Inter-RAT Mobility Robustness Optimization in Self-Organizing Networks

Vom Fachbereich 18
Elektrotechnik und Informationstechnik
der Technischen Universität Darmstadt
zur Erlangung der Würde eines
Doktor-Ingenieurs (Dr.-Ing.)
genehmigte Dissertation

von
M.Sc. Ahmad Awada
geboren am 30.04.1985 in Beirut

Referent:	Prof. Dr.-Ing. Anja Klein
Korreferent:	Prof. Dr.-Ing. habil. Andreas Mitschele-Thiel
Tag der Einreichung:	16.09.2013
Tag der mündlichen Prüfung:	12.03.2014

D 17
Darmstädter Dissertation
Darmstadt 2014

Acknowledgment

The research work of this doctoral thesis would have not been completed without the support of many people.

I would like to thank, first and foremost, Prof. Dr.-Ing. Anja Klein for giving me the opportunity to pursue a doctoral degree under her supervision, and to join the Department of Communications Engineering at Technical University of Darmstadt. Her guidance and support have been a great help to me for completing this thesis. I am grateful to all her suggestions and meticulous comments on my publications and thesis.

This thesis was funded by Nokia Siemens Networks in Munich, Germany, and I would like to thank the company for the generous support. As a member of the Radio Research Department, I have been surrounded by great supervisors and colleagues who have provided me with a productive environment to conduct research and explore new ideas. I would like to offer my special thanks to Dr.-Ing. Bernhard Wegmann for the project supervision and guidance. His professional assistance and valuable support have helped me in keeping my progress on schedule. My grateful thanks are also extended to my co-supervisor Dr.-Ing. Ingo Viering with whom I had plenty of technical discussions on diverse topics.

Special thanks go to Ömer Bulakci with whom I co-authored some of the publications in this thesis and had many insightful discussions. With his help and accompaniment, my long journey became more pleasant and cheerful. I want to thank Abdallah Bou Saleh for all the thoughtful discussions and encouragement at the beginning of the research work. I acknowledge also my master thesis student Jiasheng Liang for his work.

I would like to thank all my other co-authors Dr. Simone Redana, Dr. Dirk Rose, Andreas Lobinger, Henri Martikainen, Bernhard Raaf and Prof. Jyri Hämäläinen for their contributions. I acknowledge Michael Färber, Peter Merz and Rüdiger Halfmann for their help in offering me all the necessary resources to complete this thesis. I want to thank also all my other colleagues and friends for the good time we had together during the thesis, namely Zeid Abou-Chahine, Wolfgang Mennerich, Isil Burcu Barla, Federica Vitiello, Dereje W. Kifle, Fasil Berhan and Anteneh Atumo.

I would like to thank Prof. Dr.-Ing. habil. Andreas Mitschele-Thiel for the review of the thesis and comments. I thank also Prof. Dr.-Ing. Ralf Steinmetz and Prof. Dr.-Ing. Marius Pesavento from Technical University of Darmstadt for being members of

the thesis defense committee. The assistance provided by the secretary Lioba Fischer is greatly appreciated.

I express my sincere gratitude to all my beloved family members in Lebanon, Australia and Germany. I am deeply and forever indebted to my parents, brothers and sister for their love, encouragement and endless support throughout my life.

Finally, my heartfelt thanks go to my wife, Layal Awada, whose unwavering love, support and encouragement have been an enormous help for me.

Kurzfassung

Das starke Wachstum bei der mobilen Datenkommunikation erfordert neue effizientere Mobilfunktechnologien (engl., Radio Access Technology (RAT)) wie Long Term Evolution (LTE), welche zusätzlich als sog. Overlay-Netze zu bestehenden Mobilfunksystemen eingesetzt werden. Ein Inter-RAT Handover ist ein Wechsel des mobilen Endgeräts (engl., User Equipment (UE)) von einer Mobilfunktechnologie zu einer anderen. Ein Inter-RAT Handover wird in der Regel dadurch ausgelöst, dass der Signalpegel des momentan versorgenden RATs schwach wird, während ein ausreichend hoher Signalpegel von einem anderen RAT zur Verfügung steht. Er kann aber auch aufgrund von Traffic Steering, einer vom Betreiber gezielten Verteilung des Verkehrsaufkommens über die verschiedenen RATs ausgelöst werden. Ein störungsfreier Betrieb der Wechsel zwischen den RATs erfordert eine optimale Einstellung der Handover-Parameter, die in der Regel pro Zelle, pro Zellpaar oder sogar im besten Fall sogar für einen definierten Ortsbereich konfiguriert werden.

Die Netzplanung muss ohne Kenntnis der detaillierten Funkausbreitungsbedingungen, sowie der Bewegungsrichtungen und Geschwindigkeiten der mobilen Endgeräte auskommen und kann somit nur eine grobe Voreinstellung der Parameter bereitstellen, die dann später während des Netzbetriebes mit Hilfe von Drive-Tests und Expertenwissen optimiert werden müssen. Diese manuelle Optimierung erfordert umfangreiche menschliche Eingriffe, die erhöhte Betriebskosten (engl., Operational Expenses (OPEX)) für den Mobilfunkbetreiber bedeutet. Außerdem führt aufgrund der begrenzten Mittel für eine detailliertere Ursachenanalyse die manuelle Optimierung zu einer suboptimalen Handover-Qualität. Deshalb wurden von Mobilfunkbetreibern Mechanismen angefordert, die eine automatische Optimierung der Handover-Parameter ermöglichen. Dieser Mechanismus für den Inter-RAT Fall ist in der 3rd Generation Partnership Project (3GPP) als Inter-RAT Mobility Robustness Optimization (MRO) bekannt und gehört zu den Anwendungsfällen, welche in Rahmen von Self-Organizing Networks (SON) definiert sind.

Die technische Komplexität und die Anforderungen an MRO machen eine effiziente und gründliche Optimierung mittels manueller Methoden nahezu unmöglich. Da ein Mobilfunknetz aus einer großen Anzahl von Zellen besteht, ist die gleichzeitige Optimierung der zellspezifischen Handover-Parameter eine große Herausforderung. Darüber hinaus machen die Abhängigkeiten und Wechselwirkungen der Handover-Schwellen zwischen den verschiedenen Nachbarzellen die Anforderungen an MRO noch schwieriger und komplizierter. Bekannte Optimierungsmethoden, etwa lokale Suchverfahren wie Simulated Annealing, könnten prinzipiell offline während der Planungsphase verwendet

werden, aber nicht im online-Modus unter Echtzeitbedingungen, wo dynamisch auf die Veränderungen in der Umgebung sowie hinsichtlich des Verkehrsaufkommens reagiert werden muss. Aus dieser Perspektive werden neue Optimierungsverfahren benötigt, die den Herausforderungen und Einschränkungen von MRO genügen. Diesbezüglich werden in dieser Arbeit mehrere neue inter-RAT MRO Verfahren vorgeschlagen und analysiert, die diesen Anforderungen genügen.

Zur detaillierten Analyse der Mobilitätsprobleme, die beim technologieübergreifenden Zellwechsel auftreten können, werden neue Key Performance Indikatoren vorgeschlagen. Ein Inter-RAT Handover wird von einem Ereignis ausgelöst, welches vom Erreichen der Schwellwerte zweier Messgrößen abhängt, nämlich wenn die Signalstärke der bedienenden Zelle unter den ersten Schwellwert fällt und gleichzeitig die Signalstärke einer benachbarten Zielzelle einer anderen RAT über der entsprechenden zweiten Schwelle liegt. Ein Verbindungsausfall (engl., Radio Link Failure (RLF)) durch einen zu spät veranlassten Handover (ein sog. Too Late Handover (TLH)) bedarf wegen der Abhängigkeit von zwei Schwellen einer genaueren Analyse, da nicht unmittelbar klar ist, welche der beiden Schwellen nicht erreicht wurde. Wegen der dualen Schwellenmessung gibt es im Gegensatz zum intra-RAT Fall zwei unterschiedliche Typen des TLHs.

Der Standard sieht derzeit vor, dass die Schwellen zum Auslösen eines Inter-RAT Handovers zellspezifisch konfiguriert und optimiert werden. Das heißt, die UEs werden mit ein und denselben Messschwellen konfiguriert, unabhängig von der benachbarten Zelle. In dieser Arbeit wird zunächst die Leistungsfähigkeit einer zellspezifischen Optimierung analysiert und ein neuer zellgruppenspezifischer Optimierungsansatz vorgeschlagen, wo unterschiedliche Schwellenwerte in Bezug auf eine Gruppe von benachbarten Zielzellen konfiguriert werden können. Für beide Ansätze, den zellspezifischen und zellgruppenspezifischen, wird ein Algorithmus entwickelt, der eine automatische Optimierung der inter-RAT Handover Schwellen ermöglicht. Zug um Zug werden weitere Parameter, die die Auslösung des Handovers beeinflussen, analysiert und in den Algorithmus eingebunden. So auch das Zeitintervall zwischen der Erfüllung der beiden Ereignisbedingungen und der Meldung des Ereignisses an die Basisstation, genannt Time-to-trigger (TTT). Der Algorithmus wurde dahingehend erweitert, dass eine gemeinsame Optimierung der Handover-Schwellenwerte mit dem TTT möglich ist. Basierend auf den während der Arbeit erworbenen Erkenntnissen, dass auch zellgruppenspezifische Handover-Parameter nicht alle Mobilitätsprobleme lösen können, da selbst entlang einer Zellgrenze die Funkbedingungen nicht als stationär angenommen werden können, wird noch ein ortsbezogener Ansatz vorgeschlagen und untersucht. Im Gegensatz zu den zellbasierten Optimierungsansätzen werden die Handoverschwellen nun ortsspezifisch konfiguriert und optimiert, wobei in einer verfeinerten Variante diese auch noch

hinsichtlich der benachbarten Zielzelle unterschieden werden können.

Die Leistungsfähigkeit der verschieden Inter-RAT MRO Ansätze wird mittels simulativer Untersuchungen bewertet. Eine wichtige Erkenntnis war unter anderem, dass sich die inter-RAT Mobilitätsprobleme auf einige bestimmte Zellen beschränken. Dementsprechend sind es immer die gleichen UEs, die von Handoverproblemen betroffen sind, was zu einer hohen Unzufriedenheit dieser Benutzer führt. Diese örtliche Beschränkheit ist ein klares Indiz für die Notwendigkeit von mindestens zellspezifischen Handover-Schwellen. Bessere Ergebnisse lassen sich erzielen, wenn die Handover-Parameter auch noch bezüglich der Zielzelle oder einer Zielzellgruppe unterschiedlich konfiguriert werden. Bei der gemeinsamen Optimierung der Schwellenwerte zusammen mit dem TTT hat sich gezeigt, dass eine zellspezifische Optimierung der Handover-Schwellen der zellgruppenspezifischen überlegen ist. Alle Handoverprobleme, die nicht durch zellbasierte Optimierungsansätze gelöst werden, können durch den ortsspezifischen Ansatz behoben werden.

Die hier vorgestellten Untersuchungen und Konzepte haben direkt den Arbeitsbereich SON des Standardisierungsgremiums 3GPP beeinflusst. Einige Beiträge im Zusammenhang mit den zellspezifischen und zellgruppenspezifischen Optimierungsansätze wurden eingereicht und sind im Rahmen von LTE Release (Rel.) 11 verabschiedet worden.

Abstract

The massive growth in mobile data communication requires new more efficient Radio Access Technology (RAT) such as Long Term Evolution (LTE) being deployed on top of legacy mobile communication systems. Inter-RAT handovers are triggered either when the signal level of the serving RAT becomes weak while a sufficiently high signal level is measured from another RAT, or by traffic steering policies for balancing the load among different RATs, for example. Trouble-free operation of inter-RAT handovers requires an optimal setting of the handover parameters which is typically different for each cell and even location. Without knowing the detailed radio propagation conditions, directions and speeds of User Equipments (UEs), network planning can only provide a default setting which needs to be manually optimized during network operation with the aid of drive tests and expert knowledge. This manual optimization requires extensive human intervention which increases Operational Expenses (OPEX) of mobile operators and yields sub-optimal mobility performance due to limited means for more detailed root cause analysis. Therefore, automatic mechanisms have been requested by mobile operators to optimize the inter-RAT handover parameters. This optimization is known as inter-RAT Mobility Robustness Optimization (MRO) which is one of the use cases in Self-Organizing Network (SON).

The technical complexities and requirements on MRO are too difficult to be tackled efficiently and properly by existing manual optimization methods. Considering that mobile networks consist of a high number of cells, the number of handover thresholds to be optimized in a network is significant. Moreover, the intricate dependencies and interactions among the handover thresholds of different neighboring cells make MRO problems even more challenging and complicated. Current optimization methods such as the local search method Simulated Annealing, for example, can be used offline in the network planning phase, however, they cannot be applied online in real-time networks to dynamically react on the changes in the environment and traffic. From that perspective, new optimization methods are needed to address the challenges and limitations imposed by MRO. In this thesis, several novel and feasible inter-RAT MRO methods have been proposed and analyzed.

New key performance indicators which capture the different types of mobility failure events are proposed by the author of this thesis for the inter-RAT scenario. An inter-RAT handover is triggered by a dual-threshold measurement event where the first threshold corresponds to the serving cell and the second to the neighboring target cell of another RAT. This dual-threshold measurement event requires a more precise analysis of Too Late Handovers (TLHs). A TLH which is caused by the misconfigured

serving cell threshold is distinguished from that which can be resolved by the target cell threshold. Thus, there are two types of TLHs in contrast to the intra-RAT case where a single type of TLH handover exists.

Inter-RAT handover thresholds of currently standardized RATs are configured and optimized cell-specifically. That is, the same handover thresholds are applied by the UEs irrespective of the neighboring handover target cell. The limitations of a cell-specific optimization approach are analyzed and a new cell-group specific optimization approach where the handover thresholds are differentiated with respect to a group of neighboring target cells is proposed. For both cell-specific and cell-group specific optimization approaches, an automatic algorithm is developed to optimize the inter-RAT handover thresholds. In order to analyze the impact of Time-to-Trigger (TTT), which is a time interval affecting the triggering of handovers, the MRO algorithm is extended to allow a joint optimization of handover thresholds and TTT. Based on findings that even cell-group specific parameters cannot resolve all mobility failure events in some cells where radio conditions are not stationary along the cell border, a more advanced location-specific approach is proposed. Unlike cell-based optimization approaches, the handover thresholds are configured and optimized per cell-area and they can be differentiated with respect to neighboring target cells.

Simulative investigations are carried out to evaluate the performance of the different optimization approaches. It has been shown that mobility failure events are rather located in specific cells. Accordingly, the same UEs are probably affected all the time by these mobility failures which leads to high user dissatisfaction. This clearly indicates the need of cell-specific handover thresholds to resolve the mobility problems in some cells. Moreover, it is shown that the optimization of target cell threshold in a cell-group specific manner yields an additional performance improvement compared to cell-specific optimization approach. The joint optimization approach of handover thresholds and TTT has shown advantages only when the handover thresholds are configured cell-specifically rather than cell-group specifically. The mobility failure events that are not resolved by cell-based optimization approaches are mitigated by cell-area based optimization approach.

The investigations and concepts in this thesis have directly impacted 3rd Generation Partnership Project (3GPP) standard. Several contributions related to cell-specific and cell-group specific optimization approaches have been submitted and adopted by LTE Release (Rel.) 11 standard.

Contents

Chapter 1

Introduction

1.1 Self-Organizing Radio Networks

Nowadays, mobile communications becomes a staple commodity which is indispensable for daily life. The advances in mobile technologies have enabled the emergence of new classes of mobile devices such as smart phones and tablets. These mobile devices allow the users to access the internet and benefit from a wide range of online services. Moreover, the open architecture of some mobile operating systems has boosted the development of a significant number of mobile applications which have great impact on individuals as well as on businesses [Has12]. The high diversity in user applications and services has caused mobile communications to become an integral part of everyday life.

The explosive growth in wireless data usage [Ame11] has fostered mobile networks to evolve from circuit switched paradigm with hierarchical network architecture to a flexible packet switched radio access technique with flat architecture as realized in LTE. New 4th Generation (4G) systems such as LTE are being deployed by mobile operators on top of legacy 2nd Generation (2G) or 3rd Generation (3G) mobile system. The co-existence of multiple RATs offers mobile operators an efficient means to meet the different data rate requirements of the users [BAE+09]. For further improvements, small cells such as femto and pico cells are foreseen to provide more coverage and offload some of the macro cells [AEaG13, ONY+11]. This heterogeneity in RATs and types of cells makes the network more diverse and complicated.

The extension of the network to comprise new RATs and sites increases drastically the costs and the operational effort of mobile operators. The deployment of new mobile networks and sites increases Capital Expenses (CAPEX) comprising engineering and installation services [Cel08, MPJC10]. On the other hand, the parallel operation and maintenance of multiple networks increases significantly OPEX [ERX+13]. It is estimated that about 24 % of a typical mobile operator revenue is spent on OPEX [She05]. At the same time, the multitude of tunable radio network parameters and intricate interactions among RATs impose new operational challenges [vdBLE+08]. Mobile networks are becoming more difficult to configure, optimize and maintain due to technological complexities.

The increase in CAPEX and OPEX is accompanied, unfortunately, by a stagnation in the revenues of mobile operators [Has12, PZW11]. Despite the spectral efficiency gains of the new wireless technologies, the revenue measured on a per-Megabit (Mb) basis is dropping due to the rapid growth in data throughput [Ame11]. Moreover, the revenues are declining because of the high competition resulting in new flat-rate contracts for voice and data communications [Has12]. To remain competitive, mobile operators are seeking new techniques which cut their CAPEX and OPEX while maintaining a high quality network service.

The common objective of 3GPP standard [3GP07], mobile operator's lobby Next Generation Mobile Networks (NGMN) [NGM06] and research projects such as FP7 SOCRATES [SOC08b] is to minimize the human involvement in network planning and optimization tasks. Currently, the configuration and optimization of the network is manually performed requiring the intervention of technical experts in network planning, drive tests, optimization and maintenance tasks [ALS+08]. Moreover, the network optimization processes are repetitive and need to be performed permanently in order to respond to the dynamic changes in network, environmental conditions and traffic [Ame11]. Considering the large-scale deployment of the mobile networks comprising multiple RATs and thousands of sites, the network configuration and optimization costs are significant. As a means to reduce costs without degrading Quality of Service (QoS), manual operational tasks are replaced by automatic functionalities running autonomously at the network side. Networks having such automatic configuration and optimization functionalities are called SONs.

The benefits of introducing self-organization to mobile wireless networks are in terms of CAPEX and OPEX reductions as well as performance enhancements [vdBLE+08]. The permanent and costly human involvement in network operation is minimized by using automatic functionalities which are always online in all nodes of the network. Minimization of the human intervention leads directly to a reduction in OPEX. In addition, the foreseen performance gains from self-organization exceed those obtained by traditional configuration and optimization methods [vdBLE+08]. The instantaneous acquisition of information from the network enables self-organization applications to be less error-prone and to respond faster to the changes in the network. The performance gains in coverage, capacity and QoS help to reduce the number of sites or allow for a delayed investment in additional cells which directly shrinks CAPEX.

The functionalities of SON include self-configuration, self-optimization and self-healing [FS08]:

- Self-configuration procedures are responsible for the initial configuration and ba-

sic setup of the Base Stations (BSs). Self-configuration is active in pre-operational phase when the BSs are powered up for the first time and prior to Radio Frequency (RF) transmission.

- Self-optimization procedures are used to auto-tune the radio network parameters. These procedures work in operational phase and respond online to the changes in the network. The optimizations rely on the measurements of UEs and BSs as well as on performance measurements.

- Self-healing procedures detect automatically operational failures in BSs and apply self-healing mechanisms to recover from these failures.

1.2 Inter-RAT Mobility Robustness Optimization

For each of the three SON functionalities described in Section 1.1, a set of use cases are defined in [NGM07, 3GP11]. For instance, the main use cases of self-optimization are neighbor cell list optimization [LH11], coverage and capacity optimization [NuIAJHMT10, NuIMT12a, NuIMT12b], mobility load balancing [LSJB10, AWVK10a, AWVK10b] and MRO [KKYK11, HL12]. The recommendations and requirements on each use case are given in [NGM08, SOC08a]. They mainly describe the technical and business requirements of each use case and its corresponding expected outcome. Mobile operators have identified MRO as one the key tasks that requires automation as it is performed in their day-to-day operations [Ame11]. For this reason, MRO use case is considered in this thesis and it is described in detail in the following.

The general aim of MRO use case in SON is the automatic optimization of the parameters affecting the handovers of UEs for the sake of ensuring a proper end-user mobility in the network [HSS12], i.e., when moving from a source cell to a target cell. Incorrect handover parameter settings can negatively impact the user experience and waste network resources by causing mobility problems such as Handover Failures (HOFs), Radio Link Failures (RLFs) and Unnecessary Handovers (UHs). RLFs or HOFs can lead to a call drop if the connection of the UE is not re-established, and consequently have more impact on user perception than other mobility problems. Costly handovers such as Ping-Pongs (PPs), which are consecutive back and forth handovers during a short time, lead mainly to inefficient usage of network resources.

Different types of handovers exist depending on the RAT and operating carrier frequencies of source and target cells. The handover types are shown in Fig. 1.1. Intra-RAT

handover occurs between a source and target cell of the same RAT. On the other hand, inter-RAT handover occurs between a source and target cell of different RATs operating at two different carrier frequencies, e.g., LTE and 3G. Moreover, the intra-

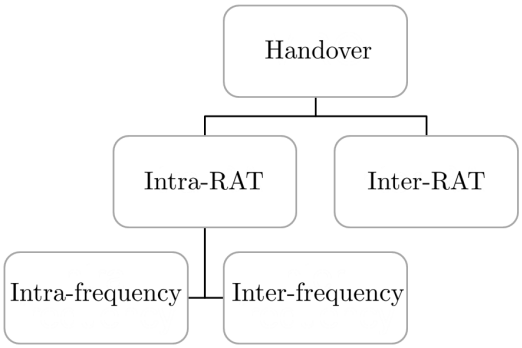

Figure 1.1. Different types of handovers.

RAT handover is further differentiated between intra-frequency and inter-frequency. In the former case, the source and target cells of the same RAT operate at the same carrier frequency whereas in the latter case the two cells operate at different carrier frequencies.

The main difference between intra-frequency and inter-frequency handover, including inter-RAT case, is the interference experienced by the UE during the handover. In intra-frequency handover, the handed over UE suffers from the interference between source and target cells. This is schematically illustrated in Fig. 1.2(a) that shows the received signal strengths of a UE from both source and target cells as a function of its distance from the BS. If the UE is handed over to the target cell before it reaches the border of the source cell (dashed line), determined by the mobility handover parameter settings, the interference induced by the previously serving cell would be high, which in turn can cause an RLF due to a Too Early Handover (TEH). On the other hand, if the handover is executed after the UE has crossed the border of the serving cell, an RLF could occur due to a TLH. Thus, the success of intra-frequency handover highly depends on the time instant of handover execution.

In inter-frequency handover, a UE does not experience any interference from the source cell if it is handed over to the target cell. This is illustrated in Fig. 1.2(b) which shows an inter-frequency example of a UE attempting to hand over from a source cell in RAT A to a co-sited target cell in RAT B. In inter-frequency handover, there is no so-called “cell edge problem” as source and target cells operate at different frequencies. Moreover, there is a large area where the UE can connect either to the source or target cell with good signal level.

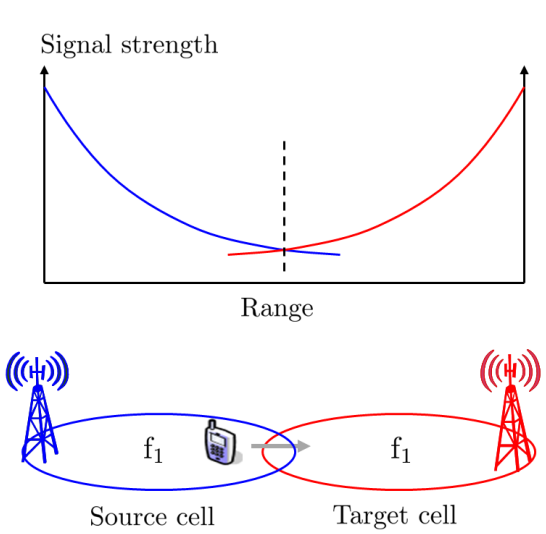

(a) Intra-frequency handover: The target cell is an interferer.

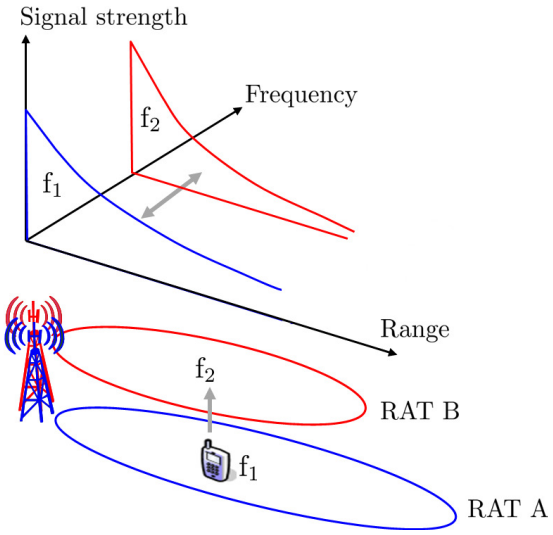

(b) Example of an inter-frequency handover: No interference between different operating frequencies.

Figure 1.2. Impact of interference during the handover of a UE in intra-frequency (left) and inter-frequency (right) scenarios.

This thesis focuses on MRO between two RATs. As an example, an LTE network overlaying with a 3G network is considered. Nevertheless, the presented concepts and optimization approaches could be, in principle, applied for all types of RATs, e.g., 2G or Worldwide Interoperability for Microwave Access (WiMAX).

The co-existence of two overlaying LTE and 3G networks provides mobile operators a high degree of flexibility for matching network resources to application requirements. As LTE provides much higher peak throughput than 3G [HT09], high data rate users can be served by LTE and the rest by 3G network. Thus, a better utilization of radio resources can be achieved by handing over LTE capable users having high data rate requirements from 3G to the LTE network. This kind of inter-RAT handover is called traffic steering based handover as it yields a better distribution of load and traffic in both RATs [NPS11].

The handover of an UE to another RAT is also necessary when the coverage of the serving RAT becomes weak and a strong coverage from a different RAT exists. The radio coverage of a RAT can be insufficient in two cases: a) One RAT is deployed only for a limited geographical area while the other RAT is covering the full serving area, or b) Coverage holes exist in one RAT, mainly caused by physical obstructions such as buildings, tunnels or hills, and at the same time a good coverage exists from the other RAT. In order to provide a service continuity, a user reaching the end of coverage area or approaching a coverage hole should be handed over to another RAT if possible.

The inter-RAT handover of a UE relies on filtered signal measurements of the serving and target cells. The impact of fast fading on signal measurements is averaged out by applying first Layer 1 (L1) averaging, then Layer 3 (L3) filtering using a filter coefficient parameter [3GP12b, 3GP12g]. These filtered measurements are reported by the UE to the serving BS either periodically or event-triggered. In the latter case, the measurements are reported when the serving signal is below a first threshold and the target signal is higher than a second threshold for a certain TTT interval. Once the measurement report is received, the inter-RAT handover is prepared and executed by the BS. The parameters affecting the inter-RAT handovers are namely the two aforementioned thresholds, TTT and filter coefficient parameter. The objective of inter-RAT MRO is to optimize automatically all or some of the handover parameters of each cell in order to ensure seamless handovers of UEs between RATs.

1.3 State of the Art

This section provides an overview of the previous works related to SON and MRO use case. The first part briefly describes the evolution of the methods followed in network configuration and optimization that yielded later on the inclusion of SON in future networks [Has12]. The second part discusses the relevant literature on MRO use case.

The development of new RATs and network architectures have made the configuration and optimization operations much more difficult and complex. With the introduction of Wideband Code Division Multiple Access (WCDMA) along with new data services, the optimization trade-offs and the number of configuration parameters have increased significantly compared to 2G system [Has12, SPRSG+11]. As a result, new approaches and tools were required to support the network planning configuration and optimization processes [ZYAW06]. Some of these tools have incorporated automated optimization functionalities which made the network design more time-efficient and reduced the network deployment and maintenance costs [ABH+04, BJAPO05, NDA06, SVY06]. Driven by the pressure from mobile operators to further reduce costs, SON is envisioned and introduced by 3GPP in 4G systems such as LTE to configure and optimize the cellular network automatically. Mobile operators have identified SON as one of the key means to reduce costs and to simplify the network management [SPRSG+11]. The previous investigations on MRO use case are described in the following.

The research topic of intra-RAT MRO in SON has been extensively discussed in literature, especially for LTE networks [JBT+10, Wei10, BJS+11, JBS+11, VWL+11]. However, few papers deal with inter-RAT MRO in the context of SON. This is because

inter-RAT MRO was given at first a lower priority than intra-RAT MRO which was specified by 3GPP in Rel. 9 and Rel. 10. Inter-RAT MRO has been specified in Rel. 11 and has been fed with results from this thesis. There was almost no prior art for inter-RAT MRO with the exception of basic network planning optimization methods which provide recommendations or techniques on how to set the handover parameters of legacy technologies such as 2G and 3G. In the following, the most relevant techniques for setting the inter-RAT handover parameters of 2G and 3G systems are summarized.

The work in [SSJC05] proposes a design for an inter-RAT handover algorithm in Universal Mobile Telecommunication System (UMTS) and Global System for Mobile Communications (GSM) networks. The deployment scenario consists of an island of UMTS cells surrounded by an ubiquitous GSM network. The main idea of the optimization algorithm is to set a hysteresis value between the parameters affecting in-going and out-going inter-RAT handovers. The authors show that for well-designed hysteresis values, a good trade off can be achieved between call drop rates, intra- and inter-RAT handover rates.

In [BGM+06], field tests measurements are used to find proper settings for the parameters controlling the inter-RAT handover from a WCDMA to a GSM network. The RF measurements are logged during a drive test in a route which is leaving WCDMA coverage and they are passed to an emulator for processing. The impact of different parameter settings on inter-RAT handover performance has been investigated. Using the test results, the authors recommend a set of handover parameters that lead to significant reductions in call drop rates in WCDMA.

Cell-specific parameterization of inter-RAT handover parameters has been suggested in [FSL+07] for a UMTS network overlaying partly with a GSM network. That is, each cell applies specific values of handover parameters. The UMTS cells are distinguished according to their neighbor cell relationships and coverage areas. The following three types of cells are defined: Inner cell, transit cell and border cell. The inner cell is fully surrounded by nearby neighbors and has restricted coverage. The handover parameters of this kind of cell are configured such that inter-RAT handovers are almost disabled. A transit cell is fully surrounded by a lower number of neighbors than that of inner cell and has a larger coverage. This kind of cell should be more prepared for executing inter-RAT handovers to react on weak radio conditions. Finally, a border cell refers to an outer cell of the UMTS network which is not fully surrounded by nearby neighboring cells. For this cell, the inter-RAT handover of a UE to the GSM network should be triggered in time before a call drop happens due to missing coverage.

1.4 Open Issues

The automatic optimization of inter-RAT handover parameters in SON is a relatively new topic which has not been addressed much in literature as mentioned in Section 1.3. For this reason, many issues related to inter-RAT MRO are still open. In this section, the most important open issues are summarized as follows.

1. How to model and design a multi-RAT cellular system for investigating inter-RAT MRO while keeping the computational complexity low?
2. Which inter-RAT mobility failure types are needed for appropriate root cause analysis?
3. What is the new offline optimization method that can take into account the interactions among the configuration parameters, and how can it be used in network planning phase to efficiently optimize the handover parameters?
4. How to make use of Physical Cell IDs (PCIs) of neighboring target cells of handover in order to overcome the limitations of the current cell-specific optimization approach of handover thresholds in SON?
5. How to design an efficient algorithm for automatically optimizing the inter-RAT handover thresholds of each cell?
6. How to make use of the additional TTT parameter which is defined in Section 1.2 to improve the performance of the automatic algorithm optimizing only the handover thresholds of cells?
7. How to make use of the locations of mobility failure events to achieve an inter-RAT MRO solution which is better than cell-based optimization approaches where the handover thresholds are configured per cell?

1.5 Contributions and Outline of the Thesis

In this section, the outline of the thesis is given and the main contributions which answer the open issues of Section 1.4 are summarized.

Chapter 2 presents the system model of the multi-RAT cellular system and two relevant deployment scenarios for investigating inter-RAT MRO. This chapter addresses

the challenges of open Question 1. The handover measurements and downlink Signal-to-Interference and Noise Ratio (SINR) are modeled such that the computational complexity of the inter-RAT MRO is reduced. The impact of fast fading is considered in handover measurements by generating and filtering the samples offline due to the small time granularity of L1 filtering procedure. Moreover, the models of the handover procedure and detection of RLFs are simplified in comparison with those specified in the 3GPP standard. Two deployment scenarios are considered for LTE and 3G co-sited networks. The scenarios are designed such that the user distribution is stationary over time, which is necessary for the evaluation of any automatic inter-RAT MRO algorithm.

The handover parameters and mobility failure types used for inter-RAT scenario are described in Chapter 3. The inter-RAT handover parameters: handover thresholds, TTT and filter coefficient are explained along with the factors affecting their settings. This chapter answers open Question 2. In contrast to the intra-RAT case, two types of TLHs exist: The first one is a TLH which is due to the misconfiguration of the serving cell threshold and the second is a TLH which is due to the misconfiguration of the target cell threshold. A scheme is proposed to classify a TLH into one of these types. The proposal to differentiate between the two types of TLHs has been recently adopted by LTE Rel. 11 standard [3GP12c].

The manual optimization of inter-RAT handover thresholds, which requires human intervention, is presented in Chapter 4. The handover thresholds are initialized with a best network-wide setting, i.e., same handover thresholds for all cells of the network, and optimized later cell-specifically during network operation. Cell-specific optimization of handover thresholds can be performed as well using offline optimization methods during the network planning phase. This chapter answers open Question 3. Taguchi's method for experiment design is a promising offline optimization method that was developed at first for manufacturing processes. The method has been applied by the author of this thesis to optimize for the first time radio network parameters. The advantage of Taguchi's method compared to others, such as Simulated Annealing, is that it considers explicitly the interactions among the configuration parameters. Taguchi's method is based originally on orthogonal array [Roy01] which is difficult to construct for arbitrary number of parameters while keeping the complexity of the method low. This limitation has been addressed by replacing the orthogonal array with a nearly orthogonal array [AWVK11c] which can be constructed for arbitrary number of parameters and provides more flexibility in controlling the complexity of the method. Simulation results are shown to evaluate the performance of the newly introduced Taguchi's method, Simulated Annealing and best network-wide setting of handover thresholds.

The automatic optimization of handover thresholds in SON is presented in Chapter 5. Currently, the handover thresholds are configured cell-specifically by the 3GPP standard [3GP12b, 3GP12g]. The cell-specific optimization problem is formulated by the author of this thesis using the values of the Key Performance Indicators (KPIs) which are collected periodically in each cell. Moreover, the optimization limitations of cell-specific optimization problem are derived analytically. This chapter addresses open Question 4. Using the PCIs of neighboring target cells, the values of the KPIs can be differentiated with respect to neighboring target cells of handover. This allows for a cell-group specific optimization of the handover thresholds where a dedicated value can be configured with respect to a group of neighboring target cells. It is shown in this thesis that configuring only the target cell threshold in a cell-group specific manner is beneficial. This contribution of configuring the target cell threshold in a cell-group specific way has been submitted to LTE Rel. 11 standard [NN12]. Chapter 5 answers also open Question 5 of Section 1.4. The optimization loop of the handover thresholds, configured cell-specifically or cell-group specifically, is described in Section 5.6. To obtain steady improvements, a feedback controller is used to change the values of handover thresholds. The performance of the newly introduced cell-group specific optimization approach is compared by means of simulations to that of the cell-specific optimization approach and the best network-wide setting of handover thresholds.

The automatic algorithm of Chapter 5 optimizing only the handover thresholds is extended to include the TTT parameter. The joint optimization algorithm of the handover thresholds and TTT is presented in Chapter 6. This chapter answers open Question 6. The inter-RAT mobility failure events are classified into two sets of KPIs: The first set comprises the mobility failure events which can be resolved only by the handover thresholds and the second one comprises the mobility failure events which can be resolved by TTT. Based on the values of these two sets of KPIs, a decision is made on whether to change either the handover thresholds or TTT. The performance of the joint optimization algorithm of the handover thresholds and TTT is compared with that of the algorithm optimizing only the handover thresholds. The performance comparison is carried out for cell-specific and cell-group specific target cell thresholds.

In Chapter 7, a cell-area based optimization algorithm of handover thresholds is presented. This chapter provides the answer of open Question 7. Unlike cell-based optimization approaches of Chapter 5, the coverage area of each cell is decomposed into small tiles or areas and dedicated handover thresholds are assigned for each area. The cell-area based optimization problem is formulated in terms of the mobility failure events which are collected periodically for each area. The optimization of the handover thresholds of each area can be performed with respect to all neighboring cells or a group of neighboring cells. The former and latter new optimization approaches

are denoted by cell-area specific and cell-area group specific optimization approaches, respectively, in analogy to cell-specific and cell-group specific optimization approaches of Chapter 5. The performance of the cell-area based optimization approach is compared with that of the best network-wide setting, cell-based optimization approaches of handover thresholds and joint optimization of handover thresholds and TTT.

The thesis is concluded in Chapter 8 which summarizes the main results and provides an outlook on future work.

Chapter 2
System Model

2.1 Introduction

This chapter presents the system model and the scenarios that are used for inter-RAT MRO investigation.

Traditional models for system level simulators are not appropriate for SON mechanisms since they focus on scheduling and Radio Resource Management (RRM) which operate at a small time scale, generally in the order of Transmission Time Interval (TTI) in ms [VDL09]. The underlaying variations in the environment which are tracked by MRO are rather slow and do not require a fast adaptation [MYYZ12]. Changes in propagation conditions, traffic and mobility behavior, e.g., new streets, would be visible for mobile operators when only enough statistics of mobility failure events are obtained. Reliable statistics are typically collected from the network during time intervals of minutes, or even hours depending on the traffic in the considered cell [VWL+11]. From that perspective, the time scale of MRO is large unlike other highly adaptive functionalities such as RRM. In addition to this temporal aspect, MRO has another spatial aspect which is the simultaneous occurrence of mobility problems in different cells and the interdependencies among cells. A change of a handover parameter in a cell might trigger MRO in other neighboring intra- or inter-RAT cells, and if mobility problems are distributed in different areas of the network, many cells may apply MRO simultaneously. These temporal and spatial aspects of MRO increase the complexity of the simulative investigation.

To consider time periods of several minutes or hours, low complexity models of the network are necessary for efficient simulative investigation. In this chapter, models for the measurements of the UE, handover procedure, RLF detection and average SINR in downlink are proposed. The models of the UE measurements consider effects varying on a small time scale such as fast fading without increasing the computational complexity. This is accomplished by generating the samples of fast fading offline and adding them to the measurements during the simulation. In addition, the author proposes two deployment scenarios of overlaying LTE and 3G networks for inter-RAT MRO investigation.

This chapter is organized as follows. The network layouts of LTE and 3G networks are described in Section 2.2. The radio signal propagation model comprising the effect

of path loss, shadowing and antenna beam pattern is discussed in Section 2.3. The measurements of the UE which are used for handover decisions are described in Section 2.4 along with the filtering procedures applied for measurements. The model of the average SINR in downlink is presented in Section 2.5 for a UE served by an LTE or 3G cell. Section 2.6 explains the handover procedure model of UE. The detection model of RLF is provided in Section 2.7. The last Section 2.8 introduces the two deployment scenarios for simulative MRO investigation which consist of two partially or fully overlaying LTE and 3G co-sited networks.

2.2 Cellular Layouts of LTE and 3G Networks

This section describes the cellular layouts of LTE and 3G networks.

Each LTE and 3G BS has a tri-sector antenna. All transmit antennas of BSs are mounted at a height h_{bs}. The index of the BS is $b = 1, \ldots, N_{\text{bs}}$, where N_{bs} is the total number of LTE and 3G BSs. The cell index is $c = 1, \ldots, N_{\text{c}}$, where N_{c} is the total number of LTE and 3G cells. The set of LTE and 3G cells is given by $\mathcal{C} = \{1, \ldots, N_{\text{c}}\}$. Each cell c is served by a BS at position $\mathbf{p}_c$. Due to sectorization, some cells have the same BS position. The network to which each cell c belongs is given by $\ell_c = w \in \{1, 2\}$, where w equal to 1 and 2 indicates LTE and 3G network, respectively. The set of inter-RAT neighbors of cell c is given by $\mathcal{N}_c$ defined as

$$\mathcal{N}_c = \{i_1, \ldots, i_k, \ldots, i_K | i_k \in \mathcal{C}, \ell_{i_k} \neq \ell_c\} \tag{2.1}$$

where k is the index of the K inter-RAT neighbors of cell c. The total number of UEs is denoted by N_{ue}. Each UE u is located at a position $\mathbf{v}_u$ on the ground, i.e., UE height is zero.

2.3 Radio Signal Propagation Model

In this section, the models of path loss, shadowing and 3-Dimensional (3-D) antenna beam pattern are described. Fast fading is not considered as it is discussed in Section 2.4 where measurements of UEs and filtering procedures are presented.

The path loss is the attenuation in signal strength of a transmitted signal and depends only on the distance between the transmitter and receiver [Gol05]. The distance between a BS serving cell c and UE u is denoted by $d_{c,u} = |\mathbf{p}_c - \mathbf{v}_u|$. The path loss model

is given in dB scale by

$$L_{\mathrm{p}}(d_{c,u}) = \alpha_{\mathrm{p}} + \beta_{\mathrm{p}} \cdot 10 \log_{10}(d_{c,u}\ [\mathrm{km}]) \tag{2.2}$$

where α_{p} is a propagation constant and β_{p} is the path loss exponent [3GP06].

Shadowing, also referred to as small scale fading, is modeled as a random process caused by obstacles in the environment which attenuate the power of the transmitted signal [Gol05]. For simulations, shadowing is considered by using a so-called shadowing map for each BS, which is a deterministic function of a particular position of a UE u in the network [VDL09]. The samples of the shadowing map are log-normally distributed with zero mean and standard deviation σ_{sf} given in dB [Rap02]. In addition, the shadowing maps of cells served by the same BS are fully correlated.

The shadowing value corresponding to UE u located at position $\mathbf{v}_u$ with respect to BS b is denoted by $M_b(\mathbf{v}_u)$. According to [VVGZ94], $M_b(\mathbf{v}_u)$ can be expressed as the sum of two independent components $\xi_w(\mathbf{v}_u)$ and $\eta_b(\mathbf{v}_u)$: The former refers to the near field component and is common for all BSs of the same network w, whereas the latter is BS-specific, and in turn independent for different BSs. Thus, $M_b(\mathbf{v}_u)$ is formulated as

$$M_b(\mathbf{v}_u) = \sqrt{\zeta_{\mathrm{bs}}} \cdot \xi_w(\mathbf{v}_u) + \sqrt{1-\zeta_{\mathrm{bs}}} \cdot \eta_b(\mathbf{v}_u) \tag{2.3}$$

with

$$\begin{aligned} \mathrm{E}[\xi_w(\mathbf{v}_u)] &= \mathrm{E}[\eta_b(\mathbf{v}_u)] = 0, & (2.4)\\ \mathrm{Var}[\xi_w(\mathbf{v}_u)] &= \mathrm{Var}[\eta_b(\mathbf{v}_u)] = \sigma_{\mathrm{sf}}^2 \text{ for all } b, & (2.5)\\ \mathrm{E}[\xi_w(\mathbf{v}_u)\eta_b(\mathbf{v}_u)] &= 0 \text{ for all } b, & (2.6) \end{aligned}$$

and

$$\mathrm{E}[\eta_{b_1}(\mathbf{v}_u)\eta_{b_2}(\mathbf{v}_u)] = 0 \text{ for all } b_1 \neq b_2, \tag{2.7}$$

where E[.] and Var[.] denotes the mean and variance operator, respectively. The parameter ζ_{bs} is the correlation coefficient pertaining to shadowing values of two BSs of the same network and it is given by

$$\frac{\mathrm{E}[M_{b_1}(\mathbf{v}_u)M_{b_2}(\mathbf{v}_u)]}{\sigma_{\mathrm{sf}}^2} = \zeta_{\mathrm{bs}}, \text{ and } b_1 \text{ where } b_2 \text{ are of same network.} \tag{2.8}$$

There is also spatial correlation between the shadowing values of a single shadowing map which is given by the de-correlation distance d_{corr}. Two shadowing values $M_b(\mathbf{v}_1)$ and $M_b(\mathbf{v}_2)$ have some correlation if they are separated by a distance smaller than d_{corr} [3GP06].

The correlation coefficient pertaining to shadowing values of two fully co-sited BSs of different networks is denoted by $0 \leq \zeta_{\text{nw}} \leq 1$. The setting of ζ_{nw} is elaborated in Section 2.8 which discusses the deployment scenarios of LTE and 3G networks.

Apart from path loss and shadowing, the signal strength received by a UE depends on the tilt and azimuth orientation of the transmit antenna. A 3-D antenna beam pattern is used and is approximated by summing up the azimuth and vertical patterns.

The azimuth pattern of the antenna serving cell c is determined by azimuth orientation Φ_c, azimuth beam width Δ_ϕ and maximum azimuth attenuation B_{h}. The azimuth pattern $B_\phi(\Phi_c, \phi)$ of the antenna serving cell c is given by [3GP10] as

$$B_\phi(\Phi_c, \phi) = -\min\left(B_{\text{h}}, 12 \cdot \left(\frac{\phi - \Phi_c}{\Delta_\phi}\right)^2\right) \tag{2.9}$$

where angle $\phi = \angle(\mathbf{p}_c - \mathbf{v}_u)$.

Similarly, the tilt of the antenna serving cell c and the elevation beam width are denoted by Θ_c and Δ_θ, respectively. The vertical pattern $B_\theta(\Theta_c, \theta)$ of the antenna is given by

$$B_\theta(\Theta_c, \theta) = -\min\left(B_{\text{v}}, 12 \cdot \left(\frac{\theta - \Theta_c}{\Delta_\theta}\right)^2\right) \tag{2.10}$$

where B_{v} is the maximum elevation attenuation and angle $\theta = \arctan(h_{\text{bs}}/|\mathbf{p}_c - \mathbf{v}_u|)$.

The 3-D pattern of the antenna in sector c is expressed as a sum of the two aforementioned patterns as given by

$$B(\Phi_c, \phi, \Theta_c, \theta) = -\min\left\{-\left(B_\phi(\Phi_c, \phi) + B_\theta(\Theta_c, \theta)\right), B_{\text{a}}\right\} \tag{2.11}$$

where B_{a} is the maximum backward attenuation [Hop03].

The overall signal attenuation $A_c(d_{c,u}, \mathbf{v}_u, \Phi_c, \Theta_c)$ at the UE u served by a cell c of BS b is computed as

$$A_c(d, \mathbf{v}_u, \Phi_c, \Theta_c) = L_{\text{p}}(d_{c,u}) - G_{\text{gain}} - B(\Phi_c, \phi, \Theta_c, \theta) + L_{\text{pn}} + M_b(\mathbf{v}_u) \tag{2.12}$$

where G_{gain}, expressed in dBi, is the antenna gain and L_{pn} is the penetration loss.

2.4 UE Measurements and Filtering

2.4.1 Introduction

The handover decision relies basically on downlink signal measurements which are performed by the UE. The UE is configured to carry out measurements for the serving cell and neighboring cells. Depending on the measurement configuration, the UE measures the signals of neighboring cells of the same or different RATs. Two measurement quantities are used for handover decisions: Signal strength or signal quality measurements [3GP12e]. The latter quantity considers the received signal strength of the serving cell in relation to the interference of other neighboring cells of same RAT. The raw UE measurements are impacted by fast fading and other measurement errors. To eliminate these short-term variations and inaccuracies, two steps of filtering are applied to the measurements prior to any measurement reporting. First, L1 filtering is used to filter out the effect of fast fading and obtain stable estimates [3GP12d]. Then, L3 filtering is applied to smoothen the measurements received from L1 by filtering out measurement errors and residual signal fluctuations [3GP12g].

This section is organized as follows. The model of fast fading is given in Section 2.4.2. The measurements of the UE are given in Section 2.4.3. L1 filtering of fast fading is explained in Section 2.4.4. The model of measurement error is provided in Section 2.4.5 followed by a description of L3 filtering in Section 2.4.6.

2.4.2 Fast Fading Model

Fast fading refers to the rapid fluctuations in the signal amplitude resulting from multipath propagation [Sin10]. If the number of scattering objects is large and there is no light-of-sight signal path between the transmitter and receiver, the amplitude of the signal can be modeled according to a Rayleigh distribution given by

$$f_{\mathbf{x}_{\mathrm{ff}}}(x_{\mathrm{ff}}) = \frac{x_{\mathrm{ff}}}{\sigma_{\mathrm{ff}}^2} \cdot e^{-\frac{x_{\mathrm{ff}}^2}{2\sigma_{\mathrm{ff}}^2}} \tag{2.13}$$

where x_{ff} is a realization of the Rayleigh distributed Random Variable (RV) $\mathbf{x}_{\mathrm{ff}}$ [Mol03].

According to [SOZ11], an LTE capable UE should be equipped with at least two receive antennas. As this investigation studies inter-RAT MRO between LTE and 3G,

all UEs are assumed to be LTE capable. Assuming that the multipath fast fading processes at each of the two receive antennas are statistically independent, a diversity order of two is achieved resulting in less critical fading power attenuation. This is shown in Fig. 2.1 which plots the power envelope, i.e., square of the amplitude, of the multipath fast fading in dB as a function of time in ms for a UE moving at a speed of 3 km/h: The red and blue curves correspond to the case when the UE is equipped with one receive antenna and two receive antennas, respectively. According to Fig. 2.1, the

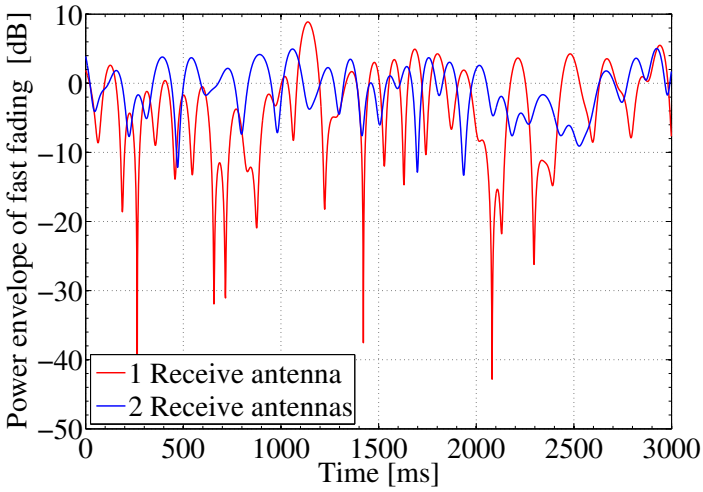

Figure 2.1. The power envelope of the multipath fast fading in dB as a function of time in ms for a UE moving at a speed of 3 km/h: The red and blue curves correspond to the case when the UE is equipped with one receive antenna and two receive antennas, respectively.

power envelope of the multipath fast fading corresponding to a single receive antenna experiences higher number of severe dips compared to that of two receive antennas. In other words, fast fading is less critical in case the UE is equipped with two receive antennas.

In case of a single receive antenna, the power envelope of the multipath fast fading is computed by taking the power of realizations of $\mathbf{x}_{\text{ff}}$, generated according to the Jakes model [Jak74] for Rayleigh flat fading. In this case, the power envelope of the multipath fast fading is exponentially distributed [Sha11] and its corresponding probability distribution function (pdf) is shown in red in Fig. 2.2. In case of two receive antennas, the power envelope of the multipath fast fading is obtained by generating two independent realizations of $\mathbf{x}_{\text{ff}}$ and averaging their corresponding power values. As a result, the power envelope of the multipath fast fading is chi-squared distributed with four degrees of freedom [Sha11] as shown in blue in Fig. 2.2. For both one and two receive antennas, the average of the power envelope of the multipath fast fading is zero in dB.

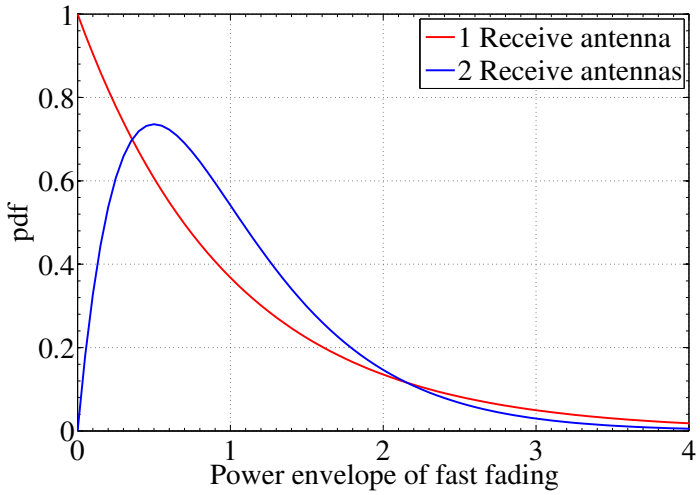

Figure 2.2. The pdf of the power envelope of the multipath fast fading: The red and blue curves correspond to the case when the UE is equipped with one receive antenna and two receive antennas, respectively.

2.4.3 Modeling of UE Measurements

2.4.3.1 Introduction

The serving BS in an LTE or 3G network configures the UE to perform signal measurements for the serving and intra- or inter-RAT neighboring cells. For instance, the UE can be configured to start measuring the neighboring inter-RAT cells when the signal measurement of the serving cell falls below a certain network configured threshold. In this study, it is assumed that inter-RAT measurements are performed by the UE at each time step t_n where n is the index for the time steps. The time elapsed between two simulation time steps is fixed and is indicated by the time step size T_{n} which is expressed in ms. Moreover, in order to perform signal measurements for neighboring inter-RAT cells, a UE has to interrupt its serving connection for measurement gaps [KH08]. From that perspective, inter-RAT measurements are quite costly unlike intra-RAT measurements which do not require any measurement gaps. Different measurement quantities can be configured by each BS. The measurement quantities are described first for LTE cells then for 3G cells.

2.4.3.2 Measurements of LTE Cells

The first measurement quantity is the Reference Signal Received Power (RSRP) which is a signal strength measurement, expressed in dBm. RSRP is defined as the linear

average over the power contributions of the resource elements that carry cell-specific reference signals within the considered measurement bandwidth [3GP12e]. The resource element is the smallest frequency and time unit which is used for downlink transmission and corresponds to a single 15 kHz sub-carrier during one Orthogonal Frequency Division Multiplexing (OFDM) symbol interval [Tol11]. The transmit power of cell c on a single resource element is given by $P_c^{(\text{tx,re})}$ in dBm. Considering a total transmit power $P_c^{(\text{tx})}$ and an LTE system bandwidth W, $P_c^{(\text{tx,re})}$ is computed as

$$P_c^{(\text{tx,re})} = P_c^{(\text{tx})} - 10 \cdot \log_{10}\left(\frac{W\ [\text{MHz}]}{15 \cdot 10^{-3}\ [\text{MHz}]}\right), \tag{2.14}$$

where $15 \cdot 10^{-3}$ is the sub-carrier bandwidth in MHz.

The RSRP of an LTE cell c measured by a UE u at time step t_n is modeled in dB scale as

$$RSRP_{u,c}(t_n) = P_c^{(\text{tx,re})} - A_c(d, \mathbf{v}_u(t_n), \Phi_c, \Theta_c) + \alpha_{u,c}(t_n), \tag{2.15}$$

where $A_c(d, \mathbf{v}_u(t_n), \Phi_c, \Theta_c)$ defined in (2.12) is the overall signal attenuation of UE u at time step t_n and $\alpha_{u,c}(t_n)$ in dB is the power envelope of the multipath fast fading on the link between cell c and UE u at time step t_n. The power envelope $\alpha_{u,c}(t_n)$ is chi-squared distributed with four degrees of freedom. The linear form of $RSRP_{u,c}(t_n)$ is denoted by $RSRP_{u,c}(t_n)|_{(\text{lin})}$.

The second measurement quantity is the Reference Symbol Received Quality (RSRQ) which is a signal quality measurement, expressed in dB. RSRQ is defined in linear scale as the ratio between RSRP and Received Signal Strength Indicator (RSSI) [3GP12e]. RSSI comprises the linear average of the total received power observed only in OFDM symbols containing reference symbols [3GP12e]. Thus, RSSI includes the signal strength of the serving cell, interference from neighboring cells of the same RAT in addition to noise power. As the RSSI measurement comprises signal strength measurements of different cells, it is assumed that multipath fast fading is averaged out in the measurement process.

A Resource Block (RB) spans 12 contiguous sub-carriers and seven OFDM symbols in one slot with a duration of 0.5 ms [Sau10]. In a single RB, each of the two OFDM symbols out of seven contain two reference symbols. The transmit power of cell c on a single RB is denoted by $P_c^{(\text{tx,rb})}$ in dBm and is computed as

$$P_c^{(\text{tx,rb})} = P_c^{(\text{tx})} - 10 \cdot \log_{10}\left(\frac{W\ [\text{MHz}]}{12 \cdot 15 \cdot 10^{-3}\ [\text{MHz}]}\right). \tag{2.16}$$

Excluding the effect of fast fading, the received power on a single RB of a cell c measured by a UE u at time step t_n is expressed in dB scale as

$$P_{u,c}^{(\mathrm{rx,rb})}(t_n) = P_c^{(\mathrm{tx,rb})} - A_c(d, \mathbf{v}_u(t_n), \Phi_c, \Theta_c). \tag{2.17}$$

The linear form of $P_{u,c}^{(\mathrm{rx,rb})}(t_n)$ is given by $P_{u,c}^{(\mathrm{rx,rb})}(t_n)\Big|_{(\mathrm{lin})}$.

The value of RSSI depends on the load of the serving and neighboring cells of the same RAT. The load of a cell c is denoted by $0 \leq \rho_c \leq 1$. In this study, a full buffer traffic model [VDL09] is assumed for users. That is, all RBs are used as soon as there is a single UE, and the load is $\rho_c = 1$. If the cell is empty, i.e., it does not serve any UE, the load is $\rho_c = 0$. Considering a single RB, the contribution of a fully loaded neighboring cell c in RSSI is the total received power $P_{u,c}^{(\mathrm{rx,rb})}\Big|_{(\mathrm{lin})}$. On the other hand, the contribution of an empty cell in RSSI is the received power on two sub-carriers carrying reference symbols and is approximated by 2/12 of $P_{u,c}^{(\mathrm{rx,rb})}\Big|_{(\mathrm{lin})}$.

The RSRQ of an LTE cell c measured by a UE u at time step t_n is modeled in linear scale as

$$RSRQ_{u,c}(t_n)\Big|_{(\mathrm{lin})} = \frac{RSRP_{u,c}(t_n)\Big|_{(\mathrm{lin})}}{RSSI_u(t_n)\Big|_{(\mathrm{lin})}}, \text{ where} \tag{2.18}$$

$$RSSI_u(t_n)\Big|_{(\mathrm{lin})} = \sum_{s \in \mathcal{C} | \ell_s = \ell_c} \left(\rho_s \cdot P_{u,s}^{(\mathrm{rx,rb})}(t_n)\Big|_{(\mathrm{lin})} + (1-\rho_s) \cdot \frac{2}{12} \cdot P_{u,s}^{(\mathrm{rx,rb})}(t_n)\Big|_{(\mathrm{lin})} \right) + P_{\mathrm{N}}^{(\mathrm{rb})}\Big|_{(\mathrm{lin})} \tag{2.19}$$

where $P_{\mathrm{N}}^{(\mathrm{rb})}\Big|_{(\mathrm{lin})}$ is the linear form of the noise power $P_{\mathrm{N}}^{(\mathrm{rb})}$ on a single RB in dBm.

2.4.3.3 Measurements of 3G Cells

The signal strength measurement of a 3G cell is the Received Signal Code Power (RSCP) which is measured over the full 3G system bandwidth W of (2.14). RSCP is expressed in dBm and is analogous to RSRP of an LTE cell. RSCP is defined as the received power on one code measured on the primary Common Pilot Channel (CPICH) [3GP12e]. The transmit power on CPICH channel, expressed by $P_c^{(\mathrm{tx,cpich})}$ in dBm, is equal in linear scale to 10 % of the total transmit power $P_c^{(\mathrm{tx})}$ on the full 3G system bandwidth. The RSCP of a 3G cell c measured by a UE u at time step t_n is modeled in dB scale as

$$RSCP_{u,c}(t_n) = P_c^{(\mathrm{tx,cpich})} - A_c(d, \mathbf{v}_u(t_n), \Phi_c, \Theta_c) + \alpha_{u,c}(t_n). \tag{2.20}$$

The linear form of $RSCP_{u,c}(t_n)$ is given by $RSCP_{u,c}(t_n)\Big|_{(\text{lin})}$.

The signal quality measurement of a 3G cell is called Ec/N_0 and is analogous to RSRQ of an LTE cell. Ec/N_0 is expressed in dB and is defined in linear scale as the ratio between RSCP and RSSI [3GP12e]. Similar to the RSRQ case, it is assumed that multipath fast fading is averaged out in the RSSI measurement. Excluding the effect of fast fading, the total received power of cell c by UE u at time step t_n is expressed in dB scale as

$$P_{u,c}^{(\text{rx})}(t_n) = P_c^{(\text{tx})} - A_c(d, \mathbf{v}_u(t_n), \Phi_c, \Theta_c). \tag{2.21}$$

The linear form of $P_{u,c}^{(\text{rx})}(t_n)$ is denoted by $P_{u,c}^{(\text{rx})}(t_n)\Big|_{(\text{lin})}$.

The contribution of a fully loaded neighboring cell c in RSSI is the total received power $P_{u,c}^{(\text{rx})}\Big|_{(\text{lin})}$. As for an empty cell, the contribution in RSSI is the received power on control channels which is approximated by 20% of the total received power $P_{u,c}^{(\text{rx})}\Big|_{(\text{lin})}$. The Ec/N_0 of a 3G cell c measured by a UE u at time step t_n is modeled in linear scale as

$$[Ec/N_0]_{u,c}(t_n)\Big|_{(\text{lin})} = \frac{RSCP_{u,c}(t_n)\Big|_{(\text{lin})}}{RSSI_u(t_n)\Big|_{(\text{lin})}}, \text{ where} \tag{2.22}$$

$$RSSI_u(t_n)\Big|_{(\text{lin})} = \sum_{s\in\mathcal{C}|\ell_s=\ell_c} \left(\rho_s \cdot P_{u,s}^{(\text{rx})}(t_n)\Big|_{(\text{lin})} + (1-\rho_s)\cdot 0.2 \cdot P_{u,s}^{(\text{rx})}(t_n)\Big|_{(\text{lin})}\right) + P_{\text{N}}\Big|_{(\text{lin})} \tag{2.23}$$

where $P_{\text{N}}\Big|_{(\text{lin})}$ is the linear form of the total noise power P_{N} in dBm.

2.4.4 Layer 1 Filtering

The L1 filtering is a procedure which is applied by the UE to average out fast fading. The procedure of L1 filtering is not specified by 3GPP. Typically, the L1 averaging length of intra-RAT and inter-RAT measurements is 200 ms and 480 ms, respectively [3GP12d].

The L1 filtering procedure of fast fading acts on a subframe basis in LTE and 3G. One subframe in LTE consists of two slots with a duration of 1 ms [HT09] whereas one subframe in 3G consists of three slots with a duration of 2 ms [HT07]. Thus, applying an online L1 filtering to RSRP and RSCP measurements would require a small simulation time step T_{n} of 1 ms. The use of such small time step would hinder the investigation

of inter-RAT MRO which requires long simulation periods to collect statistics about mobility failures. Moreover, L1 of the UE provides L3 with a measurement every 50, 100 or 200 ms depending on the implementation of the UE [SS10]. As a result, the smallest value which should be configured for T_{n} is 50 ms.

In order to consider L1 filtering and keep at the same time $T_{\mathrm{n}} \geq 50$ ms, the values of the power envelope of the multipath fast fading are generated offline and L1 filtering is applied only to the fast fading component of RSRP and RSCP measurements which are described in (2.15) and (2.20), respectively. The other component $A_c(d, \mathbf{v}_u(t_n), \Phi_c, \Theta_c)$ of the measurement which is defined in (2.12) and corresponding to the overall signal attenuation due to path loss, shadowing and antenna beam pattern, is not considered in L1 filtering. The error resulting from filtering only the fast fading component of the measurement is negligible since path loss and shadowing do not really change during L1 filtering period.

The L1 filtered value of the power envelope $\alpha_{u,c}(t_n)$ of the multipath fast fading is denoted by $\widehat{\alpha}_{u,c}(t_n)$ in dB. The samples of the power envelope $\alpha_{u,c}$ of the multipath fast fading are generated offline with a granularity of 1 ms. For intra-RAT measurements, the samples of $\widehat{\alpha}_{u,c}$ are computed by considering every 50th sample of $\alpha_{u,c}$ and averaging in the linear scale over the last four values. Thus, four samples in 200 ms are averaged for intra-RAT measurement. As for inter-RAT measurement, the first five consecutive samples of $\alpha_{u,c}$ of each 50 ms block are first averaged resulting in a new sample $\bar{\alpha}_{u,c}$. The samples of $\widehat{\alpha}_{u,c}$ are then computed by averaging over the last nine samples of $\bar{\alpha}_{u,c}$. Hence, nine samples in 450 ms are averaged in case of inter-RAT measurement. The L1 averaging length used for inter-RAT measurement differs slightly from 480 ms which is stated in [3GP12d]. For both intra- and inter-RAT measurements, a sample of $\widehat{\alpha}_{u,c}$ is generated every 50 ms.

The L1 filtered measurement of $RSRP_{u,c}(t_n)$ is expressed in dB scale as

$$\widehat{RSRP}_{u,c}(t_n) = P_c^{(\mathrm{tx,re})} - A_c(d, \mathbf{v}_u(t_n), \Phi_c, \Theta_c) + \widehat{\alpha}_{u,c}(t_n). \tag{2.24}$$

The L1 filtered measurement of RSRQ can be directly calculated in linear scale by taking the ratio between L1 filtered measurement of RSRP and RSSI defined in (2.19).

Similarly, the L1 filtered measurement of $RSCP_{u,c}(t_n)$ is expressed in dB scale as

$$\widehat{RSCP}_{u,c}(t_n) = P_c^{(\mathrm{tx,cpich})} - A_c(d, \mathbf{v}_u(t_n), \Phi_c, \Theta_c) + \widehat{\alpha}_{u,c}(t_n). \tag{2.25}$$

As for the L1 filtered measurement of Ec/N_0, it is calculated in linear scale by taking the ratio between L1 filtered measurement of RSCP and RSSI defined in (2.23). The

L1 measured quantity of cell c performed by UE u is denoted by $\widehat{MQ}_{u,c}(t_n)$ in dB scale at time step t_n irrespective of the measurement quantity, e.g., signal strength or signal quality measurement.

2.4.5 Measurement Error Model

The L1 filtered measurement is not perfectly accurate and comprises a measurement error. According to [HT04b], this measurement error is log-normally distributed with zero mean and σ_{me} standard deviation with σ_{me} given in dB. The measurement error is added to $\widehat{MQ}_{u,c}(t_n)$ prior to the application of L3 filtering. The value of σ_{me} depends on the measurement bandwidth [ADCO+07]. The larger the measurement bandwidth, the smaller the measurement error is. For instance, σ_{me} corresponding to measurement bandwidth of 2.5 MHz, 5 MHz and 10 MHz is 0.6, 0.45 and 0.35, respectively [ADCO+07]. The L1 filtered measurement, impacted by the measurement error, can be expressed in dB scale as

$$\widetilde{MQ}_{u,c}(t_n) = \widehat{MQ}_{u,c}(t_n) + \alpha_{u,c}^{(\text{me})}(t_n) \tag{2.26}$$

where $\alpha_{u,c}^{(\text{me})}(t_n)$ is the measurement error pertaining to $\widehat{MQ}_{u,c}(t_n)$ at time step t_n.

2.4.6 Layer 3 Filtering

The L3 filtering is used in order to smooth the measurements received from L1. 3GPP has defined a recursive averaging method based on a filter factor a_{L3} [3GP12b,3GP12g]. L3 filtering is applied to L1 measurement prior to any measurement reporting. In this way, the effect of measurement errors and residual signal fluctuations are suppressed and, in turn, unreliable handover decisions are minimized. The value of the filter factor depends on a filter coefficient k_{L3} which is signaled by the serving BS to the UE. The L3 filtered measurement $MQ_{u,c}(t_n)$ is computed as follows:

$$MQ_{u,c}(t_n) = (1 - a_{\text{L3}}) \cdot MQ_{u,c}(t_{n-1}) + a_{\text{L3}} \cdot \widetilde{MQ}_{u,c}(t_n) \tag{2.27}$$

where $a_{\text{L3}} = 0.5^{k_{\text{L3}}/2}$ and $a_{\text{L3}} = 0.5^{k_{\text{L3}}/4}$ are used for 3G and LTE measurements, respectively. The L3 filtering in (2.27) assumes that L1 filtered measurements are generated every 200 ms. However, as mentioned in Section 2.4.4, L1 can generate measurements at a faster rate depending on the implementation of the UE, e.g., 50 or 100 ms. If L1 is assumed to generate measurements every $T_{\text{n}} < 200$ ms, then a new filter factor a'_{L3} shall be used in order to ensure that the impulse response of the

filter remains consistent [SS10]. The value of the new filter factor satisfies the following equality:

$$(1 - a_{\mathrm{L3}}) = (1 - a'_{\mathrm{L3}})^{\frac{200\ [\mathrm{ms}]}{T_{\mathrm{n}}}}. \tag{2.28}$$

2.5 Model of the Average SINR in Downlink

The average SINR of a UE served by an LTE cell is approximated using the model defined in [VDL09]. The downlink SINR of a UE u served by an LTE cell c at time step t_n is given in linear scale by

$$\gamma_{u,c}(t_n)\Big|_{(\mathrm{lin})} = \frac{P^{(\mathrm{rx,rb})}_{u,c}(t_n)\Big|_{(\mathrm{lin})}}{\sum\limits_{s\in\mathcal{C}|\ell_s=\ell_c,s\neq c}\left(\rho_s \cdot P^{(\mathrm{rx,rb})}_{u,s}(t_n)\Big|_{(\mathrm{lin})}\right) + P^{(\mathrm{rb})}_{\mathrm{N}}\Big|_{(\mathrm{lin})}}, \tag{2.29}$$

where the numerator defined in (2.17) represents the received signal power of the serving cell c on a single RB and the sum in the denominator refers to the total interference power from all cells of the same network of cell c. In dB scale, the SINR is expressed by $\gamma_{u,c}(t_n)$.

Similarly, the average SINR of a UE served by the 3G cell is given in linear scale by

$$\gamma_{u,c}(t_n)\Big|_{(\mathrm{lin})} = \frac{P^{(\mathrm{rx})}_{u,c}(t_n)\Big|_{(\mathrm{lin})}}{\sum\limits_{s\in\mathcal{C}|\ell_s=\ell_c,s\neq c}\left(\rho_s \cdot P^{(\mathrm{rx})}_{u,s}(t_n)\Big|_{(\mathrm{lin})} + (1-\rho_s)\cdot 0.2 \cdot P^{(\mathrm{rx})}_{u,s}(t_n)\Big|_{(\mathrm{lin})}\right) + P_{\mathrm{N}}\Big|_{(\mathrm{lin})}}, \tag{2.30}$$

where the numerator defined in (2.21) represents the total desired received power and the denominator refers to the total interference power which is equal to RSSI of (2.23) excluding the signal power of the serving cell.

2.6 Modeling of Handover Procedure

In this section, the procedure of handing over a UE to a neighboring intra- or inter-RAT cell is explained.

In LTE and 3G networks, the handover of a UE u is triggered by the serving BS, typically when a measurement report is received from this UE. The reporting of the

UE measurements to the serving BS can be either periodic or event triggered. In the latter case, the measurement report is sent when a certain condition, called the entering condition of the measurement event, is fulfilled for a certain time interval. The parameters of the entering condition are configured by the serving BS and are called handover parameters although they do not necessarily lead to a handover. The evaluation of the entering condition requires the UE to perform signal measurements for the serving cell and intra- or inter-RAT neighboring cells.

The entering condition of the measurement event used for intra-RAT handover expires at time step t_0 when the measurement of an intra-RAT neighboring cell $c_0 \in \mathcal{C}$ exceeds the measurement of serving cell c by an offset φ for a certain time interval denoted by $T_{\mathrm{T}}^{(\mathrm{intra})}$ [3GP12b, 3GP12g], i.e.,

$$MQ_{u,c_0}(t_n) > MQ_{u,c}(t_n) + \varphi \text{ for } t_0 - \left\lceil T_{\mathrm{T}}^{(\mathrm{intra})}/T_{\mathrm{n}} \right\rceil < t_n < t_0 \tag{2.31}$$

where $\lceil . \rceil$ is the ceiling operator. In (2.31), the time interval $T_{\mathrm{T}}^{(\mathrm{intra})}$, called also TTT, is converted from absolute number in ms to a number of simulation time steps. For instance, $T_{\mathrm{T}}^{(\mathrm{intra})} = 128$ ms corresponds to a duration of three time steps if $T_{\mathrm{n}} = 50$ ms. Both handover parameters, φ and $T_{\mathrm{T}}^{(\mathrm{intra})}$, should guarantee the reliability of the measurement event and the following handover decision.

For inter-RAT handover, a dual threshold measurement event is configured by the serving BS [3GP12b, 3GP12g]. The measurement event which is used to hand over UEs from 3G to LTE and vice-versa is called measurement event 3A and B2, respectively. The entering condition of this measurement event expires at time step t_0 when the measurement of the serving cell c falls below a threshold $Q_c^{(1)}$ and the measurement of an inter-RAT neighboring cell exceeds another threshold $Q_c^{(2)}$ for a certain time interval TTT denoted by $Q_c^{(3)}$, i.e.,

$$MQ_{u,c}(t_n) < Q_c^{(1)} \ \wedge \ MQ_{u,i_k}(t_n) > Q_c^{(2)} \text{ for } t_0 - \left\lceil Q_c^{(3)}/T_{\mathrm{n}} \right\rceil < t_n < t_0. \tag{2.32}$$

The three inter-RAT handover parameters in (2.32) are the threshold $Q_c^{(1)}$ corresponding to the serving cell, the threshold $Q_c^{(2)}$ corresponding to neighboring cell and the TTT parameter $Q_c^{(3)}$. The index for the three handover parameters is denoted by $m = 1, \ldots, M, M+1$, where M is the total number of handover thresholds, i.e., $M = 2$ in inter-RAT case. That is, the index $m = 1, 2$ and 3 are used for serving cell threshold, target cell threshold and TTT, respectively. The cell-specific value of the m^{th} inter-RAT handover parameter is denoted by $Q_c^{(m)}$.

After the entering condition of the measurement event is fulfilled for TTT time interval, the following steps [VWL+11] are executed to hand over the UE to an intra- or inter-RAT cell:

1. The UE sends a measurement report to the serving BS. The measurement report can contain the measurements of many neighboring cells. The transmission of the measurement report has some probability to fail, especially if the UE is already far from the serving BS.

2. Upon receiving the measurement report, the BS sends a handover request to the neighboring cell corresponding to the strongest measurement and waits for either an acknowledgment or a rejection. This induces an additional delay which is typically called handover preparation time, and is denoted by $T_{\mathrm{hp}}^{(\mathrm{intra})}$ and $T_{\mathrm{hp}}^{(\mathrm{inter})}$ for intra- and inter-RAT handover, respectively.

3. The BS informs the UE to connect to the prepared target neighboring cell by sending a handover command. The transmission of the handover command can fail, in particular if the UE was moving during preparation and is already in the coverage area of another cell. This failure is modeled by checking, after the handover preparation time, the SINR of the UE with respect to the serving cell if it is below a certain threshold Q_{HC} in dB.

4. Once the handover command is successfully received, the UE will try to access the target cell of handover using the Random Access Channel (RACH) [3GP12f]. This random access can fail as well and is modeled by checking, after the handover preparation time, the SINR of the UE with respect to the target cell if it is below a certain threshold Q_{RACH} in dB [MZMT12].

5. The UE is finally handed over upon a successful access of the target cell.

Thus, the handover of the UE is executed after the handover preparation time if the SINRs of the UE with respect to the serving and target cells are high enough. Otherwise, the handover fails and the UE stays in the previously serving cell where it might experience later an RLF. In particular, if the handover failure is due to a weak SINR with respect to the target cell, an RLF is directly detected and the UE selects a new cell.

The cell c serving a UE u at time step t_n is given by the connection function $x_u(t_n) = c$. An intra-RAT handover of UE u is executed from cell c to a neighboring cell c_0 of the same network at time step t_{HO} if the following conditions hold:

$$x_u(t_n) = c_0 \quad \text{for} \quad t_n > t_{\mathrm{HO}}$$

$$\text{if } MQ_{u,c_0}(t_n) > MQ_{u,c}(t_n) + \varphi$$

$$\text{for } t_{\mathrm{HO}} - \left\lceil T_{\mathrm{hp}}^{(\mathrm{intra})}/T_{\mathrm{n}} \right\rceil - \left\lceil T_{\mathrm{T}}^{(\mathrm{intra})}/T_{\mathrm{n}} \right\rceil < t_n < t_{\mathrm{HO}} - \left\lceil T_{\mathrm{hp}}^{(\mathrm{intra})}/T_{\mathrm{n}} \right\rceil,$$

$$\gamma_{u,c}(t_{\mathrm{HO}}) > Q_{\mathrm{HC}} \text{ and } \gamma_{u,c_0}(t_{\mathrm{HO}}) > Q_{\mathrm{RACH}}. \tag{2.33}$$

Similarly, the UE is handed over to a neighboring cell i_k of a different network if the following conditions hold:

$$\begin{gathered} x_u(t_n) = i_k \quad \text{for} \quad t_n > t_{\mathrm{HO}} \\ \text{if } MQ_{u,c}(t_n) < Q_c^{(1)} \ \wedge \ MQ_{u,i_k}(t_n) > Q_c^{(2)} \\ \text{for } t_{\mathrm{HO}} - \left\lceil T_{\mathrm{hp}}^{(\mathrm{inter})}/T_{\mathrm{n}} \right\rceil - \lceil Q_c^{(3)}/T_{\mathrm{n}} \rceil < t_n < t_{\mathrm{HO}} - \left\lceil T_{\mathrm{hp}}^{(\mathrm{inter})}/T_{\mathrm{n}} \right\rceil, \\ \gamma_{u,c}(t_{\mathrm{HO}}) > Q_{\mathrm{HC}} \text{ and } \gamma_{u,i_k}(t_{\mathrm{HO}}) > Q_{\mathrm{RACH}}. \end{gathered} \tag{2.34}$$

2.7 Modeling of Radio Link Failure Detection

In this section, the detection model of RLF is presented for LTE and 3G UEs.

The connection of the UE, whose intra-RAT handover procedure fails, might be lost due to the high interference power of other neighboring cells. Similarly, the connection of a UE approaching a coverage hole in the serving RAT might be lost if it is not handed over in time from one network to another. In both cases, the UE is getting out of sync for the time when the communication is no longer possible and considers the connection to be failed. This is typically called RLF which might yield either a service interruption or a call drop.

In this model, an RLF is detected at time step t_{RLF} if the SINR of UE u with respect to the serving cell c falls below a certain threshold Q_{RLF} in dB for a certain time interval T_{RLF} [VWL+11], i.e.,

$$\gamma_{u,c}(t_n) < Q_{\mathrm{RLF}} \text{ for } t_{\mathrm{RLF}} - \lceil T_{\mathrm{RLF}}/T_{\mathrm{n}} \rceil < t_n < t_{\mathrm{RLF}}. \tag{2.35}$$

After the RLF is detected, the UE will connect to a new cell with sufficient signal level. If the cause of the RLF is a coverage problem, it may take time for the UE to find a new cell. In contrast, if the cause of the RLF was a wrong handover decision or a missed handover opportunity, it is very likely that the UE connects immediately to a new cell.

2.8 Deployment Scenarios

2.8.1 Introduction

The roll out of a new LTE network requires either the acquisition of new sites for installing BSs or reusing the existing sites of 3G network. In the former case, the deployment cost is high because, in addition to the acquisition cost, installing LTE BSs needs additional infrastructure such as power supply and cooling systems [NSN12]. Moreover, it is typically difficult to acquire new sites due to restrictions on RF radiation exposure and regulations from authorities [HT04a]. Alternatively, co-siting 3G and LTE networks is an efficient way to reduce the deployment cost. Co-siting allows the mobile operators to share existing premises and infrastructure enabling a fast and cost-efficient deployment of LTE network. For this reason, co-sited LTE and 3G network model is adopted in this thesis.

2.8.2 Partially Overlaying LTE and 3G Co-Sited Networks with Limited LTE Coverage

The LTE network will be rolled out gradually on top of the legacy 3G network starting in areas where high data traffic is expected. Thus, the LTE deployment will be limited at the beginning to urban areas whereas 3G network provides full coverage for urban and suburban areas. A typical irregular network layout for partially overlaying inter-RAT deployment is shown in Fig. 2.3(a). The complete 9×9 km^2 area (urban and suburban areas) is served by a 3G network, shown in red, while LTE covers only the urban area, shown in blue. The total number N_{bs} of tri-sectored BSs is 24, among which 9 LTE and 3G BSs are co-sited. The cell index c is shown in Fig. 2.3(b): Numbers 1 to 27 are used for LTE cells (blue) and 28 to 72 for 3G cells (red).

Some of the UEs move randomly in the serving area whereas others move at specified trajectories defined by the street grid which is shown in black in Fig. 2.3(a). The velocity of the UEs moving randomly and on the streets is denoted by v_{mr} and v_{st}, respectively. The UEs are uniformly distributed on the streets and randomly select a direction at every intersection.

This scenario comprising partially overlaying LTE and 3G co-sited networks is used only to highlight some practical aspects which are considered by the 3GPP standard.

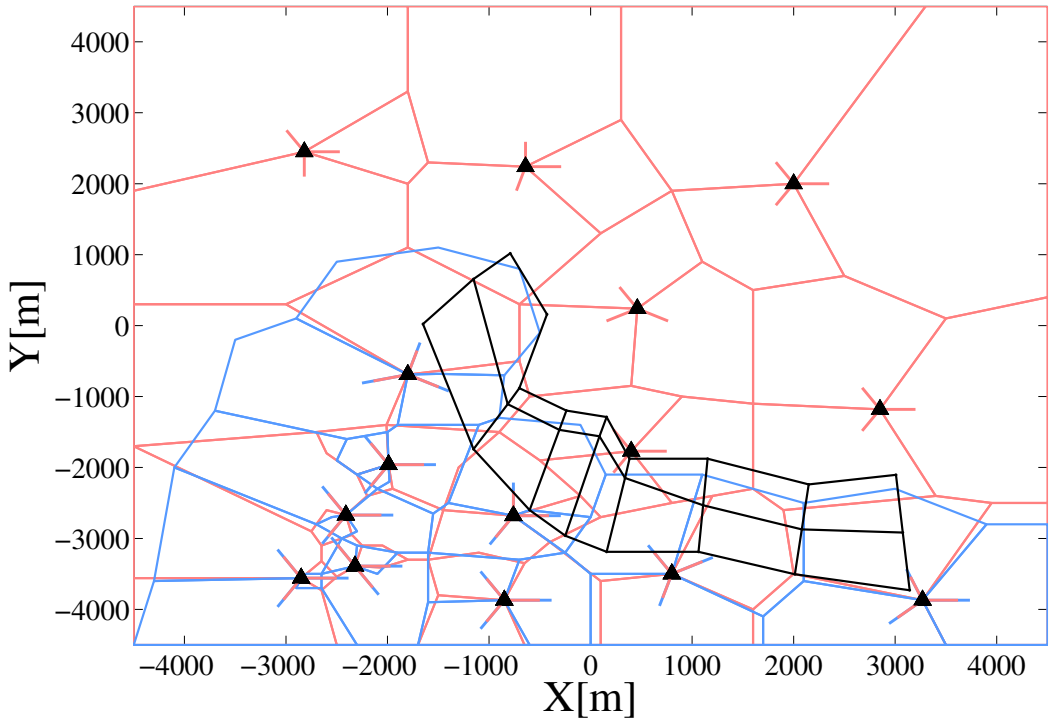

(a) The LTE network (blue) partially overlays the 3G network (red). The street grid is shown in black.

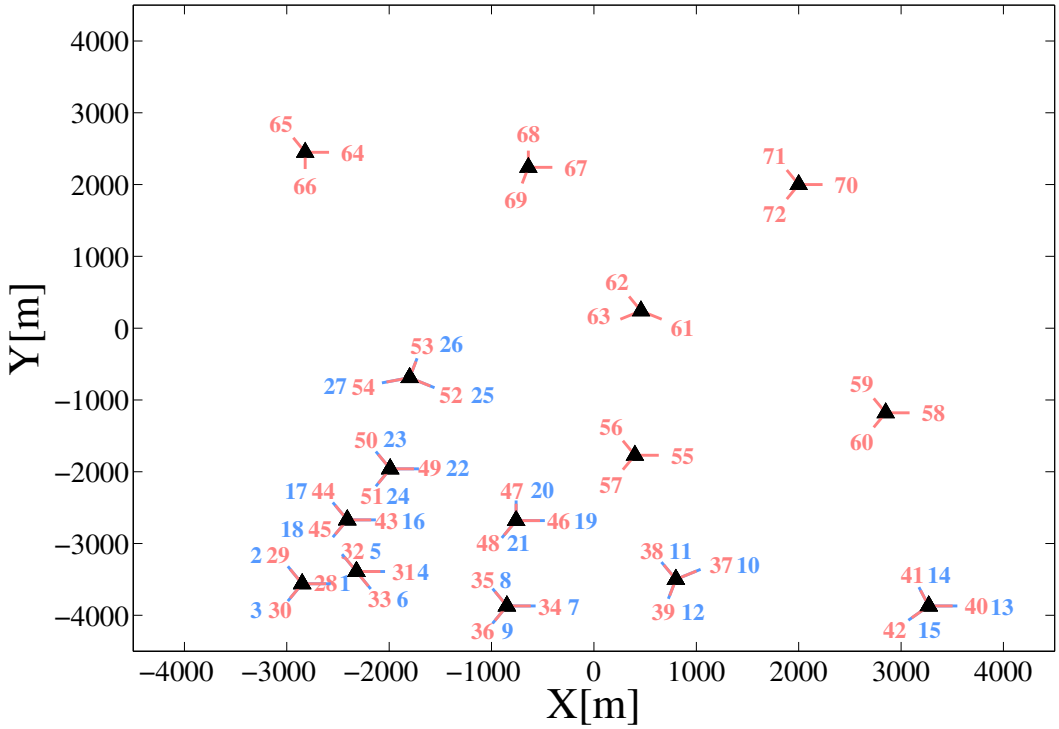

(b) Numbers 1 to 27 are used for LTE cells (blue) and 28 to 72 for 3G cells (red).

Figure 2.3. Partially overlaying LTE (blue) and 3G (red) co-sited networks with limited LTE coverage.

3GPP considers this scenario to be the most prevalent in the first stage of LTE deployment. The assumptions which were adopted for this scenario with respect to the conditions triggering the inter-RAT handovers from the LTE to the 3G network and vice-versa are explained in the following. It is presumed that the handovers from LTE to 3G are triggered only where there is no LTE coverage. On the other hand, the handovers from 3G to LTE are triggered only by the operator's traffic steering policy to achieve an optimal distribution of the traffic across multiple RATs and better spectrum efficiency [NN12]. In other words, radio-driven inter-RAT handovers from 3G to LTE are not triggered. The shadowing values of two fully co-sited LTE and 3G BSs are assumed to be fully correlated, i.e., $\zeta_{\mathrm{nw}} = 1$. In this case, a coverage hole area in 3G corresponds also to a coverage hole in LTE assuming that the two networks operate at two different frequency bands which are not far from each other. In this study, the carrier frequencies of 3G and LTE networks are 2.1 GHz and 2.6 GHz, respectively. As the 3G network operates at a lower carrier frequency, the link budget of a 3G cell is slightly better than that of a co-sited LTE cell assuming that both have the same shadowing component, i.e., $\zeta_{\mathrm{nw}} = 1$.

For traffic steering based handovers, the measurement event 3C is typically configured to hand over a UE in 3G to a RAT of higher priority which is LTE in this case [3GP12g]. The entering condition of this measurement event expires at time step t_0 when the measured quantity of the LTE neighbor i_k of a 3G cell c exceeds a certain threshold Q_{ts} for $T_{\mathrm{T}}^{(\mathrm{ts})}$ time interval, i.e.,

$$MQ_{u,i_k}(t_n) > Q_{\mathrm{ts}} \text{ for } t_0 - \left\lceil T_{\mathrm{T}}^{(\mathrm{ts})}/T_{\mathrm{n}} \right\rceil < t_n < t_0. \tag{2.36}$$

A traffic steering policy is necessary to bring the UEs back from 3G to LTE. Without traffic steering, all UEs would end up connected with the 3G network. This is clearly seen in Fig. 2.4(a) which shows the number of UEs in each network as a function of time without any traffic steering from 3G to LTE. The reason for the decay in the number of UEs in LTE is that after each RLF, the UE would select a 3G cell rather than an LTE cell due to the difference in the link budget. As a result, no inter-RAT handovers would be triggered and the investigation of inter-RAT MRO would not be possible. Thus, traffic steering is necessary to obtain more or less an even distribution of UEs in each network. This can be seen in Fig. 2.4(b) which shows the number of UEs in each network as a function of time with traffic steering from 3G to LTE. According to the figure, the number of UEs in each network remains more or less the same as a function of time which is necessary for the inter-RAT MRO investigation.

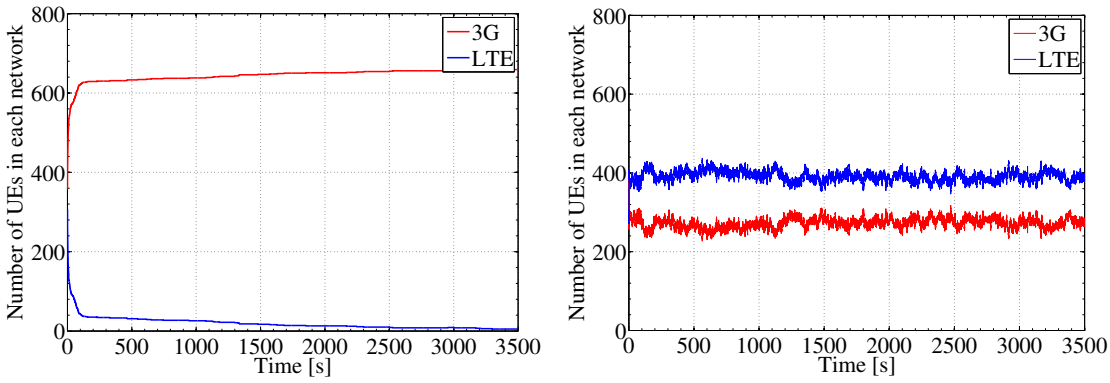

(a) Without traffic steering from 3G to LTE. (b) With traffic steering from 3G to LTE.

Figure 2.4. The number of UEs in each network as a function of time in s.

2.8.3 Fully Overlaying LTE and 3G Co-Sited Networks

In later stages of LTE deployment, it is expected that the 3G and LTE networks will be fully overlaying. The 3GPP Case 3 network layout with Inter-Site Distance (ISD) of 1732 [3GP10] is considered as shown in Fig. 2.5 for fully overlaying inter-RAT deployment. A large ISD has been chosen since it is difficult to obtain coverage holes with small ISD of 500 corresponding to 3GPP Case 1 scenario. The total number N_{bs}

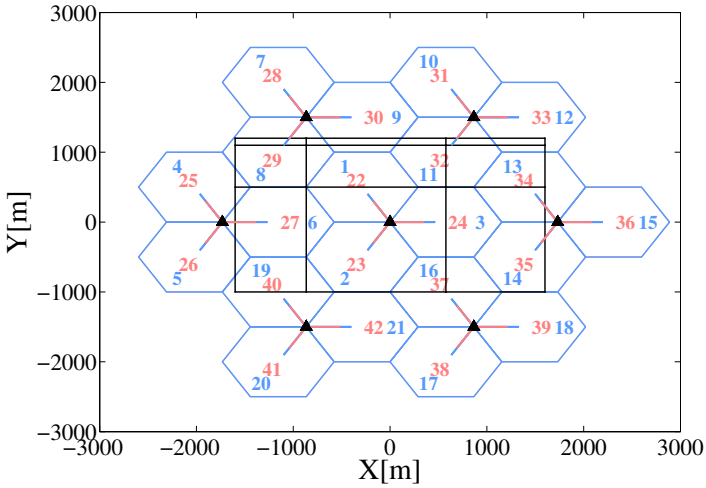

Figure 2.5. Fully overlaying LTE (blue) and 3G (red) co-sited networks. The street grid is shown in black.

of BSs is 14 among which 7 LTE and 3G BSs are co-sited. Each BS serves tri-sectored homogeneous and hexagonal cells. The cell indices 1 to 21 (blue) are used for LTE cells and 22 to 42 for 3G cells (red).

Similar to the partially overlaying LTE and 3G scenario, some of the UEs move randomly and others move on a street grid which is shown in black in Fig. 2.5. The streets are placed in a specific way that covers most of the areas which are interesting for inter-RAT MRO study. Two streets pass through the same boundary of cells 8, 9, 11 and 12. Another street passes through an area which is directly below the antenna of cell 6. Two perpendicular streets pass through a three cell area which is common for cells 1, 6 and 8. Two parallel and perpendicular streets pass through the same boundaries of cells 3 and 11. A single street is perpendicular to the boundary of cell 16. Another single street passes along the boundary of cell 2. Finally, a single street passes through a three cell area which is common for cells 2, 6 and 19.

This scenario comprising two fully overlaying LTE and 3G co-sited networks is used to study radio-driven inter-RAT handovers from both directions, i.e., to exclude the traffic steering policy from 3G to LTE which was adopted for partially overlaying network scenario, described in Section 2.8.2. A radio-driven inter-RAT handover from the 3G to the LTE network can be only triggered if coverage holes exist in the 3G network and at the same time there is a good coverage from LTE. This case can only happen if the shadowing values of two fully co-sited LTE and 3G BSs are uncorrelated, i.e., $\zeta_{\text{nw}} = 0$ which is rather an aggressive assumption. However, setting $\zeta_{\text{nw}} = 0$ provides a proper scenario where the stationarity of UEs in each network is generated without the use of any traffic steering policy. This is clearly seen in Fig. 2.6 which shows the number of UEs in each network for $\zeta_{\text{nw}} = 1$ in Fig. 2.6(a) and $\zeta_{\text{nw}} = 0$ in Fig. 2.6(b).

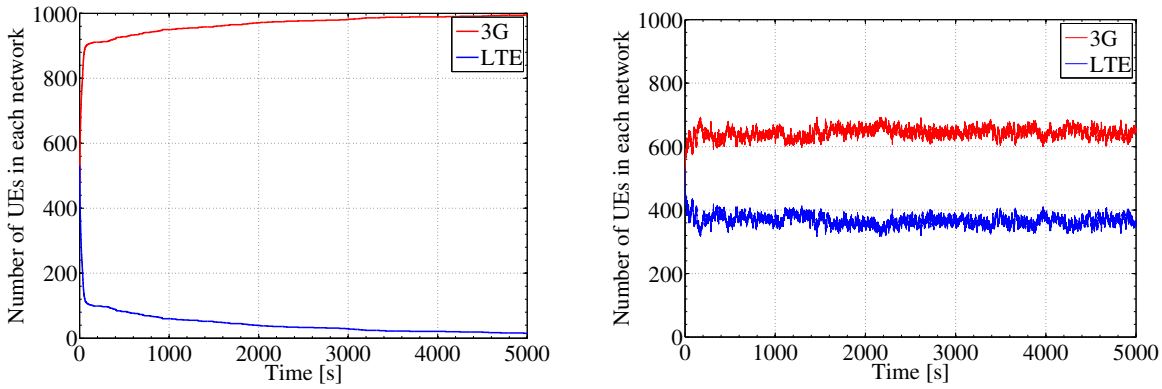

(a) Correlated shadowing values of co-sited LTE and 3G BSs, ζ_{nw}=1.

(b) Uncorrelated shadowing values of co-sited LTE and 3G BSs, ζ_{nw}=0.

Figure 2.6. The number of UEs in each network as a function of time in s.

According to Fig. 2.6(a), the number of UEs in LTE decays as time passes. This is because the UEs are kept in the 3G network and are not handed over to LTE since any 3G coverage hole corresponds also to an LTE coverage hole assuming that LTE

and 3G operate at carrier frequencies of 2.6 GHz and 2.1 GHz, respectively. On the other hand, if ζ_{nw} is set to 0, the number of UEs remains more or less the same in each network which is necessary for inter-RAT MRO investigation. In addition, the assumption $\zeta_{\text{nw}} = 0$ makes the scenario more challenging for studying inter-RAT MRO since in this case, radio driven inter-RAT handovers are triggered from both directions, LTE to 3G network and vice versa.

Chapter 3

Inter-RAT Handover Parameters and Mobility Failure Types

3.1 Introduction

The inter-RAT handover decisions rely basically on the measurement reports which are sent by UEs to the serving BS. These reports are triggered by the handover parameters and reporting criteria which are configured by the BS [HSS12]. The most relevant inter-RAT handover parameters are the two handover thresholds $Q_c^{(1)}$ and $Q_c^{(2)}$ corresponding to the measurements of the serving and target cells, respectively. Other parameters such as the time interval $Q_c^{(3)}$ which refers to TTT and the filter coefficient k_{L3} used for L3 filtering of the measurements have also an impact on the robustness of handovers. The two handover thresholds are currently configured cell-specifically, i.e., can be set differently in each cell.

The setting of the handover parameters in a cell is mainly affected by three factors. The first factor is the radio propagation condition which varies in each cell. As long as a cell does not have any coverage holes, there is no need for inter-RAT handovers and in turn no need to optimize its corresponding handover parameters. On the contrary, other cells have coverage holes and their corresponding handover parameters may need to be properly configured to avoid any inter-RAT mobility problems. The second factor is the user path in the cell. The coverage holes in a cell are not critical unless the users are passing through them. In this case, the users need to be handed over to another RAT early enough before they approach these coverage holes. The third and last factor is the user velocity. Fast moving UEs are typically more vulnerable to mobility problems due to the rapid changes in their signal measurements.

The mobility failure types which are defined for inter-RAT scenarios can be divided into two categories: The first consists of inter-RAT RLFs and the second includes the undesired costly inter-RAT handovers which should be avoided [3GP12c]. The author has proposed to differentiate between two types of TLHs in inter-RAT scenarios: 1) A TLH due to the misconfiguration of serving cell threshold and 2) A TLH due to the misconfiguration of target cell threshold. This proposal has been accepted and specified by the 3GPP Rel. 11 standard [3GP12c]. In this study, all inter-RAT mobility failure types are considered though 3GPP standard has focused only on a subset of

them [3GP12f] which are relevant for a partially overlaying LTE deployment as defined in Section 2.8.2.

As in many other optimization problems, inter-RAT MRO underlies trade-offs. Since the considered handover thresholds are currently cell-specifics, it might be challenging in some cells to reduce all mobility problems. It can happen that a reduction in one type of mobility failure is possible only at the expense of an increase in the values of other types. Typically, resolving most critical failure types is prioritized over others. These trade-offs in inter-RAT MRO are discussed in detail in this chapter along with the inter-RAT handover parameters and mobility failure types.

This chapter is organized as follows. The inter-RAT handover parameters are discussed in Section 3.2. The factors affecting the setting of the handover parameters are elaborated in Section 3.3. The different types of mobility failures which are defined for inter-RAT scenarios are explained in Section 3.4. Finally, the trade-offs in inter-RAT MRO problem are highlighted in Section 3.5.

3.2 Inter-RAT Handover Parameters

3.2.1 Handover Thresholds

The two thresholds $Q_c^{(1)}$ and $Q_c^{(2)}$, corresponding to the measurements of the serving and target cells, respectively, are typically considered to be the main parameters for controlling inter-RAT handovers. For clarity, the execution of the inter-RAT handover of a UE u from cell c to neighboring cell i_k at time step t_{HO} is depicted in Fig. 3.1. The measurement quantities of the serving and target cells are given by $MQ_{u,c}(t_n)$ and $MQ_{u,i_k}(t_n)$, respectively. The handover is executed $T_{\mathrm{hp}}^{(\mathrm{inter})}$ of (2.34) after the entering condition of the measurement event is fulfilled for $Q_c^{(3)}$ time interval of (2.34), i.e., the connection function $x_u(t_n)$ of (2.33) is changed from c to i_k at time instant t_{HO}. The entering condition of the measurement event is fulfilled if $MQ_{u,c}(t_n)$ is below $Q_c^{(1)}$ and $MQ_{u,i_k}(t_n)$ is higher than $Q_c^{(2)}$.

Assuming that $Q_c^{(3)}$ and the filter coefficient k_{L3} of (2.27) are kept fixed, the parameters which can only delay or advance the handover execution are the two handover thresholds. For instance, increasing $Q_c^{(1)}$ would advance the handover execution since the entering condition of the measurement event would be fulfilled earlier. In contrast, decreasing $Q_c^{(1)}$ would delay the handover execution since the entering condition of the

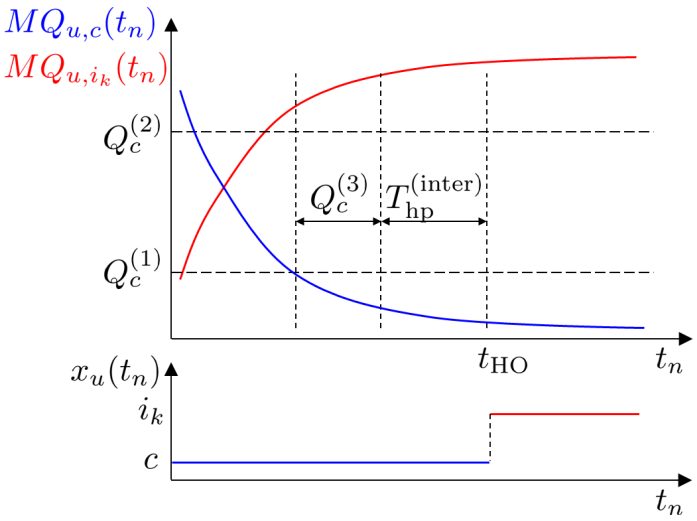

Figure 3.1. The execution of the inter-RAT handover of a UE u from cell c to neighboring cell i_k at time step t_{HO}.

measurement event would be fulfilled later. As for the second threshold, decreasing $Q_c^{(2)}$ in this example would not have any impact on the handover execution. This is because the entering condition of the measurement event would not be fulfilled earlier as long as the measurement of the serving cell falls later below $Q_c^{(1)}$. However, increasing $Q_c^{(2)}$ would delay the handover execution.

The two handover thresholds are currently configured in a cell-specific way [3GP12b, 3GP12g], i.e., each cell can configure different values for the two handover thresholds. The optimization ranges of the two handover thresholds $Q_c^{(1)}$ and $Q_c^{(2)}$ can be chosen to be the same or subsets of the ranges pertaining to the corresponding measurement quantities. The range of $MQ_{u,c}(t_n)$ values depends on whether signal strength or signal quality measurements are configured by the serving BS. For signal strength measurements, the range of $MQ_{u,c}(t_n)$ values is [-140,-44] dBm with 1 dB resolution for an LTE cell [3GP12d] and [-120,-25] dBm for a 3G cell [3GP12a]. The two ranges are on a different scales because the signal strength measurement of an LTE cell is performed over 15 kHz, bandwidth occupied by a resource element, whereas the measurement of a 3G cell is performed over the full 5 MHz bandwidth, see Section 2.4.3. For signal quality measurements, the range of $MQ_{u,c}(t_n)$ values is [-19.5,-3] dB with 0.5 dB resolution for an LTE cell [3GP12d] and [-24,0] dB for a 3G cell [3GP12a]. Accordingly, the optimization ranges of the handover thresholds can be much larger if signal strength measurements are configured.

The signal quality measurements consider the interference power of neighboring cells of the same network and, in turn, they seem to be more relevant than signal strength

measurements. However, the definition of signal quality measurement depends on the load of the measured cell, see Section 2.4.3.2 and Section 2.4.3.3, which is not desired for inter-RAT MRO. This is because for the same SINR and received signal strength, the RSRQ measurement of the UE may differ by up to 8 dB depending on the load of the serving cell [HSS12].

The load-dependency of RSRQ can cause mobility problems for UEs, especially in low loaded cells. For clarity, consider two empty cells A and B of different RATs and a single UE which is connected to cell A. If the UE starts a video download and is assigned all the radio resources, the load in cell A would increase from 0% to 100% and the RSRQ measurement of the UE with respect to cell A may drop by up to 8 dB [HSS12]. This drop in RSRQ can trigger the handover of the UE to the neighboring empty cell B. If the handover is triggered, the load in cell B would in turn increase from 0% to 100% and the RSRQ measurement of the UE with respect to cell B may also drop by up to 8 dB. As before, the UE might be again handed over back to cell A. Thus, there is a risk that the UE is handed over back and forth between the two low loaded cells A and B. Even in a fully loaded network, it has been shown in [AWVK12b] that signal quality measurements could not provide any benefit over signal strength measurements in inter-RAT MRO. Moreover, the dependency of signal quality measurements on the load of the serving cell makes the configuration of the handover thresholds more complicated in general since it might be difficult to follow the rapid changes of the load in the cell in real networks. For the aforementioned reasons, the UEs in this thesis are configured to perform signal strength measurements for inter-RAT handovers. Yet, all the concepts and optimization algorithms of this thesis are also applicable to signal quality measurements.

3.2.2 Time-to-Trigger

The measurement report of the UE is not directly sent after the entering condition of the measurement event is fulfilled. Instead, the entering condition should be fulfilled for a certain time interval indicated by the $Q_c^{(3)}$ parameter. This is necessary to avoid inter-RAT handovers which are triggered based on measurement outliers [HSS12]. Similar to the two handover thresholds, increasing $Q_c^{(3)}$ would delay the execution of the inter-RAT handover whereas decreasing $Q_c^{(3)}$ would advance the handover, see Fig. 3.1.

The value of TTT is specified by the measurement reporting configuration which contains the parameters triggering the measurement report of the UEs [3GP12g]. Moreover, each UE can still apply a scaling factor for the configured TTT value depending

on its speed [3GP12g]. Typically, fast moving UEs use a shorter TTT values than those used by slow moving UEs. The range of $Q_c^{(3)}$ values is specified in [3GP12g] with a variable resolution. The possible values of $Q_c^{(3)}$ are 0, 40, 64, 80, 100, 128, 160, 256, 320, 480, 512, 640, 1024, 1280, 2560 and 5120 in ms.

3.2.3 Filter Coefficient

The L3 filtering is applied primarily to smooth the signal measurements by averaging out fast fading and measurement errors. This is can be clearly seen in Fig. 3.2(a) which shows the signal strength measurement of an LTE cell at two filtering stages: L1 and L3 filtering measurements with different filtering coefficient k_{L3}. The L1 filtering measurement (gray dashed) fluctuates a lot which leads to many unstable inter-RAT handovers. The other curves show the L3 filtering measurements which are used to check the entering condition of the measurement event. High filter coefficient values reduce more the fluctuations, but at the expense of an additional delay in following the variations of the channel.

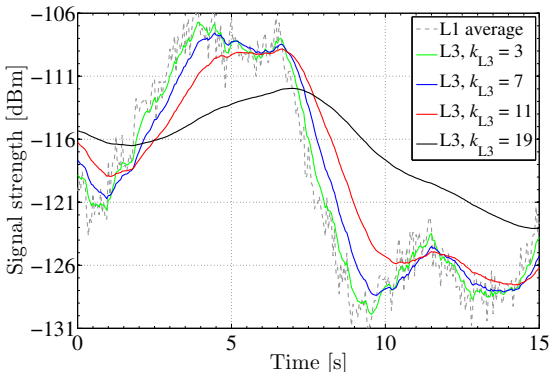

(a) Signal strength measurement of an LTE cell at two filtering stages: L1 and L3 filtered measurements with different filter coefficients k_{L3}.

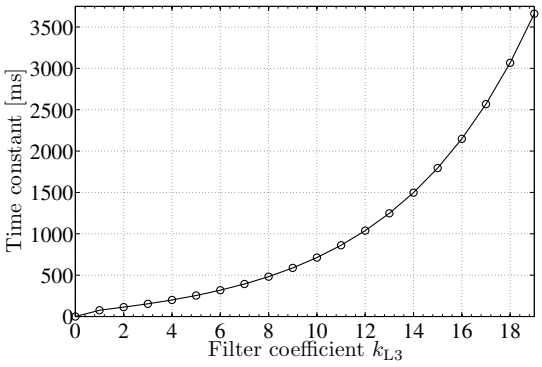

(b) Time constant T_{cst} as a function of filter coefficient k_{L3}.

Figure 3.2. Impact of L3 filter coefficient k_{L3} on the fluctuations and delay of the signal measurement.

The delay between the L1 and L3 filtering measurements can be estimated by the time constant T_{cst} which is defined as the time duration after which $(1 - a_{\text{L3}})$ of (2.27) reduces to half [HSS12]. The time constant T_{cst} corresponding to the filter coefficient

applied for LTE signal measurement is computed as

$$T_{\text{cst}} = 200 \text{ ms} \cdot \frac{\ln\left(\frac{1}{2}\right)}{\ln\left(1 - a_{\text{L3}}\right)} \tag{3.1}$$

$$= 200 \text{ ms} \cdot \frac{\ln\left(\frac{1}{2}\right)}{\ln\left(1 - 2^{\frac{-k_{\text{L3}}}{4}}\right)}, \tag{3.2}$$

where ln(.) is the natural logarithm operator.

For instance, the time constants corresponding to filter coefficients 7 and 11 are equal to 390 ms and 860 ms, respectively, as shown in Fig. 3.2(b). Moreover, extreme values of filter coefficient such as $k_{\text{L3}} = 19$ start to average out shadowing as well which is critical for triggering the handovers on time. The value of the filter coefficient is configured per measurement quantity [3GP12g], e.g., RSRP or RSRQ. The possible values of the filter coefficient which are defined by the 3GPP standard are integers 0 to 9, 11, 13, 15, 17 and 19.

3.3 Factors Affecting Handover Parameterization

3.3.1 Radio Propagation Conditions

The radio propagation conditions are different from one cell to another and even within cells at different locations. This is because shadow fading which is caused by large obstructions such as hills and large buildings causes location-dependent variations [Gol05]. Accordingly, each cell requires a specific setting of the handover parameters. For illustration, the coverage maps of 3G and LTE networks used in the simulation model are shown in Fig. 3.3(a) and Fig. 3.3(b), respectively. The areas having 3G and LTE coverage are indicated by red and blue, respectively, whereas coverage holes are indicated by black in both figures. The 3G coverage holes are determined by checking all the pixels whose RSCP levels are below the threshold of -115 dBm. Similarly, the LTE coverage holes are determined by checking all the pixels whose RSRP levels are below the threshold of -130 dBm. More coverage holes exist in the LTE network than in the 3G network. This is due to the fact that LTE operates at a higher carrier frequency,

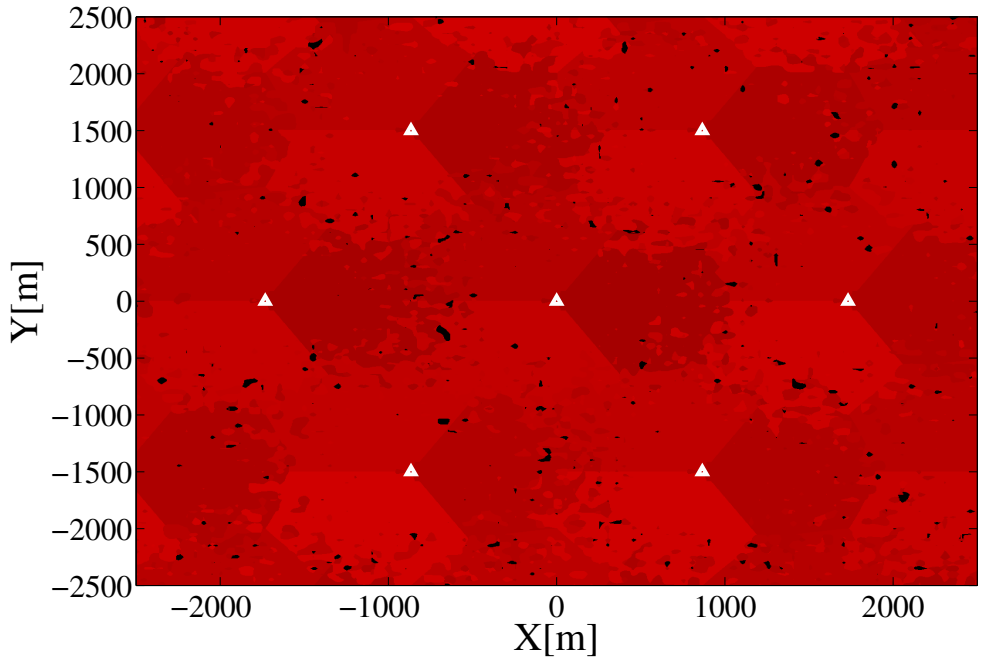

(a) The 3G network operating at 2.1 GHz carrier frequency.

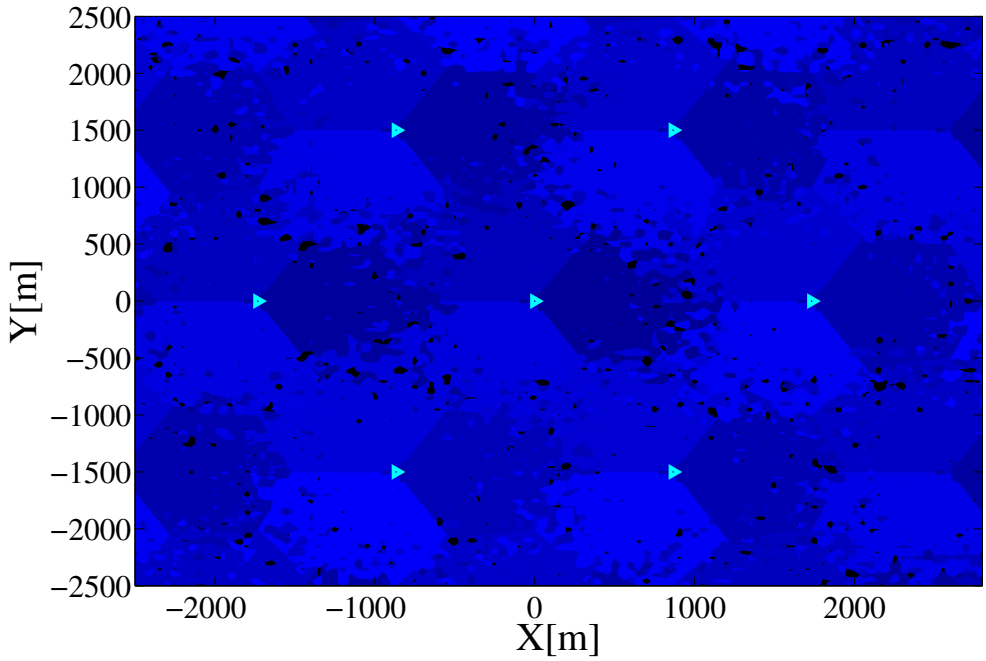

(b) The LTE network operating at 2.6 GHz carrier frequency.

Figure 3.3. Coverage maps of 3G and LTE networks. Coverage holes are indicated by black.

i.e., 2.6 GHz, resulting in a higher path loss [3GP06]. According to the figures, it can be seen that the number, size and location of the coverage holes vary in each cell. Some

of the cells have few small coverage holes whereas other cells have many large coverage holes. As a result, a setting of the handover parameters has to be found for each cell which best fits its specific radio propagation conditions.

Mobility problems which are caused by coverage holes can be resolved only if there is a good coverage from the other RAT. For illustration, the overlaying coverage map of 3G and LTE networks is shown in Fig. 3.4. The areas having coverage from both

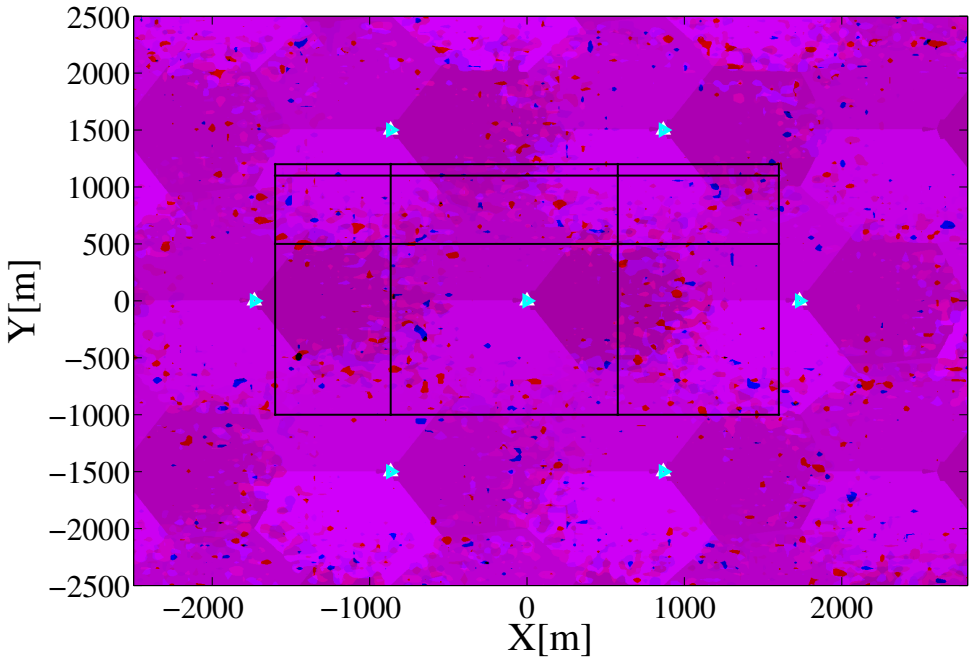

Figure 3.4. Overlaying coverage map of 3G and LTE networks. The LTE coverage holes which could be served by the 3G network are shown in red. The 3G coverage holes which could be served by the LTE network are shown in blue. Overlapping coverage holes in 3G and LTE networks are shown in black.

3G and LTE networks are indicated by magenta. The LTE coverage holes which could be served by the 3G network are shown in red. Vice versa, the 3G coverage holes which could be served by the LTE network are shown in blue. In this scenario, most of the coverage holes could be served by one of the two RATs. Only few overlapping coverage holes in 3G and LTE networks exist and they are shown in black. RLFs which are caused by these overlapping coverage holes cannot be resolved by adjusting the handover parameters. This is because there is no RAT that the UE could hand over to if it is inside or approaching such an overlapping coverage hole. These RLFs are not counted as mobility problems and might be resolved by other means pertaining to radio network planning such as adjusting the electrical tilt or the azimuth orientation of the transmit antenna. Thus, they are excluded from the investigation as they are of no interest for inter-RAT MRO.

3.3.2 User Path

The settings of the handover parameters depend also on the paths that the users are following in the network. In some cells, the users move on paths which are free from coverage holes. In this case, the handover parameters do not have to be necessarily updated. In other cells, the users might cross a single or multiple coverage holes consecutively, see Fig. 3.4. In this case, a proper setting of the handover parameters is needed. Thus, from mobility perspective, the coverage holes of a cell are critical only when they intersect the user path.

3.3.3 User Velocity

The variations in received signal of a UE depend on its velocity. The received signal of a fast moving UE varies more rapidly than that of a slowly moving UE. For instance, consider two UEs with the following velocities: 3 km/h and 120 km/h. In a time interval of 3 seconds, the slow and fast moving UE would advance 2.5 m and 100 m, respectively. For a de-correlation distance $d_{\text{corr}} = 50$ m for shadow fading [3GP06], the received signal of the slow moving UE does not vary much, i.e., 2.5 m $<$ 50 m, whereas that of the fast moving UE undergoes two independent samples of shadow fading, i.e., $100/50 = 2$. These variations in received signals have impact on the triggering events of the inter-RAT handovers, and consequently, on the number and type of mobility problems in the cell. Thus, the velocity of UEs affects indirectly the setting of the handover parameters.

3.4 Inter-RAT Mobility Failure Types

3.4.1 Radio Link Failures

In accordance with the mobility failure types defined for the intra-RAT case [3GP11], three mobility failure events are considered for inter-RAT scenario: TLH, TEH and Handover to a Wrong Cell (HWC). The latter three types of RLFs are described by their order.

1) TLH: The call is dropped before a handover is initiated or executed from one RAT to another and the UE reconnects to a cell in a RAT which is different than

that of the previously serving cell. The reason for the TLH is either that the entering condition of the measurement event had not been fulfilled or it has been fulfilled, but the RLF occurs before the inter-RAT handover is executed.

The entering condition of the measurement event is not fulfilled at the time step t_{RLF} of RLF in three different cases:

- Case A: $MQ_{u,c}(t_n)$ is higher than $Q_c^{(1)}$ and $MQ_{u,i_k}(t_n)$ is higher than $Q_c^{(2)}$, see Fig. 3.5(a).
- Case B: $MQ_{u,c}(t_n)$ is below $Q_c^{(1)}$ and $MQ_{u,i_k}(t_n)$ is below $Q_c^{(2)}$, see Fig. 3.5(b).
- Case C: $MQ_{u,c}(t_n)$ is higher than $Q_c^{(1)}$ and $MQ_{u,i_k}(t_n)$ is below $Q_c^{(2)}$, see Fig. 3.5(c).

In the other case, denoted by case D and shown in Fig. 3.5(d), the entering condition of the measurement event is fulfilled but nevertheless the RLF occurred before the inter-RAT handover is completed.

In the intra-RAT case, a single handover threshold is used and consequently, one type of TLH exists. However, in inter-RAT case there are two thresholds controlling each measurement event and the TLH can be resolved by adjusting either $Q_c^{(1)}$ or $Q_c^{(2)}$ threshold. A TLH which can be resolved by adjusting $Q_c^{(1)}$ or $Q_c^{(2)}$ is denoted by TLH-1 or TLH-2, respectively. 3GPP was following this investigation to distinguish between the two types TLH-1 or TLH-2 and has adopted this differentiation in LTE Rel. 11 standard [3GP12c]. In case A, the entering condition of the measurement event is not fulfilled because $Q_c^{(1)}$ is set to a too low value and the RLF occurred before $MQ_{u,c}(t_n)$ becomes lower than $Q_c^{(1)}$. In this case, increasing $Q_c^{(1)}$ could resolve the TLH, and consequently the TLH is classified as TLH-1. Similarly, in case B the entering condition of the measurement event is not fulfilled because $Q_c^{(2)}$ is set to a too high value which is not crossed i.e., the RLF occurred before $MQ_{u,i_k}(t_n)$ becomes higher than $Q_c^{(2)}$. In this case, decreasing $Q_c^{(2)}$ could resolve the TLH, and consequently the TLH is classified as TLH-2.

For the cases C and D, the classification of TLH is not as obvious as in cases A and B: In case C, none of the two thresholds are crossed, i.e., $MQ_{u,c}(t_n) > Q_c^{(1)}$ and $MQ_{u,i_k}(t_n) < Q_c^{(2)}$, and in case D both thresholds are crossed, i.e., $MQ_{u,c}(t_n) < Q_c^{(1)}$ and $MQ_{u,i_k}(t_n) > Q_c^{(2)}$. In case C, the TLH can be resolved by adjusting both $Q_c^{(1)}$ and $Q_c^{(2)}$ thresholds because they are not crossed. However, as each TLH should be

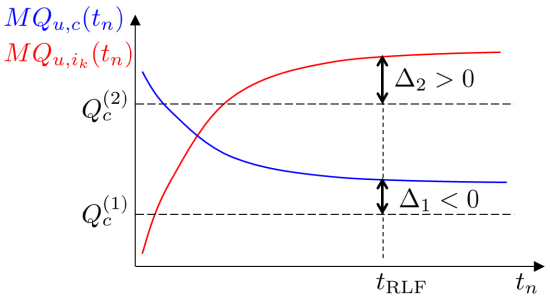

(a) Example of case A where the entering condition of the measurement event is not fulfilled at time step t_{RLF}. The TLH is classified as TLH-1.

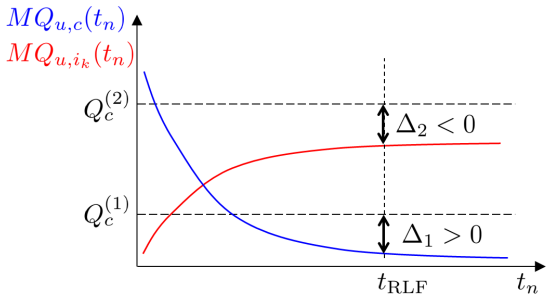

(b) Example of case B where the entering condition of the measurement event is not fulfilled at time step t_{RLF}. The TLH is classified as TLH-2.

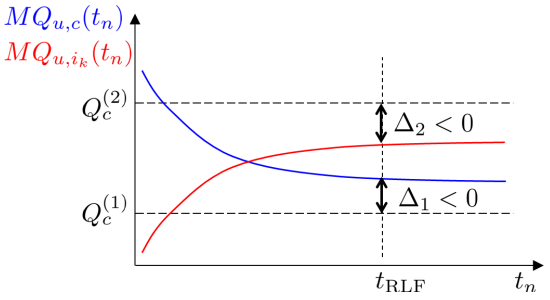

(c) Example of case C where the entering condition of the measurement event is not fulfilled at time step t_{RLF}. The TLH is classified as either TLH-1 or TLH-2 depending on the values of Δ_1 and Δ_2.

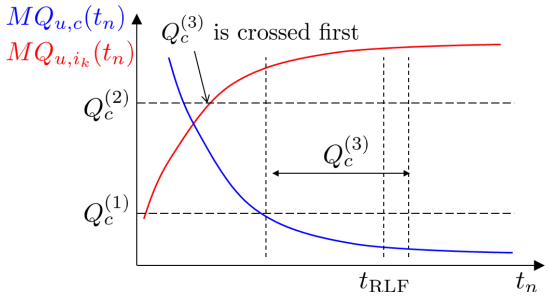

(d) Example of case D where the entering condition of the measurement event is fulfilled at time step t_{RLF}. The TLH is classified as either TLH-1 or TLH-2 depending on which threshold is crossed first.

Figure 3.5. Examples for four different cases of inter-RAT TLH.

counted as a single mobility failure event, it has to be classified either as TLH-1 or TLH-2. For this purpose, a new classification rule that is based on the differences between the values of the thresholds and their corresponding measured signal levels evaluated at t_{RLF} is used. Let $\Delta_1 = Q_c^{(1)} - MQ_{u,c}(t_{\mathrm{RLF}})$ and $\Delta_2 = MQ_{u,i_k}(t_{\mathrm{RLF}}) - Q_c^{(2)}$ be the differences corresponding to thresholds $Q_c^{(1)}$ and $Q_c^{(2)}$, respectively. The rule determines the threshold that should be adjusted first by comparing the two negative values Δ_1 and Δ_2. If $\Delta_1 < \Delta_2$, $Q_c^{(1)}$ is adjusted first and the TLH is classified as TLH-1. Otherwise, the TLH is classified as TLH-2. Once the threshold corresponding to the smallest difference is correctly adjusted in subsequent steps, i.e., its corresponding value of Δ_1 or Δ_2 becomes positive, the rule detects that the other threshold having $\Delta_1 < 0$ or $\Delta_2 < 0$ has to be adjusted. As a result, the rule needs multiple steps to detect that both thresholds have to be adjusted, and consequently resolve the TLH. The proposed routine for classifying a TLH as either TLH-1 or TLH-2 in cases A, B and C is summarized in pseudo-code 1.

As for the last case D, the classification rule of the aforementioned pseudo-code 1

Pseudo-code 1 : Routine for classifying a TLH as either TLH-1 or TLH-2.

```
Input Parameters: MQ_{u,c}(t_RLF), MQ_{u,i_k}(t_RLF), Q_c^(1) and Q_c^(2).
Calculate Δ1 = Q_c^(1) − MQ_{u,c}(t_RLF).
Calculate Δ2 = MQ_{u,i_k}(t_RLF) − Q_c^(2).
if Δ1 < Δ2 then
    TLH is classified as TLH-1.
else
    TLH is classified as TLH-2.
end if
```

does not apply. In this case, the TLH could be resolved by adjusting the threshold which is crossed later. Accordingly, the TLH is classified as TLH-1 if $Q_c^{(1)}$ is crossed later, otherwise the TLH is classified as TLH-2. For clarity, an example is shown in Fig. 3.5(d) which illustrates case D. According to the figure, the entering condition of the measurement event is fulfilled, nevertheless an RLF occurs before the $Q_c^{(3)}$ time interval is completed. The TLH could be resolved if the entering condition would have been fulfilled earlier. To this end, the threshold which delayed the fulfillment of the entering condition needs to be determined and adjusted. In this example, $Q_c^{(2)}$ is crossed before $Q_c^{(1)}$ and the threshold which should be adjusted is $Q_c^{(1)}$. Thus, the TLH is classified as TLH-1. Decreasing $Q_c^{(2)}$ would not resolve the TLH as the entering condition would not be fulfilled earlier, since $MQ_{u,c}(t_n)$ is higher than $Q_c^{(1)}$. However, if $Q_c^{(1)}$ is crossed earlier, the entering condition of the measurement event would have been fulfilled earlier and the RLF would have been avoided.

2) TEH: The UE is successfully handed over from cell A to another cell B of a different RAT. Shortly after, an RLF happens and the UE reconnects to the previous RAT, either to the same cell A or to a different one. Moreover, the inter-RAT handover failure, occurring when the UE fails during the handover to connect to the target handover cell using RACH [3GP12f], is also considered as a TEH. The handover from cell A to cell B should be avoided as the signal measurement of cell B is not strong enough to serve the UE after the handover

3) HWC: The UE is successfully handed over from cell A to another cell B of a different RAT. Shortly after, an RLF happens and the UE reconnects to a third cell C belonging to the same RAT as cell B. Similar to a TEH, the handover is triggered too early and should be delayed in order to hand over the UE directly to cell C instead of cell B.

For the detection of TEH and HWC events, the RLF should occur in cell B within a specific time interval T_{TE} after the UE is handed over from cell A. Typically, the time

interval T_{TE} is set to 3 s or 5 s.

3.4.2 Costly Inter-RAT Handovers

There are two types of costly inter-RAT handover events: Inter-RAT PP and UH from LTE to 3G network [3GP12f]. The latter mobility failure type was specifically introduced for the inter-RAT scenario in order to keep the UEs connected as much as possible to the newly deployed LTE network which is given in this study a higher priority than the 3G network. In that way, the UEs can benefit for a longer time from the LTE network which provides higher capacity and speed than 3G. The description of PPs and UHs is as follows:

1) PP: The UE is handed over to a cell of a different RAT and within a time interval T_{PP}, the UE is handed over back to the same cell or to a different cell of the previous RAT.

2) UH: The UE is handed over from a high priority RAT (LTE in this study) to a low priority RAT (3G) even though the signal quality measurement of the previous LTE cell is still good enough [3GP12f]. The UH is exclusive for the LTE network. A successful inter-RAT handover is detected as unnecessary if after the handover, the RSRQ of the previous LTE cell is higher than the threshold Q_{RSRQ} for the time interval T_{RSRQ}.

3.4.3 3GPP Specified Inter-RAT Mobility Failure Types

The 3GPP standard has focused only on a subset of the aforementioned inter-RAT mobility failure types since the investigations were based on the network scenario with partially overlaying deployment of LTE and 3G networks which is defined in Section 2.8.2 along with its adopted assumptions. The LTE Rel. 10 standard has defined the UH problem type whereas LTE Rel. 11 has recently considered TLHs from LTE to 3G, TEHs from 3G to LTE and PPs in both RATs [3GP12f].

The inter-RAT mobility failure events which are not considered by the 3GPP standard are summarized in Table 3.1. The TLH from 3G to LTE and TEH from LTE to 3G are not yet considered by 3GPP. This is because these two KPIs are relevant only when independent coverage holes in both RATs exist, i.e., a coverage hole which could be served by another RAT. These independent coverage holes can occur only if the

Table 3.1. Inter-RAT mobility failure events which are not considered yet by 3GPP.

Mobility Problem Type	Scenario
TLH from 3G to LTE	Independent coverage holes in both RATs
TEH from LTE to 3G	Independent coverage holes in both RATs
HWC in both RATs	Any

shadowing values pertaining to two co-sited BSs of different RATs are statistically independent. Thus, these two mobility failure events are relevant only for the fully overlaying deployment of 3G and LTE networks which assumes $\zeta_{\text{nw}} = 0$. As for HWC in both RATs, it is not considered by 3GPP though it can occur in any deployment of 3G and LTE networks. However, 3GPP may reconsider in the future to introduce the three mobility failure events of Table 3.1 when they start to occur more frequently in real networks.

3.5 Trade-offs in Inter-RAT MRO Problem

For each mobility failure type, there exists a set of settings for the handover thresholds that yield relatively smaller numbers of failure events compared to others. If the sets of handover thresholds corresponding to all failure types intersect, then it would be easy to find a proper setting for the handover thresholds that minimizes the number of failure events for all types. On the other hand, if the sets of handover thresholds are almost disjoint, then many trade-offs exist between different mobility failure types. In order to check if trade-offs exist in inter-RAT MRO problem, the number of mobility failure events are collected in a predefined time interval of T_{CL} and plotted as a function of the values of handover thresholds for each failure type. The results are presented after giving the simulation parameters in the following.

The scenario consists of two fully overlaying co-sited 3G and LTE networks, see Section 2.8.3. The simulation parameters that are common for the fully and partially overlaying LTE and 3G deployments are summarized in Table 3.2. The simulation parameters are set to typical values that are used as well in the rest of the thesis. The simulation parameters that are specific for each of the fully and partially overlaying 3G and LTE deployments are given in a separate table. Table 3.3 summarizes the simulation parameters that are used for the fully overlaying deployment of 3G and LTE networks. The antenna tilt θ_c is set to 6° for all cells. The total number of UEs in both networks is 1010 distributed as follows: 5 UEs moving randomly in each cell with a

Table 3.2. Common simulation parameters for fully and partially overlaying LTE and 3G deployments.

	Parameter	Value
Network	Carrier frequency	LTE: 2.6 GHz, 3G: 2.1 GHz
	System bandwidth W	LTE: 10 MHz, 3G: 5 MHz
	Height h_{bs} of BS	30 m
	Total transmit power $P_c^{(\mathrm{tx})}$	LTE: 46 dBm, 3G: 43 dBm
	Noise power $P_{\mathrm{N}}^{(\mathrm{rb})}$ on a single RB	LTE: -114 dBm
	Total noise power P_{N}	3G: -100 dBm
	Propagation constant α_{p}	LTE: 130.5 dB, 3G: 128.6 dB
	Path loss exponent β_{p}	37.6 dB
	Penetration loss L_{pn}	20 dB
	Shadowing standard deviation σ_{sf}	8 dB
	Shadowing de-correlation distance d_{corr}	50 m
	Shadowing correlation coefficient ζ_{bs} between BSs of same network	1
	Fast fading	2-tap Rayleigh fading channel
	Scale parameter σ_{ff} of Rayleigh distribution	$1/\sqrt{2}$
	Standard deviation of the measurement error σ_{me}	RSRP: 0.8 dB, RSRQ: 0.33 dB RSCP: 0.45 dB, Ec/N_0: 0.33 dB
	Filter coefficient k_{L3}	4
	Intra-RAT handover offset φ	3 dB
	Velocity of randomly moving UEs	$v_{\mathrm{mr}} = 3$ km/h
	Traffic model	Full buffer
BS Antenna	Azimuth beam width Δ_ϕ	70°
	Maximum azimuth attenuation B_{h}	20 dB
	Elevation beam width Δ_θ	10°
	Maximum elevation attenuation B_{v}	20 dB
	Maximum backward attenuation B_{a}	25 dB
	Antenna gain G_{gain}	14 dBi
Timers	Step size T_{n}	100 ms
	Intra-RAT TTT $T_{\mathrm{T}}^{(\mathrm{intra})}$	320 ms
	Handover preparation time $T_{\mathrm{hp}}^{(\mathrm{intra})}$	150 ms
	Handover preparation time $T_{\mathrm{hp}}^{(\mathrm{inter})}$	250 ms
	Time intervals T_{TE}, T_{PP} and T_{RSRQ}	3 s
	Time interval T_{RLF}	500 ms
	Time interval T_{CL}	150 s
Detection Thresholds	Q_{HC} and Q_{RLF}	-8 dB
	Q_{RACH}	-7 dB
	Q_{RSRQ}	-17.7 dB

speed of $v_{\mathrm{mr}} = 3$ km/h and 800 UEs moving on streets with a speed of $v_{\mathrm{st}} = 60$ km/h. In addition, the value of inter-RAT TTT is set to $Q_c^{(3)} = 320$ ms.

Table 3.3. Simulation parameters which are specific for fully overlaying LTE and 3G deployment.

Parameter	Value
Antenna tilt θ_c	6°
Number N_{ue} of UEs	1010
	Moving randomly: 5 per cell
	Moving on streets: 800

The values of $Q_c^{(1)}$ and $Q_c^{(2)}$ are swept from -129 dBm to -118 dBm and from -111 dBm to -100 dBm for each LTE cell, respectively. The number of mobility failure events are collected from the LTE network during a time interval of $T_{\text{CL}} = 150$ s. The total number of events in the LTE network are shown in Fig. 3.6 for different failure types and values of the serving and target cell thresholds. The number of events is indicated

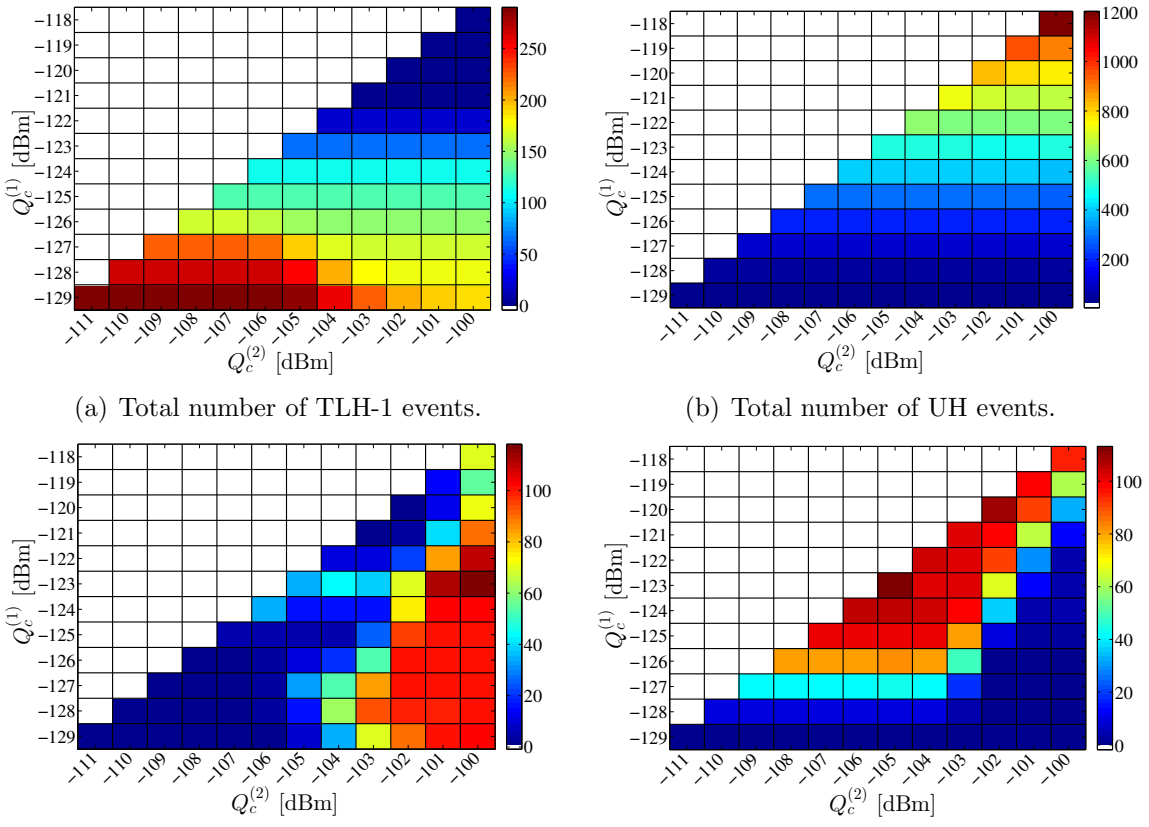

(a) Total number of TLH-1 events.

(b) Total number of UH events.

(c) Total number of TLH-2 events.

(d) Sum of the numbers of TEH and HWC events.

Figure 3.6. Total number of events in LTE network for different failure types and values of the serving and target cell thresholds.

by a specific color for each setting of handover thresholds and failure type. The smallest

numbers of events are indicated by blue and the highest numbers by red. The blank quadrants are not simulated. According to the figure, it can be seen that the set of handover thresholds minimizing the number of events, i.e., indicated by blue color, is to some extent different for each failure type. As a result, many trade-offs exist indeed in inter-RAT MRO. These trade-offs between the mobility failure types are explained in the following.

The total number of TLH-1 events is shown in Fig. 3.6(a). For a fixed target cell threshold, the number of TLH-1 events decreases as the serving cell threshold increases. This is because the inter-RAT handovers are triggered earlier before the UEs experience RLFs. However, this decrease in the number of TLH-1 events is possible only at the expense of an increase in the number of UHs which is shown in Fig. 3.6(b). A higher value for $Q_c^{(1)}$ can avoid more TLHs of type 1 in some areas of the cell, however, in other areas the inter-RAT handovers of UEs would be triggered earlier resulting in a higher number of UHs. Thus, a high value for $Q_c^{(1)}$ can shrink the LTE coverage as UEs would be handed over earlier to 3G network.

Another trade-off exists between the number of TLH-2 events, shown in Fig. 3.6(c), and the sum of the numbers of TEH and HWC events, shown in Fig. 3.6(d). For a fixed serving cell threshold, the number of TLHs of type 2 increases as the target cell threshold increases. This is because it is more difficult to hand over the UEs to another neighboring cell having a higher signal strength level. On the contrary, the sum of the numbers of TEH and HWC events increases as the target cell threshold decreases. The reason for this is that the entering condition of the measurement event can be fulfilled more easily with smaller target cell threshold. Consequently, many inter-RAT handovers could be triggered to target cells having weak signal strength levels resulting in TEHs or HWC.

Chapter 4

Manual Optimization of Handover Thresholds

4.1 Introduction

To exploit the existence of multiple RATs and provide users with the best QoS, the numbers of inter-RAT mobility failures experienced by UEs should be minimized. This can be achieved by properly configuring the inter-RAT handover parameters of the BSs. Among these parameters, the inter-RAT handover thresholds of the measurement event controlling the triggering of the measurement reports are typically the first to optimize. The handover thresholds can be configured network-wide where each cell in a RAT applies the same settings or cell-specifically [3GP12b, 3GP12g]. Currently, all the optimization methods of the handover thresholds are manual requiring an extensive skilled human intervention, either by evaluating performance metric data or performing drive tests. This work is tedious and time consuming, and therefore rather expensive as the handover thresholds need to be reconfigured manually each time there is a change in the environment or mobility conditions.

The current network planning and optimization methods typically provide a fixed network-wide setting for the handover thresholds of all the cells in the roll-out phase. This approach is simple, however, it does not yield the best network performance as the radio propagation conditions in each cell are different requiring a cell-specific adaptation of the handover thresholds [FSL+07]. Therefore, in a following optimization phase during the network operation, cells that later show considerable mobility problems in operation mode are optimized manually with the aid of drive tests and expert knowledge. This kind of optimization is performed in an operating network and requires several iterations. In the following, it is called online optimization.

Offline optimization means can be also used during the network planning phase as long as the cell-specific radio conditions can be determined and modeled. The optimization methods of network planning tools allow to find near-optimal settings for radio network parameters, and therefore they can be applied to find a proper cell-specific setting for the handover thresholds. The optimization methods are basically testing several sets of parameter settings and the performance of each parameter setting is evaluated in an experiment against a predefined optimization function. Each evaluation corresponds to

a single simulation run in the network planning tool. Though these offline optimization methods provide some sort of automation for setting the handover thresholds, they are still considered in this study as manual optimization methods since they require the intervention of skilled experts to run and analyze the simulation results. Different offline optimization methods exist for obtaining cell-specific inter-RAT handover thresholds and they are described in the following.

The tabu search [ACMS02, TK05] and Simulated Annealing (SA) [Hur02, SY08] are two optimization methods which have been commonly used in network planning tools. These methods start from a candidate solution vector comprising an initial guess for the settings of the parameters and then move iteratively to a better neighbor solution. The search for the new candidate solution is performed by exploring locally the neighborhood of the current candidate solution. Other heuristic search methods such as genetic algorithm can be also used in network planning tools [MTR00]. While SA creates a new candidate solution by modifying the current solution with a local move, the genetic algorithm creates new candidate solutions by combining two different solutions.

Taguchi's Method (TM) for experiment design is another promising optimization method which follows different approach than the aforementioned local search methods. The major advantage of TM is the ability to consider explicitly the interactions existing among the configuration parameters. Moreover, it explores the search space in a scientifically disciplined manner unlike meta-heuristic local search methods. TM was first developed for the optimization of manufacturing processes [Roy90], and then imported into many engineering fields, to name but a few, hardware design [Tag01], power electronics [HHL+05, IHTT06, KRR08], microwave circuits [VE93] and wireless communications [CL05]. This method has been applied by the author of this thesis in [AWVK11a] to optimize for the first time radio parameters of an LTE network. TM uses a so-called Orthogonal Array (OA) [Roy01] which is not to be mixed up with orthogonal antenna array. The OA is invented by C. R. Rao and was used by Genichi Taguchi to develop the base of what is currently known as TM. By using an OA, a reduced set of representative parameter combinations is selected to be tested from the full search space. The number of selected parameter combinations determines the number of experiments being carried out and evaluated against an optimization function. Using all the experiments' results, a candidate solution is found and the process is repeated till a desired criterion is fulfilled.

The construction of an OA is challenging and might not exist for any number of configuration parameters. As a result, TM applying OA cannot be used for any optimization problem. A good replacement for OA is Nearly Orthogonal Array (NOA) which was proposed by the author of this thesis in [AWVK11c]. NOA can be constructed for any

number of configuration parameters and has statistical properties which are comparable to those of an OA. Consequently, NOA enables the application of TM in any optimization problem and provides more flexibility in selecting the desired number of experiments and in turn controlling the computational complexity. TM applying NOA has been applied by the author of this thesis in [AWV+11] to jointly optimize the antenna parameters of BSs in an LTE network and the power control parameters in LTE advanced relay networks [BABS+11, BABS+13].

The two offline optimization methods SA and TM are not applicable as automatic optimization algorithms in real operating networks. This is because they are based on arbitrary high number of experiments which may significantly harm the performance of UEs. In this study, these two methods are mainly used for benchmarking with the automatic optimization algorithm of the inter-RAT handover thresholds. Moreover, they are used to show how to obtain, in offline mode, a cell-specific handover threshold setting which outperforms the best network-wide setting found during the network planning phase.

This chapter is organized as follows. The network-wide optimization of the handover thresholds is presented in Section 4.2. The current methods which are used to optimize the handover thresholds in a cell-specific way are described in Section 4.3: The online optimization procedure of the handover thresholds using drive tests is explained in Section 4.3.1 and the two offline optimization methods, SA and TM, which are used in network planning tools are described in Section 4.3.2 and Section 4.3.3, respectively. More specifically, for TM the description of OA and NOA is given in Section 4.3.3.2 and Section 4.3.3.3, respectively, and the new optimization procedure applying NOA is presented in Section 4.3.3.4. Finally, the performance of SA, TM applying NOA and the best network-wide setting is compared in Section 4.3.4.

4.2 Network-Wide Optimization of Handover Thresholds

The inter-RAT handover thresholds are initially configured with a proper network-wide setting. This configuration is necessary to minimize, as much as possible, the numbers of mobility problems which impact negatively the user experience. The network-wide setting of the handover thresholds can be only optimized for a specific setup and parameter configuration [VWL+11]. Thus, the resulting setting might not be necessarily optimal if the value of any parameter, which has been considered as fixed such as

the speed of UEs or inter-RAT TTT $Q_c^{(3)}$, is changed. Nevertheless, this optimized network-wide setting represents the most reliable setting and it is typically used when a RAT is rolled out and firstly configured. Therefore, the best network-wide setting is used as a reference for the automatic optimization algorithm for all speeds of UEs and values of inter-RAT TTT $Q_c^{(3)}$. For this purpose, a parameter sweep of the handover thresholds is performed and the values of the mobility failure events are collected during a time interval of $T_{\mathrm{CP}} = 150$ s. The scenario consists of two fully overlaying co-sited 3G and LTE networks, see Section 2.8.3. The speed of UEs on streets is set to $v_{\mathrm{st}} = 60$ km/h and the value of inter-RAT TTT is fixed to $Q_c^{(3)} = 320$ ms. The rest of the simulation parameters are summarized in Table 3.3 and Table 3.2.

The total number of mobility failure events in 3G and LTE networks is shown in Fig. 4.1 for different network-wide settings of serving and target cell thresholds. The total sum of RLFs, i.e., sum of the numbers of TLHs of type 1 and 2, TEHs and handovers to wrong cell, and PPs in both networks is indicated by a specific color in Fig. 4.1(a) for each setting of handover thresholds. The target cell thresholds $Q_c^{(2)}$ of all LTE and 3G cells are indicated by the pair of values which are shown on the x-axis. For instance, the first and second value of the pair $(-111,-126)$ dBm denotes the target cell threshold of all LTE and 3G cells, respectively. Similarly, the serving cell thresholds $Q_c^{(1)}$ of all LTE and 3G cells are indicated by the pair of values which are shown on the y-axis.

Typically, a higher priority is given to the numbers of RLFs and PPs than the number of UHs which is shown in Fig. 4.1(b). Therefore, the selection of the best network-wide setting is primarily based on the numbers of RLFs and PPs and secondarily on the number of UHs. According to Fig. 4.1(a), there are five network-wide settings, corresponding to blue quadrants, which have smaller numbers of RLFs and PPs compared to other settings. Among these five settings, the best network-wide setting is ($Q_c^{(1)}$,$Q_c^{(2)}$) = (-121,-100) dBm for LTE network and (-106,-115) dBm for 3G network. The serving cell threshold of the best setting is relatively high compared to others and yields a high number of UHs as shown in Fig. 4.1(b). This high number of UHs can be tolerated by mobile operators at the beginning as opposed to high numbers of RLFs and PPs which have more impact on QoS. Later, during the network operation the handover thresholds of the LTE cells having high number of UHs are optimized manually with the aid of drive tests and technical experts.

The selected network-wide setting yields as well the smallest number of RLFs and PPs in each network separately. The total numbers of RLFs and PPs in 3G and LTE networks are shown in Fig. 4.2 and Fig. 4.3, respectively. According to the figures, it is shown that for the selected network-wide setting, the number of RLFs is the smallest in both the LTE and the 3G network. Moreover, the number of inter-RAT PPs is very

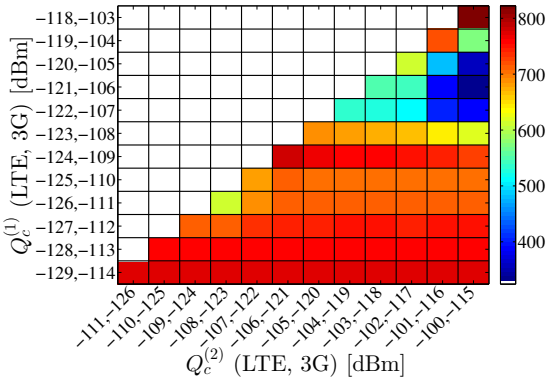

(a) Sum of RLFs and PPs in LTE and 3G networks.

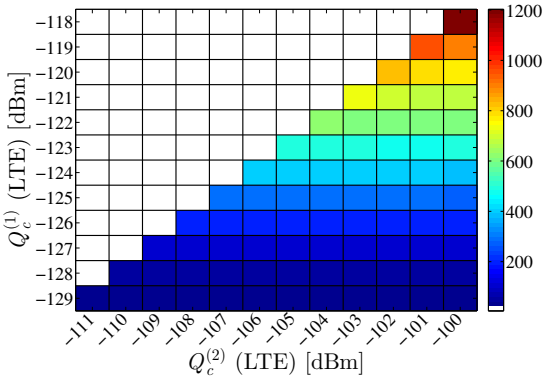

(b) Total number of UHs in LTE network.

Figure 4.1. Total number of mobility failure events in 3G and LTE networks for different network-wide settings of serving and target cell thresholds.

small for both networks. The reason for this is that the difference between the serving and target cell thresholds pertaining to LTE or 3G cell measurements is high and equal to 6 dB, i.e., -115+121 = 6 dB and -100+106 = 6 dB, and in turn it is difficult to have two consecutive inter-RAT handovers in a short time interval of $T_{\mathrm{PP}} = 3$ s.

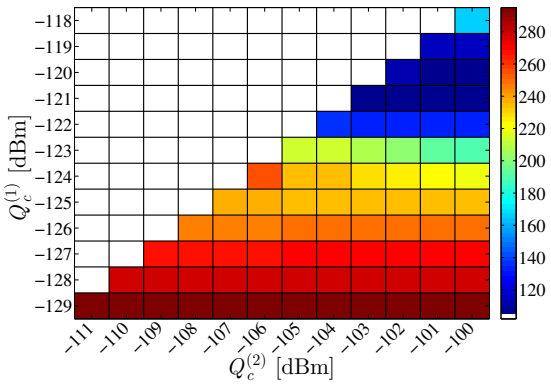

(a) Total number of RLFs in LTE network.

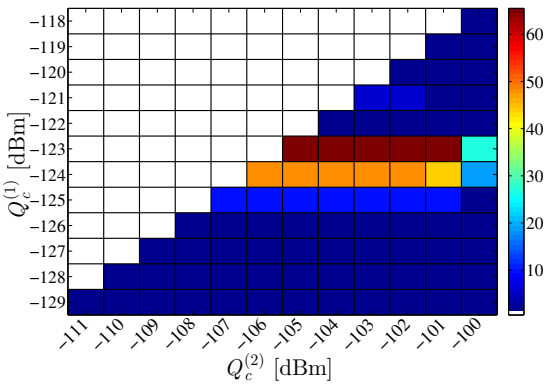

(b) Total number of PPs in LTE network.

Figure 4.2. Total number of mobility failure events in LTE network for different LTE network-wide settings of serving and target cell thresholds.

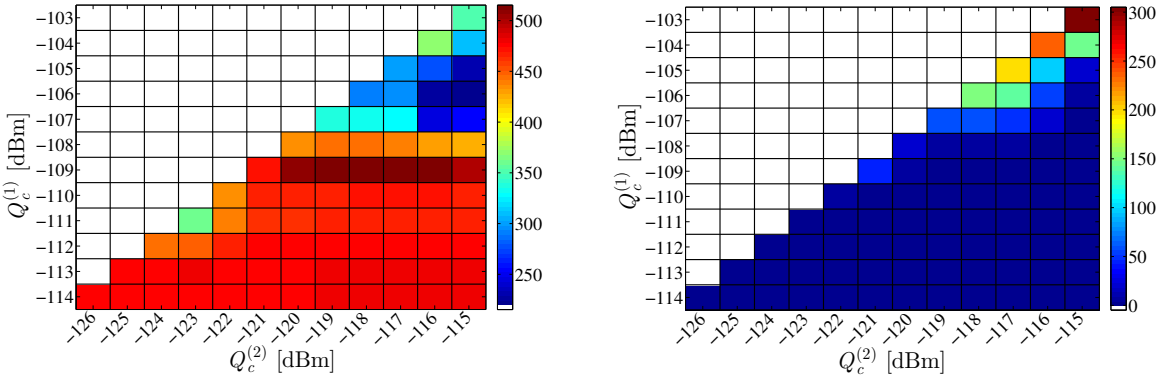

(a) Total number of RLFs in 3G network.

(b) Total number of PPs in 3G network.

Figure 4.3. Total number of mobility failure events in 3G network for different 3G network-wide settings of serving and target cell thresholds.

4.3 Cell-Specific Optimization of Handover Thresholds

4.3.1 Online Optimization using Drive Tests

In the first phase of the LTE or 3G network roll-out, the inter-RAT handover thresholds are configured with the best network-wide setting. This setting works well for most cells of the network. However, there is a limited number of cells which still experience significant numbers of mobility problems during the network operation. For mobile operators, it is extremely important to solve the mobility failure events in this limited number of cells because the same UEs are experiencing regularly these failure. Resolving the mobility failure events in those cells results in a better user-perceived quality. Therefore, the handover thresholds of the cells which show later a significant number of mobility problems are optimized online using drive tests. The online optimization procedure of handover thresholds can be summarized in the following three steps:

1. The mobility performance is monitored in the network in order to determine the cells which still have mobility problems after applying the best network-wide setting of the handover thresholds. The performance metrics that are used for monitoring are called KPIs. In prior art, these KPIs are completely proprietary and unspecified by 3GPP. Typically, the KPIs which are used are the handover success rate, call drop rate and number of handovers. These KPIs do not provide detailed information about the types of mobility failure events which are defined in Section 3.4. The mechanisms that are needed to differentiate between

the different types of RLFs and costly inter-RAT handovers have been recently specified by 3GPP in Rel. 9, 10 and 11 for MRO use case in SON.

2. In order to collect more detailed information about the mobility problems, drive tests are performed in the aforementioned cells. A drive test is a technique consisting of a vehicle containing measurement equipment that can detect and log signal strength measurements and handover information. The vehicle moves in the geographical areas which are covered by the cells having mobility problems and performs measurements.

3. The data collected from drive tests are analyzed by radio network engineers. Based on this analysis, the root cause of the mobility problems is identified in each cell and a decision is taken on the new handover threshold settings. The handover thresholds are then updated manually using the Operation and Maintenance (OAM) configuration tool.

The three aforementioned steps are repeated until the optimization procedure converges to final values of handover thresholds.

4.3.2 Offline Optimization using Simulated Annealing

The cell-specific handover thresholds which are obtained online using drive tests can be as well found using offline optimization methods. SA is a well-known offline local search method which provides a near-optimal solution vector $\mathbf{x}$ for the minimization of a predefined multidimensional function y [HJJ03]. SA is a general optimization method which works irrespective of the definitions of $\mathbf{x}$ and y. In this study, the vector $\mathbf{x} = [x_1, \ldots, x_p, \ldots, x_{2 \cdot N_\mathrm{c}}]$ contains the serving and target handover thresholds of all N_c 3G and LTE cells: The first N_c parameters can be assigned for the serving cell thresholds, e.g, $x_1 = Q_1^{(1)}$, and the rest for target cell thresholds. The steps of SA are explained in the following.

SA has an explicit strategy to avoid the local minimum. Unlike other optimization methods which always moves in the direction of improvement, SA allows non-improving moves to escape from the local minimum [KGV83]. The probability of accepting a move which degrades the value of the optimization function y is decreased during the search. The acceptance probability is controlled by the so-called temperature parameter T and the value of the increase δ in the optimization function [HJJ03]. At a fixed temperature, the higher the difference δ, the lower the probability to accept the move is. Moreover, the higher the temperature T, the greater the acceptance probability is.

The steps of the SA algorithm are outlined in pseudo-code 2. The value of the opti-

Pseudo-code 2 : Simulated annealing with solution space Ω and neighborhood structure $N(\mathbf{x})$ [HJJ03].

```
1: Select an initial candidate solution x = x_0 ∈ Ω;
2: Select an initial temperature T = T_0 > 0;
3: Select a neighborhood structure N(x);
4: Select a temperature reduction function ϱ(T);
5: Select the number N_it of iterations executed at each temperature T;
6: Select the number of times N_tp the temperature is reduced;
7: Set the counter h of the number of times the temperature is reduced to 0;
8: repeat
9:    Set the counter q of the number of iterations executed at each temperature T to
      0;
10:   repeat
11:      Randomly generate x' ∈ N(x);
12:      Compute δ = f(x') − f(x);
13:      if δ ≤ 0 then
14:         x ← x';
15:      else
16:         Generate a random number ϑ uniformly distributed between 0 and 1;
17:         if ϑ < exp(−δ/T) then
18:            x ← x';
19:         end if
20:      end if
21:      q ← q + 1;
22:   until q = N_it;
23:   T ← ϱ(T);
24:   h ← h + 1;
25: until h = N_tp;
```

mization function y evaluated for $\mathbf{x}$ is indicated by $f(\mathbf{x})$. SA starts by generating an initial candidate solution $\mathbf{x} \in \Omega$ where Ω is the solution space defined as the set of all feasible candidate solutions. In each step, a new candidate $\mathbf{x}'$ is generated from the neighborhood $N(\mathbf{x})$ of the current solution. If $f(\mathbf{x}') \leq f(\mathbf{x})$, $\mathbf{x}'$ is accepted as current solution in the next step, otherwise it is accepted with some probability depending on the parameters T and $\delta = f(\mathbf{x}') - f(\mathbf{x})$. During the search, the temperature T is decreased slowly and the process is repeated until the algorithm converges into a steady state.

As SA is a heuristic search method, there are no general rules that guide the choice of the input parameters [Hur02]. Therefore, decisions have to be made on the initial temperature T_0, the neighborhood structure $N(\mathbf{x})$ and the temperature reduction function $\varrho(T)$. In this work, the initial temperature T_0 is set such that a non-improving move

with a maximum increase $\delta_{\max}$ in the value of the optimization function is accepted in the beginning with a predefined probability $\mu_{\text{pb}} = \exp(-\delta_{\max}/T_0)$ [SY08]. As a result,

$$T_0 = \frac{-\delta_{\max}}{\ln(\mu_{\text{pb}})} \tag{4.1}$$

where ln(.) is the natural logarithm operator. The neighborhood structure $N(\boldsymbol{x})$ is often defined as the set of candidate solutions that slightly differ from the current solution $\mathbf{x}$ [MN00]. In this work, a new candidate solution $\mathbf{x}'$ is obtained by giving a small and random displacement υ for all the handover threshold values in $\mathbf{x}$ [PYS08]. The displacement υ is generated by selecting a random number in the range $(-\upsilon_{\max}, \upsilon_{\max})$ where $\upsilon_{\max}$ is the maximum displacement value. To lower the temperature T every N_{tp} iterations, a standard geometric temperature reduction function is used as in [Hur02], i.e., $\varrho(T) = \nu_{\text{T}} \cdot T$, where ν_{T} is a reduction ratio.

4.3.3 Offline Optimization using Taguchi's Method

4.3.3.1 Introduction

TM is another offline optimization method that was originally used to find a near-optimal setting for a small number of configuration parameters. The method relies on an OA, which should be constructed, to test different parameter settings. However, the construction of an OA becomes much more complicated when the number of parameters is high which is the case in most challenging optimization problems. To overcome this issue, the author proposes to replace an OA by NOA. NOA is easier to construct for any number of configuration parameters, and consequently allows the use of TM in any optimization problem. By introducing NOA, the author has modified the optimization procedure based on TM to use NOA instead of an OA. The new method is applied in this study to optimize the handover thresholds of each cell in the network.

This section is organized as follows. OA is explained in Section 4.3.3.2 along with its properties. Then, NOA is introduced in Section 4.3.3.3. The new iterative optimization procedure based on TM applying NOA is presented in Section 4.3.3.4.

4.3.3.2 Orthogonal Array

An OA is an array which contains a reduced set of N_{exp} parameter combinations to be tested from the full search space Ω [HSS99]. The total number of parameters,

serving and target handover thresholds of all 3G and LTE cells, is indicated by $N_{\mathrm{p}} = 2 \cdot N_c$. Every parameter x_p has a set of testing values corresponding to a set of levels $\mathcal{L} = \{1, \ldots, \ell, \ldots, N_{\mathrm{v}}\}$ where N_{v} is the total number of levels. For instance, if a parameter x_p can take three values 5, 6 and 7, level 1 refers to value 5, level 2 to value 6 and level 3 to value 7. Each row $e = 1, \ldots, N_{\mathrm{exp}}$ of the OA describes a possible combination of parameter levels to be tested in a corresponding experiment. Hence, an OA determines the testing level of each parameter in each experiment. To perform the experiments, each level of a parameter determined by the OA is mapped to a corresponding testing value. The optimization function y is evaluated for each parameter combination determined by row e of the OA resulting in a measured response y_e. In every iteration of TM, the levels of each parameter are mapped to different testing values based on the candidate solution found in the previous iteration. Hence, a new set of N_{exp} parameter combinations is tested in each iteration. The properties of the OA are described in the following.

By definition, an $N_{\mathrm{exp}} \times N_{\mathrm{p}}$ matrix $\mathbf{A}$, having elements from $\mathcal{L}$, is said to be an orthogonal array OA($N_{\mathrm{exp}}, N_{\mathrm{p}}, N_{\mathrm{v}}, S$) with N_{v} levels, strength S and index λ if every $N_{\mathrm{exp}} \times S$ sub-array of $\mathbf{A}$ contains each S-tuple based on $\mathcal{L}$ exactly λ times as a row [HSS99]. Thus, λ denotes the number of times each S-tuple based on $\mathcal{L}$ is tested. The higher the strength S, the more the OA considers the interactions among the configuration parameters. In this study, each column in the OA corresponds to a handover threshold value x_p. The first N_{c} columns can be assigned for the serving cell thresholds and the rest for target cell thresholds. For illustration, an example of an OA(9,4,3,2) having $N_{\mathrm{exp}} = 9$ which is 9 times smaller than all $3^4 = 81$ possible combinations, $N_{\mathrm{p}} = 4$ configuration parameters, $N_{\mathrm{v}} = 3$ levels and strength $S = 2$ is depicted in Table 4.1.

Table 4.1. An illustrative OA(9,4,3,2) with the measured responses and their corresponding SN ratios.

Experiment	x_1	x_2	x_3	x_4	**Measured response**	**SN ratio**
1	1	1	1	1	y_1	SN_1
2	1	2	2	3	y_2	SN_2
3	1	3	3	2	y_3	SN_3
4	2	1	2	2	y_4	SN_4
5	2	2	3	1	y_5	SN_5
6	2	3	1	3	y_6	SN_6
7	3	1	3	3	y_7	SN_7
8	3	2	1	2	y_8	SN_8
9	3	3	2	1	y_9	SN_9

In any 9×2 sub-array of the OA in Table 4.1, the following nine row combinations (1,1), (1,2), (1,3), (2,1), (2,2), (2,3), (3,1), (3,2), (3,3) are found and each pair appears the same number of times, i.e., $\lambda = 1$. In other words, every level of a parameter x_p is tested with every other level of a parameter $x_{p'} \neq x_p$ exactly $\lambda = 1$ times. This property of the OA accounts for the interactions that might exist between the parameters. Therefore, the OA depicted in Table 4.1 does not only analyze the individual impact of each parameter on the performance, but also the effect of the combination of any two parameters.

A basis property of the OA is that each parameter is tested at each level the same number of times. This allows for a fair and balanced manner of testing the values of the parameters. In Table 4.1, each level is tested three times for every parameter. Moreover, any sub-array of $\mathbf{A}$ is also an OA. Therefore, a new OA having a smaller number of parameters can be obtained from an existing one by removing one or more columns. This property is especially useful when the number of parameters of an optimization problem is smaller than N_p. In this case, an OA can be directly obtained from $\mathbf{A}$ without the need to construct it.

Another fundamental issue is the construction and existence of an OA. Many techniques are known for constructing OAs based on Galois fields and finite geometries. More details about how to construct an OA are found in [HSS99]. Besides, it is not always possible to construct an OA with the desired number N_exp of experiments. The higher N_exp, the higher is the computational complexity. If the values of $N_\mathrm{p}, N_\mathrm{v}$, and S are specified, there is a lower bound on the minimum number N_exp of experiments so that an OA exists. The Rao's bounds, defined in [Rao47] for an OA of strength two and three, set a restriction on the number N_exp of experiments and, therefore, the computational complexity of the algorithm. The parameters of the OA$(N_\mathrm{exp}, N_\mathrm{p}, N_\mathrm{v}, S)$ should satisfy the following inequalities

$$N_\mathrm{exp} \geq \sum_{g=0}^{s} \binom{N_\mathrm{p}}{g} (N_\mathrm{v} - 1)^g, \text{ if } S = 2s, s > 0 \tag{4.2}$$

$$N_\mathrm{exp} \geq \sum_{g=0}^{s} \binom{N_\mathrm{p}}{g} (N_\mathrm{v} - 1)^g + \binom{N_\mathrm{p} - 1}{s} (N_\mathrm{v} - 1)^{s+1}, \text{if } S = 2s + 1, s \geq 0. \tag{4.3}$$

In principle, N_exp is much smaller than the number $N_\mathrm{v}^{N_\mathrm{p}}$ of all possible parameter combinations, i.e., $N_\mathrm{exp} \ll N_\mathrm{v}^{N_\mathrm{p}}$.

Many OAs having different number N_p of configuration parameters have been already constructed and archived in the database maintained in [Slo]. Thus, the required

OA can be directly selected from this database if found, otherwise, it needs to be constructed. The construction of an OA having high number N_{p} of parameters might be challenging or even not possible. This is because an OA would exist only if it satisfies the inequalities of (4.2). Moreover, even if the OA exists, it is not always obvious how to construct it. Thus, the TM based on OA can be used only for a limited number of optimization problems whose OA exists and can be constructed.

4.3.3.3 Nearly Orthogonal Array

In order to use TM in all optimization problems, it is necessary to relax Rao's bound of (4.2) and keep at the same time most of the properties of an OA. One good replacement for OA is NOA which can be constructed for any value of $N_{\mathrm{exp}}, N_{\mathrm{p}}$ and N_{v} and has statistical properties similar to an OA. Considering that the number of handover thresholds to be optimized in this study is high, NOA can be used instead of an OA. The construction and properties of NOA are explained in the following.

Various algorithms exist for constructing NOAs. In this work, NOAs are constructed using the algorithm described in [Xu02]. For illustration, Table 4.2 shows an example of an NOA(6,4,3) having $N_{\mathrm{exp}} = 6$, $N_{\mathrm{p}} = 4$ and $N_{\mathrm{v}} = 3$ which can be used as a replacement for the OA(9,4,3,2) of Table 4.1. In this example, the number N_{exp} of

Table 4.2. An illustrative NOA(6,4,3) with the measured responses and their corresponding SN ratios.

Experiment	x_1	x_2	x_3	x_4	**Measured response**	**SN ratio**
1	1	1	2	2	y_1	SN_1
2	1	2	1	1	y_2	SN_2
3	2	3	3	1	y_3	SN_3
4	2	1	1	3	y_4	SN_4
5	3	2	3	2	y_5	SN_5
6	3	3	2	3	y_6	SN_6

experiments of an NOA is 33% lower than that of an OA. This reduction in N_{exp} and in turn computational complexity is possible only at the expense of considering partially the interactions among the configuration parameters. In a NOA, each testing level of a parameter x_p is not necessarily tested with every other level of $x_{p'} \neq x_p$. For instance, considering the first two parameters x_1 and x_2 in Table 4.2, the following three row combinations are missing (1,3), (2,2) and (3,1). Fortunately, it is not necessary in radio network optimization problems to fully exploit the interactions among the parameters.

This is because the parameters of non-neighboring cells are to some extent independent from each other.

The high degree of freedom that a NOA offers compared to an OA makes TM much more vulnerable to the choice of the input parameters N_{exp} and N_{v} according to the results published by the author of this thesis in [AWVK11c]. Currently, there are no rules that guide the choice of these two parameters. In general, the values of the input parameters depends on the size of the optimization range as well as on the computational complexity of the experiments. For instance, for a large optimization range the input parameters should be set in general to high values in order to have a statistically representative set of experiments from the full search space. However, it will be shown in Section 4.3.4 that TM applying NOA can converge with small number of experiments and levels even though the selected optimization range of handover thresholds is relatively large.

4.3.3.4 Optimization Procedure Applying Nearly Orthogonal Array

An iterative optimization procedure based on TM applying an OA is described in [WYE07, AWVK11a]. In order to use TM in optimization problems having high number N_{p} of configuration parameters, the optimization procedure should be modified to include NOA instead of OA. The flowchart of the new optimization procedure, which is proposed by the author of this thesis, is depicted in Fig. 4.4 and is discussed in details in the following.

The first step in the optimization procedure is to construct a proper NOA. For this purpose, the number N_{p} of configuration parameters has to be determined. Moreover, a decision has to be made on the number N_{exp} of experiments and number N_{v} of levels. In each iteration r, the parameter levels which are determined by the NOA are mapped to testing values depending on the previously found candidate solution. To this end, let $V_p^{(\min)}$ and $V_p^{(\max)}$ be the minimum and maximum feasible values for parameter x_p, respectively. In the first iteration, the center value of the optimization range for parameter x_p is defined as

$$V_p^{(r)} = \frac{V_p^{(\min)} + V_p^{(\max)}}{2}. \tag{4.4}$$

In every iteration r, the level $\ell = \lceil N_{\text{v}}/2 \rceil$ is always mapped to $V_p^{(r)}$. The other $N_{\text{v}} - 1$ levels are distributed around $V_p^{(r)}$ by adding or subtracting a multiple integer of a step size $\beta_p^{(r)}$. For $r = 1$, the step size is defined as

$$\beta_p^{(r)} = \frac{V_p^{(\max)} - V_p^{(\min)}}{N_{\text{v}} + 1}. \tag{4.5}$$

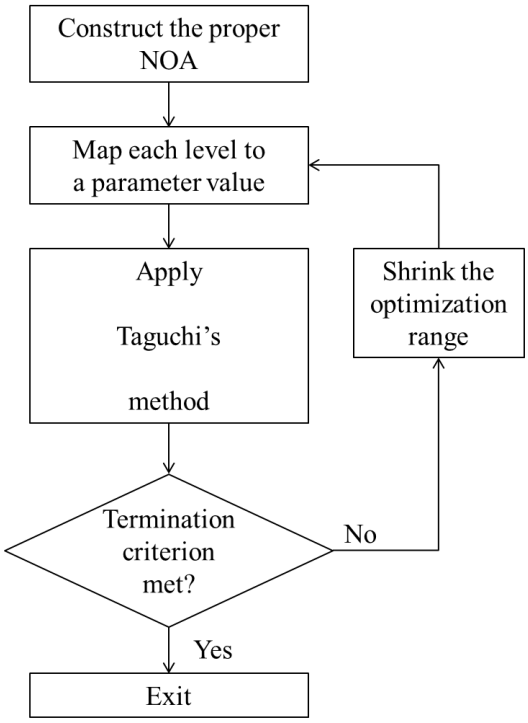

Figure 4.4. The new iterative optimization procedure based on TM applying NOA rather than OA.

In iteration r, the mapping function $f_p^{(r)}(\ell)$ of a level ℓ to a dedicated value of the parameter x_p can be described as follows

$$f_p^{(r)}(\ell) = \begin{cases} V_p^{(r)} - (\lceil N_\mathrm{v}/2 \rceil - \ell) \cdot \beta_p^{(r)} & 1 \leq \ell \leq \lceil N_\mathrm{v}/2 \rceil - 1 \\ V_p^{(r)} & \ell = \lceil N_\mathrm{v}/2 \rceil \\ V_p^{(r)} + (\ell - \lceil N_\mathrm{v}/2 \rceil) \cdot \beta_p^{(r)} & \lceil N_\mathrm{v}/2 \rceil + 1 \leq \ell \leq N_\mathrm{v}. \end{cases} \tag{4.6}$$

For instance, consider a parameter x_1 having a minimum value $V_p^{(\min)} = 0$ and a maximum $V_p^{(\max)} = 15$. If x_1 is tested with three levels, i.e., $N_\mathrm{v} = 3$, level 2 is mapped in first iteration to $(0 + 15)/2 = 7.5$, level 1 to $7.5 - \beta_1^{(1)} = 3.75$ and level 3 to $7.5 + \beta_1^{(1)} = 11.25$. The values of $V_p^{(r)}$ and $\beta_p^{(r)}$ are updated at the end of each iteration if the termination criterion is not met. After mapping the levels to parameter values, the experiments arranged by the NOA are performed and the values of the optimization function y is evaluated for each experiment e.

To interpret the experimental results, TM converts the measured responses to Signal-to-Noise (SN) ratios which are not to be confused with Signal-to-Noise Ratio (SNR) of UEs. If the aim is to minimize the measured response y_e, the following definition of SN ratio applies for each experiment e:

$$SN_e = -10 \cdot \log_{10}(y_e^2) \text{ [dB]}. \tag{4.7}$$

The average SN ratio is then computed for each parameter and level. In the example of Table 4.2, the average SN ratio of x_2 at level $\ell = 1$ is computed by averaging in dB the SN ratios of the experiments where x_2 is tested at level 1, i.e., SN_1 and SN_4. The best level of each parameter is the level having the highest average SN ratio. Using the mapping function $f_p^{(r)}(\ell)$, the best setting of a parameter x_p in iteration r is found and denoted by $V_p^{(\text{best},r)}$.

At the end of each iteration, the termination criterion is checked. If it is not met, the best values found in iteration r are used as center values for the parameters in the next iteration $r + 1$:

$$V_p^{(r+1)} = V_p^{(\text{best},r)}. \tag{4.8}$$

It may happen that the best value of a parameter x_p found in iteration r is close to $V_p^{(\min)}$ or $V_p^{(\max)}$. In this case, there is need for a procedure to consistently check if the mapped value of a level is within the optimization range. Moreover, the optimization range is reduced by multiplying the step size of each parameter x_p by a reduction factor $\xi < 1$, i.e.,

$$\beta_p^{(r+1)} = \xi \beta_p^{(r)}. \tag{4.9}$$

With every iteration, the optimization range is reduced and the possible values of a parameter are closer to each other. Hence, the set used to select a near-optimal value for a parameter becomes smaller. The optimization procedure terminates when all step sizes of the parameters are less than a predefined threshold ϵ i.e.,

$$\beta_p^{(r)} < \epsilon \ \forall p. \tag{4.10}$$

4.3.4 Performance Comparison between Simulated Annealing, Taguchi's Method and Best Network-Wide Setting

The performances of the two offline optimization methods SA and TM applying NOA are compared with that of the best network-wide setting of the handover thresholds which is explained in Section 4.2. The two offline methods provide a cell-specific setting for the handover thresholds which should in principle outperform the best network-wide setting.

The optimization function y is defined such that the comparison between the offline optimization methods and the best network-wide setting or automatic optimization algorithm is fair with respect to performance evaluation. The number of UHs in a cell has lower priority than RLFs and should be minimized only if no TLHs exist. The coverage of the LTE cell is increased only if the UEs could continue in the source cell

without problems as stated in [3GP12f]. The existence of TLHs is an indication that the UEs could not stay longer in the cell and should be handed over earlier. Having an explicit conditional rule for reacting on UHs is not possible in SA and TM which update the handover thresholds based on the value of a single optimization function y. As a result, the total number $N_{\text{all}}^{(\text{UH})}$ of UHs is excluded. In this study, the optimization function y is defined as the sum of the total number $N_{\text{all}}^{(\text{RLF})}$ of RLFs and the number $N_{\text{all}}^{(\text{PP})}$ of PPs in both 3G and LTE networks, i.e.,

$$y = N_{\text{all}}^{(\text{RLF})} + N_{\text{all}}^{(\text{PP})}. \tag{4.11}$$

Hence, SA and TM will be used as benchmark only with respect to the total number of RLFs and PPs which have higher priority than UHs.

The scenario consists of two fully overlaying co-sited LTE and 3G networks, which is explained in Section 2.8.3. The speed of UEs on streets is set to $v_{\text{st}} = 60$ km/h which is the speed used in optimizing the best network-wide setting. The inter-RAT TTT $Q_c^{(3)}$ is set to the optimal value which minimizes the optimization function y evaluated for the best network-wide setting of handover thresholds. For this purpose, the value of the optimization function y is shown in Fig. 4.5 for the best network-wide setting with $Q_c^{(3)}$ as parameter. According to the figure, it is shown that the value of the

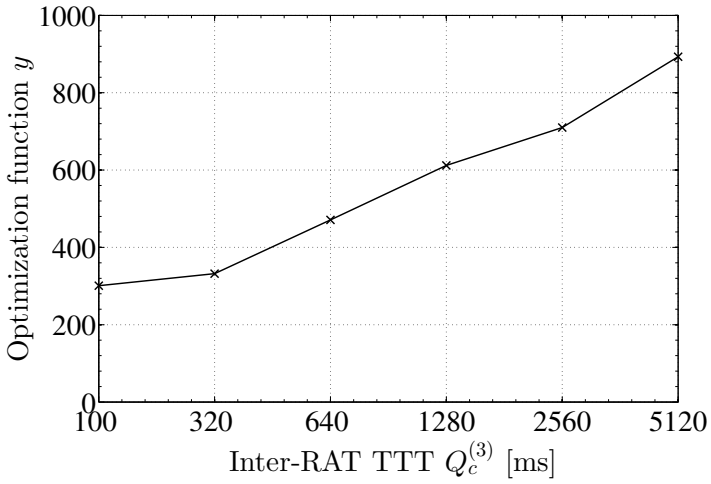

Figure 4.5. The value of the optimization function y evaluated for the best network-wide setting versus inter-RAT TTT $Q_c^{(3)}$.

optimization function increases with higher values of $Q_c^{(3)}$. As a result, the value $Q_c^{(3)}$ is set to 100 ms which provides a slightly better performance than $Q_c^{(3)} = 320$ ms. The rest of the simulation parameters are summarized in Table 3.2 and Table 3.3.

The optimization function y is evaluated in each network trial. In case of SA, each network trial corresponds to a single evaluation $f(\mathbf{x})$ of the optimization function. As

for TM, each experiment arranged by the NOA corresponds to one network trial. For both methods, the optimization function is evaluated in each network trial using the values of the KPIs collected during $T_{\mathrm{CP}} = 150$ ms time interval.

The input parameters of SA and TM have been selected such that the two optimization methods converge within an acceptable number of network trials. Due to limitations in computational complexity and memory resources, it is difficult to go beyond 250 network trials with the aforementioned value of T_{CP} and a time step size of $T_{\mathrm{n}} = 100$ ms. The parameters of SA are summarized in Table 4.3. A good guess for the initial

Table 4.3. Simulation parameters for SA.

Parameter	Value
Initial candidate solution $\mathbf{x_0}$	Best network-wide setting
Number N_{it} of iterations at each temperature	10
Number N_{tp} the temperature is reduced	24
Initial acceptance probability μ_{pb}	0.5
Maximum displacement value v_{max}	3 dB
Temperature reduction ratio ν_{T}	0.7
Maximum increase δ_{max} in y	40

candidate solution $\mathbf{x_0}$ is the best network-wide setting which is found in Section 4.2. The total number of network trials is set to $N_{\mathrm{tp}} \cdot N_{\mathrm{it}} = 24 \cdot 10 = 240$. The initial temperature T_0 is selected such that an increase of $\delta_{\mathrm{max}} = 40$ in the value of the optimization function y is accepted at the beginning with a probability $\mu_{\mathrm{pb}} = 0.5$. The value of T is shown in Fig 4.6 as a function of the number of network trials.

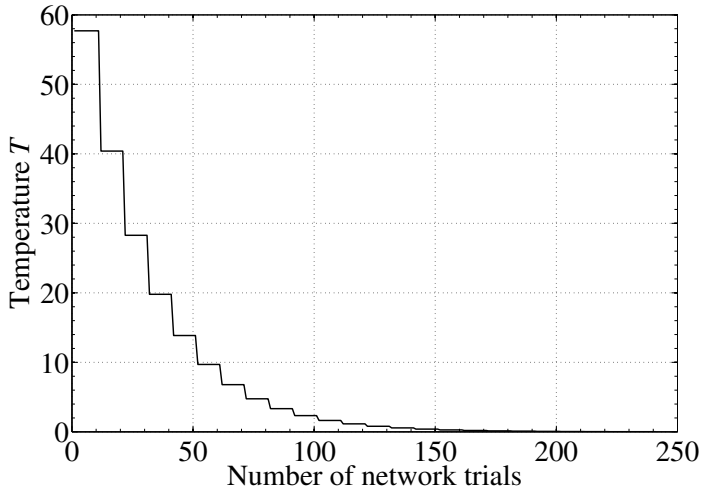

Figure 4.6. The value of the temperature T as a function of the number of networks trials.

The parameters of TM are summarized in Table 4.4. The selected NOA has $N_{\text{exp}} =$

Table 4.4. Simulation parameters for TM applying NOA.

Parameter	Value
NOA(N_{exp}, N_{p}, N_{v})	NOA(20, 84, 5)
$V_{\text{p}}^{(\text{min})}, V_{\text{p}}^{(\text{max})}$ of LTE serving cell threshold	-131, -121 dBm
$V_{\text{p}}^{(\text{min})}, V_{\text{p}}^{(\text{max})}$ of LTE target cell threshold	-103, -97 dBm
$V_{\text{p}}^{(\text{min})}, V_{\text{p}}^{(\text{max})}$ of 3G serving cell threshold	-116, -106 dBm
$V_{\text{p}}^{(\text{min})}, V_{\text{p}}^{(\text{max})}$ of 3G target cell threshold	-118, -112 dBm
Optimization range reduction ratio ξ	0.75
Termination threshold ϵ	0.25

20 experiments, $N_{\text{p}} = 84$ serving and target cell thresholds and $N_{\text{v}} = 5$ levels. For an OA to exist with such parameters, the minimum number N_{exp} of experiments should be higher than or equal to 337 for strength $S = 2$, see (4.2). This minimum number of N_{exp} already exceeds the total number 250 of possible network trials. As a result, the optimization procedure based on TM which is described in Section 4.3.3.4 cannot even complete the first iteration if such an OA is used. On the other hand, if the aforementioned NOA is used the optimization procedure based on TM can complete up to $250/N_{\text{exp}} \approx 12$ iterations which are typically enough for convergence. The optimization range of the serving and target cell thresholds are given by the values $V_{\text{p}}^{(\text{min})}$ and $V_{\text{p}}^{(\text{max})}$ for each parameter. The reduction ratio ξ and the termination threshold ϵ are set to 0.75 and 0.25, respectively.

The value of the optimization function y is plotted as a function of the number of network trials for SA and TM in Fig. 4.7. In the first network trial, SA has the same optimization function value of the best network-wide setting. However, TM does not have any initial setting and in turn the value of the optimization function is different than that of SA in the first network trial. According to the figure, it is shown that SA and TM achieve optimization function values which are 27% and 35% lower than that of the best network-wide setting, respectively. Thus, there exist cell-specific settings for the handover threshold values which outperform the best network-wide setting. By applying these cell-specific handover thresholds, the number of mobility failures experienced by UEs in the network would decrease. Moreover, it is shown that the value of the optimization function y fluctuates a lot during the optimization, in particular for TM. These fluctuations in the value of the optimization function would be critical if these methods are applied online as they impact negatively the user perception.

The cell-specific values of serving and target cell thresholds of the considered LTE network are shown in Fig. 4.8 for SA and TM. The best network-wide setting which is

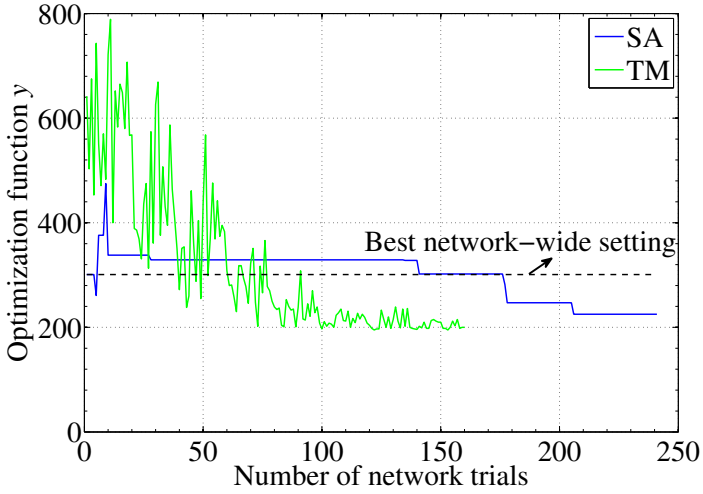

Figure 4.7. The value of the optimization function y as a function of the number of network trials for SA and TM. The speed of UEs on streets is $v_{\mathrm{st}} = 60$ km/h and the inter-RAT TTT $Q_c^{(3)} = 100$ ms.

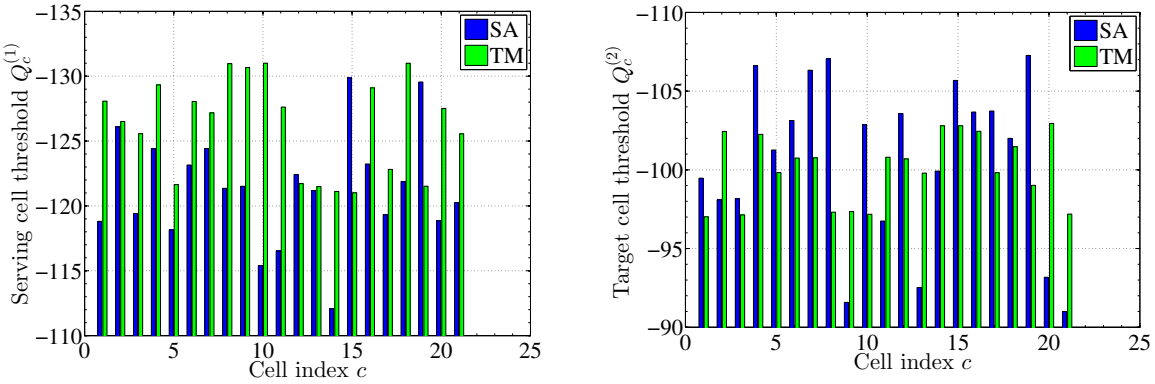

(a) Optimized values of $Q_c^{(1)}$ for LTE cells.

(b) Optimized values of $Q_c^{(2)}$ for LTE cells.

Figure 4.8. The optimized values of serving and target cell thresholds of LTE network.

used for LTE is ($Q_c^{(1)}$,$Q_c^{(2)}$) = (-121,-100) dBm. According to the figure, the handover threshold values obtained by the two offline optimization methods are different. This is due to the fact that the size of the optimization range is large and there is more than one cell-specific handover threshold setting which outperforms the best network-wide setting. These results can assist the experts during the network planning phase to configure cell-specific values of handover thresholds.

Chapter 5

Automatic Optimization of Handover Thresholds

5.1 Introduction

In order to tackle the challenges of manual optimization methods such as time-consuming drive testing and labor-intensive evaluation of testing data, automatic optimization of handover thresholds is highly demanded. Thus, MRO is one of the most prominent use case of SON. An automatic optimization algorithm requires mechanisms that permanently analyze mobility failure events and check if any cell experiences mobility problems. The mobility failure events are counted periodically using performance metrics which are also called KPIs. The performance monitoring over time of the KPI values is explained in Section 5.2.

The automatic optimization of inter-RAT handover thresholds is performed currently in a cell-specific way. In theory, the automatic optimization of the handover thresholds could be performed as well in a network-wide manner. In this approach, the same handover thresholds are configured for all cells and the optimization does not differentiate among the cells. On the contrary, in cell-specific optimization the automatic algorithm can set different handover thresholds for each cell. This additional degree of freedom makes the cell-specific optimization approach more appealing compared to network-wide optimization. For this reason, the network-wide optimization of the handover thresholds is discussed briefly in Section 5.3 whereas Section 5.4 explains the cell-specific optimization approach in detail. More specifically, the optimization problem is formulated by the author of this thesis for the cell-specific optimization approach, and the advantages and limitations of this approach compared to the best network-wide setting configured initially during the network planning phase are highlighted.

In a cell-specific optimization approach, there is a single handover threshold which is configured irrespective of the neighboring cell. Thus, the optimized handover setting of a cell results from averaging over the KPI values regardless to which neighbor the UE has been handed over to, and therefore some of the mobility problems cannot be resolved. To address this limitation, the author proposes to configure and optimize a dedicated handover threshold value with respect to a group of neighboring target cells. This advanced approach, denoted by cell-group specific optimization, provides

additional degrees of freedom compared to cell-specific optimization and, in turn, it can adapt better to the mobility problems occurring with respect to specific target cells. The cell-group specific optimization approach is described in Section 5.5. The optimization problem is formulated and an analysis, which encompasses all the aspects related to the cell-group specific optimization approach, is presented.

For both cell-specific and cell-group specific optimization approaches, a general automatic optimization algorithm is proposed by the author of this thesis in Section 5.6 for the inter-RAT handover thresholds. The algorithm is designed to run in each cell of both 3G and LTE networks. Each cell periodically collects its KPI statistics and updates its handover thresholds based on these statistics. The changes in the values of the handover thresholds of each cell are determined by a feedback controller [BB08]. In the vocabulary of control theory, the two main components of the feedback controller are the proportional control block [BB08] and the gain scheduler [PDH97, LF06]. The change in the value of each handover threshold is determined by the first control block and is proportional to a predefined error signal. The gain scheduler alters the behavior of the proportional control block by modifying its parameters [PDH97,LF06] depending on the mobility conditions in each cell.

The performance of cell-specific and cell-group specific optimization approach is evaluated in Section 5.7 on a network and cell level. The evaluation is carried out for different speeds of UEs and values of inter-RAT TTT. In addition, for the cell-specific optimization approach the performance of the automatic optimization algorithm using all mobility failure types is compared with that using only the 3GPP specified ones in partially and fully overlaying deployments of LTE and 3G networks, see Section 2.8. Moreover, a performance comparison between the automatic optimization algorithm, SA and TM is presented. The work of this chapter has been partially presented by the author of this thesis in [AWR+11, AWVK11b, AWVK12a, WAKV13, AWVK13b].

5.2 Performance Monitoring over Time

In this section, the monitoring over time of the number of mobility failure events in each cell is explained in detail. The mobility failure events are collected by each cell of which the misconfiguration of its handover thresholds is responsible for those failures. The 3GPP standard has specified the mobility failure types and the mechanisms for the root cause analysis procedure. The cell that missed or initiated an early inter-RAT handover is responsible for that failure and has to count it. For TLHs, the responsible cell and the cell where the RLF happened are the same whereas for TEHs and HWC the

responsible cell is the cell triggering the inter-RAT handover before the RLF occurred. Similarly, PPs are counted by the cell triggering the first inter-RAT handover and UHs are counted by the previously serving LTE cells.

The metrics used for performance monitoring and counting mobility failure events are called inter-RAT KPIs. The 3GPP specified mechanisms for root cause analysis allow the definition of KPIs that can provide detailed information about the mobility failure types [3GP12f] which are discussed in Section 3.4. In this study, it is assumed that for each mobility failure type a dedicated KPI exists. Thus, a KPI exists for TLH of type 1, TLH of type 2, TEH, HWC, PP and UH, i.e., six KPIs are defined in total. The collected values of KPIs can be either held in a central unit or distributed in the BSs controlling the cells.

The values of the KPIs are collected periodically by each cell. The duration of a KPI collection period is T_{CL} which can be of the order of minutes, hours and even days depending on the user traffic in the cell. The index for the KPI collection period is denoted by κ. In each KPI collection period κ, new values of the KPIs are collected. A trade-off exists between the reliability and the ability to react on KPI statistics depending on the time interval T_{CL} [HSS12]. This trade-off is depicted in Fig. 5.1. According to the figure, the longer the time interval T_{CL} the more reliable and stable

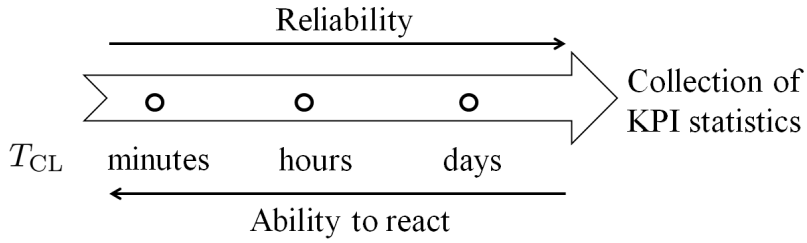

Figure 5.1. Trade off between the reliability and the ability to react on KPI statistics depending on the time interval T_{CL} [HSS12].

the KPI statistics are. It is necessary that the values of the KPIs are stable over collection periods for given fixed values of inter-RAT handover thresholds. The reason for this is that the automatic algorithm reacts only on reliable values of KPIs. However, the reaction on KPI statistics is delayed with increasing value of T_{CL}. Thus, T_{CL} should be set such that the KPI statistics are reliable enough and the reaction to the mobility problems is not delayed.

An example is given in Fig. 5.2 that show the numbers of mobility problems for LTE and 3G cells as a function of KPI collection period κ. Only the cells having significant

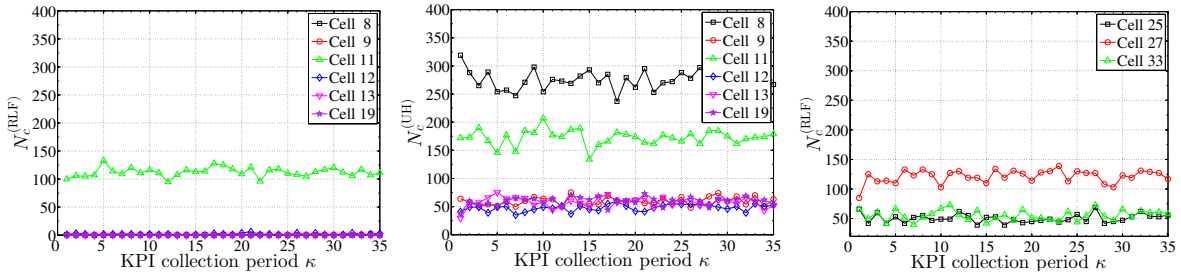

(a) Number $N_c^{(\mathrm{RLF})}$ of RLFs for LTE cells. (b) Number $N_c^{(\mathrm{UH})}$ of UHs for LTE cells. (c) Number $N_c^{(\mathrm{RLF})}$ of RLFs for 3G cells.

Figure 5.2. Numbers of mobility problems for LTE and 3G cells as a function of KPI collection period κ for the best network-wide setting of the handover thresholds.

number of mobility failure events are shown in the figure. The time interval T_{CL} is set to 150 s and the handover thresholds of all the cells are fixed and configured with the best network-wide setting which is described in Section 4.2. The values of TLH-1, TLH-2, TEH, HWC, PP and UH KPIs collected from cell c are denoted by $N_c^{(\mathrm{TLH-1})}$, $N_c^{(\mathrm{TLH-2})}$, $N_c^{(\mathrm{TEH})}$, $N_c^{(\mathrm{HWC})}$, $N_c^{(\mathrm{PP})}$ and $N_c^{(\mathrm{UH})}$, respectively. The total number of RLFs in cell c is computed by summing over the values of TLH-1, TLH-2, TEH and HWC KPIs, i.e.,

$$N_c^{(\mathrm{RLF})} = N_c^{(\mathrm{TLH-1})} + N_c^{(\mathrm{TLH-2})} + N_c^{(\mathrm{TEH})} + N_c^{(\mathrm{HWC})}. \tag{5.1}$$

The values of the KPIs are to some extent stable over KPI collection periods for the selected value of the time interval T_{CL}. According to the figure, the number of LTE and 3G cells which still have mobility problems after applying the best network-wide setting is 6 out of 21 (≈29%) and 3 out 21 (≈14%), respectively, i.e., the total number of 3G or LTE cells is 21. Cell 11 is the only LTE cell which still has RLFs whereas there are three cells 25, 27 and 33 in 3G network. Cells which still have UHs are cells 8, 9, 11, 12, 13 and 19. The handover thresholds of the cells which still have mobility failure events have to adjusted either by using drive tests or an automatic inter-RAT MRO algorithm.

5.3 Network-Wide Optimization of Handover Thresholds

The automatic optimization of the handover thresholds in network-wide manner is to some extent redundant and inefficient. The handover thresholds are already optimized during the network planning phase by configuring the best network-wide setting as explained in Section 4.2. As a result, a network-wide optimization of the handover

thresholds during the network operation might not achieve any additional performance gain compared to the best setting. Moreover, a network-wide setting results from averaging over all the mobility problems in the network. Thus, there will be many cells in the network which still have mobility problems even after the optimization. In addition, the three factors: radio propagation, path and speed of UEs which are explained in Section 3.3 vary between the cells. Therefore, cell-specific handover thresholds are needed to resolve the specific mobility problems of each cell.

An automatic network-wide optimization of the handover thresholds cannot react on UHs with presence of TLHs in the network. Typically, in the network planning phase the mobile operators configure a conservative network-wide setting minimizing the number of TLHs at the expense of a high number of UHs, see Section 4.2. Generally, the number of TLHs is given a higher priority than UHs and in turn it may not be possible to react during network operation on UHs as it may increase the number of TLHs. In this case, the coverage of the LTE network cannot be expanded without using cell-specific handover thresholds. The expansion of the LTE coverage is actually very critical for mobile operators who invested a lot in deploying the LTE network. In this study, the automatic network-wide optimization of the handover thresholds is not investigated as it does not yield any additional performance gains compared to the existing cell-specific optimization approach.

5.4 Cell-Specific Optimization of Handover Thresholds

5.4.1 Formulation of the Optimization Problem

In this section, the cell-specific optimization problem is formulated in terms of the values of the KPIs which are collected by each cell during the time interval T_{CL}. The index for the inter-RAT KPI is indicated by $a = 1, \ldots, A$ where A is the total number of KPIs. For each cell c, a normalized weight value $0 \leq w_{c,a} \leq 1$ is assigned for the value of the a^{th} KPI. The weights of the KPIs values are packed in vector $\mathbf{w}_c \in \mathbb{R}^{A \times 1}$, i.e.,

$$\mathbf{w}_c = \begin{bmatrix} w_{c,1} \\ \vdots \\ w_{c,a} \\ \vdots \\ w_{c,A} \end{bmatrix}. \tag{5.2}$$

The value of the a^{th} KPI collected by cell c during the time interval T_{CL} with respect to the k^{th} inter-RAT neighboring cell i_k is indicated by $f_{c,i_k}^{(a)}$. The values of the KPIs with respect to each neighbor of cell c are packed in matrix $\mathbf{F}_c \in \mathbb{Z}^{A\times K}$ where $\mathbb{Z}$ is the set of integers, i.e.,

$$\mathbf{F}_c = \begin{bmatrix} f_{c,i_1}^{(1)} & \cdots & f_{c,i_k}^{(1)} & \cdots & f_{c,i_K}^{(1)} \\ \vdots & & \ddots & & \vdots \\ f_{c,i_1}^{(a)} & \cdots & f_{c,i_k}^{(a)} & \cdots & f_{c,i_K}^{(a)} \\ \vdots & & \ddots & & \vdots \\ f_{c,i_1}^{(A)} & \cdots & f_{c,i_k}^{(A)} & \cdots & f_{c,i_K}^{(A)} \end{bmatrix} = [\mathbf{f}_{c,i_1}, \ldots, \mathbf{f}_{c,i_k}, \ldots \mathbf{f}_{c,i_K}]\,. \tag{5.3}$$

The vector $\mathbf{f}_{c,i_k}$ is the k^{th} column of matrix $\mathbf{F}_c$ and corresponds to all the KPI values of cell c with respect to the neighboring cell i_k.

The handover thresholds of each cell c are packed into vector $\mathbf{q}_c$ which is defined as

$$\mathbf{q}_c = [Q_c^{(1)}, \ldots, Q_c^{(m)}, \ldots, Q_c^{(M)}] \tag{5.4}$$

where M is the total number of the handover thresholds. In an inter-RAT scenario, there are two handover thresholds $Q_c^{(1)}$ and $Q_c^{(2)}$ corresponding to the serving and target cell, respectively. Thus, M is equal to 2.

In theory, the handover thresholds of each cell can be optimized to minimize the total weighted number of mobility problems in 3G and LTE networks. This joint optimization problem of the handover thresholds can be formulated as

$$\{\widehat{\mathbf{q}}_1, \ldots, \widehat{\mathbf{q}}_c, \ldots, \widehat{\mathbf{q}}_C\} = \underset{\mathbf{q}_1,\ldots,\mathbf{q}_c,\ldots,\mathbf{q}_C}{\arg\min} \sum_{c=1}^{C}\sum_{k=1}^{K}\sum_{a=1}^{A} w_{c,a} f_{c,i_k}^{(a)} \tag{5.5}$$

where $\widehat{\mathbf{q}}_c$ is the optimized vector of $\mathbf{q}_c$. The optimization function is computed by summing over all the values of the KPIs, number i_k of neighboring target cells and cells. The advantage of the joint optimization is that it considers the intricate interactions and dependencies among the handover thresholds of different cells. However, in joint optimization there is a high risk that some individual cells show exceptionally bad performance which affects the same UEs. For mobile operators, it is not acceptable to have bad performance in some cells of the network as it may increases the churn rate. For these reasons, the joint optimization of the handover thresholds is replaced by the independent optimization where each cell optimizes its specific handover thresholds with respect to its own KPI statistics. The advantage of the independent optimization is that each cell can improve the mobility performance with respect to its corresponding cell-specific radio conditions. Moreover, the independent optimization does not require

any additional signaling messages between BSs and in turn it is less complex. The independent optimization problem of the handover thresholds is formulated as

$$\left\{\widehat{Q}_c^{(1)},\ldots,\widehat{Q}_c^{(m)},\ldots,\widehat{Q}_c^{(M)}\right\} = \underset{Q_c^{(1)},\ldots,Q_c^{(m)},\ldots,Q_c^{(M)}}{\arg\min} \sum_{k=1}^{K}\sum_{a=1}^{A} w_{c,a} f_{c,i_k}^{(a)} \quad \forall c \tag{5.6}$$

where $\widehat{Q}_c^{(m)}$ is the optimized value of $Q_c^{(m)}$.

For the cell-specific configuration, the handover threshold is used irrespective of the neighboring target cell. Consequently, the values of the KPIs in matrix $\mathbf{F}_c$ are not differentiated with respect to neighboring cells and they are summed up over index k resulting in vector

$$\boldsymbol{\ell}_c = \sum_{k=1}^{K} \mathbf{f}_{c,i_k} \in \mathbb{Z}^{A\times 1}. \tag{5.7}$$

Thus, each element of the vector $\boldsymbol{\ell}_c$ is the sum of the values of a KPI in cell c with respect to all neighboring cells. The procedure followed in manual optimization of the handover thresholds is imported to the automatic algorithm. In order to react on a specific value of a KPI, the experts identify first the handover threshold which needs to be tuned and then determine the action to be performed on the threshold, i.e., increase or decrease. Following the same approach, the total values of the KPIs in $\boldsymbol{\ell}_c$ are grouped into two correction directives: $D_c^{(+),m}$ and $D_c^{(-),m}$ which are the total number of mobility failure events that require an increase and a decrease, respectively, in the value of the threshold $Q_c^{(m)}$. The two correction directives are packed in vector $\mathbf{d}_m \in \mathbb{R}^{1\times 2}$, i.e.,

$$\mathbf{d}_m = \left[D_c^{(+),m}, D_c^{(-),m}\right]. \tag{5.8}$$

In order to obtain the vector $\mathbf{d}_m$ from $\boldsymbol{\ell}_c$, a matrix $\mathbf{G}_m$ should be designed to group the values of the KPIs into the aforementioned correction directives. By defining $\mathbf{G}_m \in \mathbb{R}^{A\times 2} = [\mathbf{g}_{1,m}, \mathbf{g}_{2,m}]$ where $\mathbb{R}$ is the set of real numbers, $\mathbf{d}_m$ can be computed as follows:

$$\boldsymbol{\ell}_c^{\mathrm{T}} \mathbf{G}_m = \mathbf{d}_m \tag{5.9}$$

where $(.)^{\mathrm{T}}$ is the transpose operator. The two vectors $\mathbf{g}_{1,m}$ and $\mathbf{g}_{2,m}$ of matrix $\mathbf{G}_m$ should be designed such that the weights of the KPI values are considered and each mobility failure event is not counted more than once. Thus, the constraint imposed on the design of matrix $\mathbf{G}_m$ can be written as

$$\sum_{m=1}^{M} (\mathbf{g}_{1,m} + \mathbf{g}_{2,m}) = \mathbf{w}_c \tag{5.10}$$

where $\mathbf{w}_c$ is the vector containing the weight of each KPIs value, see (5.2). Different designs for $\mathbf{G}_m$ exist. An efficient design for $\mathbf{G}_m$ is proposed in Section 5.6.4.

Using the correction directives of each handover threshold, the independent optimization problem which is formulated in (5.6) can now be decomposed into M sub-problems as follows:

$$\widehat{Q}_c^{(m)} = \underset{Q_c^{(m)}}{\arg\min} \left(D_c^{(+),m} + D_c^{(-),m} \right) \quad \forall m \text{ and } c. \tag{5.11}$$

Thus, each handover threshold is optimized with respect to the sum of its corresponding correction directives. It is shown in Appendix A.1 that

$$\sum_{k=1}^{K} \sum_{a=1}^{A} w_{c,a} f_{c,i_k}^{(a)} = \sum_{m=1}^{M} \left(D_c^{(+),m} + D_c^{(-),m} \right) \tag{5.12}$$

holds if the constraint of (5.10) is fulfilled.

5.4.2 Advantages and Limitations of Cell-Specific Optimization

5.4.2.1 Advantages over Initially Configured Network-Wide Setting

This section describes the advantages of the cell-specific optimization approach over the best network-wide setting which is configured initially during the network planning phase. The advantages of the cell-specific optimization approach can be illustrated using the two correction directives $D_c^{(+),m}$ and $D_c^{(-),m}$. In cell-specific optimization, the action on a handover threshold depends on the difference between the values of the two aforementioned correction directives. The possible actions which are performed on a handover threshold are either increase, decrease or do not change. Accordingly, the three cases are distinguished as follows:

Case 1: $D_c^{(+),m} >> D_c^{(-),m}$: The number of mobility failure events in cell c requiring an increase in the handover threshold $Q_c^{(m)}$ is much higher than that requiring a decrease. In this case, the handover threshold can be increased as it can well reduce the dominant number of mobility failure events requiring an increase in the handover threshold.

Case 2: $D_c^{(+),m} << D_c^{(-),m}$: The number of mobility failure events in cell c requiring a decrease in the handover threshold $Q_c^{(m)}$ is much higher than that requiring an increase. In this case, the handover threshold can be decreased as it can well reduce the dominant number of mobility failure events requiring a decrease in the handover threshold.

Case 3: $D_c^{(+),m} \approx D_c^{(-),m}$: The number of mobility failure events in cell c requiring an increase in the handover threshold $Q_c^{(m)}$ is approximately equal to that requiring a decrease. In this case, the correction directives require contradicting handover threshold

actions. Changing the threshold in one direction could decrease one of the correction directives more than the other one is increased, however, it would be difficult to predict the correct action. Moreover, the gain would be minimal, if it at all exists, since none of the correction directives can be well reduced without a significant increase in the other one. Thus, if the handover threshold is updated the correction directives would most likely start to oscillate. Reducing the oscillations in the values of the KPIs is an important aspect in SON as they directly impact the users. Therefore, the handover threshold is not changed.

The cell-specific optimization approach can achieve performance gains compared to the best network-wide setting of handover thresholds in cells belonging to cases 1 and 2 only. In these two cases, the handover thresholds can be tailored for each cell according to its specific mobility conditions. However, it is not necessary that all the mobility problems of the cells belonging to cases 1 and 2 are resolved. It can happen during the optimization that the correction directives become similar to each other as in case 3 and the handover threshold cannot be updated anymore. The optimization limitations of the cell-specific approach are discussed in the following section.

5.4.2.2 Optimization Limitations

Based on the analysis of Section 5.4.2.1, the set $\mathcal{C}$ of all cells in 3G and LTE networks can be decomposed in three disjoint sets based on the values of their corresponding correction directives. The three sets are defined as follows

$$\mathcal{U}^{(m)} = \left\{ c \in \mathcal{C} | D_c^{(+),m} >> D_c^{(-),m} \right\}, \tag{5.13}$$

$$\mathcal{V}^{(m)} = \left\{ c \in \mathcal{C} | D_c^{(+),m} << D_c^{(-),m} \right\}, \text{ and} \tag{5.14}$$

$$\mathcal{O}^{(m)} = \left\{ c \in \mathcal{C} | D_c^{(+),m} \approx D_c^{(-),m} \right\}. \tag{5.15}$$

The automatic optimization algorithm can react to the mobility problems of all cells belonging to sets $\mathcal{U}^{(m)}$ and $\mathcal{V}^{(m)}$ requiring an increase and decrease, respectively, in the handover threshold $Q_c^{(m)}$. The handover threshold $Q_c^{(m)}$ is not modified for all cells in set $\mathcal{O}^{(m)}$, and in turn their corresponding mobility problems cannot be resolved by the cell-specific optimization approach. To resolve the mobility problems of the cells in set $\mathcal{O}^{(m)}$, more degrees of freedom are needed in configuring the handover thresholds. Thus, the cell-specific optimization approach cannot react in any cell of the network if the sets $\mathcal{U}^{(m)}$ and $\mathcal{V}^{(m)}$ are empty for all the handover thresholds, i.e.,

$$\bigcup_{m=1}^{M} \left(\mathcal{U}^{(m)} \bigcup \mathcal{V}^{(m)} \right) = \emptyset. \tag{5.16}$$

In this case, the cell-specific optimization approach would have the same performance of the initially configured network-wide setting. However, it is unlikely that (5.16) holds in large networks having hundreds of cells. Therefore, the cell-specific optimization approach is expected to outperform the best network-wide setting.

5.5 Cell-Group Specific Optimization of Handover Thresholds

5.5.1 Motivation

The cell-specific optimization approach is convenient since it has few numbers of handover thresholds and counters and, therefore it is simple. However, the cell-specific optimization fails when the values of the correction directives are similar to each other, i.e., $D_c^{(+),m} \approx D_c^{(-),m}$. The mobility failure events of $D_c^{(+),m}$ can either occur with respect to the same or different target cells than those of $D_c^{(-),m}$. In the latter case, the mobility failure events can be resolved if the handover thresholds can be distinguished with respect to neighboring target cells. Configuring and optimizing dedicated thresholds with respect to a group of neighboring target cells is denoted by cell-group specific optimization of handover thresholds. This additional degree of freedom in the configuration of the handover thresholds should allow, in principle, to tackle more efficiently the mobility problems and achieve an inter-RAT MRO solution which is better than the cell-specific optimization approach.

5.5.2 Configuration of Handover Thresholds

In cell-group specific optimization, each handover threshold of cell c can be configured in principle with respect to a subset of the neighboring cells in set $\mathcal{N}_c$. For clarity, an example is depicted in Fig. 5.3 which shows the cell-specific and cell-group specific configurations of the handover thresholds of cell c with respect to neighbor cells. In Fig. 5.3(a), it is shown that in cell-specific configuration a single handover threshold $Q_c^{(m)}$ is configured with respect to all neighbor cells in set $\mathcal{N}_c$. In contrast, in cell-group specific configuration a dedicated handover threshold is configured with respect to a subset of neighbor cells as shown in Fig. 5.3(b). For each handover threshold m, different subsets of neighbor cells can be selected. In this example, the set $\mathcal{N}_c$ is decomposed in two disjoints subsets $\mathcal{S}_{c,1}^{(m)}$ and $\mathcal{S}_{c,2}^{(m)}$. As a result, two handover thresholds $Q_{c,1}^{(m)}$ and $Q_{c,2}^{(m)}$ are configured with respect to sets $\mathcal{S}_{c,1}^{(m)}$ and $\mathcal{S}_{c,2}^{(m)}$, respectively.

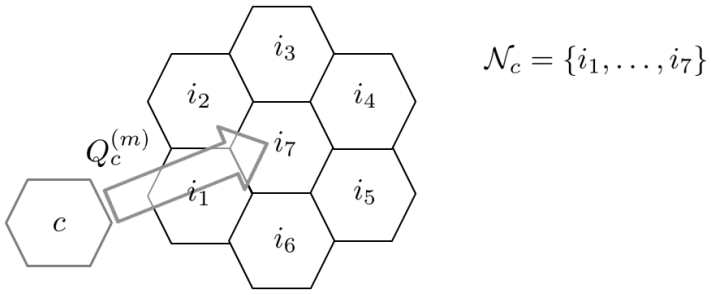

(a) Cell-specific configuration.

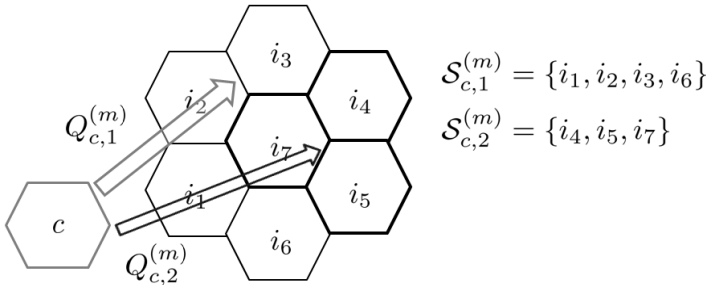

(b) Cell-group specific configuration.

Figure 5.3. Cell-specific and cell-group specific configurations of the handover threshold of cell c with respect to a subset of neighboring cells in set $\mathcal{N}_c$.

5.5.3 Formulation of the Optimization Problem

The formulation of the cell-group specific optimization problem follows the same approach which is used for cell-specific optimization in Section 5.4.1. For each handover threshold m, the set $\mathcal{N}_c$ of neighbors of cell c is decomposed into J_m disjoint subsets

$$\mathcal{S}_{c,j}^{(m)} \subseteq \mathcal{N}_c, \bigcup_{j=1}^{J_m} \mathcal{S}_{c,j}^{(m)} = \mathcal{N}_c, \bigcap_{j=1}^{J_m} \mathcal{S}_{c,j}^{(m)} = \emptyset \text{ and } \left|\mathcal{S}_{c,j}^{(m)}\right| \geq 1 \tag{5.17}$$

where $j \in \mathcal{J}_m$ is the index of the subset and $\mathcal{J}_m = \{1, \ldots, J_m\}$. The index for the elements of $\mathcal{S}_{c,j}^{(m)}$ is indicated by $v = 1, \ldots, V$ where V is the total number of elements. The v^{th} element of $\mathcal{S}_{c,j}^{(m)}$ is denoted by ζ_v, i.e.,

$$\mathcal{S}_{c,j}^{(m)} = \{\zeta_1, \ldots, \zeta_v, \ldots, \zeta_V\}. \tag{5.18}$$

In each KPI collection period κ, the values of the KPIs with respect to each neighbor of cell c are packed in matrix $\mathbf{F}_c \in \mathbb{Z}^{A \times K}$ which is defined in (5.3). The handover threshold $Q_{c,j}^{(m)}$ is optimized only with respect to the values of the KPIs corresponding to the neighboring cells in set $\mathcal{S}_{c,j}^{(m)}$. Therefore, a selection matrix $\mathbf{S}_{c,j}^{(m)} \in \mathbb{B}^{K \times V}$ where $\mathbb{B} = \{0, 1\}$ is used to retrieve the columns of $\mathbf{F}_c$ corresponding to the neighboring cells in $\mathcal{S}_{c,j}^{(m)}$. The columns which are selected by $\mathbf{S}_{c,j}^{(m)}$ are packed in matrix $\mathbf{R}_{c,j}^{(m)} \in \mathbb{Z}^{A \times V}$,

i.e.,

$$\mathbf{F}_c \mathbf{S}_{c,j}^{(m)} = \mathbf{R}_{c,j}^{(m)}. \tag{5.19}$$

For instance, consider the example depicted in Fig. 5.3(b). The two selections matrices $\mathbf{S}_{c,1}^{(m)}$ and $\mathbf{S}_{c,2}^{(m)}$ are

$$\mathbf{S}_{c,1}^{(m)} = \begin{bmatrix} 1 & 0 & 0 & 0 \\ 0 & 1 & 0 & 0 \\ 0 & 0 & 1 & 0 \\ 0 & 0 & 0 & 0 \\ 0 & 0 & 0 & 0 \\ 0 & 0 & 0 & 1 \\ 0 & 0 & 0 & 0 \end{bmatrix} \text{ and } \mathbf{S}_{c,2}^{(m)} = \begin{bmatrix} 0 & 0 & 0 \\ 0 & 0 & 0 \\ 0 & 0 & 0 \\ 1 & 0 & 0 \\ 0 & 1 & 0 \\ 0 & 0 & 0 \\ 0 & 0 & 1 \end{bmatrix}. \tag{5.20}$$

The matrix $\mathbf{R}_{c,j}^{(m)}$ is then expressed as

$$\mathbf{R}_{c,j}^{(m)} = [\mathbf{f}_{c,\zeta_1}, \ldots, \mathbf{f}_{c,\zeta_v}, \ldots, \mathbf{f}_{c,\zeta_V}] \tag{5.21}$$

where $\mathbf{f}_{c,\zeta_v}$ is the column containing the values of the KPIs in cell c with respect to neighboring cell ζ_v. As a single handover threshold is configured with respect to the neighboring cells in $\mathcal{S}_{c,j}^{(m)}$, the values of the KPIs in $\mathbf{R}_{c,j}^{(m)}$ are not differentiated between the selected neighboring cells. Thus, the values of the KPIs in $\mathbf{R}_{c,j}^{(m)}$ are summed up over the index v resulting in vector

$$\boldsymbol{\ell}_{c,j}^{(m)} = \sum_{v=1}^{V} \mathbf{f}_{c,\zeta_v} \in \mathbb{Z}^{A \times 1}. \tag{5.22}$$

Each element of $\boldsymbol{\ell}_{c,j}^{(m)}$ is the sum of all the values of a KPI with respect to all neighboring cells in set $\mathcal{S}_{c,j}^{(m)}$. Following the same approaches in Section 5.4, the values of the KPIs in $\boldsymbol{\ell}_{c,j}^{(m)}$ are grouped into two correction directives: $D_{c,j}^{(+),m}$ and $D_{c,j}^{(-),m}$ which are the total number of mobility failure events which require an increase and a decrease, respectively, of the value of the threshold $Q_{c,j}^{(m)}$. In order to obtain the correction directives, the same matrix $\mathbf{G}_m \in \mathbb{R}^{A \times 2} = [\mathbf{g}_{1,m}, \mathbf{g}_{2,m}]$ which is defined in Section 5.4 is used to group the values of the KPIs as follows:

$$\boldsymbol{\ell}_{c,j}^{(m)^{\mathrm{T}}} \mathbf{G}_m = \mathbf{d}_{c,j}^{(m)}, \tag{5.23}$$

where

$$\mathbf{d}_{c,j}^{(m)} = \left[D_{c,j}^{(+),m}, D_{c,j}^{(-),m} \right]. \tag{5.24}$$

Using the aforementioned correction directives, the independent optimization problem which is formulated in (5.6) can now be decomposed into $\sum_{m=1}^{M} J_m$ sub-problems as follows:

$$\widehat{Q}_{c,j}^{(m)} = \underset{Q_{c,j}^{(m)}}{\arg\min} \quad \left(D_{c,j}^{(+),m} + D_{c,j}^{(-),m} \right) \quad \forall m, j \text{ and } c. \tag{5.25}$$

Thus, each handover threshold $Q_{c,j}^{(m)}$ is optimized with respect to the sum of its corresponding correction directives. It is shown in Appendix A.2 that

$$\sum_{k=1}^{K}\sum_{a=1}^{A} w_{c,a} f_{c,i_k}^{(a)} = \sum_{m=1}^{M}\sum_{j=1}^{J_m}\left(D_{c,j}^{(+),m} + D_{c,j}^{(-),m}\right) \tag{5.26}$$

holds if the constraint of (5.10) is fulfilled.

The value of J_m determines the configuration type of the handover threshold as shown in Table 5.1. The cell-specific configuration of the handover thresholds is a special

Table 5.1. Three different handover threshold configurations based on the value of J_m.

Case	$\mathcal{S}_{c,j}^{(m)}$	$Q_{c,j}^{(m)}$	Optimization function	Configuration
$J_m = 1$	$\mathcal{N}_c$	$Q_c^{(m)}$	$\left(D_c^{(+),m} + D_c^{(-),m}\right)$	Cell-specific
$1 < J_m < \lvert\mathcal{N}_c\rvert$	$\mathcal{S}_{c,j}^{(m)}$	$Q_{c,j}^{(m)}$	$\left(D_{c,j}^{(+),m} + D_{c,j}^{(-),m}\right)$	Cell-group specific
$J_m = \lvert\mathcal{N}_c\rvert$	$\left\lvert\mathcal{S}_{c,j}^{(m)}\right\rvert = 1$	$Q_{c,j}^{(m)}$	$\left(D_{c,j}^{(+),m} + D_{c,j}^{(-),m}\right)$	Cell-pair specific

case of the cell-group specific configuration approach. If $J_m = 1$, the set $\mathcal{S}_{c,j}^{(m)} = \mathcal{N}_c$ and the handover threshold $Q_{c,j}^{(m)}$ is configured with respect to all neighboring cells. In this case, the matrix $\mathbf{S}_{c,j}^{(m)}$ is equal to the identity matrix $\mathbf{I} \in \mathbb{B}^{K\times K}$. On the other hand, if $J_m = |\mathcal{N}_c|$ then each set $\mathcal{S}_{c,j}^{(m)}$ consists of a single neighboring cell and the handover threshold $Q_{c,j}^{(m)}$ is configured with respect to each neighboring cell. In this case, the cell-group specific configuration approach is denoted by cell-pair specific. If $1 < J_m < |\mathcal{N}_c|$, then there exists at least one handover threshold $Q_{c,j}^{(m)}$ which is not configured with respect to a single neighboring cell. In this case, the configuration of the handover threshold is cell-group specific.

5.5.4 Advantages and Limitations of Cell-Group Specific Optimization

5.5.4.1 Comparison between Cell-Group Specific Serving and Target Cell Threshold Configuration

The cell-group specific configuration is not advantageous for all handover thresholds. Configuring the serving cell threshold in a cell-group specific way is risky as it may yield a high number of RACH failures which occur when the UE fails during the handover to connect to the target cell, see Section 2.6.

For clarity, an example is depicted in Fig. 5.4 which shows the serving cell c overlaying with neighboring cell i_1 and three other neighboring cells i_2, i_3 and i_4, i.e., the total number of neighbors is $K = 4$. In this example, the cell-pair specific configuration of the

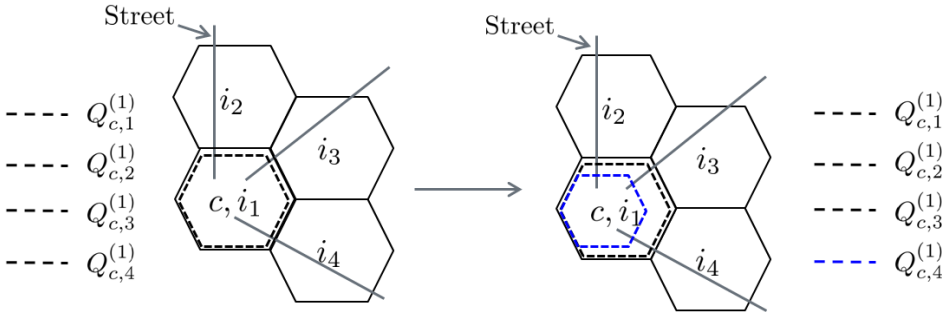

(a) The serving cell threshold $Q_{c,4}^{(1)}$ configured with respect to neighboring cell i_4 is increased.

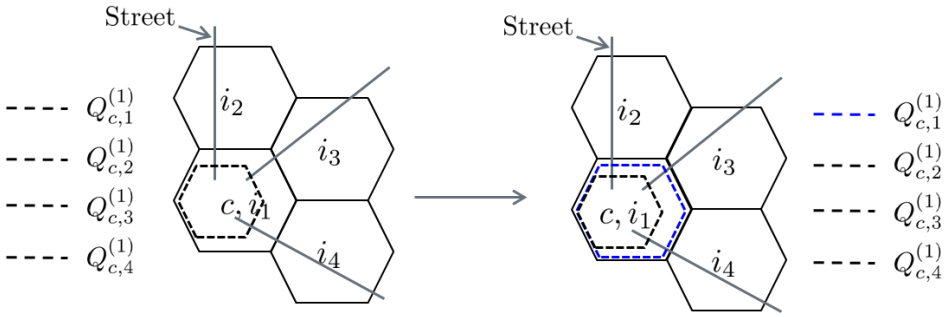

(b) The serving cell threshold $Q_{c,1}^{(1)}$ configured with respect to neighboring cell i_1 is decreased.

Figure 5.4. Increasing and decreasing the serving cell threshold in a cell-pair specific way.

handover threshold is considered. That is, the serving cell threshold $Q_{c,j}^{(1)}$ is configured with respect to each set $\mathcal{S}_{c,j}^{(1)}$ comprising a single neighboring cell, i.e., $J_1 = 4$. For instance, the threshold $Q_{c,1}^{(1)}$ is configured with respect to neighboring cell i_1, $Q_{c,2}^{(1)}$ with respect to neighboring cell i_2 and so on. The black or blue dashed line indicates the handover border of cell c corresponding to each serving cell threshold.

In Fig. 5.4(a), the serving cell threshold $Q_{c,4}^{(1)}$ configured with respect to neighboring cell i_4 is increased. The other serving cell thresholds are kept fixed. It is shown that increasing $Q_{c,4}^{(1)}$ does not only shift the handover border of cell c with respect to the street passing through neighboring cell i_4, but also with respect to other streets which are far from i_4. As $Q_{c,4}^{(1)}$ is higher than all other serving cell thresholds, there is a high risk that the UEs moving on all streets would try to handover first to neighboring cell i_4. However, the UEs moving on streets which are far from neighboring cell i_4 would most probably fail to access the target cell during the handover. In this case, the UEs would detect RACH failures and lose the connection.

The RACH failures may occur as well when the serving cell threshold is decreased cell-pair specifically. In Fig. 5.4(b), the serving cell threshold $Q_{c,1}^{(1)}$ configured with respect to neighboring cell i_1 is decreased while others are kept fixed. As $Q_{c,1}^{(1)}$ is smaller than other three thresholds, the UEs would try first to handover to neighboring cells i_2, i_3 and i_4 instead of i_1. However, these UEs are far from the BSs serving cells i_2, i_3 and i_4, and, consequently, they would fail to access these neighboring cells during the handover. Thus, also in this case the UE detects a RACH failure.

In contrast to the serving cell threshold, the configuration of the target cell threshold in a cell-pair specific way does not lead to RACH failures. The reason is that increasing or decreasing the target cell threshold affects only the handover border of the neighboring cell rather than that of the serving cell. This is illustrated in Fig. 5.5 which shows a serving cell c and four other neighboring cells. The black or blue line indicates the

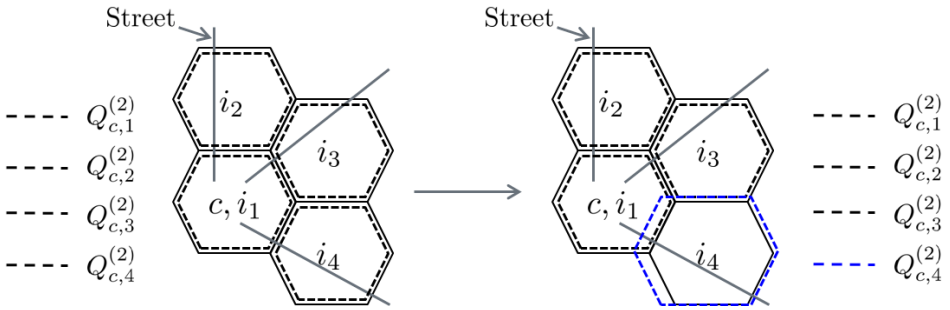

(a) The target cell threshold $Q_{c,4}^{(2)}$ configured with respect to neighboring cell i_4 is decreased.

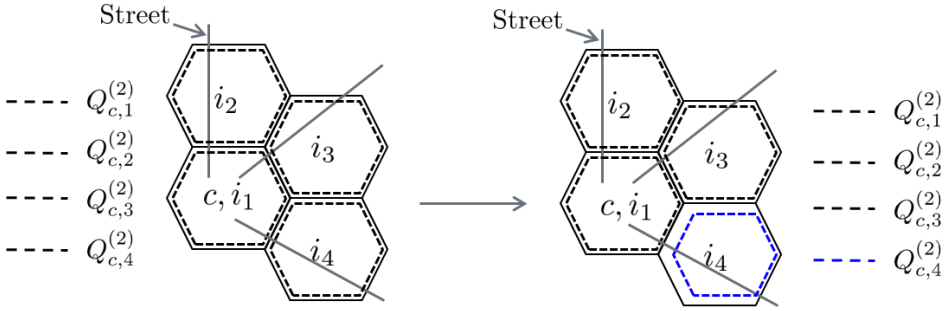

(b) The target cell threshold $Q_{c,4}^{(2)}$ configured with respect to neighboring cell i_4 is increased.

Figure 5.5. Decreasing and increasing the target cell threshold in a cell-pair specific way.

handover border of a neighboring cell corresponding to a target cell threshold. It is shown in Fig. 5.5(a) that decreasing the target cell threshold $Q_{c,4}^{(2)}$ expands the handover border of the neighboring cell i_4 without affecting other streets or neighboring cells. Similarly, it is shown in Fig. 5.5(b) that increasing the target cell threshold $Q_{c,4}^{(2)}$ affects only the handover border of the neighboring cell i_4. Thus, the cell-group specific con-

figuration of the target cell threshold can be beneficial and provide additional degrees of freedom for resolving the mobility problems as explained in the next section.

5.5.4.2 Advantages over Cell-Specific Optimization

In this section, the advantages of optimizing the target cell threshold in cell-group specific way over cell-specific is highlighted analytically. The target cell threshold $m = 2$ of (2.32) is optimized with respect to the sum $\Psi(\kappa)$ of its corresponding correction directives in KPI collection period κ. Using (5.12) and (5.26), the sum $\Psi(\kappa)$ is expressed in KPI collection period κ as

$$\Psi(\kappa) = D_c^{(+),2}(\kappa) + D_c^{(-),2}(\kappa) = \sum_{j=1}^{J_2} \left(D_{c,j}^{(+),2}(\kappa) + D_{c,j}^{(-),2}(\kappa) \right) \tag{5.27}$$

where J_2 is the total number of selected subsets $\mathcal{S}_{c,j}^{(2)}$ for target cell threshold. Moreover, as the matrix $\mathbf{G}_2$ of (5.9) and (5.23) used to derive the correction directives of the target cell threshold is common for both optimization approaches, the following equalities hold:

$$D_c^{(+),2}(\kappa) = \sum_{j=1}^{J_2} D_{c,j}^{(+),2}(\kappa) \text{ and} \tag{5.28}$$

$$D_c^{(-),2}(\kappa) = \sum_{j=1}^{J_2} D_{c,j}^{(-),2}(\kappa). \tag{5.29}$$

The aim is to analyze the impact on $\Psi(\kappa)$ when the target cell threshold is updated in cell-specific or cell-group specific way. For this purpose, the value of $\Psi(\kappa)$ in the next period $\kappa + 1$ is expressed in terms of the correction directives of the current and next collection periods for both optimization approaches. In the following, the expression of $\Psi(\kappa)$ is derived first for the cell-specific optimization approach then for cell-group specific optimization.

The sum of $D_{c,j}^{(+),2}(\kappa)$ and $D_{c,j}^{(-),2}(\kappa)$ is upper bounded by the total number $H_{c,j}^{(2)}(\kappa)$ of missed (TLHs) and successful handovers from cell c with respect to neighboring cells of set $\mathcal{S}_{c,j}^{(2)}$, i.e.,

$$\left(D_{c,j}^{(+),2}(\kappa) + D_{c,j}^{(-),2}(\kappa) \right) \leq H_{c,j}^{(2)}(\kappa) \ \forall j. \tag{5.30}$$

Any successful handover is counted as a mobility failure event if the UE detects an RLF shortly after, i.e., TEH or HWC.

The set $\mathcal{J}_2$ of indices for the subsets $\mathcal{S}_{c,j}^{(m)}$ of neighboring cells is decomposed in three disjoint sets as follows

$$\mathcal{U}_c^{(2)} = \left\{ j \in \mathcal{J}_2 | D_{c,j}^{(+),2}(\kappa) >> D_{c,j}^{(-),2}(\kappa) \right\}, \tag{5.31}$$

$$\mathcal{V}_c^{(2)} = \left\{ j \in \mathcal{J}_2 | D_{c,j}^{(+),2}(\kappa) << D_{c,j}^{(-),2}(\kappa) \right\}, \text{ and} \tag{5.32}$$

$$\mathcal{O}_c^{(2)} = \left\{ j \in \mathcal{J}_2 | D_{c,j}^{(+),2}(\kappa) \approx D_{c,j}^{(-),2}(\kappa) \right\}. \tag{5.33}$$

The sets $\mathcal{U}_c^{(2)}$, $\mathcal{V}_c^{(2)}$ and $\mathcal{O}_c^{(2)}$ contain the indices of the subsets $\mathcal{S}_{c,j}^{(2)}$ of neighboring cells requiring an increase, decrease and no change, respectively, in $Q_{c,j}^{(2)}$. Using these sets, the sum $\Psi(\kappa)$ in (5.27) can be rewritten as

$$\begin{aligned}\Psi(k) = &\sum_{\mu \in \mathcal{U}_c^{(2)}} \left(D_{c,\mu}^{(+),2}(\kappa) + D_{c,\mu}^{(-),2}(\kappa) \right) + \sum_{\nu \in \mathcal{V}_c^{(2)}} \left(D_{c,\nu}^{(+),2}(\kappa) + D_{c,\nu}^{(-),2}(\kappa) \right) \\ &+ \sum_{o \in \mathcal{O}_c^{(2)}} \left(D_{c,o}^{(+),2}(\kappa) + D_{c,o}^{(-),2}(\kappa) \right). \end{aligned} \tag{5.34}$$

In cell-specific optimization, the handover threshold is updated based on the difference in the values of the correction directives $D_c^{(+),2}(\kappa)$ and $D_c^{(-),2}(\kappa)$ as described in Section 5.4.2.1. Three cases are distinguished as follows.

1. $D_c^{(+),2}(\kappa) >> D_c^{(-),2}(\kappa)$: In this case, $D_c^{(+),2}(\kappa)$ is dominant in the cell and the handover threshold $Q_{c,j}^{(2)}$ is increased. This action on the handover threshold aims at reducing $D_c^{(+),2}(\kappa)$ in the cell which is the sum of $D_{c,j}^{(+),2}(\kappa)$ over index j. Thus, $D_{c,j}^{(+),2}(\kappa+1)$ can be expressed as

$$D_{c,j}^{(+),2}(\kappa+1) = \Delta_{c,j}^{(+),2} \cdot D_{c,j}^{(+),2}(\kappa) \quad \forall j \tag{5.35}$$

where the factor $\Delta_{c,j}^{(+),2} \geq 0$. In the best case, all the mobility failure events of $D_{c,j}^{(+),2}(\kappa+1)$ are resolved, i.e., $\Delta_{c,j}^{(+),2} = 0$.

Reducing $D_c^{(+),2}(\kappa+1)$ might lead to an increase in $D_c^{(-),2}(\kappa+1)$ as both correction directives require contradicting threshold actions to be performed on the same handover threshold $Q_c^{(2)}$. The correction directive $D_{c,j}^{(-),2}(\kappa+1)$ can be expressed as a fraction of the residual number of missed and successful handovers as

$$\begin{aligned} D_{c,j}^{(-),2}(\kappa+1) &= \lambda_{c,j}^{(-),2} \cdot \left(H_{c,j}^{(2)}(\kappa+1) - D_{c,j}^{(+),2}(\kappa+1) \right) \\ &= \lambda_{c,j}^{(-),2} \cdot R_{c,j}^{(-),2}(\kappa+1) \quad \forall j \end{aligned} \tag{5.36}$$

where the factor $0 \leq \lambda_{c,j}^{(-),2} \leq 1$. The factor $\lambda_{c,j}^{(-),2}$ is upper bounded by 1 since the sum of the correction directives cannot be higher than $H_{c,j}^{(2)}(\kappa+1)$ of (5.30).

Using (5.34), (5.35) and (5.36), the sum $\Psi(\kappa+1)$ in collection period $\kappa+1$ can be expressed in this case as

$$\begin{aligned}\Psi(k+1) = &\sum_{\mu\in\mathcal{U}_c^{(2)}} \left(\Delta_{c,\mu}^{(+),2}\cdot D_{c,\mu}^{(+),2}(\kappa) + \lambda_{c,\mu}^{(-),2}\cdot R_{c,\mu}^{(-),2}(\kappa+1)\right)\\ &+ \sum_{\nu\in\mathcal{V}_c^{(2)}} \left(\Delta_{c,\nu}^{(+),2}\cdot D_{c,\nu}^{(+),2}(\kappa) + \lambda_{c,\nu}^{(-),2}\cdot R_{c,\nu}^{(-),2}(\kappa+1)\right)\\ &+ \sum_{o\in\mathcal{O}_c^{(2)}} \left(\Delta_{c,o}^{(+),2}\cdot D_{c,o}^{(+),2}(\kappa) + \lambda_{c,o}^{(-),2}\cdot R_{c,o}^{(-),2}(\kappa+1)\right). \end{aligned} \tag{5.37}$$

It is shown in (5.37) that increasing the target cell threshold cell-specifically is proper with respect to all the neighboring cells of subsets $\mathcal{S}_{c,j}^{(2)}\Big|_{j\in\mathcal{U}_c^{(2)}}$. However, this handover threshold update is inappropriate with respect to neighboring cells of subsets $\mathcal{S}_{c,j}^{(2)}\Big|_{j\in\mathcal{V}_c^{(2)}}$. This is because $D_{c,j}^{(-),2}(\kappa)\Big|_{j\in\mathcal{V}_c^{(2)}}$ is dominant with respect to these neighboring cells, and consequently the target cell threshold should be decreased. Hence, increasing $Q_c^{(2)}$ may even degrade the mobility conditions with respect to the neighboring cells of subsets $\mathcal{S}_{c,j}^{(2)}\Big|_{j\in\mathcal{V}_c^{(2)}}$. In addition, the target cell threshold should not be modified with respect to the neighboring cells of subsets $\mathcal{S}_{c,j}^{(2)}\Big|_{j\in\mathcal{O}_c^{(2)}}$ because none of their corresponding correction directives can be well reduced without a significant increase in one of them.

2. $D_c^{(+),2}(\kappa) << D_c^{(-),2}(\kappa)$: In this case, $D_c^{(-),2}(\kappa)$ is dominant in the cell and the handover threshold $Q_{c,j}^{(2)}$ is decreased. This action on the handover threshold aims at reducing $D_c^{(-),2}(\kappa)$ in the cell which is the sum of $D_{c,j}^{(-),2}(\kappa)$ over index j. Thus, $D_{c,j}^{(-),2}(\kappa+1)$ can be expressed as

$$D_{c,j}^{(-),2}(\kappa+1) = \Delta_{c,j}^{(-),2}\cdot D_{c,j}^{(-),2}(\kappa) \quad \forall j \tag{5.38}$$

where the factor $\Delta_{c,j}^{(-),2} \geq 0$.

Similar to the previous case, reducing $D_c^{(-),2}(\kappa+1)$ might lead to an increase in $D_c^{(+),2}(\kappa+1)$. The correction directive $D_{c,j}^{(+),2}(\kappa+1)$ can be expressed as a fraction of the residual number of missed and successful handovers as

$$\begin{aligned} D_{c,j}^{(+),2}(\kappa+1) &= \lambda_{c,j}^{(+),2}\cdot\left(H_{c,j}^{(2)}(\kappa+1) - D_{c,j}^{(-),2}(\kappa+1)\right)\\ &= \lambda_{c,j}^{(+),2}\cdot R_{c,j}^{(+),2}(\kappa+1) \quad \forall j \end{aligned} \tag{5.39}$$

where the factor $0 \leq \lambda_{c,j}^{(+),2} \leq 1$.

Using (5.34), (5.38) and (5.39), the sum $\Psi(\kappa+1)$ in period $\kappa+1$ can be expressed

in this case as

$$\begin{aligned}\Psi(\kappa+1) = &\sum_{\mu\in\mathcal{U}_c^{(2)}} \left(\lambda_{c,\mu}^{(+),2}\cdot R_{c,\mu}^{(+),2}(\kappa+1) + \Delta_{c,\mu}^{(-),2}\cdot D_{c,\mu}^{(-),2}(\kappa)\right)\\ &+ \sum_{\nu\in\mathcal{V}_c^{(2)}} \left(\lambda_{c,\nu}^{(+),2}\cdot R_{c,\nu}^{(+),2}(\kappa+1) + \Delta_{c,\nu}^{(-),2}\cdot D_{c,\nu}^{(-),2}(\kappa)\right)\\ &+ \sum_{o\in\mathcal{O}_c^{(2)}} \left(\lambda_{c,o}^{(+),2}\cdot R_{c,o}^{(+),2}(\kappa+1) + \Delta_{c,o}^{(-),2}\cdot D_{c,o}^{(-),2}(\kappa)\right). \end{aligned} \tag{5.40}$$

It is shown in (5.40) that decreasing the target cell threshold cell-specifically is proper with respect to all the neighboring cells of subsets $\mathcal{S}_{c,j}^{(2)}\Big|_{j\in\mathcal{V}_c^{(2)}}$. However, this handover threshold update is inappropriate with respect to neighboring cells of subsets $\mathcal{S}_{c,j}^{(2)}\Big|_{j\in\mathcal{U}_c^{(2)}}$. This is because $D_{c,j}^{(+),2}(\kappa)\Big|_{j\in\mathcal{U}_c^{(2)}}$ is dominant with respect to these neighboring cells, and consequently the target cell threshold should be increased. Hence, decreasing $Q_c^{(2)}$ may even degrade the mobility conditions with respect to the neighboring cells of subsets $\mathcal{S}_{c,j}^{(2)}\Big|_{j\in\mathcal{U}_c^{(2)}}$. In addition, the target cell threshold should not be modified with respect to the neighboring cells of subsets $\mathcal{S}_{c,j}^{(2)}\Big|_{j\in\mathcal{O}_c^{(2)}}$ because none of their corresponding correction directives can be well reduced without a significant increase in one of them.

3. $D_c^{(+),2}(\kappa) \approx D_c^{(-),2}(\kappa)$: In this case, the cell c does not modify the target cell threshold $Q_c^{(2)}$. In principle, $D_c^{(+),2}(\kappa+1)$ and $D_c^{(-),2}(\kappa+1)$ should be equal to the previous values of $D_c^{(+),2}(\kappa)$ and $D_c^{(-),2}(\kappa)$, respectively. However, they might be different if other neighboring cells have updated their handover thresholds leading to a shift in cell borders in the next period. Therefore, the sum of $D_c^{(+),2}(\kappa+1)$ and $D_c^{(-),2}(\kappa+1)$ can be expressed in general as a fraction of $H_{c,j}^{(2)}(\kappa)$ as follows

$$\left(D_{c,j}^{(+),2}(\kappa+1) + D_{c,j}^{(-),2}(\kappa+1)\right) = \lambda_{c,j}^{(2)}\cdot H_{c,j}^{(2)}(\kappa+1)\ \forall j \tag{5.41}$$

where the factor $0 \le \lambda_{c,j}^{(2)} \le 1$. Keeping the target cell threshold unchanged is a proper action with respect to neighboring cells of subsets $\mathcal{S}_{c,j}^{(2)}\Big|_{j\in\mathcal{O}_c^{(2)}}$. However, this action is inappropriate with respect to neighboring cells of subsets $\mathcal{S}_{c,j}^{(2)}\Big|_{j\in\mathcal{U}_c^{(2)}}$ and $\mathcal{S}_{c,j}^{(2)}\Big|_{j\in\mathcal{V}_c^{(2)}}$ where one of the correction directives is dominant, and consequently their corresponding target cell thresholds should be increased or decreased, respectively. This case $D_c^{(+),2}(\kappa) \approx D_c^{(-),2}(\kappa)$ is the most critical in cell-specific optimization since the automatic algorithm cannot react to the mobility problems of neighboring cells of both subsets of $\mathcal{S}_{c,j}^{(2)}\Big|_{j\in\mathcal{U}_c^{(2)}}$ and $\mathcal{S}_{c,j}^{(2)}\Big|_{j\in\mathcal{V}_c^{(2)}}$.

In contrast to cell-specific optimization, a dedicated handover threshold is configured with respect to each subset of neighboring cells in cell-group specific optimization. Consequently, the appropriate target cell threshold action can be performed with respect

to neighboring cells of each subset: The target cell threshold is increased with respect to neighboring cells of subset $\mathcal{S}_{c,j}^{(2)}\Big|_{j\in\mathcal{U}_c^{(2)}}$, decreased with respect to neighboring cells of $\mathcal{S}_{c,j}^{(2)}\Big|_{j\in\mathcal{V}_c^{(2)}}$, not changed with respect to neighboring cells of $\mathcal{S}_{c,j}^{(2)}\Big|_{j\in\mathcal{O}_c^{(2)}}$. In cell-group specific optimization, the sum $\Psi(\kappa+1)$ in collection period $\kappa+1$ can be written as

$$\begin{aligned}\Psi(\kappa+1) = &\sum_{\mu\in\mathcal{U}_c^{(2)}} \left(\Delta_{c,\mu}^{(+),2}\cdot D_{c,\mu}^{(+),2}(\kappa) + \lambda_{c,\mu}^{(-),2}\cdot R_{c,\mu}^{(-),2}(\kappa+1)\right)\\ &+ \sum_{\nu\in\mathcal{V}_c^{(2)}} \left(\lambda_{c,\nu}^{(+),2}\cdot R_{c,\nu}^{(+),2}(\kappa+1) + \Delta_{c,\nu}^{(-),2}\cdot D_{c,\nu}^{(-),2}(\kappa)\right)\\ &+ \sum_{o\in\mathcal{O}_c^{(2)}} \lambda_{c,o}^{(2)}\cdot H_{c,o}^{(2)}(\kappa+1). \end{aligned} \tag{5.42}$$

Thus, as opposed to cell-specific optimization, the cell-group specific approach can tackle the mobility failure events with respect to neighboring cells of $\mathcal{S}_{c,j}^{(2)}\Big|_{j\in\mathcal{U}_c^{(2)}}$ and $\mathcal{S}_{c,j}^{(2)}\Big|_{j\in\mathcal{V}_c^{(2)}}$ even when $D_c^{(+),2}(\kappa)\approx D_c^{(-),2}(\kappa)$.

5.5.4.3 Optimization Limitations

A handover threshold $Q_{c,j}^{(m)}$ that is configured cell-group specifically cannot be adjusted by the automatic optimization algorithm if its corresponding correction directives are similar to each other, i.e.,

$$D_{c,j}^{(+),m} \approx D_{c,j}^{(-),m}. \tag{5.43}$$

In this case, the mobility failure events occurring with respect to the subset $\mathcal{S}_{c,j}^{(m)}$ of neighboring cells require contradicting actions to be performed on the same handover threshold $Q_{c,j}^{(m)}$, and consequently none of the correction directives can be well reduced without a significant increase in one of them. As it is shown in Section 5.5.4.1 that only the configuration of the target cell threshold in cell-group specific way is beneficial, the optimization limitation in (5.43) holds only for the target cell threshold, i.e., $m=2$. If the serving cell threshold $m=1$ is configured in cell-specific way as it should be, the automatic algorithm cannot update the serving cell threshold when

$$D_c^{(+),1} \approx D_c^{(-),1}. \tag{5.44}$$

In this case, the mobility failure events occurring with respect to all neighboring cells require contradicting actions to be performed on the same serving cell threshold $Q_c^{(1)}$.

5.6 Optimization Loop of Handover Thresholds

5.6.1 Introduction

The optimization loop of the inter-RAT handover thresholds is shown in Fig. 5.6. It is carried out independently per each cell of LTE and 3G networks. In each KPI collection

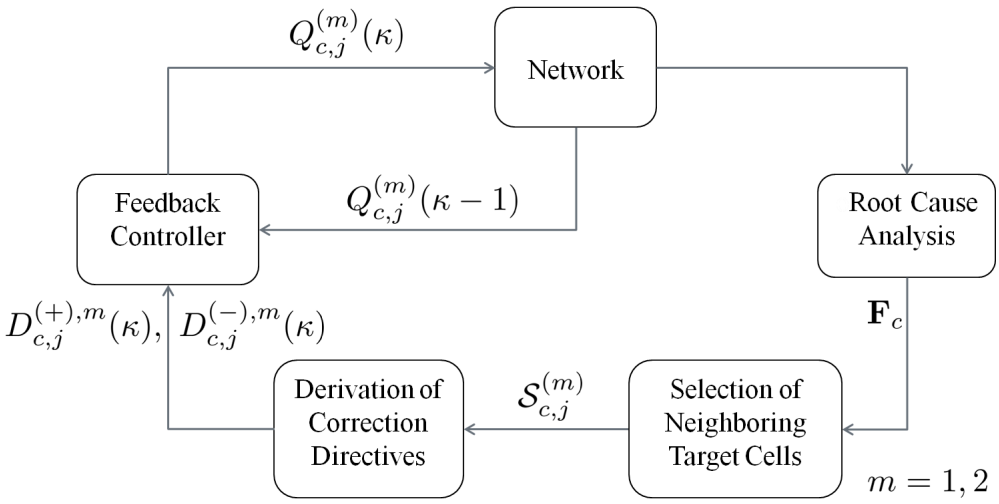

Figure 5.6. The optimization loop of the inter-RAT handover thresholds.

period, a root cause analysis is performed by each cell for the collected mobility failure events. Then, the subsets $\mathcal{S}_{c,j}^{(m)}$ of (5.17) are selected for each handover threshold m. Using these subsets, the two correction directives $D_{c,j}^{(+),m}(\kappa)$ and $D_{c,j}^{(-),m}(\kappa)$ of (5.23) are computed for KPI collection period κ. Next, the new handover threshold $Q_{c,j}^{(m)}(\kappa)$ is calculated by the feedback controller based on the two correction directives and the previous handover threshold $Q_{c,j}^{(m)}(\kappa-1)$. The optimization loop is repeated until the algorithm converges.

5.6.2 Root Cause Analysis

Each cell updates its corresponding handover thresholds based on the values of the KPIs which are collected periodically during time interval T_{CL}. The mobility failure events are counted by the responsible cell of which the misconfiguration of its handover thresholds is the root cause for those failures as explained in Section 5.2. The values of the KPIs collected by cell c with respect to each k^{th} inter-RAT neighboring cell i_k are packed in the matrix $\mathbf{F}_c$ of (5.3). In each KPI collection period κ, a new matrix $\mathbf{F}_c$ is obtained by each cell c.

5.6.3 Selection of Neighboring Target Cells for Handover Thresholds

After the root cause analysis, the collection of the values of the KPIs is stopped and the subsets $\mathcal{S}_{c,j}^{(m)}$ of neighboring target cells are selected for each handover threshold m. The same subsets are used in each KPI collection period for each handover threshold. The serving and target cell handover thresholds can be configured either in cell-specific or cell-group specific way. In the latter case, a dedicated value of the handover threshold m is configured with respect to each subset $\mathcal{S}_{c,j}^{(m)}$ of neighboring cells as explained in Section 5.5.3. Typically, the set of neighboring cells $\mathcal{N}_c$ is decomposed such that each subset $\mathcal{S}_{c,j}^{(m)}$ consists of a single neighboring cell, i.e., $J_m = |\mathcal{N}_c|$. This case corresponds to the cell-pair specific optimization approach. If the handover threshold is configured cell-specifically, there is only one subset $\mathcal{S}_{c,j}^{(m)}$ which is set to $\mathcal{N}_c$, i.e., $J_m = 1$ since the same value of the handover threshold is configured with respect to all inter-RAT neighbors of cell c.

5.6.4 Derivation of Correction Directives for Handover Thresholds

Having obtained $\mathbf{F}_c$ and decided on the subsets $\mathcal{S}_{c,j}^{(m)}$, the correction directives $D_{c,j}^{(+),m}$ and $D_{c,j}^{(-),m}$ can be computed using (5.23). For this purpose, the matrix $\mathbf{G}_m \in \mathbb{R}^{A\times 2} = [\mathbf{g}_{1,m}, \mathbf{g}_{2,m}]$ needs to be designed for each handover threshold m. The total number of inter-RAT KPIs is $A = 6$ and each KPI has a weight $0 \leq w_{c,a} \leq 1$. The index $a = 1, 2, 3, 4, 5$ and 6 is used for TLH-1, TLH-2, TEH, HWC, PP and UH, respectively. The numbers of RLFs should be minimized as they have a direct impact on the user perception. Thus, the weights of the values of TLH-1, TLH-2, TEH and HWC KPIs are all set to the highest value 1. As for PPs and UHs, they are successful handovers which impact the users less than RLFs. However, PPs incur a lot of signaling overhead and reducing them is important for mobile operators. The values of the PP and UH KPIs are given the weights $0 \leq w_{\mathrm{PP}} \leq 0$ and w_{UH}, respectively. The number of UHs in a cell has lower priority than RLFs and should be minimized only if no TLHs exist [3GP12f]. Accordingly, in each KPI collection period the weight w_{UH} of cell c is set as follows:

$$w_{\mathrm{UH}} = \begin{cases} 1, & \text{if no TLHs in cell } c \text{ with respect to neighboring cells of set } \mathcal{S}_{c,j}^{(1)} \\ 0, & \text{otherwise.} \end{cases} \tag{5.45}$$

The values of the KPIs which are grouped into the correction directives corresponding to serving cell threshold $Q_{c,j}^{(1)}$ are shown in Fig. 5.7. The value of the weight $w_{c,a}$ is

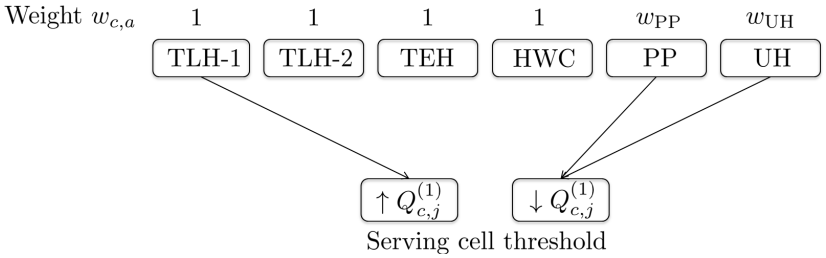

Figure 5.7. Values of the KPIs which are grouped into the correction directives corresponding to serving cell threshold $Q_{c,j}^{(1)}$.

shown for each KPI value. For instance, the weight of the first 4 KPI values is 1. By definition, a TLH of type 1 is resolved by increasing the serving cell threshold. A PP can be resolved by delaying the first inter-RAT handover. This can be achieved by decreasing the serving cell threshold. Similarly, an UH is resolved by decreasing $Q_{c,j}^{(1)}$ and keeping the UE longer in the LTE network.

The values of the KPIs which are grouped into the correction directives corresponding to target cell threshold $Q_{c,j}^{(2)}$ are shown in Fig. 5.8. By definition, a TLH of type 2 is resolved by decreasing $Q_{c,j}^{(2)}$. For TEH and HWC, the RLF occurs in the target neighboring cell. Thus, $Q_{c,j}^{(2)}$ should be increased in order to guarantee that the signal of the target cell is strong enough. In addition to decreasing $Q_{c,j}^{(1)}$, a PP can be resolved as well by increasing $Q_{c,j}^{(2)}$ and delaying the first inter-RAT handover.

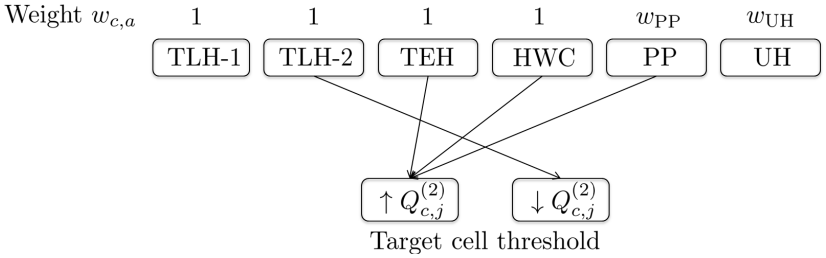

Figure 5.8. Values of the KPIs which are grouped into the correction directives corresponding to target cell threshold $Q_{c,j}^{(2)}$.

Using Fig. 5.7 and Fig. 5.8, the matrices $\mathbf{G}_1$ and $\mathbf{G}_2$ of (5.23) corresponding to $Q_{c,j}^{(1)}$ and $Q_{c,j}^{(2)}$ thresholds, respectively, can be expressed as follows

$$\mathbf{G}_1 = \begin{bmatrix} 1 & 0 \\ 0 & 0 \\ 0 & 0 \\ 0 & 0 \\ 0 & w_{\text{PP}}/2 \\ 0 & w_{\text{UH}} \end{bmatrix} \text{ and } \mathbf{G}_2 = \begin{bmatrix} 0 & 0 \\ 0 & 1 \\ 1 & 0 \\ 1 & 0 \\ w_{\text{PP}}/2 & 0 \\ 0 & 0 \end{bmatrix}. \tag{5.46}$$

The proposed design of $\mathbf{G}_1$ and $\mathbf{G}_2$ fulfills the constraint of (5.10), i.e., $\sum_{m=1}^{M}(\mathbf{g}_{1,m}+\mathbf{g}_{2,m})=\mathbf{w}_c$.

5.6.5 Correction of the Values of Handover Thresholds using Feedback Controller

5.6.5.1 Introduction

The feedback controller, which is shown in Fig. 5.6, is composed of two components: A proportional control block and a gain scheduler as depicted in Fig. 5.9. The handover threshold $Q_{c,j}^{(m)}(\kappa)$ of period κ is computed based on the values of the two correction directives $D_{c,j}^{(+),m}(\kappa)$ and $D_{c,j}^{(-),m}(\kappa)$ and the previous handover threshold $Q_{c,j}^{(m)}(\kappa-1)$ of KPI collection period $\kappa-1$. The change in handover threshold $Q_{c,j}^{(m)}(\kappa)$ is denoted

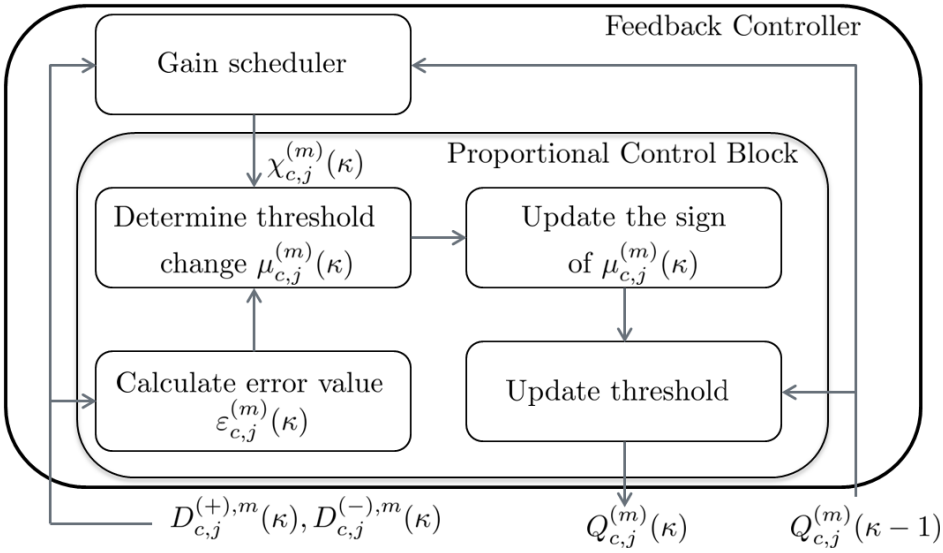

Figure 5.9. The feedback controller consisting of a proportional control block and a gain scheduler.

by $\mu_{c,j}^{(m)}(\kappa)$ which is expressed in dB. The threshold $Q_{c,j}^{(m)}(\kappa)$ is increased or decreased by $\mu_{c,j}^{(m)}(\kappa)$ only if one or both correction directives $D_{c,j}^{(+),m}(\kappa)$ and $D_{c,j}^{(-),m}(\kappa)$ exceed a certain limit denoted by $D_{\mathrm{thr}}^{(\mathrm{min})}$. The value of $D_{\mathrm{thr}}^{(\mathrm{min})}$ depends mainly on the time interval T_{CL} as well as the number of handover attempts in the cell, i.e., the number of TLHs and successful handovers. The threshold $D_{\mathrm{thr}}^{(\mathrm{min})}$ should be set high enough so that the correction directives can be considered statistically significant and in turn avoid reacting on outliers.

The value of $\mu_{c,j}^{(m)}(\kappa)$ depends on the difference between $D_{c,j}^{(+),m}(\kappa)$ and $D_{c,j}^{(-),m}(\kappa)$ as shown in Fig. 5.10. The larger the difference between the correction directives, the

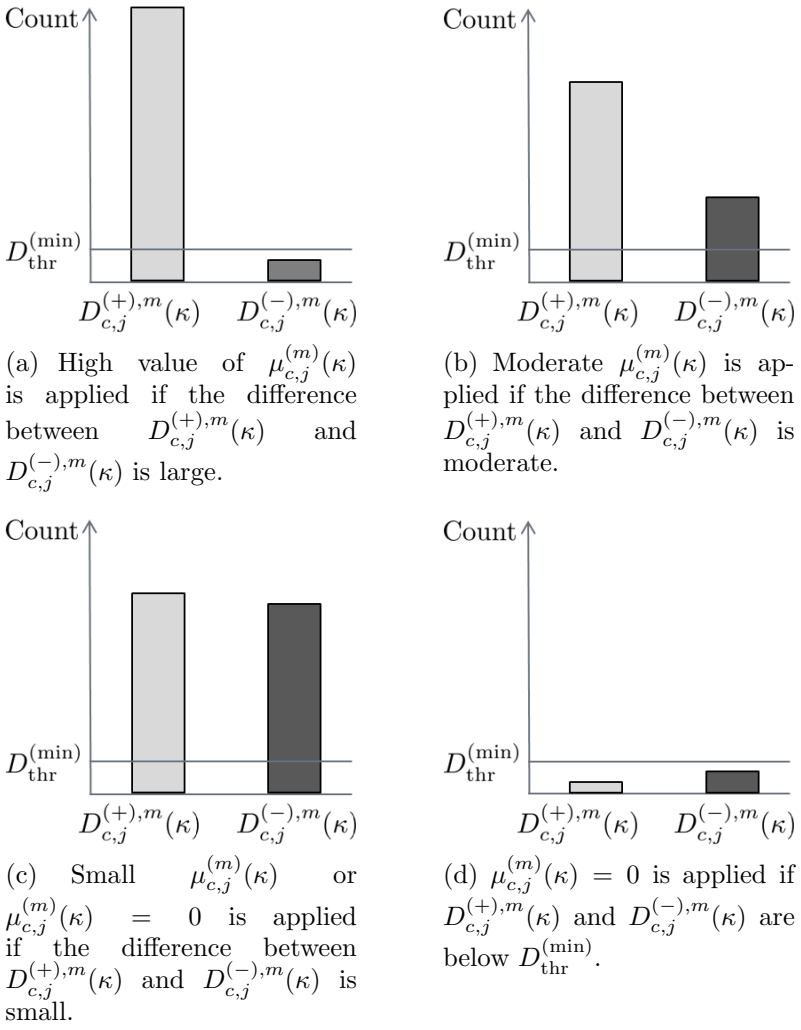

(a) High value of $\mu_{c,j}^{(m)}(\kappa)$ is applied if the difference between $D_{c,j}^{(+),m}(\kappa)$ and $D_{c,j}^{(-),m}(\kappa)$ is large.

(b) Moderate $\mu_{c,j}^{(m)}(\kappa)$ is applied if the difference between $D_{c,j}^{(+),m}(\kappa)$ and $D_{c,j}^{(-),m}(\kappa)$ is moderate.

(c) Small $\mu_{c,j}^{(m)}(\kappa)$ or $\mu_{c,j}^{(m)}(\kappa) = 0$ is applied if the difference between $D_{c,j}^{(+),m}(\kappa)$ and $D_{c,j}^{(-),m}(\kappa)$ is small.

(d) $\mu_{c,j}^{(m)}(\kappa) = 0$ is applied if $D_{c,j}^{(+),m}(\kappa)$ and $D_{c,j}^{(-),m}(\kappa)$ are below $D_{\text{thr}}^{(\text{min})}$.

Figure 5.10. The value of $\mu_{c,j}^{(m)}(\kappa)$ depends on the difference between $D_{c,j}^{(+),m}(\kappa)$ and $D_{c,j}^{(-),m}(\kappa)$.

larger $\mu_{c,j}^{(m)}(\kappa)$ is. If the difference between the correction directives is significant as in Fig. 5.10(a), a large $\mu_{c,j}^{(m)}(\kappa)$ is used since one specific value is dominating and can be well-reduced. However, it may happen that the values of the correction directives are similar as depicted in Fig. 5.10(c). In this case, the mobility failure events require contradicting handover threshold updates and none of the correction directives can be well reduced without a significant increase in the other correction directive. Therefore, a small $\mu_{c,j}^{(m)}(\kappa)$ is applied or the handover threshold is not changed, i.e., $\mu_{c,j}^{(m)}(\kappa) = 0$.

5.6.5.2 Proportional Control Block

The proportional control block performs corrective actions based on the value of a predefined error value which is denoted by $\varepsilon_{c,j}^{(m)}(\kappa)$ in KPI collection period κ. For this purpose, the metric $M_{c,j}^{(m)}(\kappa)$ corresponding to handover threshold $Q_{c,j}^{(m)}(\kappa)$ is defined as

$$M_{c,j}^{(m)}(\kappa) = \frac{\max\{D_{c,j}^{(+),m}(\kappa), D_{c,j}^{(-),m}(\kappa)\}}{\min\{D_{c,j}^{(+),m}(\kappa), D_{c,j}^{(-),m}(\kappa)\}} \geq 1. \tag{5.47}$$

The larger $M_{c,j}^{(m)}(\kappa)$, the larger $\mu_{c,j}^{(m)}(\kappa)$ is. On the contrary, a small $M_{c,j}^{(m)}(\kappa)$ requires a small $\mu_{c,j}^{(m)}(\kappa)$. The error $\varepsilon_{c,j}^{(m)}(\kappa)$ is defined as a function of the aforementioned metric. The higher the error value, the larger the change in the value of a handover threshold is. The handover threshold is not updated when the error is close to zero which occurs when both correction directives are below $D_{\text{thr}}^{(\min)}$ or they are close to each other, e.g., $M_{c,j}^{(m)}(\kappa) = 1$. Therefore, the error $\varepsilon_{c,j}^{(m)}(\kappa)$ is defined as

$$\varepsilon_{c,j}^{(m)}(\kappa) = \begin{cases} M_{c,j}^{(m)}(\kappa) - 1 \geq 0, & \text{if } D_{c,j}^{(+),m}(\kappa) > D_{\text{thr}}^{(\min)} \text{ or } D_{c,j}^{(-),m}(\kappa) > D_{\text{thr}}^{(\min)}, \\ 0, & \text{otherwise.} \end{cases} \tag{5.48}$$

The aim of the controller is to minimize this error value.

Many models exist for expressing $\mu_{c,j}^{(m)}(\kappa)$ as a function of the error $\varepsilon_{c,j}^{(m)}(\kappa)$. One simple model is to express $\mu_{c,j}^{(m)}(\kappa)$ as a linear function of $\varepsilon_{c,j}^{(m)}(\kappa)$. In other words, the value of $\mu_{c,j}^{(m)}(\kappa)$ is proportional to the error $\varepsilon_{c,j}^{(m)}(\kappa)$. To this end, let $\mu^{(\max)}(\kappa)$ be the maximum predefined change that can be applied to $Q_{c,j}^{(m)}(\kappa)$ in KPI collection period κ. The change $\mu^{(\max)}(\kappa)$ is applied when the error value $\varepsilon_{c,j}^{(m)}(\kappa)$ exceeds the maximum predefined error value $\varepsilon^{(\max)}$. The value of $\mu_{c,j}^{(m)}(\kappa)$ is calculated as

$$\mu_{c,j}^{(m)}(\kappa) = \begin{cases} \mu^{(\max)}(\kappa) & \text{, if } \varepsilon_{c,j}^{(m)}(\kappa) \geq \varepsilon^{(\max)}, \\ \chi_{c,j}^{(m)}(\kappa) \cdot \varepsilon_{c,j}^{(m)}(\kappa) & \text{, if } 0 \leq \varepsilon_{c,j}^{(m)}(\kappa) < \varepsilon^{(\max)}, \end{cases} \tag{5.49}$$

where the controller gain $\chi_{c,j}^{(m)}(1)$ is equal to $\mu^{(\max)}(1)/\varepsilon^{(\max)}$ in the first KPI collection period, i.e., $\kappa = 1$. The values of $\chi_{c,j}^{(m)}(\kappa)$ and $\mu^{(\max)}(\kappa)$ are updated by the gain scheduler to reduce the oscillations in the system, see Section 5.6.5.3. In the context of control theory, the interval $\left(0,\ \varepsilon^{(\max)}\right)$ is called the proportional band because the behavior of the controller is linear when the error lies in this interval. For clarity, the unquantized value of $\mu_{c,j}^{(m)}(\kappa)$ is shown in Fig. 5.11 as a function of the error $\varepsilon_{c,j}^{(m)}(\kappa)$ for $\varepsilon^{(\max)} = 3$ and different values for the pair $\left(\chi_{c,j}^{(m)}(\kappa), \mu^{(\max)}(\kappa)\right)$.

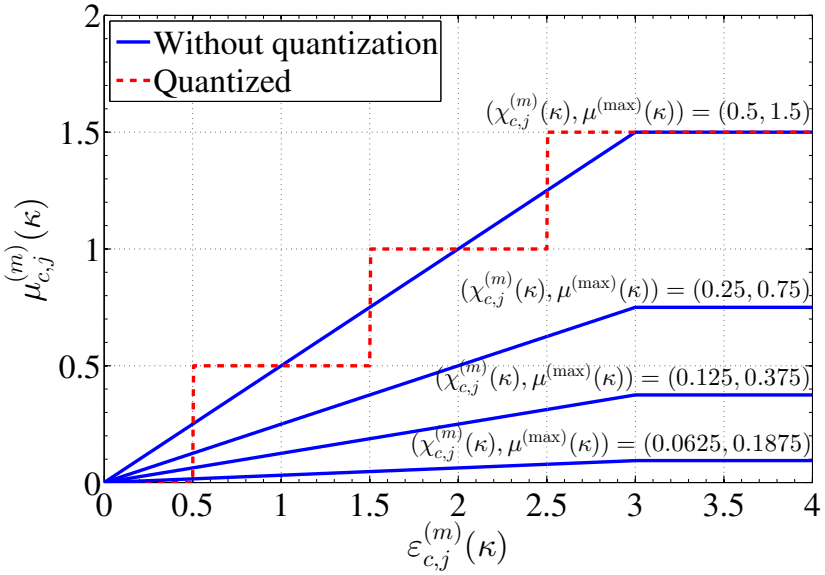

Figure 5.11. The value of $\mu_{c,j}^{(m)}(\kappa)$ as a function of the error $\varepsilon_{c,j}^{(m)}(\kappa)$ for $\varepsilon^{(\max)} = 3$ and different values for the pair $\left(\chi_{c,j}^{(m)}(\kappa), \mu^{(\max)}(\kappa)\right)$.

The sign of $\mu_{c,j}^{(m)}(\kappa)$ depends on whether $D_{c,j}^{(+),m}(\kappa)$ is greater than $D_{c,j}^{(-),m}(\kappa)$ or vice versa. A new value $\widetilde{\mu_{c,j}^{(m)}}(\kappa)$ is computed based on $\mu_{c,j}^{(m)}(\kappa)$ and the two correction directives as follows:

$$\widetilde{\mu_{c,j}^{(m)}}(\kappa) = \begin{cases} \mu_{c,j}^{(m)}(\kappa), & \text{if } D_{c,j}^{(+),m}(\kappa) > D_{c,j}^{(-),m}(\kappa), \\ -\mu_{c,j}^{(m)}(\kappa), & \text{if } D_{c,j}^{(+),m}(\kappa) < D_{c,j}^{(-),m}(\kappa). \end{cases} \tag{5.50}$$

The updated handover threshold $Q_{c,j}^{(m)}(\kappa)$ is signaled to the UEs via measurement configuration messages. To reduce the signaling overhead, the number of changes in the value of a handover threshold is limited by quantizing $\widetilde{\mu_{c,j}^{(m)}}(\kappa)$ with a quantization step size Λ_{dB}. An example is depicted in Fig. 5.11 which shows the quantized value of $\widetilde{\mu_{c,j}^{(m)}}(\kappa) = \mu_{c,j}^{(m)}(\kappa)$ with $\Lambda_{\text{dB}} = 0.5$ dB. The quantized value of $\widetilde{\mu_{c,j}^{(m)}}(\kappa)$ is denoted by $\widehat{\mu_{c,j}^{(m)}}(\kappa)$. The value of handover threshold $Q_{c,j}^{(m)}(\kappa)$ is finally updated as follows:

$$Q_{c,j}^{(m)}(\kappa) = Q_{c,j}^{(m)}(\kappa - 1) + \widehat{\mu_{c,j}^{(m)}}(\kappa). \tag{5.51}$$

The handover threshold is updated and the optimization process is repeated until the algorithm converges.

5.6.5.3 Gain Scheduler

The gain scheduler updates the parameters of the proportional control block depending on the mobility conditions in each cell. With the proportional control block, a cell achieves stability when the correction directives are either of similar or equal values as shown in Fig. 5.10(c) or lower than the threshold $D_{\text{thr}}^{(\min)}$ as in Fig. 5.10(d). In both cases, no handover threshold update is performed, i.e., $\mu_{c,j}^{(m)}(\kappa) = 0$. However, the cell may not always reach one of the latter two stable cases. For instance, it may happen that reducing $D_{c,j}^{(+),m}(\kappa)$ leads to a large increase in $D_{c,j}^{(-),m}(\kappa)$ and vice versa. In this case, the correction directives oscillate with each handover threshold update.

One example of an oscillation in the correction directives is shown in Fig. 5.12. In KPI collection period $\kappa - 2$, $D_{c,j}^{(+),m}(\kappa-2) > D_{c,j}^{(-),m}(\kappa-2)$ and the threshold $Q_{c,j}^{(m)}(\kappa-2)$ is increased accordingly. The increase in the handover threshold has caused an increase

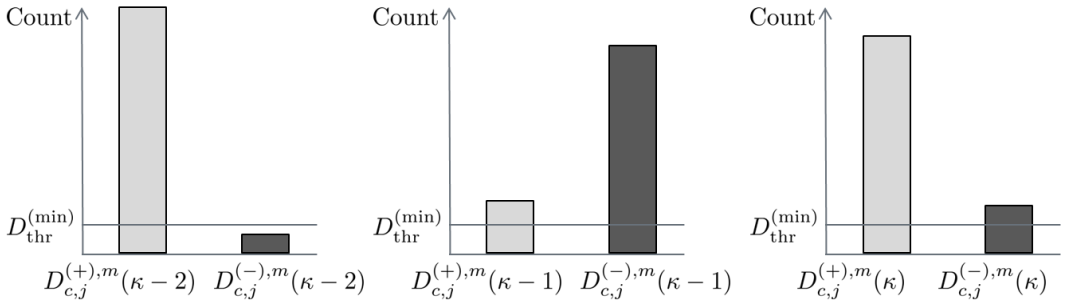

Figure 5.12. Example of an oscillation in the correction directives detected in KPI collection period κ.

in $D_{c,j}^{(-),m}(\kappa-1)$ in KPI collection period $\kappa - 1$. The handover threshold $Q_{c,j}^{(m)}(\kappa-1)$ is then decreased. In KPI collection period κ, the decrease in the handover threshold has caused again an increase in $D_{c,j}^{(+),m}(\kappa)$ and a decrease in $D_{c,j}^{(-),m}(\kappa)$. In this case, an oscillation in the correction directives is detected. Therefore, in this situation the handover thresholds are constantly updated up and down and stability is not reached.

The role of the gain scheduler is to modify the control parameters of the proportional control block depending on the mobility conditions in each cell which are identified by the observable variables or so-called scheduling variables in the vocabulary of control theory [LF06]. The first observable variable used by the gain scheduler is a boolean flag indicating if an oscillation in the correction directives occurred as depicted in Fig. 5.12. Once an oscillation in the correction directives is detected, the gain scheduler reduces the controller gain $\chi_{c,j}^{(m)}(\kappa)$ by the reduction ratio $\varpi < 1$, respectively, as follows:

$$\chi_{c,j}^{(m)}(\kappa) = \varpi \cdot \chi_{c,j}^{(m)}(\kappa - 1). \tag{5.52}$$

As a result, the gain scheduler modifies the behavior of the proportional control block with every oscillation in the correction directives. Decreasing the controller gain $\chi_{c,j}^{(m)}(\kappa)$ by ϖ leads to a reduction in the value of $\mu_{c,j}^{(m)}(\kappa)$ by a factor of ϖ if the error $\varepsilon_{c,j}^{(m)}(\kappa)$ lies within the proportional band, see (5.49). Therefore, the value of $\mu_{c,j}^{(m)}(\kappa)$ is reduced each time an oscillation is detected. If the number of oscillations is large, the value of $\mu_{c,j}^{(m)}(\kappa)$ approaches 0 and stability is achieved. Keeping the error value $\varepsilon^{(\max)}$ fixed, the value of $\mu^{(\max)}(\kappa)$ is also updated as follows:

$$\mu^{(\max)}(\kappa) = \chi_{c,j}^{(m)}(\kappa) \cdot \varepsilon^{(\max)}. \tag{5.53}$$

For instance, in Fig. 5.11 the value of $\mu_{c,j}^{(m)}(\kappa)$ is plotted as a function of the error $\varepsilon_{c,j}^{(m)}(\kappa)$ with $\chi_{c,j}^{(m)}(\kappa)$ and $\mu^{(\max)}(\kappa)$ as parameters. Initially, $\left(\chi_{c,j}^{(m)}(\kappa), \mu^{(\max)}(\kappa)\right) = (0.5, 1.5)$ is used. Once an oscillation is detected in the correction directives, the gain scheduler reduces the correction directives by $\varpi = 0.5$ resulting in $\left(\chi_{c,j}^{(m)}(\kappa), \mu^{(\max)}(\kappa)\right) = (0.25, 0.75)$ curve. If two additional oscillations are detected, the control parameters are further reduced resulting in $\left(\chi_{c,j}^{(m)}(\kappa), \mu^{(\max)}(\kappa)\right) = (0.0625, 0.1875)$. In this case, the value of $\mu_{c,j}^{(m)}(\kappa)$ is lower than 0.25 for all error values and if quantization is considered with $\Lambda_{\mathrm{dB}} = 0.5$, $Q_{c,j}^{(+),m}(\kappa) = 0$ is used for all values of $\varepsilon_{c,j}^{(m)}(\kappa)$ and stability is achieved.

A cell that has reduced its control parameters due to a series of oscillations may have to increase them again to react on any new changes in the number of mobility failure events in the network, e.g., caused by changes in the environment or mobility conditions of the cell. For example, if one of the correction directives requiring contradicting changes in the handover threshold has increased or decreased significantly, the automatic algorithm should be able to react again. Therefore, there should be a procedure to escape from small value of $\chi_{c,j}^{(m)}(\kappa)$ in case of an abrupt change in the correction directives of the considered cell. For instance, let $\varrho^{(+)}(\kappa)$ be the change in the value of $D_{c,j}^{(+),m}(\kappa)$ in KPI collection period κ. The parameter $\varrho^{(+)}(\kappa)$ is defined as the minimum distance between $D_{c,j}^{(+),m}(\kappa)$ and its corresponding $N_{\mathrm{samples}} \geq 1$ previous values, i.e.,

$$\varrho^{(+)}(\kappa) = \min_{s=1,\ldots,N_{\mathrm{samples}}} |D_{c,j}^{(+),m}(\kappa) - D_{c,j}^{(+),m}(\kappa - s)|. \tag{5.54}$$

The parameter N_{samples} is introduced in order to guarantee that the change $\varrho^{(+)}(\kappa)$ in $D_{c,j}^{(+),m}(\kappa)$ is not due to a statistical fluctuation, i.e., $D_{c,j}^{(+),m}(\kappa)$ might vary in each KPI collection period even if $Q_{c,j}^{(m)}(\kappa)$ is not changed. The parameter $\varrho^{(+)}(\kappa)$ is the second observable variable which is used by the gain scheduler. If the value of $\chi_{c,j}^{(m)}(\kappa - 1) < \chi_{c,j}^{(m)}(1)$, i.e., at least one oscillation had occurred during the optimization so far, $\chi_{c,j}^{(m)}(\kappa)$ is increased as follows:

$$\chi_{c,j}^{(m)}(\kappa) = \begin{cases} \chi_{c,j}^{(m)}(1), & \text{if } \varrho^{(+)}(\kappa) \geq \varrho^{(\max)} \\ a_{\mathrm{gs}} \cdot \varrho^{(+)}(\kappa) + b_{\mathrm{gs}}, & \text{if } \varrho^{(\min)} \leq \varrho^{(+)}(\kappa) < \varrho^{(\max)} \\ \chi_{c,j}^{(m)}(\kappa - 1), & \text{if } \varrho^{(+)}(\kappa) < \varrho^{(\min)}, \end{cases} \tag{5.55}$$

where

$$a_{\text{gs}} = \frac{\chi_{c,j}^{(m)}(1) - \chi_{c,j}^{(m)}(\kappa - 1)}{\varrho^{(\max)} - \varrho^{(\min)}}, \quad b_{\text{gs}} = \chi_{c,j}^{(m)}(1) - a_{\text{gs}} \cdot \varrho^{(\max)}, \tag{5.56}$$

and $\varrho^{(\min)}$ and $\varrho^{(\max)}$ are predefined thresholds for the minimum and maximum changes in $D_{c,j}^{(+),m}(\kappa)$. The larger $\varrho^{(+)}(\kappa)$, the higher the increase in $\chi_{c,j}^{(m)}(\kappa)$ is. If $\varrho^{(+)}(\kappa)$ is significantly large, e.g., $\varrho^{(+)}(\kappa) \geq \varrho^{(\max)}$, the value of $\chi_{c,j}^{(m)}(\kappa)$ is restored to its maximum value $\chi_{c,j}^{(m)}(1)$. Once the value of $\chi_{c,j}^{(m)}(\kappa)$ is changed, the value of $\mu^{(\max)}(\kappa)$ is updated according to (5.53). The same procedure is applied to $D_{c,j}^{(-),m}(\kappa)$.

5.7 Performance Evaluation and Analysis

5.7.1 Cell-Specific Optimization of Handover Thresholds

5.7.1.1 Network Level Performance Evaluation

The performance of cell-specific optimization of handover thresholds is compared with that of the best network-wide setting, which is found in Section 4.2. The performance of each approach is evaluated using the values of the KPIs which are collected from both 3G and LTE networks during $T_{\text{CL}} = 150$ s time interval. Moreover, the performance comparison is carried out for different velocities v_{st} of UEs on streets and values of inter-RAT TTT $Q_c^{(3)}$. The scenario consists of two fully overlaying co-sited LTE and 3G networks, which is discussed in Section 2.8.3. The simulation parameters which are used for the scenario are summarized in Table 3.2 and Table 3.3.

The handover thresholds are initialized to the best network-wide setting of handover thresholds, found in Section 4.2. The parameters that are used by the automatic algorithm of the inter-RAT handover thresholds are summarized in Table 5.2. In this study, a PP is given the same weight $w_{\text{PP}} = 1$ as an RLF. This is because PPs incur a lot of signaling overhead and reducing them is important for mobile operators. The value of $D_{\text{thr}}^{(\min)}$ is set to 15 and 10 for the cell-specific and cell-pair specific optimization approach, respectively. The maximum change $\mu^{(\max)}$ in dB that can be applied to a handover threshold is set to a relatively small value equal to 1. The reason for that is to avoid any significant oscillations in the correction directives and allow incremental improvements in each KPI collection period. Moreover, the change $\widetilde{\mu_{c,j}^{(m)}}$ in a handover threshold is further quantized with a step size $\Lambda_{\text{dB}} = 0.25$. As for the gain scheduler, the controller gain is reduced by a factor $\varpi = 0.5$ each time an oscillation in the correction directives is detected. The controller gain is increased again if the change

Table 5.2. The parameters that are used by the automatic algorithm of the inter-RAT handover thresholds.

Parameter	Value
Weight w_{PP} of PPs	1
Minimum threshold $D_{\mathrm{thr}}^{(\mathrm{min})}$ for cell-specific optimization approach	15
Minimum threshold $D_{\mathrm{thr}}^{(\mathrm{min})}$ for cell-pair specific optimization approach	10
Maximum change $\mu^{(\mathrm{max})}$ in $Q_{c,j}^{(m)}$ handover threshold	1
Maximum error value $\varepsilon^{(\mathrm{max})}$	1
Quantization step size Λ_{dB} for $\widetilde{\mu_{c,j}^{(m)}}$	0.25
Reduction ratio ϖ for controller gain $\chi_{c,j}^{(m)}$	0.5
Number N_{samples} of samples for a correction directive	3
Threshold $\varrho^{(\mathrm{min})}$ for the minimum change in a correction directive	$D_{\mathrm{thr}}^{(\mathrm{min})}$
Threshold $\varrho^{(\mathrm{max})}$ for the maximum change in a correction directive	$2 \cdot D_{\mathrm{thr}}^{(\mathrm{min})}$

in any of the two correction directives is between the thresholds $\varrho^{(\mathrm{min})} = D_{\mathrm{thr}}^{(\mathrm{min})}$ and $\varrho^{(\mathrm{max})} = 2 \cdot D_{\mathrm{thr}}^{(\mathrm{min})}$.

The total number $N_{\mathrm{all}}^{(\mathrm{RLF})}$ of RLFs, $N_{\mathrm{all}}^{(\mathrm{PP})}$ of PPs and $N_{\mathrm{all}}^{(\mathrm{UH})}$ in both 3G and LTE networks is shown in Fig. 5.13 for the best network-wide setting (NWS) and cell-specific optimization of handover thresholds (CS Thr.). The velocity v_{st} of the UEs located on streets is 30 km/h. According to the figure, "CS Thr." achieves a better

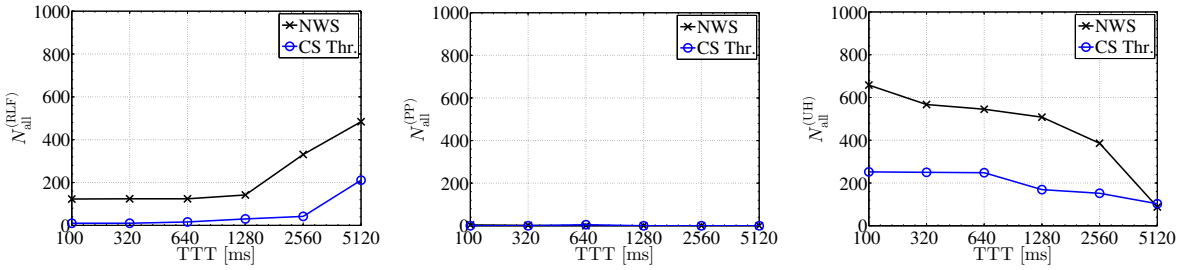

(a) Total number $N_{\mathrm{all}}^{(\mathrm{RLF})}$ of RLFs in 3G and LTE networks.

(b) Total number $N_{\mathrm{all}}^{(\mathrm{PP})}$ of PPs in 3G and LTE networks.

(c) Total number $N_{\mathrm{all}}^{(\mathrm{UH})}$ of UHs in LTE networks.

Figure 5.13. Number of mobility failure events for best network-wide setting (NWS) and cell-specific optimization of handover thresholds (CS Thr.) for $v_{\mathrm{st}} = 30$ km/h versus inter-RAT TTT.

performance in $N_{\mathrm{all}}^{(\mathrm{RLF})}$ and $N_{\mathrm{all}}^{(\mathrm{UH})}$ for all TTT values. Moreover, the performance of "NWS" and "CS Thr." depends on the initial value of TTT. For "NWS", the number $N_{\mathrm{all}}^{(\mathrm{RLF})}$ is similar only for TTT in the range between 100 ms and 1280 ms. Moreover, the number $N_{\mathrm{all}}^{(\mathrm{UH})}$ decreases with increasing value of TTT. For this velocity $v_{\mathrm{st}} = 30$ km/h, the value 640 ms of TTT is the best for "NWS" since it yields the smallest sum of $N_{\mathrm{all}}^{(\mathrm{RLF})}$ and $N_{\mathrm{all}}^{(\mathrm{PP})}$ given that RLFs have a higher priority than UHs and the weight

w_{PP} of a PP is the same as that of an RLF. For the value 640 ms of TTT, "CS Thr." resolves almost all RLFs and reduces $N_{\mathrm{all}}^{(\mathrm{UH})}$ by 53.7% compared to "NWS". These performance gains are achieved without any increase in $N_{\mathrm{all}}^{(\mathrm{PP})}$ as shown in Fig. 5.13(b).

The performance of "NWS" and "CS Thr." is compared in Fig. 5.14 for $v_{\mathrm{st}} = 60$ km/h and different values of inter-RAT TTT. Similar to the previous case of $v_{\mathrm{st}} = 30$ km/h,

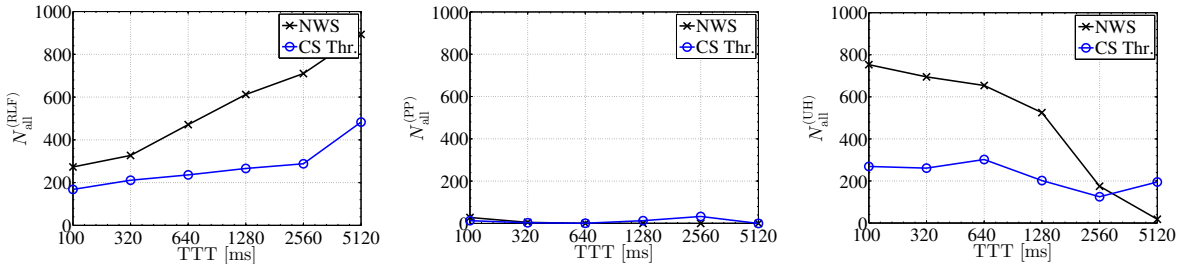

(a) Total number $N_{\mathrm{all}}^{(\mathrm{RLF})}$ of RLFs in 3G and LTE networks.

(b) Total number $N_{\mathrm{all}}^{(\mathrm{PP})}$ of PPs in 3G and LTE networks.

(c) Total number $N_{\mathrm{all}}^{(\mathrm{UH})}$ of UHs in LTE networks.

Figure 5.14. Number of mobility failure events for best network-wide setting (NWS) and cell-specific optimization of handover thresholds (CS Thr.) for $v_{\mathrm{st}} = 60$ km/h versus inter-RAT TTT.

$N_{\mathrm{all}}^{(\mathrm{RLF})}$ and $N_{\mathrm{all}}^{(\mathrm{PP})}$ increases and decreases, respectively, with increasing value of TTT. For "NWS", the value 100 ms of TTT yields the smallest sum of $N_{\mathrm{all}}^{(\mathrm{RLF})}$ and $N_{\mathrm{all}}^{(\mathrm{PP})}$ at the expense of a high value of $N_{\mathrm{all}}^{(\mathrm{UH})}$. For this value of TTT, "CS Thr." reduces $N_{\mathrm{all}}^{(\mathrm{RLF})}$ and $N_{\mathrm{all}}^{(\mathrm{UH})}$ by 38.5% and 64.3%, respectively. Moreover, the number $N_{\mathrm{all}}^{(\mathrm{PP})}$ of PPs is negligible for both "NWS" and "CS Thr.". For TTT = 5120 ms, "CS Thr." has a higher number $N_{\mathrm{all}}^{(\mathrm{UH})}$ of UHs than "NWS". This increase in $N_{\mathrm{all}}^{(\mathrm{UH})}$ is acceptable as long as the number $N_{\mathrm{all}}^{(\mathrm{RLF})}$ of RLFs which has a higher priority than $N_{\mathrm{all}}^{(\mathrm{UH}}$ is reduced, see Fig. 5.14(a).

The performance of "NWS" and "CS Thr." is compared in Fig. 5.15 for $v_{\mathrm{st}} = 90$ km/h. It is shown in Fig. 5.15(a) that for "NWS" $N_{\mathrm{all}}^{(\mathrm{RLF})}$ is much smaller for TTT = 100 ms compared to those obtained for higher values of TTT. This reduction in $N_{\mathrm{all}}^{(\mathrm{RLF})}$ is possible only at the expense of a high value of $N_{\mathrm{all}}^{(\mathrm{UH})}$ which is shown in Fig. 5.15(c). Moreover, unlike the previous two cases the number $N_{\mathrm{all}}^{(\mathrm{PP})}$ of PPs for "NWS" is relatively significant for the value 100 ms of TTT as shown in Fig. 5.15(b). For "NWS", the smallest sum of $N_{\mathrm{all}}^{(\mathrm{RLF})}$ and $N_{\mathrm{all}}^{(\mathrm{PP})}$ corresponds to the value 100 ms of TTT. For this value of TTT, "CS Thr." reduces $N_{\mathrm{all}}^{(\mathrm{RLF})}$, $N_{\mathrm{all}}^{(\mathrm{PP})}$ and $N_{\mathrm{all}}^{(\mathrm{UH})}$ by 74%, 92.7% and 72.9%, respectively.

In Fig. 5.16, the performance of "NWS" and "CS Thr." is compared for $v_{\mathrm{st}} = 120$ km/h and different inter-RAT TTT values. For this high velocity, $N_{\mathrm{all}}^{(\mathrm{RLF})}$ corresponding to

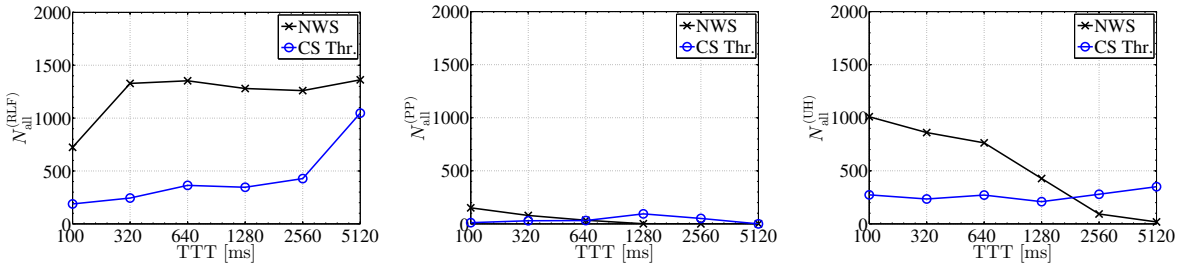

(a) Total number $N_{\text{all}}^{(\text{RLF})}$ of RLFs in 3G and LTE networks.

(b) Total number $N_{\text{all}}^{(\text{PP})}$ of PPs in 3G and LTE networks.

(c) Total number $N_{\text{all}}^{(\text{UH})}$ of UHs in LTE networks.

Figure 5.15. Number of mobility failure events for best network-wide setting (NWS) and cell-specific optimization of handover thresholds (CS Thr.) for $v_{\text{st}} = 90$ km/h versus inter-RAT TTT.

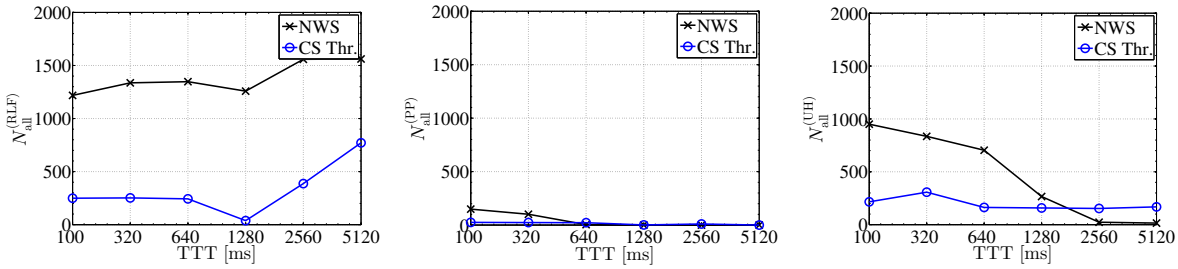

(a) Total number $N_{\text{all}}^{(\text{RLF})}$ of RLFs in 3G and LTE networks.

(b) Total number $N_{\text{all}}^{(\text{PP})}$ of PPs in 3G and LTE networks.

(c) Total number $N_{\text{all}}^{(\text{UH})}$ of UHs in LTE networks.

Figure 5.16. Number of mobility failure events for best network-wide setting (NWS) and cell-specific optimization of handover thresholds (CS Thr.) for $v_{\text{st}} = 120$ km/h versus inter-RAT TTT.

"NWS" is to some extent similar for all TTT values as shown in Fig. 5.16(a). For "NWS", the smallest sum of $N_{\text{all}}^{(\text{RLF})}$ and $N_{\text{all}}^{(\text{PP})}$ corresponds to the value 1280 ms of TTT. For this TTT value, "CS Thr." resolves almost all the RLFs as shown in Fig. 5.16(a). Moreover, the number $N_{\text{all}}^{(\text{UH})}$ of UHs is slightly smaller for "CS Thr." whereas $N_{\text{all}}^{(\text{PP})}$ is the same for both approaches.

5.7.1.2 Cell Level Performance Evaluation

The performance of the automatic algorithm is compared to that of the best network-wide setting of handover thresholds on cell level. The network-wide setting of handover thresholds has been optimized in Section 4.2 using a velocity $v_{\text{st}} = 60$ km/h for UEs on streets and inter-RAT TTT $Q_c^{(3)} = 320$ ms. Accordingly, the cell level performance comparison is carried out for this specific velocity and value of TTT. The network level performance of the automatic algorithm and the best network-wide setting of

the handover thresholds has been already shown in Fig. 5.14 for $v_{\text{st}} = 60$ km/h and different values of TTT.

The total number $N_c^{(\text{RLF})}$ of RLFs, $N_c^{(\text{PP})}$ of PPs and $N_c^{(\text{UH})}$ of UHs is shown in Fig. 5.17 as a function of the KPI collection period κ for each cell having mobility problems

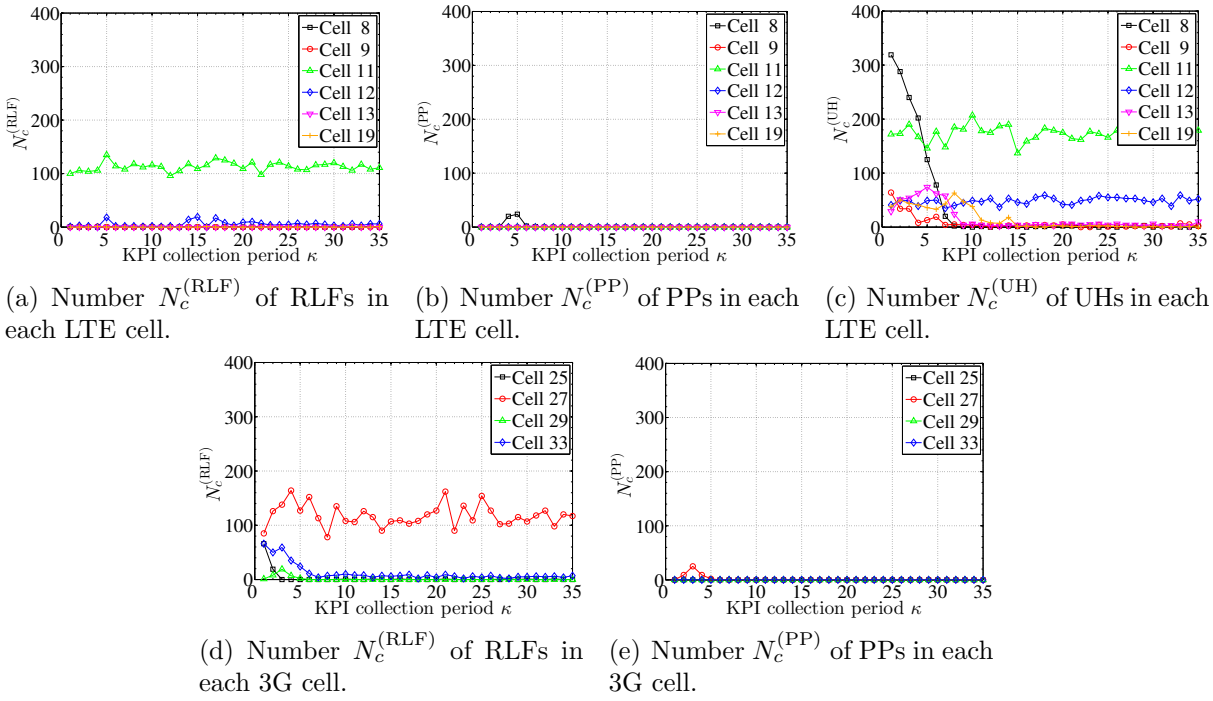

(a) Number $N_c^{(\text{RLF})}$ of RLFs in each LTE cell.

(b) Number $N_c^{(\text{PP})}$ of PPs in each LTE cell.

(c) Number $N_c^{(\text{UH})}$ of UHs in each LTE cell.

(d) Number $N_c^{(\text{RLF})}$ of RLFs in each 3G cell.

(e) Number $N_c^{(\text{PP})}$ of PPs in each 3G cell.

Figure 5.17. Cell level performance comparison between the automatic algorithm and the best network-wide setting of handover thresholds for a velocity $v_{\text{st}} = 60$ km/h and inter-RAT TTT $Q_c^{(3)} = 320$ ms.

initially or during the optimization. In the first KPI collection period $\kappa = 1$, the values of $N_c^{(\text{RLF})}$, $N_c^{(\text{PP})}$ and $N_c^{(\text{UH})}$ correspond to the initial best network-wide setting of handover thresholds. According to the figure, only $6/21 \approx 29\%$ and $4/21 \approx 19\%$ of the LTE and 3G cells, respectively, experience mobility problems. Resolving the mobility problems in those cells is important for mobile operators as it directly impacts the quality perception of UEs.

In Fig. 5.17(a), it is shown that only cell 11 has initially a high number of RLFs. This is because the initial network-wide setting of the handover thresholds has been optimized to minimize the number of RLFs at the expense of a high number of UHs as shown in Fig. 5.17(c). The automatic algorithm has failed to resolve the RLFs of cell 11 since its corresponding mobility problems require contradicting actions to be performed on the same cell-specific target cell threshold, i.e., $D_c^{(+),2} \approx D_c^{(-),2}$. As for the number $N_c^{(\text{PP})}$ of PPs, it is negligible for all LTE cells as shown in Fig. 5.17(b).

The automatic algorithm has resolved $N_c^{(\mathrm{UH})}$ of four LTE cells 8, 9, 13 and 19 and it did not react on UHs of cell 11 since it has already TLHs which are given more priority than UHs. However, the automatic algorithm has failed to resolve $N_c^{(\mathrm{UH})}$ of cell 12 because reacting on UHs in this cell has yielded a significant increase in the number of TLHs. This can be shown in Fig. 5.18 which shows the change $\widehat{\mu_{c,j}^{(1)}}$ applied to the serving cell threshold $Q_c^{(1)}$ of LTE cell 12 and the controller gain $\chi_{c,j}^{(1)}$ corresponding to $Q_c^{(1)}$, i.e., $j = 1$ in cell-specific optimization of handover thresholds, see Table 5.1. The automatic

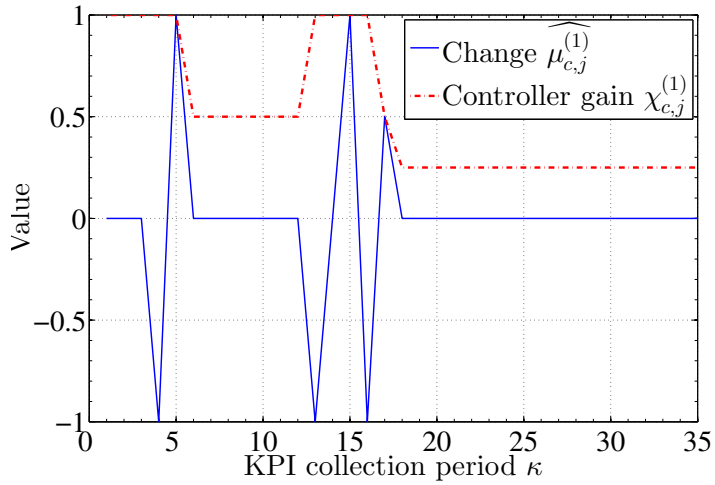

Figure 5.18. The change $\widehat{\mu_{c,j}^{(1)}}$ applied to the serving cell threshold $Q_c^{(1)}$ of LTE cell 12 and the controller gain $\chi_{c,j}^{(1)}$ corresponding to $Q_c^{(1)}$.

algorithm has tried to solve the number of UHs in KPI collection periods 4, 13 and 16 by decreasing the serving cell threshold $Q_c^{(1)}$, i.e., applying a negative change $\widehat{\mu_{c,j}^{(1)}} = -1$. However, each time $Q_c^{(1)}$ is decreased, the number of TLHs increases. Consequently, the serving cell threshold is again increased in KPI collection periods 5, 14, 17 by applying a positive change $\widehat{\mu_{c,j}^{(1)}}$. After a series of oscillations in the correction directives $D_c^{(+),1}$ and $D_c^{(-),1}$ corresponding to the serving cell threshold, the gain scheduler reduces the controller gain $\chi_{c,j}^{(1)}$ for cell 12 and stops reacting on UHs. Thus, the automatic algorithm has learned gradually that the number of UHs in cell 12 cannot be resolved and the optimization should be stopped for this specific cell.

The number $N_c^{(\mathrm{RLF})}$ of RLFs is shown in Fig. 5.17(d) for the four 3G cells 25, 27, 29 and 33. The automatic algorithm has resolved $N_c^{(\mathrm{RLF})}$ completely in cells 25, 29 and 33 whereas it has failed to resolve the RLFs of cell 27. The reason for this failure is the same as that of LTE cell 11: The number of mobility failure events requiring an increase in the target cell handover threshold is similar to the number of those requiring a decrease, i.e., $D_c^{(+),2} \approx D_c^{(-),2}$. Thus, it might be possible using cell-pair specific

handover target cell thresholds to achieve some improvement in the performance of cells 11 and 27. The number of PPs is negligible for all 3G cells as shown in Fig. 5.17(e).

The serving and target cell thresholds are shown in Fig. 5.19 for each LTE and 3G

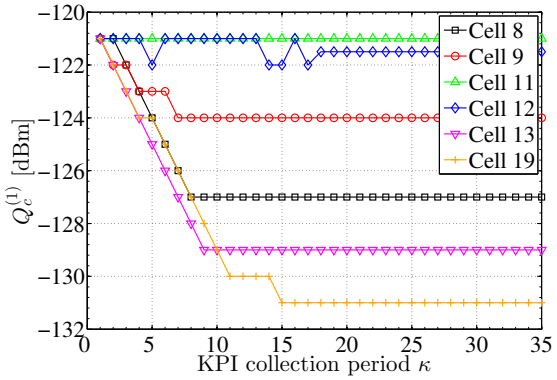

(a) The serving cell threshold $Q_c^{(1)}$ for each LTE cell.

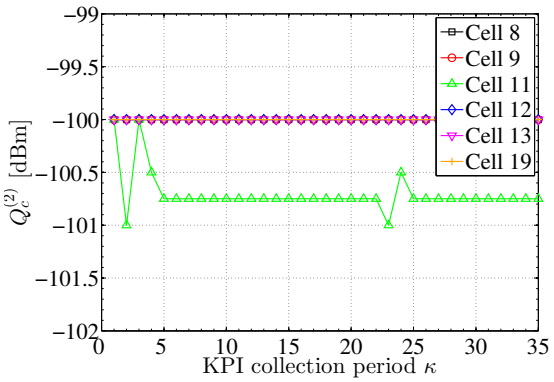

(b) The target cell threshold $Q_c^{(2)}$ for each LTE cell.

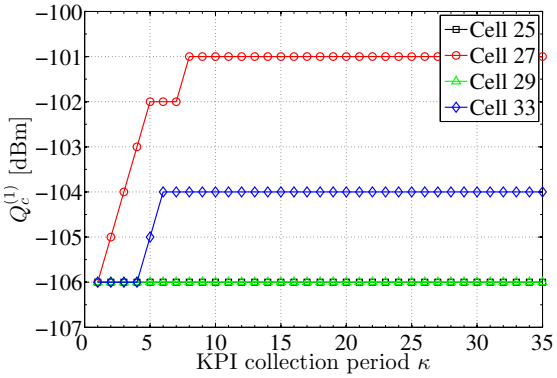

(c) The serving cell threshold $Q_c^{(1)}$ for each 3G cell.

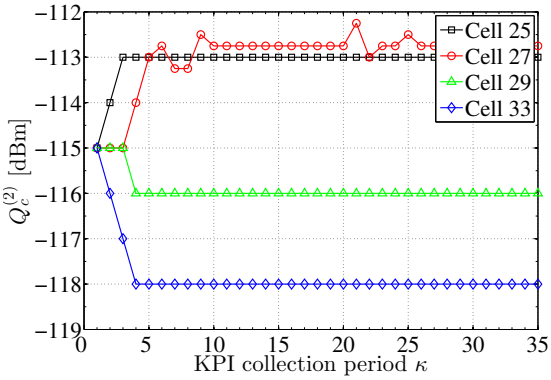

(d) The target cell threshold $Q_c^{(2)}$ for each 3G cell.

Figure 5.19. The serving and target cell thresholds as a function of the KPI collection period κ for each LTE and 3G cell.

cell as a function of the KPI collection period κ. According to the figure, the serving and target cell thresholds are cell-specific in LTE and 3G networks. The serving cell threshold $Q_c^{(1)}$ is decreased for LTE cells 8, 9, 13 and 19 in order to react on their corresponding numbers of UHs as shown in Fig. 5.19(a). On the other hand, it is shown in Fig. 5.19(c) that the serving cell thresholds of 3G cells 27 and 33 are increased to react on their corresponding values of TLH-1 KPI. Similarly, the target cell threshold $Q_c^{(2)}$ of each LTE and 3G cell is set differently as shown in Fig. 5.19(b) and Fig. 5.19(d), respectively. Thus, cell-specific handover thresholds are needed to adapt to the mobility conditions of each cell.

5.7.1.3 Performance Comparison between Automatic Algorithm, Simulated Annealing and Taguchi's Method

The performance of the automatic algorithm is compared with those of the two offline optimization methods SA and TM which are explained in Section 4.3.2 and Section 4.3.3, respectively. The scenario consists of two fully overlaying co-sited LTE and 3G networks, which is discussed in Section 2.8.3. The metric used for performance evaluation is the optimization function y that is defined in (4.11) as the sum of the total number $N_{\text{all}}^{(\text{RLF})}$ of RLFs and $N_{\text{all}}^{(\text{PP})}$ of PPs in 3G and LTE networks. The performance comparison is carried out for the four velocities $v_{\text{st}} = 30$ km/h, 60 km/h, 90 km/h and 120 km/h. For each velocity, the inter-RAT TTT $Q_c^{(3)}$ is set to the value of TTT of which the automatic algorithm achieves the smallest value of y. The value of $Q_c^{(3)}$ can be directly obtained from Fig. 5.13, Fig. 5.14, Fig. 5.15 and Fig. 5.16 showing $N_{\text{all}}^{(\text{RLF})}$ and $N_{\text{all}}^{(\text{PP})}$ for velocity $v_{\text{st}} = 30$ km/h, 60 km/h, 90 km/h and 120 km/h, respectively. The value of $Q_c^{(3)}$ minimizing the optimization function y of the automatic algorithm is equal to 320 ms, 100 ms, 100 ms and 1280 ms for $v_{\text{st}} = 30$ km/h, 60 km/h, 90 km/h and 120 km/h, respectively.

The parameters of SA are summarized in Table 4.3. As for TM, the parameters are summarized in Table 5.3. For each velocity, the optimization range is defined such that

Table 5.3. Simulation parameters for TM applying NOA.

Parameter	Value			
Velocity v_{st} of UEs on streets	30 km/h	60 km/h	90 km/h	120 km/h
NOA(N_{exp}, N_{p}, N_{v})	NOA(20, 84, 5)			
$V_{\text{p}}^{(\text{min})}, V_{\text{p}}^{(\text{max})}$ of LTE $Q_c^{(1)}$ [dBm]	-130, -121	-131, -121	-131, -118	-131, -106
$V_{\text{p}}^{(\text{min})}, V_{\text{p}}^{(\text{max})}$ of LTE $Q_c^{(2)}$ [dBm]	-106, -100	-103, -97	-108, -86	-116, -91
$V_{\text{p}}^{(\text{min})}, V_{\text{p}}^{(\text{max})}$ of 3G $Q_c^{(1)}$ [dBm]	-115, -106	-116, -106	-116, -103	-116, -91
$V_{\text{p}}^{(\text{min})}, V_{\text{p}}^{(\text{max})}$ of 3G $Q_c^{(2)}$ [dBm]	-121, -115	-118, -112	-123, -111	-131, -106
Optimization range reduction ratio ξ	0.75			
Termination threshold ϵ	0.25			

it includes the optimized values of the handover thresholds that are obtained from the automatic algorithm applying initially the best network-wide setting of the handover thresholds.

In each network trial, the optimization function y is evaluated using the values of the KPIs which are collected during $T_{\text{CL}} = 150$ s time interval. For the automatic algorithm, each network trial corresponds to one KPI collection period. The optimization

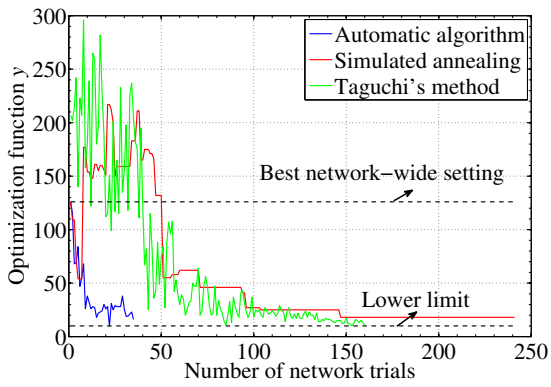

(a) Velocity $v_{\mathrm{st}} = 30$ km/h and TTT = 320 ms.

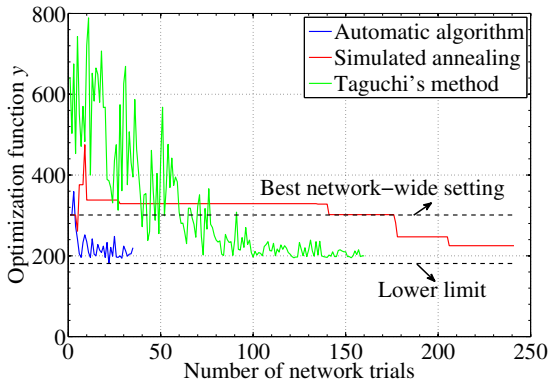

(b) Velocity $v_{\mathrm{st}} = 60$ km/h and TTT = 100 ms.

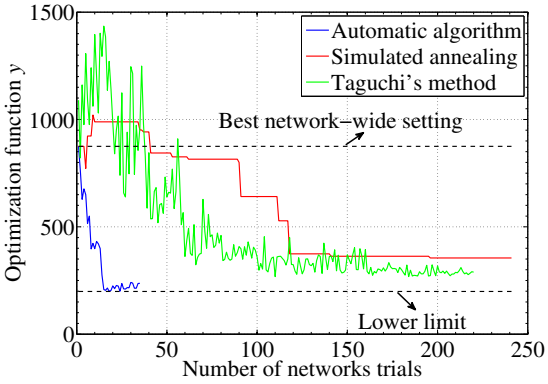

(c) Velocity $v_{\mathrm{st}} = 90$ km/h and TTT = 100 ms.

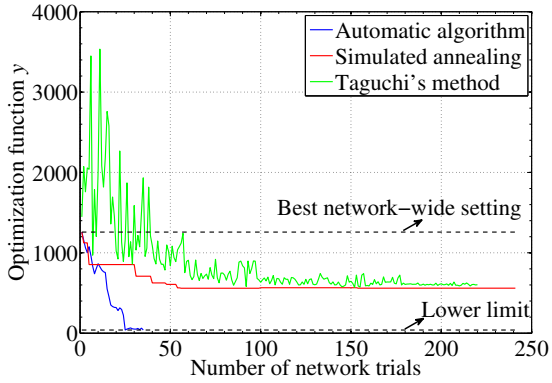

(d) Velocity $v_{\mathrm{st}} = 120$ km/h and TTT = 1280 ms.

Figure 5.20. Performance comparison between the automatic algorithm, SA and TM for four different velocities of UEs on streets.

function y is shown in Fig. 5.20 for the automatic algorithm, SA and TM with the velocity v_{st} of UEs on streets as a parameter. In each sub-figure, the upper dashed black line indicates the value of the optimization function y evaluated in the first network trial for the best network-wide setting of the handover thresholds. The lower black dashed line indicates the minimum value of y that the automatic algorithm converges to during the optimization. According to Fig. 5.20, it is shown that the automatic algorithm has a much faster convergence than SA and TM. This is because the automatic algorithm reacts directly on the handover thresholds of the cells having mobility problems whereas the other two methods explore first the predefined search space of the handover thresholds before converging.

In Fig. 5.20(a), the minimum value of the optimization function y achieved by the automatic algorithm, SA and TM is 92%, 86% and 92% lower than that of the best network-wide setting, respectively. Thus, for this velocity, the performance of automatic algorithm is similar to that of TM and better than that of SA. The same

is observed for $v_{\mathrm{st}} = 60$ km/h and 90 km/h in Fig. 5.20(b) and Fig. 5.20(c). The performance gain of the automatic algorithm, SA and TM is 40%, 26% and 35%, respectively, for $v_{\mathrm{st}} = 60$ km/h and 77%, 69% and 59%, respectively, for $v_{\mathrm{st}} = 90$ km/h. In Fig. 5.20(d), it is shown that the automatic algorithm outperforms significantly SA and TM unlike the first three cases. These simulation results clearly show that the design of the automatic algorithm of the handover thresholds is appropriate as well as efficient.

5.7.1.4 Optimization of Handover Thresholds Using Reduced Inter-RAT Mobility Failure Types as Specified by 3GPP Rel. 11

The performance of the automatic algorithm using only the specified mobility failures of 3GPP Rel. 11 is compared with that using the full set of mobility failure types which is defined in Section 3.4. The 3GPP Rel. 11 has considered only TLHs from LTE to 3G, TEHs from 3G to LTE, PPs in both RATs and UHs in LTE.

The performance comparison is carried out for partially and fully overlaying LTE and 3G deployment, described in Section 2.8.2 and Section 2.8.3, respectively, and for four velocities $v_{\mathrm{st}} = 30$ km/h, 60 km/h, 90 km/h and 120 km/h. The simulation parameters which are specific for fully and partially overlaying LTE and 3G deployment are summarized in Table 3.3 and Table 5.4, respectively. The common parameters used

Table 5.4. Simulation parameters which are specific for partially overlaying LTE and 3G deployment.

Parameter	Value
Antenna tilt θ_c	Cell-specific
Number N_{ue} of UEs	664
	Moving randomly: 2 per cell
	Moving on streets: 520
Traffic steering time interval $T_{\mathrm{T}}^{(\mathrm{ts})}$	320 ms

in both deployment scenarios are summarized in Table 3.2. The inter-RAT TTT $Q_c^{(3)}$ is set to 320 ms in the two deployment scenarios and for all velocities.

For fully overlaying LTE and 3G deployment scenario, the handover thresholds are initialized with the best network-wide setting of handover thresholds which is found in Section 4.2. As for partially overlaying LTE and 3G deployment scenario, an aggressive traffic steering policy is assumed which keeps the UEs in the LTE network as long as possible: The two handover thresholds $Q_c^{(1)}$ and $Q_c^{(2)}$ of LTE cells are set to -129 dBm

and -111 dBm, respectively, and the traffic steering threshold Q_{ts} of 3G cells, defined in (2.36), is set to -118 dBm, i.e., the UE is handed over to the LTE network if the signal strength of the LTE cell is higher than Q_{ts}.

In Fig. 5.21, the performance of the automatic algorithm using the specified mobility

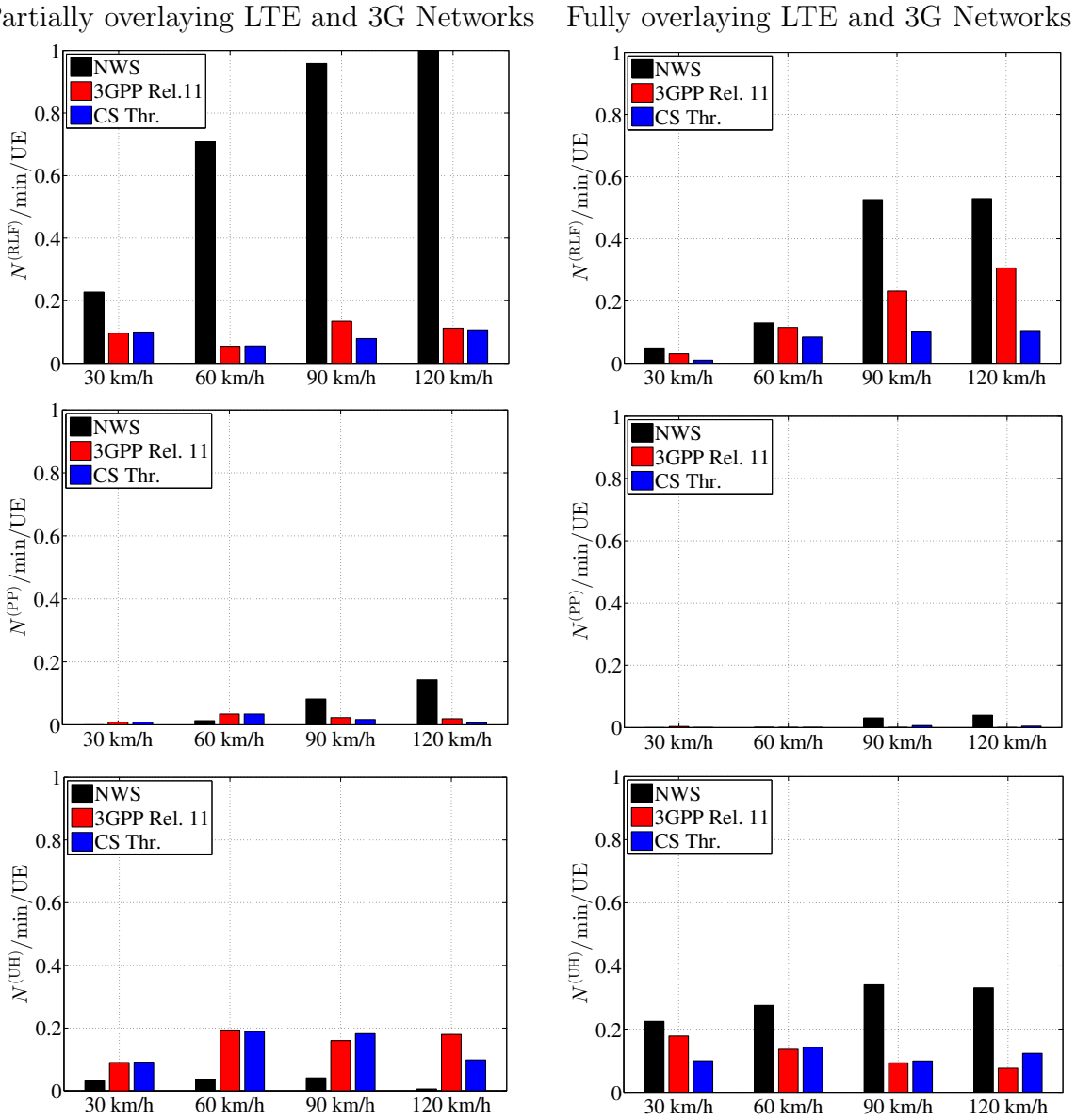

Figure 5.21. Performance of the automatic algorithm using the specified mobility failure types of 3GPP Rel. 11 (3GPP Rel. 11) and all mobility failure types (CS Thr.) in partially (left) and fully (right) overlaying LTE and 3G deployments. The performance of the initial network-wide setting is indicated by "NWS".

failure types of 3GPP Rel. 11 (3GPP Rel. 11) is compared with that using all mobility failure types (CS Thr.) in partially (left) and fully (right) overlaying LTE and

3G deployments. The performance of the initial network-wide setting is indicated by "NWS". The metrics used for performance evaluation are the numbers $N^{(\mathrm{RLF})}$ of RLFs, $N^{(\mathrm{PP})}$ of PPs and $N^{(\mathrm{UH})}$ of UHs occurring per minute and UE. The three metrics are calculated by normalizing the total number $N_{\mathrm{all}}^{(\mathrm{RLF})}$ of RLFs, $N_{\mathrm{all}}^{(\mathrm{PP})}$ of PPs and $N_{\mathrm{all}}^{(\mathrm{UH})}$ of UHs in both 3G and LTE networks by the time interval T_{CL} in minutes and total number N_{ue} of UEs.

With respect to the RLF metric, "3GPP Rel. 11" provides a very good performance in partially overlaying LTE and 3G deployment scenario which is absolutely comparable with that of "CS Thr." approach. This is expected as the 3GPP solution is explicitly designed for this limited LTE coverage scenario along with its adopted assumptions. Note that for $v_{\mathrm{st}} = 30$ km/h and 60 km/h, "3GPP Rel. 11" has a slightly lower number of RLFs than "CS Thr.". This slight difference is due to the fact that the automatic algorithm reacts on the mobility failure events of a cell only if one of the correction directives exceeds the threshold D_{thr} of (5.48).

However, when the two approaches are applied to the second fully overlaying LTE and 3G deployment it can be shown that "3GPP Rel. 11" with missing failure types such as TLH from 3G to LTE is still able to reduce a considerable number of RLFs compared to "NWS", but not to the extent of the "CS Thr." approach. Both approaches are able to reduce PPs as they are already specified in 3GPP Rel. 11 standard. The third row of the figure shows the number $N^{(\mathrm{UH})}$ of UHs which serves as a counter-part for the optimization of TLHs. The number of UHs in a cell has to be accepted as long as TLHs exist in a cell. Results show that both approaches have similar values of $N^{(\mathrm{UH})}$ in both deployment scenarios. As a conclusion, the rest of the mobility failure types which are not yet specified by 3GPP standard may be considered in future releases when they start to occur more frequently in real networks.

5.7.2 Cell-Pair Specific Optimization of Handover Thresholds

5.7.2.1 Network Level Performance Evaluation

The performance of cell-specific optimization of handover thresholds is compared with that of cell-pair specific optimization. The scenario used for evaluation is the fully overlaying LTE and 3G deployment, see Section 2.8.3. The performance is carried out for four different velocities v_{st} of UEs on streets and values of TTT. The simulation parameters which are used for the scenario are summarized in Table 3.2 and Table 3.3

whereas the parameters of the automatic algorithm are given in Table 5.2. For cell-pair specific optimization, the serving cell threshold is configured cell-specifically, i.e., $J_1 = 1$, and the target cell threshold is configured cell-pair specifically, $J_2 = |\mathcal{N}_c|$. In Fig. 5.22, the performance of the cell-pair specific optimization of handover thresholds

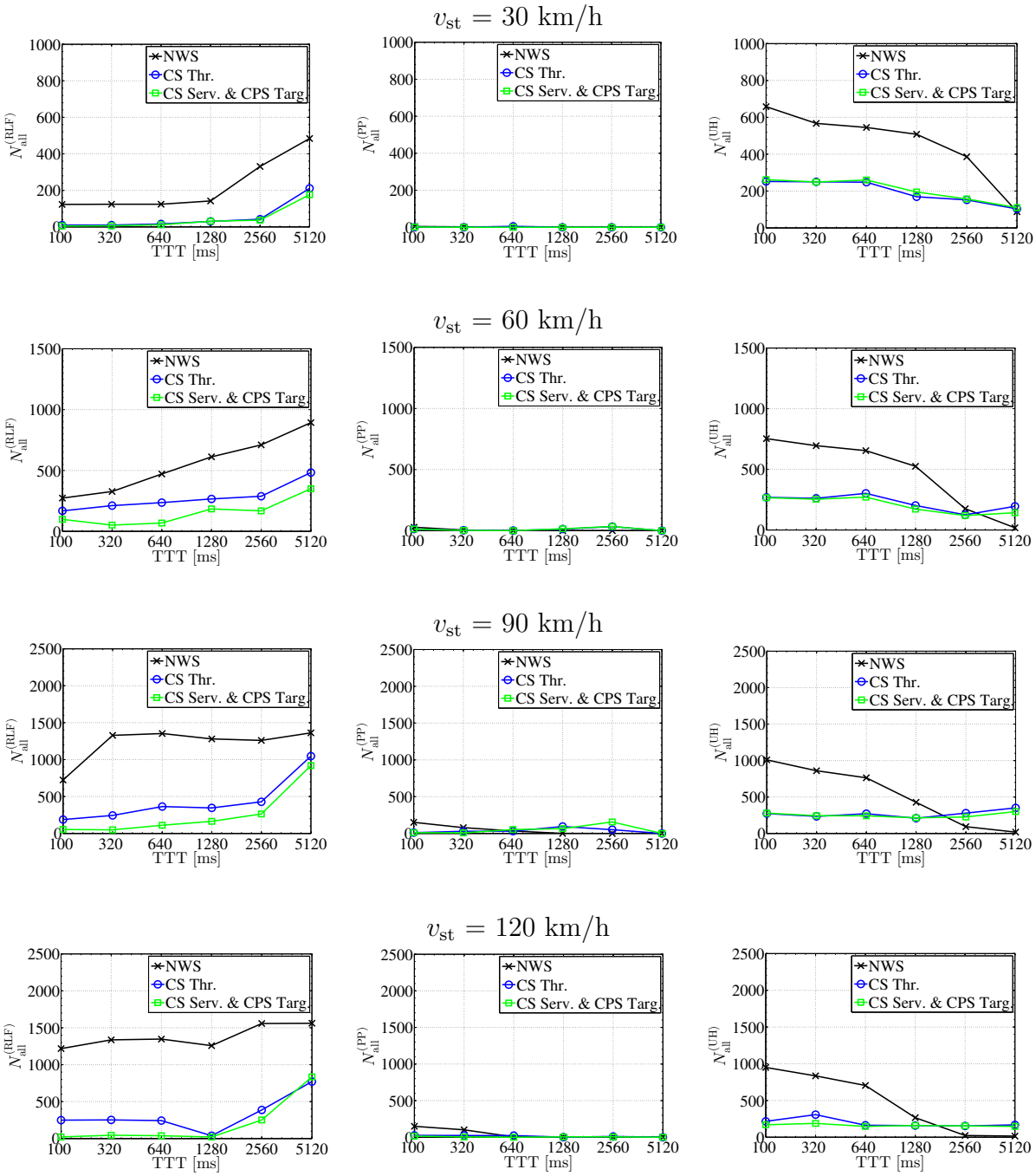

Figure 5.22. Number of mobility failure events for best network-wide setting (NWS), cell-specific (CS Thr.) and cell-pair specific (CS Serv. & CPS Targ.) optimization of handover thresholds for four different velocities v_{st} versus inter-RAT TTT.

(CS Serv. & CPS Targ.) is shown with respect to the total number $N_{\text{all}}^{(\text{RLF})}$ of RLFs, $N_{\text{all}}^{(\text{PP})}$ of PPs in both LTE and 3G networks and total number $N_{\text{all}}^{(\text{UH})}$ of UHs in LTE network.

For $v_{\text{st}} = 30$ km/h and TTT in the range between 100 ms and 2560 ms, the cell-specific optimization of handover thresholds (CS Thr.) resolves most of the RLFs compared to the network-wide setting of handover thresholds (NWS). Thus, the margin for improving the performance is small, and as a result, the cell-pair specific optimization approach achieves similar performance to the "CS Thr." approach. However, for other higher velocities the cell-pair specific optimization approach outperforms the cell-specific optimization for a wide range of TTT values. For $v_{\text{st}} = 60$ km/h and 90 km/h, the cell-pair specific optimization approach achieves lower values of $N_{\text{all}}^{(\text{RLF})}$ for all the values of TTT without any remarkable degradation in the values of $N_{\text{all}}^{(\text{PP})}$ and $N_{\text{all}}^{(\text{UH})}$. For instance, the performance gain in $N_{\text{all}}^{(\text{RLF})}$ is 85% and 76% compared to "NWS" and "CS Thr.", respectively, for $v_{\text{st}} = 60$ km/h and TTT = 320 ms.

The last row of the figure shows the performance of cell-pair specific optimization of handover thresholds for $v_{\text{st}} = 120$ km/h. It is shown that "CS Thr." resolves all RLFs only for the value 1280 ms of TTT. However, "CS Serv. & CPS Targ." resolves all RLFs for TTT in the range between 100 ms and 1280 ms. Hence, configuring the target cell thresholds in a cell-pair specific way does not only yield better performance than the cell-specific approach, but it also reduces the dependency of the performance of the automatic algorithm on the initial value of TTT. Moreover, it is shown that the performance of the cell-pair specific optimization is similar to that of the cell-specific optimization approach for very high values 2560 ms and 5210 ms of TTT. The reason for that is the misconfiguration of TTT, and consequently optimizing only the handover thresholds in a cell-pair specific way is not enough to improve the performance of the "CS Thr." approach.

5.7.2.2 Cell Level Performance Evaluation

The performance of the cell-pair specific optimization approach is compared to that of the cell-specific optimization on a cell level. The performance comparison is carried out for $v_{\text{st}} = 60$ km/h and a TTT value of 320 ms, which are the parameters used to obtain the best network-wide setting of handover thresholds in Section 4.2. The network level performance of the cell-pair specific optimization approach has been already presented in Fig. 5.22. The initial handover thresholds of the automatic algorithm are set to the best network-wide setting of handover thresholds for the cell-specific and the cell-pair specific optimization approaches.

The number $N_c^{(\mathrm{RLF})}$ of RLFs and $N_c^{(\mathrm{UH})}$ of UHs of each cell c is shown in Fig. 5.23 for cell-specific (left) and cell-pair specific (right) optimization of handover thresholds.

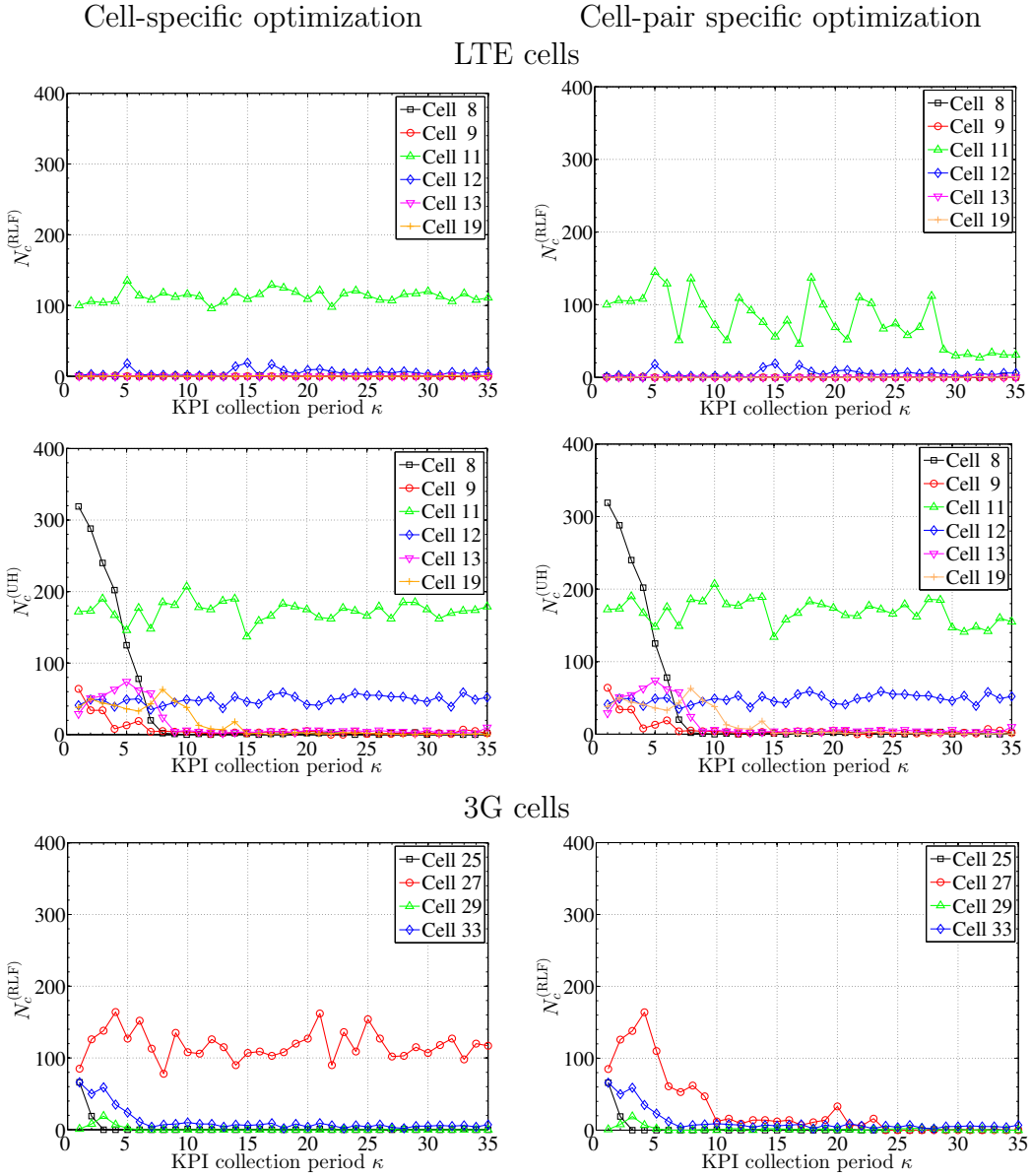

Figure 5.23. Cell level performance comparison between the cell-specific (left) and cell-pair specific (right) optimization of handover thresholds for a velocity $v_{\mathrm{st}} = 60$ km/h and inter-RAT TTT $Q_c^{(3)} = 320$ ms.

The numbers $N_c^{(\mathrm{PP})}$ of PPs are not shown because they are negligible for all cells, i.e., $N_c^{(\mathrm{PP})}$ is shown in Fig. 5.17 for the cell-specific optimization approach.

According to Fig. 5.23, it is shown that the cell-pair specific optimization approach reduces the number $N_c^{(\mathrm{RLF})}$ of RLFs for LTE cell 11 and 3G cell 27 compared to the cell-specific optimization. The rest of the cells have the same performance in the

cell-specific and cell-pair specific optimization approaches. The number of RLFs in cell 27 has been completely resolved by the cell-pair specific optimization approach because different target cell thresholds are configured with respect to neighboring cells. The remaining RLFs of cell 11 could not be resolved since the number of mobility failure events requiring an increase in the cell-pair specific target cell threshold $Q_{c,j}^{(2)}$ is approximately equal to those requiring a decrease, i.e., $D_{c,j}^{(+),2} \approx D_{c,j}^{(-),2}$. At the beginning, the value of $N_c^{(\mathrm{RLF})}$ oscillates for cell 11, however, the automatic algorithm converges at the end to a stable point by reducing the controller gain for that cell.

The serving and target cell thresholds that are obtained by the cell-pair specific optimization are shown in Fig. 5.24 for the LTE and 3G cells having mobility problems initially or during the optimization. The target cell thresholds of each cell are shown

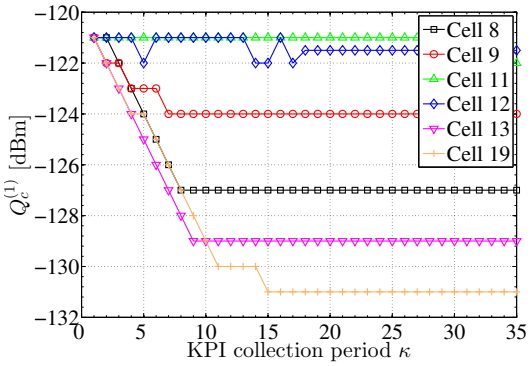

(a) The serving cell thresholds $Q_c^{(1)}$ for LTE cells.

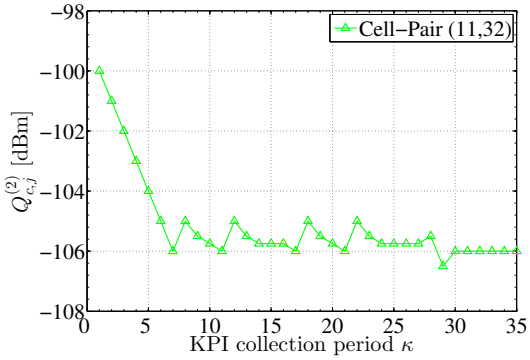

(b) The target cell thresholds $Q_{c,j}^{(2)}$ for (LTE, 3G) cell-pairs.

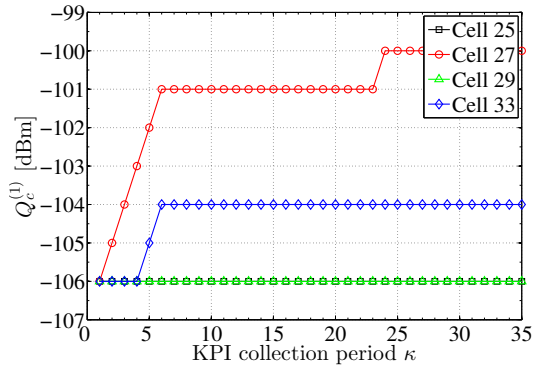

(c) The serving cell thresholds $Q_c^{(1)}$ for 3G cells.

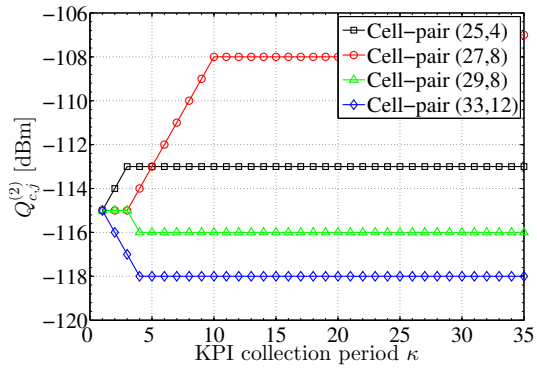

(d) The target cell thresholds $Q_{c,j}^{(2)}$ for (3G, LTE) cell-pairs.

Figure 5.24. The serving and target cell thresholds as a function of the KPI collection period κ for each LTE and 3G cell.

with respect to a neighboring cell, i.e., (serving cell, target cell). For instance, the target cell threshold of cell 11 is changed only with respect to 3G neighboring cell 32 as shown in Fig. 5.24(b). The target cell thresholds of cell 11 are not changed with

respect to other neighboring cells and they are all equal to the initial value of −100 dBm. The same applies for all other 3G cells. The target cell threshold of cell 27 is increased with respect to neighboring LTE cell 8 whereas it is not changed with respect to other neighboring cells. By setting a different target cell threshold with respect to each neighboring cell, the cell-pair specific optimization can outperform the cell-specific optimization approach as shown in Fig. 5.23 for cells 11 and 27.

Chapter 6

Joint Automatic Optimization of Handover Thresholds and Time-to-Trigger

6.1 Motivation

The inter-RAT mobility performance of UEs can be improved significantly when the handover thresholds are optimized in a cell-specific or cell-pair specific way. The simulation results presented in Chapter 5 show that the performance of the automatic algorithm optimizing the handover thresholds depends significantly on the initial value of TTT. In particular, the performance of the automatic algorithm evaluated for high values of TTT such as 2560 ms and 5120 ms is in general worse than those corresponding to smaller values of TTT. In order to achieve a performance which is independent of the initial value of TTT, both the handover thresholds and TTT parameter have to be jointly optimized for each cell. The joint optimization of these handover parameters complements the inter-RAT MRO solution which was presented in Chapter 5 for handover thresholds only.

The TTT time interval can be tuned to delay or execute earlier an inter-RAT handover. Therefore, the TTT can be used as an additional degree of freedom to tackle the mobility failure events. Unlike handover thresholds, the TTT parameter is configured per measurement reporting configuration [3GP12g]. The configuration possibilities of handover thresholds and TTT are discussed in Section 6.2.

A misconfiguration of a handover threshold is captured by high values of predefined KPIs which indicate the types and the numbers of mobility failure events. Following the same approach, the misconfiguration of TTT should be captured by specific KPIs that count the number of mobility failure events which can be resolved by adjusting the value of TTT. For this purpose, the author proposes in Section 6.3 to classify the inter-RAT mobility failure events into three categories: 1) Category I comprises the mobility failure events which can be resolved only by the handover thresholds, 2) Category II comprises the mobility failure events which can be resolved only by the TTT, and 3) Category III comprises the mobility failure events which can be resolved either by the handover thresholds or TTT. Two new sets of KPIs are proposed to count the mobility failure events of these three categories: The first set counts the mobility failure events of Category I and the second set counts the mobility failure

events of Category II and III, i.e., the mobility failure events of Category II and III are not distinguished. These two sets of KPIs cannot be fully differentiated with current 3GPP standardized means. To differentiate between the two proposed sets of KPIs, new signaling and reporting messages have to be specified by the 3GPP standard for the UEs and BSs.

Using the aforementioned two sets of KPIs, the author proposes an optimization algorithm for the handover thresholds and TTT in Section 6.4. The handover parameters are optimized based on the values of the aforementioned detailed KPIs which are collected periodically during a predefined time interval T_{CL}. As Category III comprises mobility failure events which can be resolved either by handover thresholds or TTT, one of the two handover parameters is updated in each KPI collection period. Coordinating the update of handover thresholds and TTT is necessary to avoid double reaction on the same mobility failure events.

In Section 6.5, the performance of the automatic algorithm optimizing jointly the handover thresholds and TTT is compared to that optimizing the handover thresholds only. The performance of the joint optimization is evaluated for cell-specific and cell-pair specific target cell thresholds in Section 6.5.1 and Section 6.5.2, respectively.

6.2 Configuration of Handover Thresholds and Time-to-Trigger

In this section, the configuration of the handover thresholds and TTT is discussed in detail.

The index m of (2.32) for the three inter-RAT handover parameters the serving cell threshold, the target cell threshold and TTT is equal to $1, 2, 3$, respectively. It has been shown in Section 5.5.4.1 that the serving cell threshold $Q_c^{(1)}$ should be configured in a cell-specific way whereas the target cell threshold $Q_{c,j}^{(2)}$ can be configured either in a cell-specific or cell-group specific way, i.e., a dedicated value of $Q_{c,j}^{(2)}$ is configured with respect to the j^{th} subset of neighboring cells. As for TTT which is denoted by $Q_c^{(3)}$, it is defined by the 3GPP standard per measurement reporting configuration. If the measurement events of all UEs are configured with the same value of TTT irrespective of the neighboring cell, the configuration of TTT is considered to be cell-specific in this case. In principle, the properties of TTT could be extended to allow a cell-group specific configuration. However, the configuration of TTT in a cell-group specific way

is not beneficial as it may yield to high number of RACH failures which occur when the UE fails to access the target cell threshold during the handover. This can be illustrated using Fig. 6.1 which shows a serving cell c overlaying with inter-RAT neighboring cell i_1 and three other neighboring cells i_2, i_3, i_4.

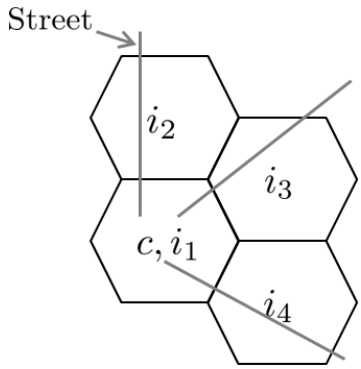

Figure 6.1. Serving cell c and its four corresponding neighboring inter-RAT cells i_1, i_2, i_3 and i_4.

Decreasing only the TTT of serving cell c with respect to neighboring cell i_4 may trigger faster the handover of UEs to neighboring cell i_4, including those which might be far from i_4. Accordingly, there is a risk that the UEs moving on the other two streets passing through i_2 and i_3 try to hand over first to neighboring cell i_4. However, these far UEs would most probably fail to access the target cell i_4 during the handover and in turn they would detect RACH failures.

The RACH failures could occur as well when the TTT is increased cell-pair specifically. For instance, assume that the TTT of serving cell c is increased only with respect to overlaying cell i_1. As the other three neighboring cells i_2, i_3 and i_4 have now smaller values of TTT, the UEs may first try to handover to one of these three neighboring cells instead of i_1. However, these UEs are far from the BSs serving cells i_2, i_3 and i_4, and consequently they would fail to access these cells during the handover. As a result, the UEs detect RACH failures and drop the call.

6.3 Classification of the Inter-RAT Mobility Failure Events into Two Sets of Key Performance Indicators

In order to make use of the TTT, the mobility failure events that can be resolved by adjusting the TTT should be differentiated from those that can be resolved by the

handover thresholds. For this reason, the mobility failure events are classified into three categories as shown in Fig. 6.2:

1. Category I comprises the mobility failure events that can be resolved only by handover thresholds.
2. Category II comprises the mobility failure events that can be resolved only by TTT.
3. Category III comprises the mobility failure events that can be resolved either by handover thresholds or TTT.

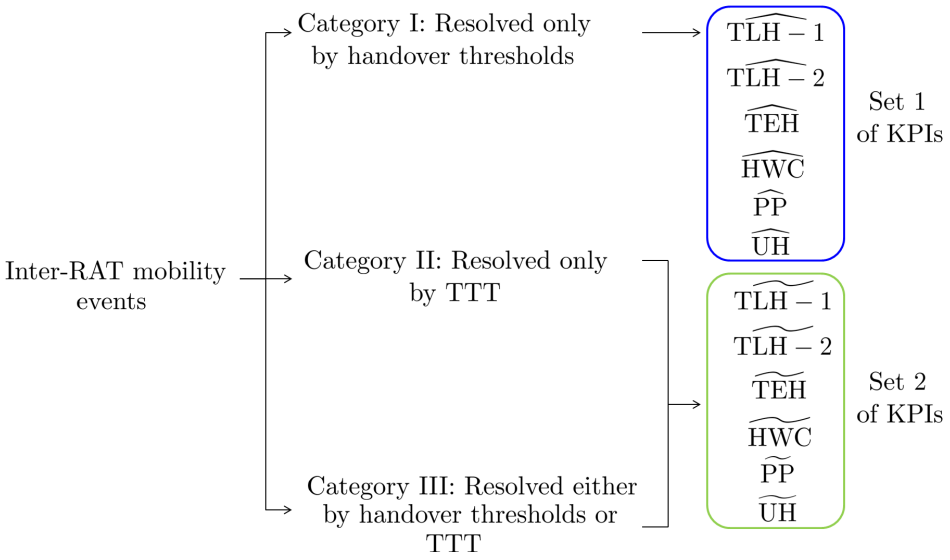

Figure 6.2. The classification of the inter-RAT mobility failure events into two sets of KPIs.

Using this classification, the mobility failure events of Category I that can be resolved only by the handover thresholds are isolated from those of Category II and III that can be resolved by adjusting the TTT. Accordingly, two sets of KPIs are proposed as shown in Fig. 6.2: The set of KPIs that counts the mobility failure events of Category I is denoted by Set 1 whereas the set of KPIs that counts the mobility failure events of Category II and Category III is denoted by Set 2. The KPIs of Set 1: $\widehat{\text{TLH}-1}$, $\widehat{\text{TLH}-2}$, $\widehat{\text{TEH}}$, $\widehat{\text{HWC}}$, $\widehat{\text{PP}}$ and $\widehat{\text{UH}}$ are used for TLH of type 1, TLH of type 2, TEH, HWC, PP and UH, respectively. Similarly, the KPIs of Set 2 are indicated by $\widetilde{\text{TLH}-1}$, $\widetilde{\text{TLH}-2}$, $\widetilde{\text{TEH}}$, $\widetilde{\text{HWC}}$, $\widetilde{\text{PP}}$ and $\widetilde{\text{UH}}$. Currently, it is not possible in 3GPP standard to differentiate between these two sets of KPIs.

Category II consists of only one case of TLH that can be resolved exclusively by TTT. This case is more probable to occur for high values of TTT and it is depicted in Fig. 6.3.

The figure shows the measurement $MQ_{u,c}(t_n)$ and $MQ_{u,i_k}(t_n)$ of a UE u corresponding to serving cell c and k^{th} inter-RAT neighboring cell i_k, respectively. The UE connected

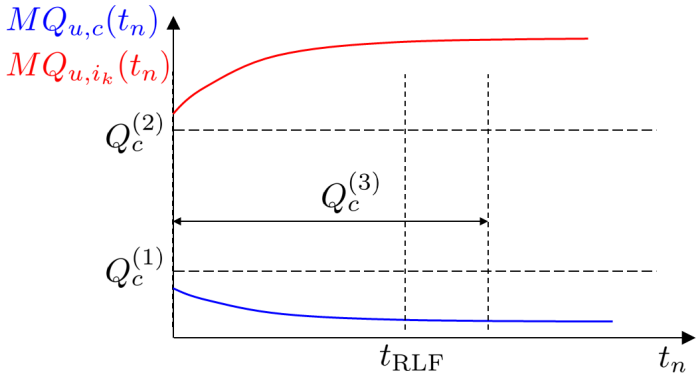

Figure 6.3. A special case of TLH which can be resolved exclusively by TTT.

to serving cell c fails to handover to neighboring cell i_k and experiences an RLF at time step t_{RLF} before the handover is initiated. This mobility failure event is counted as TLH if the UE was not handed over from the previously serving cell. Otherwise, the mobility failure event is counted as TLH only if the UE has stayed in cell c without an RLF for more than T_{TE} time interval which is defined in Section 3.4.1 to differentiate between TEHs and TLHs.

In order to resolve this case of TLH, the handover should be completed before the UE detects an RLF. Increasing the serving cell threshold $Q_c^{(1)}$ or decreasing the target cell threshold $Q_c^{(2)}$ does not help since the entering condition of the measurement event is already fulfilled from the first time instant the UE is connected to serving cell c. The only solution for this case of TLH is to decrease the TTT parameter $Q_c^{(3)}$ so that the handover is triggered prior to the RLF. The automatic algorithm optimizing only the handover thresholds cannot react to this special case of TLH. However, it can react to all the other mobility failure events of Category I and III.

The classification of mobility failure events into Set 1 or Set 2 of KPIs depends on whether the mobility event can be resolved by TTT or not. In this study, TLHs of type 1 and type 2 are called missed inter-RAT handovers whereas TEHs, HWCs, PPs and UHs are called fast inter-RAT handovers. A missed inter-RAT handover is classified into Set 2 of KPIs if the handover could be triggered prior to RLF by decreasing the value of TTT. On the other hand, a fast inter-RAT handover is classified into Set 2 of KPIs if the handover could be avoided by increasing the value of TTT.

An example of classifying a missed and a fast inter-RAT handover into Set 2 of KPIs is shown in Fig. 6.4(a) and Fig. 6.4(b), respectively. In Fig. 6.4(a), the UE detects

an RLF at time step t_{RLF} before the handover is initiated. The entering condition of the measurement event is fulfilled for the first time at time step t_1. This missed

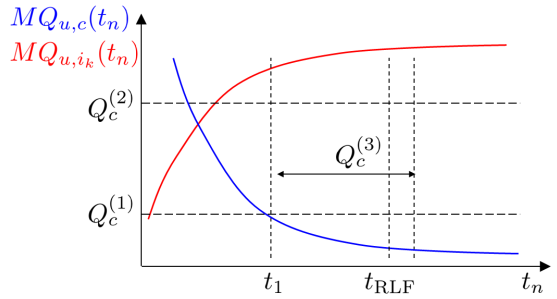

(a) Missed inter-RAT handover classified by Set 2.

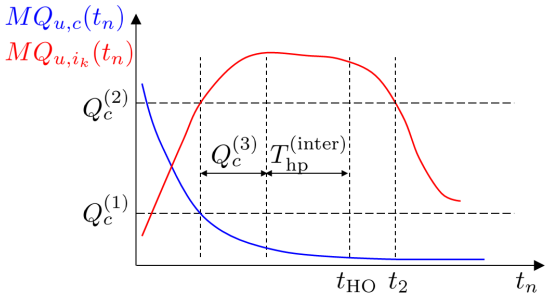

(b) Fast inter-RAT handover classified by Set 2.

Figure 6.4. An example of a missed and fast inter-RAT handover which can be resolved by decreasing and increasing the TTT parameter $Q_c^{(3)}$, respectively.

handover corresponds to a TLH of type 1 since the target cell threshold is crossed first, see Section 3.4.1. Moreover, it is classified in $\widetilde{\text{TLH}-1}$ of Set 2 if there exists a TTT value $\widetilde{Q_c^{(3)}}$ which is smaller than $Q_c^{(3)}$ and satisfies the following condition

$$\widetilde{Q_c^{(3)}} + T_{\text{hp}}^{(\text{inter})} < t_{\text{RLF}} - t_1 \tag{6.1}$$

where $T_{\text{hp}}^{(\text{inter})}$ is the inter-RAT handover preparation time. The same condition applies for TLHs of type 2. By decreasing the value of TTT, the inter-RAT handover would be completed before the RLF occurs.

An example of a fast handover is shown in Fig. 6.4(b) and is generalized for TEH, HWC, PP and UH. For all these failure types, the UE is successfully handed over from cell c to inter-RAT neighboring cell i_k at time step t_{HO}. However, shortly after 1) the UE will detect an RLF in case of TEH and HWC, 2) the UE is handed over to the previous RAT in case of PP and 3) the UE stays in the 3G inter-RAT neighboring cell in case of UH. The time step t_2 indicates the instant when the entering condition of the measurement event of the previously serving and target cells is not fulfilled for the first time after the inter-RAT handover is executed. All the aforementioned types of fast handovers are classified into Set 2 of KPIs if there exists a TTT value $\widetilde{Q_c^{(3)}}$ which is higher than $Q_c^{(3)}$ and satisfies

$$\widetilde{Q_c^{(3)}} > Q_c^{(3)} + T_{\text{hp}}^{(\text{inter})} + (t_2 - t_{\text{HO}}). \tag{6.2}$$

By increasing the value of TTT, the fast inter-RAT handover would not be triggered. The checking of (6.1) and (6.2) require the UE to log and send the signal measurements of the serving and target cells to the BS, even after the handover in case of (6.2) which

is not fully specified by the 3GPP standard, i.e., the UE can measure only the signal level of the previous LTE cell according to the 3GPP standard.

All the other mobility failure events which cannot be resolved by TTT are classified into Set 1 of KPIs. For instance, a missed handover of which the entering condition of the measurement event was never fulfilled is classified in Set 1. Two examples of missed handover that can be resolved by adjusting only the handover thresholds are shown in Fig. 6.5(a) and Fig. 6.5(b), respectively. The missed handover in Fig. 6.5(a)

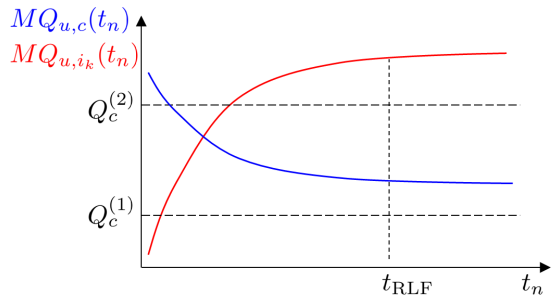

(a) Missed inter-RAT handover which can be resolved by increasing $Q_c^{(1)}$.

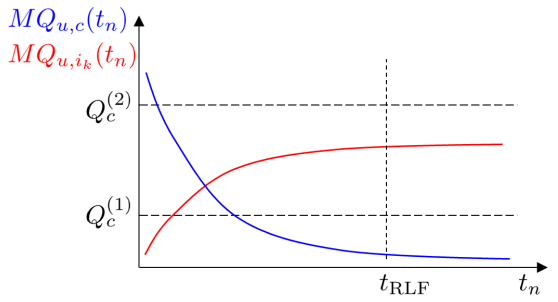

(b) Missed inter-RAT handover which can be resolved by decreasing $Q_c^{(2)}$.

Figure 6.5. Two examples of missed inter-RAT handover which can be resolved only by adjusting the handover thresholds.

and Fig. 6.5(b) can be resolved only by increasing the serving cell threshold $Q_c^{(1)}$ and decreasing the target cell threshold $Q_c^{(2)}$, respectively. Adjusting the TTT parameter in these two examples does not have any impact since the entering condition of the measurement event would never be fulfilled if the misconfigured handover threshold is not adjusted. On the other hand, a fast handover which does not fulfill the condition of (6.2) is classified in Set 1.

6.4 Optimization Loop of Handover Thresholds and Time-to-Trigger

6.4.1 Introduction

The optimization loop of the inter-RAT handover thresholds and TTT is shown in Fig. 6.6. It is carried out per each LTE or 3G cell independently. In each KPI collection period κ, a root cause analysis is performed by each cell for the collected mobility failure events. Then, the subsets $\mathcal{S}_{c,j}^{(m)}$ of (5.17) are selected for each handover parameter m.

Using these subsets, the two correction directives $D_{c,j}^{(+),m}(\kappa)$ and $D_{c,j}^{(-),m}(\kappa)$ of (5.23) are computed for each handover parameter. These correction directives are used as input for the coordination entity that decides on whether the handover thresholds or TTT should be updated in each KPI collection period. Accordingly, the handover parameters are updated and the optimization loop is repeated until the algorithm converges.

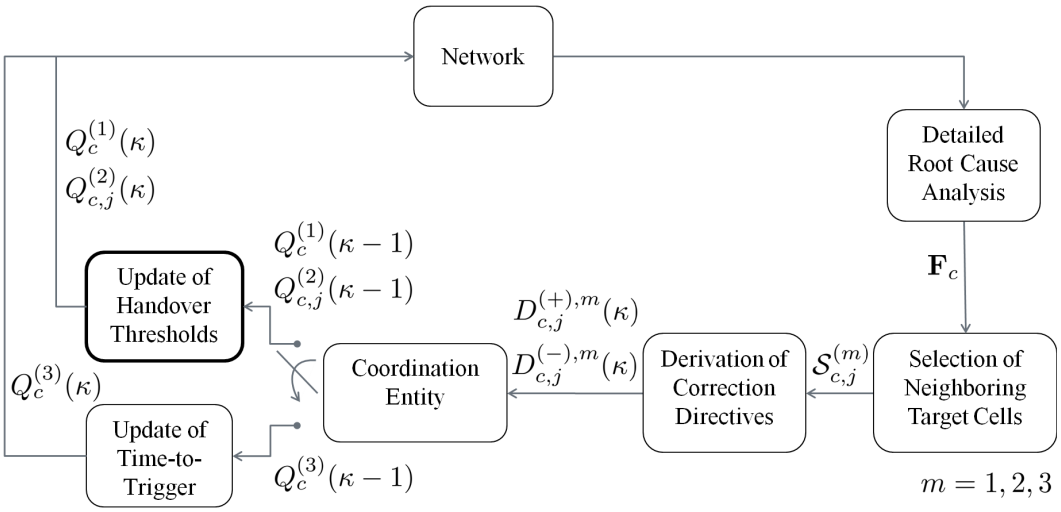

Figure 6.6. The optimization loop of the inter-RAT handover thresholds and TTT.

6.4.2 Detailed Root Cause Analysis

Each cell updates its handover parameters based on the statistics of the KPI values of Set 1 and Set 2. The values of the KPIs are collected periodically by each cell during the time interval T_{CL}. Each mobility failure event is counted by the cell of which the misconfiguration of its handover parameters is the root cause for that failure. Moreover, the mobility failure event is classified into Set 1 or Set 2 of KPIs depending on whether the mobility failure event can be resolved by TTT or not. The index $a = 1, \ldots, A$, where $A = 12$, is used for the KPIs of Set 1 and Set 2: The index $a = 1, \ldots, 6$ is used for $\widehat{\mathrm{TLH}-1}$, $\widehat{\mathrm{TLH}-2}$, $\widehat{\mathrm{TEH}}$, $\widehat{\mathrm{HWC}}$, $\widehat{\mathrm{PP}}$ and $\widehat{\mathrm{UH}}$, respectively, whereas $a = 7, \ldots, 12$ is used for $\widetilde{\mathrm{TLH}-1}$, $\widetilde{\mathrm{TLH}-2}$, $\widetilde{\mathrm{TEH}}$, $\widetilde{\mathrm{HWC}}$, $\widetilde{\mathrm{PP}}$ and $\widetilde{\mathrm{UH}}$, respectively.

The KPI values of Set 1 and Set 2 which are collected by cell c with respect to each k^{th} inter-RAT neighboring cell i_k are summarized in the matrix $\mathbf{F}_c \in \mathbb{Z}^{A\times K}$ of (5.3). The (a, k) element of $\mathbf{F}_c$, denoted by $[\mathbf{F}_c]_{a,k}$, indicates the value of the a^{th} KPI in cell c with respect to k^{th} inter-RAT neighboring cell. In each KPI collection period κ, a new matrix $\mathbf{F}_c$ is computed by cell c.

6.4.3 Selection of Neighboring Target Cells for Handover Thresholds and Time-to-Trigger

After the root cause analysis, the subsets $\mathcal{S}_{c,j}^{(m)}$ of neighboring target cells are selected for each handover parameter m, see Section 5.5.3. Using the subset $\mathcal{S}_{c,j}^{(m)}$, the matrix $\mathbf{S}_{c,j}^{(m)}$ can be derived to extract all or a fraction of the columns in $\mathbf{F}_c$ as depicted in (5.19). The selection of $\mathcal{S}_{c,j}^{(m)}$ depends on the configuration of each handover parameter. If the handover parameter is configured cell-specifically, e.g., serving cell threshold $Q_c^{(1)}$ and TTT $Q_c^{(3)}$, all values of the KPIs in $\mathbf{F}_c$ are considered. As a result, the set $\mathcal{S}_{c,j}^{(m)} = \mathcal{N}_c$ and $\mathbf{S}_{c,j}^{(m)}$ is equal to the identity matrix $\mathbf{I} \in \mathbb{B}^{K\times K}$. On the other hand, if the handover parameter is configured cell-pair specifically, e.g., target cell threshold $Q_{c,j}^{(2)}$, the set $\mathcal{N}_c$ of neighboring cells is decomposed such that each subset $\mathcal{S}_{c,j}^{(m)}$ consists of a single neighboring cell. In this case, only the values of the KPIs collected with respect to that specific neighboring cell are considered in the optimization of $Q_{c,j}^{(m)}$. The matrix $\mathbf{S}_{c,j}^{(m)} \in \mathbb{B}^{K\times 1}$ is used to select the column in $\mathbf{F}_c$ corresponding to neighboring cell of subset $\mathcal{S}_{c,j}^{(m)}$.

6.4.4 Derivation of Correction Directives for Handover Thresholds and Time-to-Trigger

Having computed $\mathbf{F}_c$ and decided on the selection matrix $\mathbf{S}_{c,j}^{(m)}$, the correction directives $D_{c,j}^{(+),m}$ and $D_{c,j}^{(-),m}$ of each handover parameter can be derived from the vector $\boldsymbol{\ell}_{c,j}^{(m)} \in \mathbb{Z}^{A\times 1}$ using (5.23), i.e., $D_{c,j}^{(+),m}$ and $D_{c,j}^{(-),m}$ are the total number of mobility failure events requiring an increase and a decrease, respectively, in handover parameter $Q_{c,j}^{(m)}$. The a^{th} element $\left[\boldsymbol{\ell}_{c,j}^{(m)}\right]_{a,1}$ of $\boldsymbol{\ell}_{c,j}^{(m)}$ is the sum of all the values of the a^{th} KPI in cell c with respect to all neighboring cells in set $\mathcal{S}_{c,j}^{(m)}$. As the serving cell threshold and TTT are configured cell-specifically, the index $j = 1$ can be dropped from $D_{c,j}^{(+),m}$, $D_{c,j}^{(-),m}$ and $\boldsymbol{\ell}_{c,j}^{(m)}$ for $m = 1, 3$, i.e., $\boldsymbol{\ell}_c = \boldsymbol{\ell}_{c,j}^{(m)}$. To obtain the correction directives, (5.23) requires the design of matrix $\mathbf{G}_m \in \mathbb{R}^{A\times 2} = [\mathbf{g}_{1,m}, \mathbf{g}_{2,m}]$ for each handover parameter.

Following the same approach as in Section 5.6.4, the RLF related KPIs have weights equal to 1 whereas PP and UH KPI is given the weight $0 \leq w_{\text{PP}} \leq 1$ and $0 \leq w_{\text{UH}} \leq 1$, respectively. The weight w_{UH} is defined in (5.45). The mobility failure events of Set 1 can be resolved only by the handover thresholds, and consequently they are not grouped into the correction directives of TTT. However, the mobility failure events of Set 2 can be resolved by TTT. In this case, TTT can be used as an additional degree of freedom to tackle the mobility failure events of Set 2. In this study, the RLF events

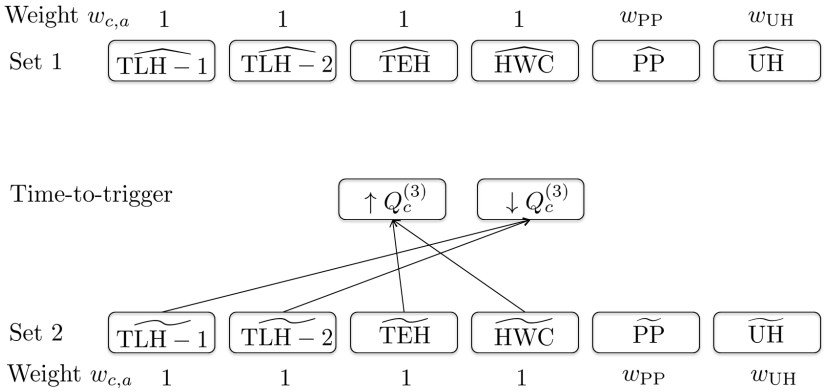

Figure 6.7. Values of the KPIs which are grouped into the correction directives corresponding to cell-specific TTT $Q_c^{(3)}$.

of Set 2 are grouped into the correction directives of TTT as shown in Fig. 6.7. The mobility failure events of $\widetilde{\mathrm{TLH}-1}$ and $\widetilde{\mathrm{TLH}-2}$ require a decrease in $Q_c^{(3)}$ whereas those of $\widetilde{\mathrm{TEH}}$ and $\widetilde{\mathrm{HWC}}$ require an increase in $Q_c^{(3)}$.

The rest of the mobility failure events in Set 1 and Set 2 are grouped into the correction directives of the handover thresholds. The values of the KPIs which are grouped into the correction directives of the serving and target cell thresholds are shown in Fig. 6.8 and Fig. 6.9, respectively. The grouping of the values of the KPIs follows the same logic which was used in Section 5.6.4 for the automatic algorithm optimizing only the handover thresholds.

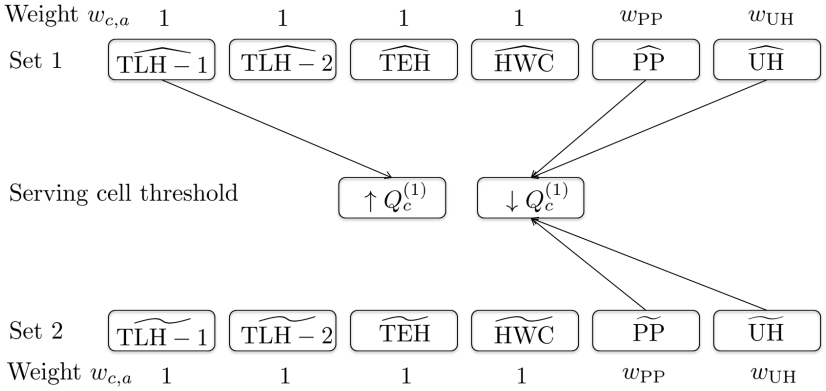

Figure 6.8. Values of the KPIs which are grouped into the correction directives corresponding to cell-specific serving cell threshold $Q_c^{(1)}$.

Using the three aforementioned figures, the matrices $\mathbf{G}_1$, $\mathbf{G}_2$ and $\mathbf{G}_3$ corresponding to

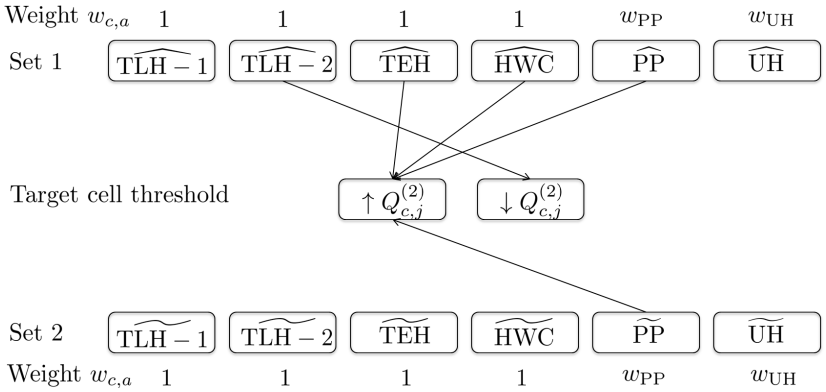

Figure 6.9. Values of the KPIs which are grouped into the correction directives corresponding to cell-pair specific target cell threshold $Q_{c,j}^{(2)}$.

$Q_c^{(1)}$, $Q_{c,j}^{(2)}$ and $Q_c^{(3)}$ thresholds, respectively, can be expressed as follows:

$$\mathbf{G}_1 = \begin{bmatrix} 1 & 0 \\ 0 & 0 \\ 0 & 0 \\ 0 & 0 \\ 0 & w_{\text{PP}}/2 \\ 0 & w_{\text{UH}} \\ 0 & 0 \\ 0 & 0 \\ 0 & 0 \\ 0 & 0 \\ 0 & w_{\text{PP}}/2 \\ 0 & w_{\text{UH}} \end{bmatrix}, \mathbf{G}_2 = \begin{bmatrix} 0 & 0 \\ 0 & 1 \\ 1 & 0 \\ 1 & 0 \\ w_{\text{PP}}/2 & 0 \\ 0 & 0 \\ 0 & 0 \\ 0 & 0 \\ 0 & 0 \\ 0 & 0 \\ w_{\text{PP}}/2 & 0 \\ 0 & 0 \end{bmatrix} \text{ and } \mathbf{G}_3 = \begin{bmatrix} 0 & 0 \\ 0 & 0 \\ 0 & 0 \\ 0 & 0 \\ 0 & 0 \\ 0 & 0 \\ 0 & 1 \\ 0 & 1 \\ 1 & 0 \\ 1 & 0 \\ 0 & 0 \\ 0 & 0 \end{bmatrix}. \tag{6.3}$$

The proposed design of $\mathbf{G}_1$, $\mathbf{G}_2$ and $\mathbf{G}_3$ fulfills the constraint of (5.10), i.e., $\sum_{m=1}^{M+1} (\mathbf{g}_{1,m} + \mathbf{g}_{2,m}) = \mathbf{w}_c$, where $M = 2$ is the number of handover thresholds and $\mathbf{w}_c$ is the vector containing the weights $w_{c,a}$ of each KPI a, i.e.,

$$\mathbf{w}_c = \begin{bmatrix} 1 \\ 1 \\ 1 \\ 1 \\ w_{\text{PP}} \\ w_{\text{UH}} \\ 1 \\ 1 \\ 1 \\ 1 \\ w_{\text{PP}} \\ w_{\text{UH}} \end{bmatrix}. \tag{6.4}$$

6.4.5 Coordination Between the Update of Handover Thresholds and Time-to-Trigger

The mobility failure events of Category III can be resolved by adjusting either the handover thresholds or TTT. To avoid double reaction on these mobility events, either the handover thresholds or TTT is changed in each KPI collection period κ. The selection between updating either the handover thresholds or TTT is summarized in pseudo-code 3.

Pseudo-code 3 : Selection between Updating either the Handover Thresholds or Time-to-Trigger.

1: Total number of missed handovers corresponding to handover thresholds: $N_{\mathrm{MH}} = D_c^{(+),1} + \sum_{j=1}^{J_2} D_{c,j}^{(-),2}$ where $D_c^{(+),1} = \boldsymbol{\ell}_c \mathbf{g}_{1,1}$ and $D_{c,j}^{(-),2} = \boldsymbol{\ell}_{c,j}^{(2)} \mathbf{g}_{2,2}$.
2: Total number of fast handovers corresponding to handover thresholds: $N_{\mathrm{FH}} = D_c^{(-),1} + \sum_{j=1}^{J_2} D_{c,j}^{(+),2}$ where $D_c^{(-),1} = \boldsymbol{\ell}_c \mathbf{g}_{2,1}$ and $D_{c,j}^{(+),2} = \boldsymbol{\ell}_{c,j}^{(2)} \mathbf{g}_{1,2}$.
3: Number of missed handovers corresponding to TTT: $D_c^{(-),3} = \boldsymbol{\ell}_c \mathbf{g}_{2,3}$.
4: Number of fast handover corresponding to TTT: $D_c^{(+),3} = \boldsymbol{\ell}_c \mathbf{g}_{1,3}$.
5: **if** $D_c^{(+),3} > D_{\mathrm{T}}^{(\min)}$ or $D_c^{(-),3} > D_{\mathrm{T}}^{(\min)}$ **then**
6: **if** $\left(N_{\mathrm{MH}} + D_c^{(-),3}\right) > \left(N_{\mathrm{FH}} + D_c^{(+),3}\right)$ **then**
7: **if** $D_c^{(-),3} > N_{\mathrm{MH}}$ **then**
8: Update Time-to-Trigger.
9: **else**
10: Update handover thresholds.
11: **end if**
12: **else**
13: **if** $D_c^{(+),3} > N_{\mathrm{FH}}$ **then**
14: Update Time-to-Trigger.
15: **else**
16: Update handover thresholds.
17: **end if**
18: **end if**
19: **else**
20: Update handover thresholds.
21: **end if**

The total number of missed and fast handovers which are grouped by the correction directives of the handover thresholds are denoted by N_{MH} and N_{FH}, respectively, in line 1-2. Similarly, the number of missed and fast handovers of TTT is given by the correction directive $D_c^{(-),3}$ and $D_c^{(+),3}$, respectively, in line 3-4. The TTT parameter is updated only if the value of one of its correction directives exceeds a minimum

threshold denoted by $D_{\mathrm{T}}^{(\min)}$, see line 5. This is necessary to avoid reacting on outlier mobility events.

If one of the TTT correction directives is higher than $D_{\mathrm{T}}^{(\min)}$, the total number $N_{\mathrm{MH}} + D_c^{(-),3}$ of missed handovers in cell c is compared to the total number of fast handovers $N_{\mathrm{FH}} + D_c^{(+),3}$, see line 6. If the total number of missed handovers is higher than that of fast handovers, the two numbers $D_c^{(-),3}$ and N_{MH} corresponding to TTT and handover thresholds, respectively, are compared. If $D_c^{(-),3} > N_{\mathrm{MH}}$, the TTT is updated since the number of missed handovers corresponding to TTT is higher than that of handover thresholds. Otherwise, the handover thresholds are updated. The same approach is followed if the total number of fast handovers in the cell is higher than that of missed handovers, see line 13-17.

The coordination entity checks also if an oscillation is detected in TTT parameter $Q_c^{(3)}$, i.e., an increase followed by a decrease or vice versa. In case the number of oscillations in $Q_c^{(3)}$ reaches the maximum number $N_{\max}^{(\mathrm{osc})}$, the optimization of TTT is stopped and the handover thresholds are updated only.

6.4.6 Update of Handover Thresholds using Feedback Controller

The algorithm updating the handover thresholds is explained in Chapter 5 in detail. The main difference with the joint optimization algorithm of handover thresholds and TTT is that the KPIs are not decomposed into two sets Set 1 and Set 2 of KPIs. The handover thresholds are updated based on the values of six KPIs: TLH-1, TLH-2, TEH, HWC, PP and UH. The value of each KPI is the total sum of the corresponding KPIs in Set 1 and Set 2. For instance, the value of TLH-1 is the sum of the values of $\widehat{\mathrm{TLH}-1}$ and $\widetilde{\mathrm{TLH}-1}$. In each KPI collection period, the values of the six KPIs are grouped into the correction directives $D_{c,j}^{(+),m}$ and $D_{c,j}^{(-),m}$ for each handover threshold m, see Section 5.6.4. The handover threshold is updated based on the values of its corresponding correction directives: The handover threshold is increased if $D_{c,j}^{(+),m} >> D_{c,j}^{(-),m}$, decreased if $D_{c,j}^{(+),m} << D_{c,j}^{(-),m}$ and not modified if $D_{c,j}^{(+),m} \approx D_{c,j}^{(-),m}$. The value of increase and decrease is determined for each handover threshold by a feedback controller which is described in Section 5.6.5.

6.4.7 Update of Time-to-Trigger

The conditions for increasing or decreasing the value of TTT are discussed in Section 6.4.5. The value of TTT is decreased/increased if the total number $N_{\mathrm{MH}} + D_c^{(-),3}$ of missed handovers in the cell is higher/smaller than that of fast handovers $N_{\mathrm{FH}} + D_c^{(+),3}$. Unlike the handover thresholds, the value of TTT is not incremented or decremented by a small change. However, a new value of TTT is applied for the next KPI collection period. In this study, the set $\mathcal{T}$ of TTT values is defined in ms as

$$\mathcal{T} = \{100,\ 128,\ 256,\ 320,\ 640,\ 1024,\ 1280,\ 2560,\ 5120\}. \tag{6.5}$$

For each mobility failure event in $\widetilde{\mathrm{TLH}-1}$, $\widetilde{\mathrm{TLH}-2}$, $\widetilde{\mathrm{TEH}}$ and $\widetilde{\mathrm{HWC}}$ KPIs, there exist more than one value $\widetilde{Q_c^{(3)}} \in \mathcal{T}$ of TTT which can resolve the mobility problem. Among these values, the highest and smallest value of $\widetilde{Q_c^{(3)}}$ is selected for each missed and fast handover, respectively. In each KPI collection period, a distribution of the values of $\widetilde{Q_c^{(3)}}$ is obtained for missed and fast handovers. If the value of TTT should be decreased, the most frequent value of $\widetilde{Q_c^{(3)}}$ in the distribution corresponding to missed handovers is applied in the next KPI collection period. On the other hand, if the value of TTT should be increased, the most frequent value of $\widetilde{Q_c^{(3)}}$ in the distribution corresponding to fast handovers is applied. After updating the values of the handover thresholds or TTT, the whole process is repeated until the optimization algorithm converges.

6.5 Performance Evaluation and Analysis

6.5.1 Joint Optimization of Cell-Specific Handover Thresholds and Time-to-Trigger

6.5.1.1 Network Level Performance Evaluation

The performance of the joint optimization of cell-specific handover thresholds and TTT is compared to that of cell-specific optimization of handover thresholds only on a network level. The scenario consists of two fully overlaying LTE and 3G co-sited networks and it is described in Section 2.8.3. The simulation parameters which are used for the scenario are summarized in Table 3.2 and Table 3.3. As for the parameters of the automatic algorithm, the minimum threshold $D_{\mathrm{T}}^{(\min)}$ and the maximum number

$N_{\max}^{(\mathrm{osc})}$ of oscillations in TTT is set to 20 and 2, respectively. The initial cell-specific values of TTT are set to a fixed network-wide value which is varied in each simulation run: The initial value of TTT is set to 100 ms, 320 ms, 640 ms, 1280 ms, 2560 ms and 5120 ms. The rest of the parameters are given in Table 5.2.

The performance evaluation is based on the total number $N_{\mathrm{all}}^{(\mathrm{RLF})}$ of RLFs, $N_{\mathrm{all}}^{(\mathrm{PP})}$ of PPs in both LTE and 3G networks and number $N_{\mathrm{all}}^{(\mathrm{UH})}$ of UHs in LTE network. The three metrics are shown in Fig. 6.10 for best network-wide setting (NWS), cell-specific optimization of handover thresholds (CS Thr.) and joint optimization of cell-specific handover thresholds and TTT (CS Thr., TTT). The network-wide setting has been already optimized in Section 4.2. The performance comparison is carried out for four velocities v_{st} of UEs on streets: 30 km/h, 60 km/h, 90 km/h and 120 km/h. The x-axis of each sub-figure shows the initial value of TTT for all cells. For "CS Thr., TTT" approach, the values of TTT are changed during the optimization whereas they are fixed for "NWS" and "CS Thr." approaches. Plotting the number of mobility failure events for different initial values of TTT helps to investigate the sensitivity of the optimization approaches with respect to the initial configuration of TTT.

According to Fig. 6.10, $N_{\mathrm{all}}^{(\mathrm{RLF})}$ of "CS Thr., TTT" is more or less independent of the initial value of TTT in contrast to the "CS Thr." approach. Moreover, "CS Thr." and "CS Thr., TTT" have similar $N_{\mathrm{all}}^{(\mathrm{RLF})}$ for some specific value of TTT which varies for each velocity v_{st}. For v_{st} = 30 km/h, 60 km/h and 90 km/h, $N_{\mathrm{all}}^{(\mathrm{RLF})}$ of "CS Thr." and "CS Thr., TTT" are similar for the initial TTT value of 100 ms. However, for v_{st} = 120 km/h both approaches have the same $N_{\mathrm{all}}^{(\mathrm{RLF})}$ for the initial TTT value of 1280 ms which is different than that used for the other three velocities. Furthermore, "CS Thr., TTT" outperforms "CS Thr." and achieves smaller $N_{\mathrm{all}}^{(\mathrm{RLF})}$ for all other values of TTT. As for UHs and PPs, it is shown that both approaches have comparable values of $N_{\mathrm{all}}^{(\mathrm{PP})}$ and $N_{\mathrm{all}}^{(\mathrm{UH})}$. In some cases such as v_{st} = 120 km/h and TTT = 640 ms, "CS Thr., TTT" has a higher $N_{\mathrm{all}}^{(\mathrm{UH})}$ than "CS Thr.". The performance degradation in the number of UHs is acceptable as long as the number $N_{\mathrm{all}}^{(\mathrm{RLF})}$ of RLFs having higher priority than UHs is reduced.

6.5.1.2 Cell Level Performance Evaluation

The performance of the joint optimization of cell-specific handover thresholds and TTT is compared to that of cell-specific optimization of handover thresholds only on a cell level. The performance comparison is carried out for v_{st} = 60 km/h and a TTT value of 320 ms, which are the parameters used to obtain the best network-wide setting

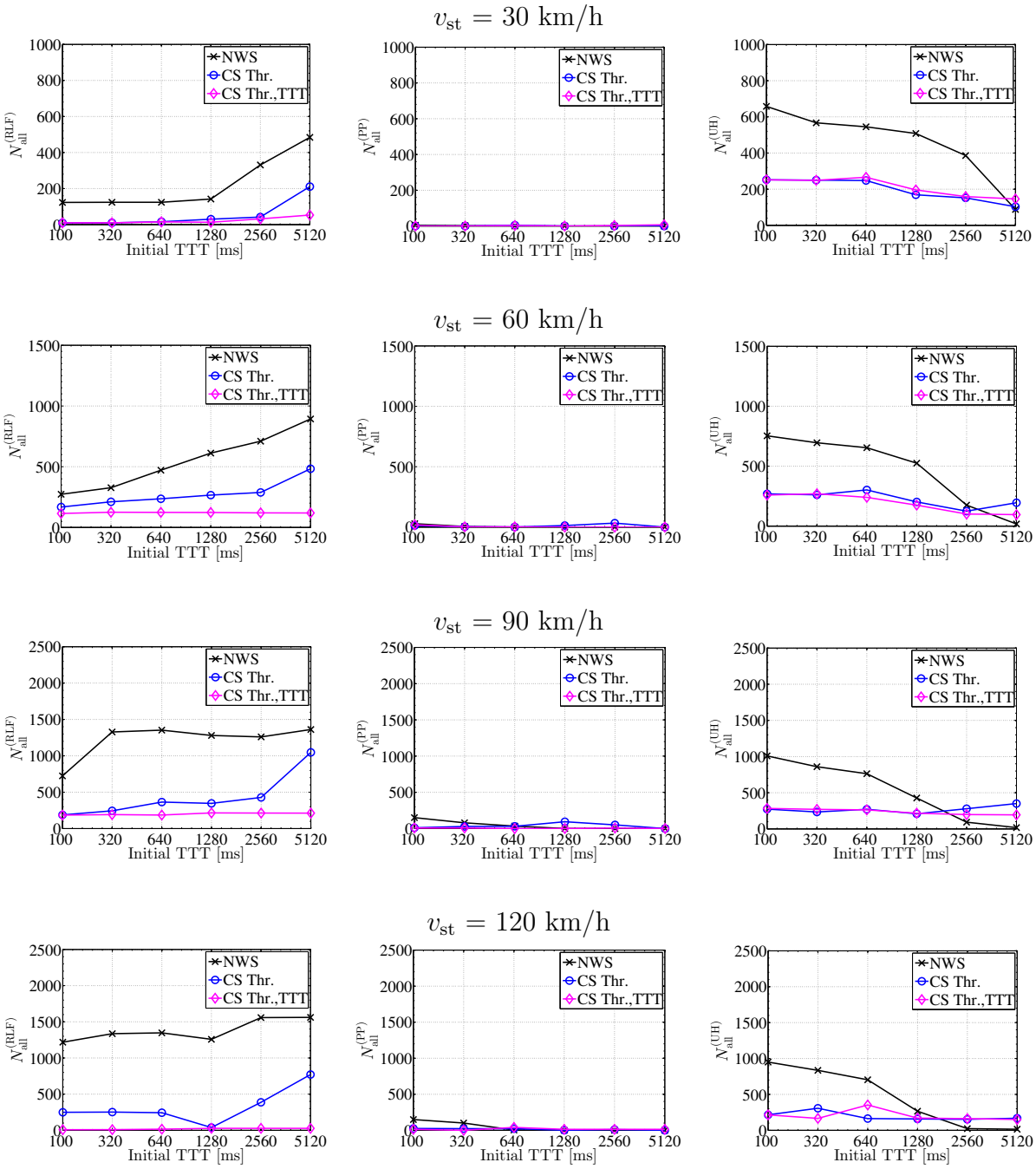

Figure 6.10. Number of mobility failure events for four different velocities v_{st} versus initial inter-RAT TTT.

of handover thresholds in Section 4.2. The network-level performance of the joint optimization approach has already been presented in Fig. 6.10.

The number $N_c^{(\mathrm{RLF})}$ of RLFs and $N_c^{(\mathrm{UH})}$ of UHs of each cell c is shown in Fig. 6.11 for cell-specific optimization of handover thresholds (left) and joint cell-specific optimization of handover thresholds and TTT (right). The numbers $N_c^{(\mathrm{PP})}$ of PPs are not

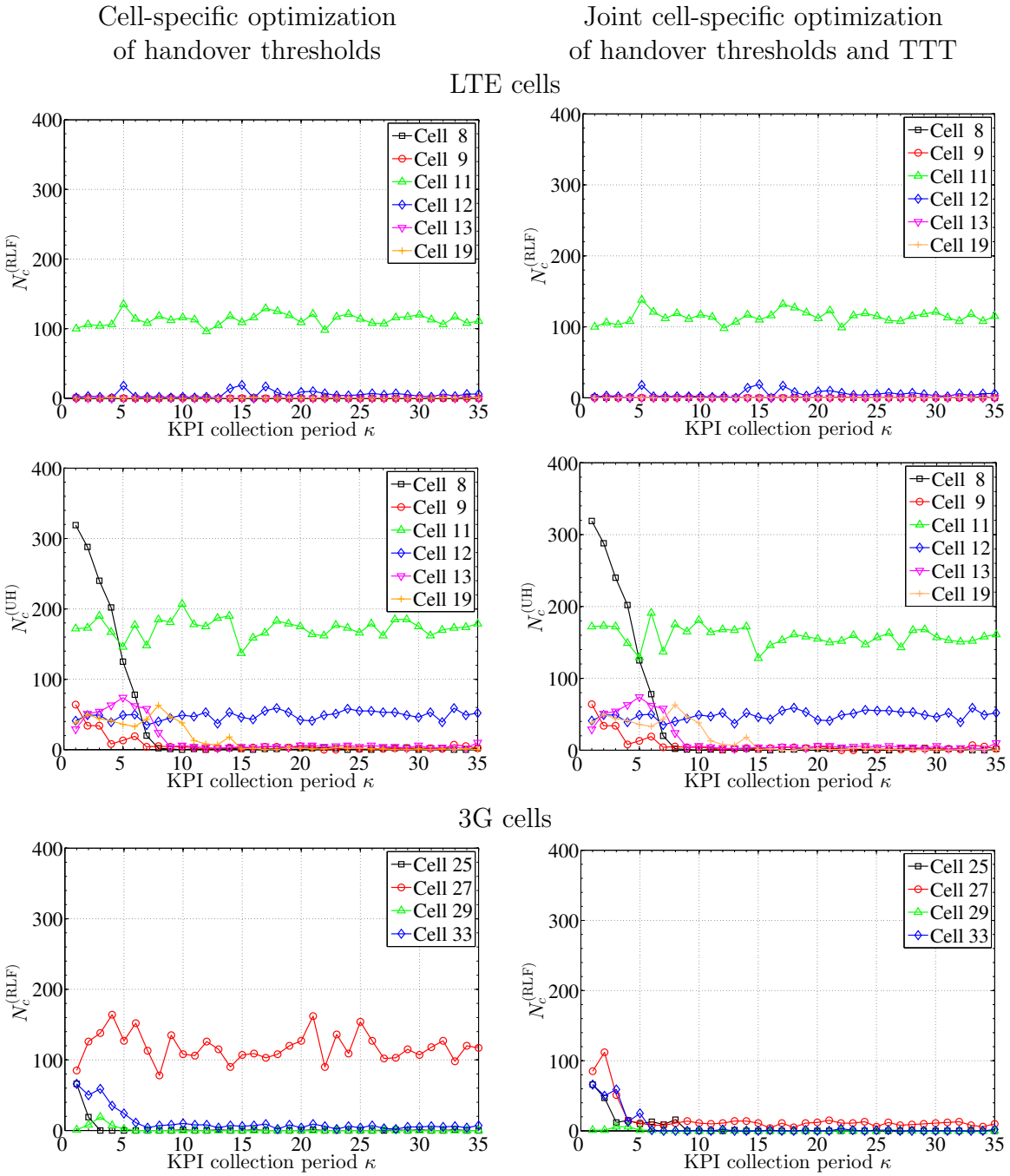

Figure 6.11. Cell level performance comparison between cell-specific optimization of handover thresholds (left) and joint cell-specific optimization of handover thresholds and TTT (right) for velocity $v_{\text{st}} = 60$ km/h and inter-RAT TTT $Q_c^{(3)} = 320$ ms.

shown in Fig. 6.11 because they are negligible for all cells. $N_c^{(\text{PP})}$ has been already shown in Fig. 5.17 for cell-specific optimization approach. According to Fig. 6.11, the joint cell-specific optimization approach resolves completely the number of RLFs in 3G cell 27 as opposed to the cell-specific optimization of handover thresholds. This is

because the joint optimization approach can adjust, in addition to the two handover thresholds, the TTT of each cell and in turn make use of this additional degree of freedom to achieve a better performance. The rest of the cells have similar performance for both optimization approaches.

In Fig. 6.12, the cell-specific values of the inter-RAT TTT $Q_c^{(3)}$ are shown for the velocity $v_{\text{st}} = 60$ km/h and an initial $Q_c^{(3)}$ value of 320 ms (left) and 5120 ms (right). According to the figure, it is shown that $Q_c^{(3)}$ of each cell converges to a different value

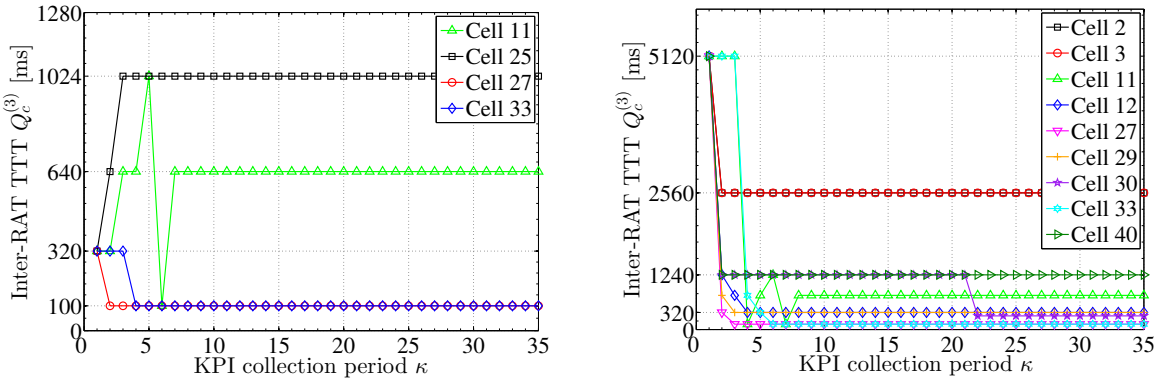

(a) Initial $Q_c^{(3)} = 320$ ms. (b) Initial $Q_c^{(3)} = 5120$ ms.

Figure 6.12. Cell-specific values of the inter-RAT TTT $Q_c^{(3)}$ for the velocity $v_{\text{st}} = 60$ km/h and initial $Q_c^{(3)}$ value of 320 ms (left) and 5120 ms (right).

of TTT. In Fig. 6.12(a), the TTT value of cell 27 is decreased from 320 ms to 100 ms. Without this adjustment of TTT, the RLFs of cell 27 could not be resolved as shown in Fig. 6.11 for cell-specific optimization of handover thresholds (left). The joint optimization of handover thresholds and TTT approach can as well cope with any misconfiguration of the initial value of TTT. In Fig. 6.12(b), it is shown how the automatic joint optimization algorithm can correct the initial extreme value of TTT which is configured at the beginning for LTE and 3G cells.

6.5.2 Joint Optimization of Cell-Specific Serving Cell Threshold and Time-to-Trigger, and Cell-Pair Specific Target Cell Threshold

6.5.2.1 Network Level Performance Evaluation

In this section, the performance of the joint optimization of handover thresholds and TTT is evaluated for cell-pair specific target cell threshold $Q_c^{(2)}$, i.e., $J_2 = |\mathcal{N}_c|$.

The performance evaluation is based on the total number $N_{\text{all}}^{(\text{RLF})}$ of RLFs, $N_{\text{all}}^{(\text{PP})}$ of PPs in both LTE and 3G networks and number $N_{\text{all}}^{(\text{UH})}$ of UHs in LTE network. These three

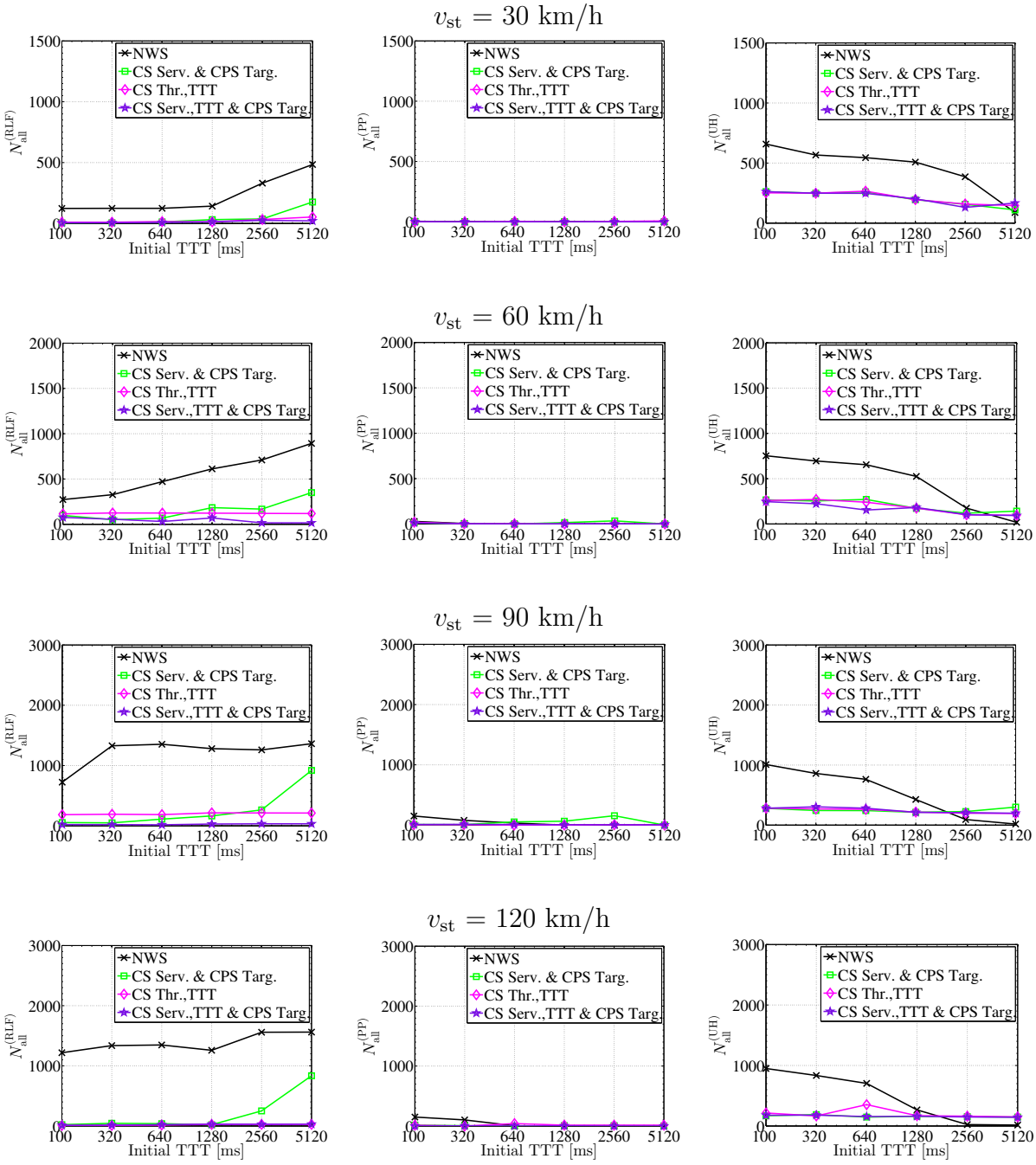

Figure 6.13. Number of mobility failure events for best network-wide setting (NWS), optimization of cell-specific serving cell threshold and cell-pair specific target cell threshold (CS Serv. & CPS Targ.), joint optimization of cell-specific handover thresholds and TTT (CS Thr., TTT) and joint optimization of cell-specific serving cell threshold and TTT, and cell-pair specific target cell threshold (CS Serv., TTT & CPS Targ.).

performance metrics are shown in Fig. 6.13 for best network-wide setting (NWS), opti-

mization of cell-specific serving cell threshold and cell-pair specific target cell threshold (CS Serv. & CPS Targ.), joint optimization of cell-specific handover thresholds and TTT (CS Thr., TTT) and joint optimization of cell-specific serving cell threshold and TTT, and cell-pair specific target cell threshold (CS Serv., TTT & CPS Targ.). The network-wide setting has already been optimized in Section 4.2. The performance comparison is carried out for four velocities v_{st} of UEs on streets: 30 km/h, 60 km/h, 90 km/h and 120 km/h. The x-axis of each sub-figure shows the initial value of TTT for all cells. For "CS Thr., TTT" and "CS Serv., TTT & CPS Targ.", the values of TTT are changed during the optimization whereas they are fixed for "NWS" and "CS Serv. & CPS Targ." approaches.

In Fig. 6.13, it is shown that $N_{\mathrm{all}}^{(\mathrm{RLF})}$ of "CS Serv., TTT & CPS Targ." is independent of the initial value of TTT in contrast to the "CS Serv. & CPS Targ." approach. However, for all velocities, "CS Serv. & CPS Targ." achieves similar performance as that of "CS Serv., TTT & CPS Targ." for the initial values 100 ms and 320 ms of TTT. Thus, the optimization of the additional TTT parameter becomes less critical if the target cell threshold $Q_c^{(2)}$ is configured cell-pair specifically and the TTT is set relatively to a small value, i.e., 100 ms or 320 ms. This is because configuring $Q_c^{(2)}$ in a cell-pair specific way provides already a high number of degrees of freedom to tackle the numbers of RLFs and PPs. In addition, it is shown in the figure that "CS Serv., TTT & CPS Targ." outperforms "CS Thr., TTT" in terms of $N_{\mathrm{all}}^{(\mathrm{RLF})}$ for $v_{\mathrm{st}} = 60$ km/h and 90 km/h. Again, these results show that configuring $Q_c^{(2)}$ in a cell-pair specific way is advantageous.

Among the different optimization approaches, it is shown in Fig. 6.13 that the joint optimization of handover thresholds and TTT with cell-pair specific $Q_c^{(2)}$ is the most effective in tackling the number of RLFs and PPs for all initial values of TTT. However, all the optimization approaches perform similarly in terms of the number of UHs. The reason is that the number of TLHs is given higher priority than UHs and the cell reacts on $N_{\mathrm{all}}^{(\mathrm{UH})}$ only if it does not have any TLHs. To tackle the remaining number of UHs, more degrees of freedom are needed.

6.5.2.2 Cell Level Performance Evaluation

The cell level performance of the joint optimization approach with cell-pair specific target cell threshold (CS Serv., TTT & CPS Targ.) is compared with the three following optimization approaches: Cell-specific optimization of handover thresholds (CS Thr.), joint optimization of cell-specific handover thresholds and TTT (CS Thr., TTT), optimization of cell-specific serving cell threshold and cell-pair specific target cell threshold

(CS Serv. & CPS Targ.). The performance comparison is carried out for $v_{\mathrm{st}} = 60$ km/h and a TTT value of 320 ms, which are the parameters used to obtain the best network-wide setting of handover thresholds (NWS) in Section 4.2. The performance of each approach is evaluated based on the number $N_c^{(\mathrm{RLF})}$ of RLFs and number $N_c^{(\mathrm{UH})}$ of UHs. The number $N_c^{(\mathrm{PP})}$ of PPs is not considered since it is insignificant for the aforementioned values of v_{st} and TTT.

The number $N_c^{(\mathrm{RLF})}$ of RLFs in LTE and 3G cells is shown in Fig. 6.14(a) for all the optimization approaches. According to the figure, there are four cells which initially

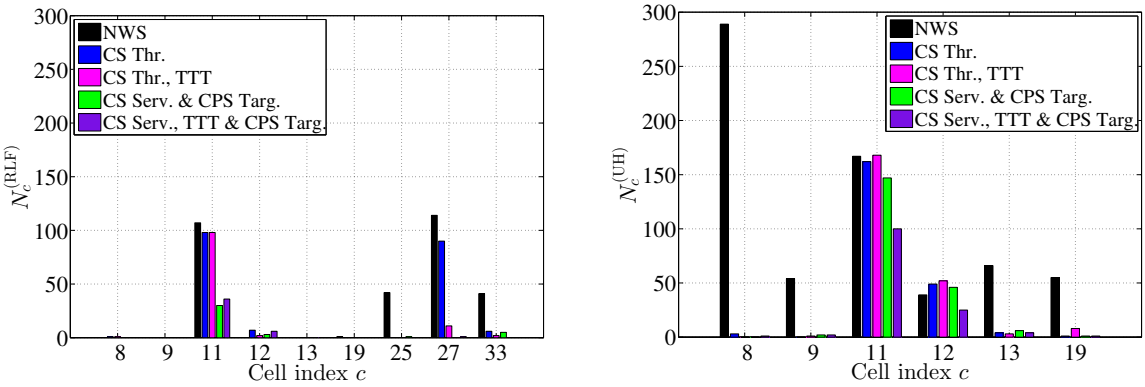

(a) Number $N_c^{(\mathrm{RLF})}$ of RLFs in LTE and 3G cells.

(b) Number $N_c^{(\mathrm{UH})}$ of UHs in LTE cells.

Figure 6.14. Cell level performance of best network-wide setting (NWS), cell-specific optimization of handover thresholds (CS Thr.), joint optimization of cell-specific handover thresholds and TTT (CS Thr., TTT), optimization of cell-specific serving cell threshold and cell-pair specific target cell threshold (CS Serv. & CPS Targ.) and joint optimization of cell-specific serving cell threshold and TTT, and cell-pair specific target cell threshold (CS Serv., TTT & CPS Targ.).

have relevant number of RLFs: Cell 11, 25, 27 and 33. The first optimization approach "CS Thr." has resolved only $N_c^{(\mathrm{RLF})}$ of cells 25 and 33. The second approach "CS Thr., TTT" has resolved $N_c^{(\mathrm{RLF})}$ of cell 27 in addition to those of cells 25 and 33. The last two approaches "CS Serv. & CPS Targ." and "CS Serv., TTT & CPS Targ." have resolved completely $N_c^{(\mathrm{RLF})}$ of cells 25, 27, 33 and a large portion of $N_c^{(\mathrm{RLF})}$ of cell 11. As for the number $N_c^{(\mathrm{UH})}$ of UHs, all the four optimization approaches have resolved completely $N_c^{(\mathrm{UH})}$ of cells 8, 9, 13, 19. These results show that "CS Serv. & CPS Targ." approach can provide similar results to the "CS Serv., TTT & CPS Targ.", yet at a lower complexity.

Chapter 7

Cell Area-Based Automatic Optimization of Handover Thresholds

7.1 Motivation

The two inter-RAT handover thresholds corresponding to serving and neighboring target cells are currently configured cell-specifically by 3GPP [3GP12b, 3GP12g]. That is all the UEs served by a cell apply the same two handover thresholds when handing over to any neighboring cell of a different RAT. The cell-specific optimization of the two handover thresholds is convenient since it has few numbers of thresholds and counters. However, the optimization can fail when the mobility failure events occurring with respect to different neighboring cells require contradicting actions to be performed on the same handover threshold, i.e., increase and decrease. This optimization limitation has been addressed in Chapter 5 by proposing a cell-group specific configuration for the handover thresholds where a dedicated threshold value is configured with respect to a group of neighboring cells. The cell-group specific optimization provides more degrees of freedom to address different radio conditions towards different neighboring cells. However, it can still fail since the radio conditions can be even not stationary along the border of the same neighboring cell, especially in inter-RAT scenario where the area of potential handover between the serving and the overlaying neighboring cell is large.

In addition to handover thresholds, the inter-RAT TTT parameter is another degree of freedom which can be used to tackle the mobility failure events. The handover thresholds and TTT have been jointly optimized in Chapter 6. The simulation results have shown that the optimization of TTT can make the performance of the automatic algorithm independent of the initial value of TTT. Moreover, the joint optimization of cell-specific handover thresholds and TTT outperforms the cell-specific optimization of handover thresholds in terms of RLFs. Nevertheless, there are still some RLFs and UHs which are not resolved for some cells. To tackle these remaining mobility failure events, more degrees of freedom are needed when configuring the handover thresholds and one of them is the location of the UE.

The mobility failure events occur generally in some specific areas of the cell. By configuring dedicated handover thresholds for each area, the mobility failure events occurring

in different areas of the cell can be decoupled which is not possible for cell-specific or cell-group specific optimization approaches. The configuration of the handover thresholds per area provides abounding spatial degrees of freedom if the areas are designed small enough. These additional degrees of freedom can be used to tackle different types of mobility failure events occurring with respect to the same neighboring cell. Moreover, they help to reduce the number of UHs which are optimized only if no TLHs exist in the cell. The automatic optimization of the handover thresholds per area has been proposed by the author of this thesis and is called cell-area based optimization.

This chapter is organized as follows. The configuration of the handover thresholds per area is explained in Section 7.2. The cell area-based optimization problem is formulated in Section 7.3. Here, cell-area specific and cell-area group specific optimization of handover thresholds are differentiated by the author of this thesis. A UE applies the handover thresholds of an area if it is inside the area or in its proximity. This location-based application of handover thresholds is discussed in Section 7.4. In Section 7.5, the advantages and limitations of the cell-area based optimization approach are presented. The proposed cell area-based optimization loop of handover thresholds is described in Section 7.6. The performance of the cell-area based automatic optimization is compared in Section 7.7 with those of cell-specific and cell-pair specific optimizations, and joint optimization approaches of handover thresholds and TTT. The work in this chapter has been partially presented in [AWVK13a].

7.2 Configuration of Handover Thresholds

In cell-area based optimization, dedicated handover thresholds are assigned for different areas of the same cell. The coverage area of cell c is decomposed into a grid of small tiles or square areas as shown in Fig. 7.1. The z^{th} area of serving cell c is indicated by $\mathrm{r}_{c,z}$, where $z = 1, \ldots, Z_c$ is the index for each area and Z_c is the total number of areas in cell c. The side length of each area is given by d. The center of each area $\mathrm{r}_{c,z}$ is indicated by the vector $\mathbf{r}_{c,z}$.

Similar to cell-specific and cell-group specific configurations, the handover thresholds of each area $\mathrm{r}_{c,z}$ can be configured with respect to all neighboring cells in set $\mathcal{N}_c$ or with respect to a subset of neighboring cells. The former approach is denoted by cell-area specific configuration whereas the latter is denoted by cell-area group specific configuration. For clarity, an example is shown in Fig. 7.2. The figure shows a cell area $\mathrm{r}_{c,z}$ and seven neighboring cells i_1, ..., i_7. In cell-area specific configuration, a single value $Q_{c,z}^{(m)}$ of handover threshold m is configured with respect to all neighboring cells

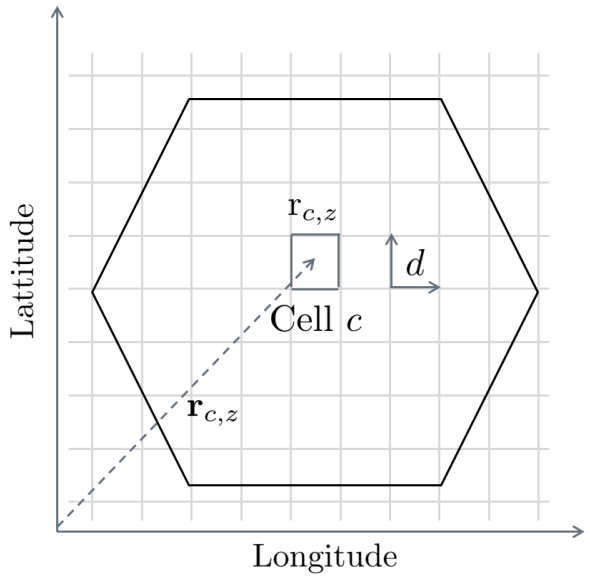

Figure 7.1. Decomposition of the coverage area of serving cell c into a grid of small areas with side length d.

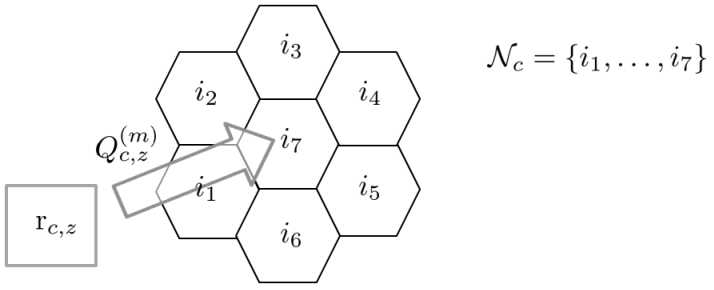

(a) Cell-area specific configuration.

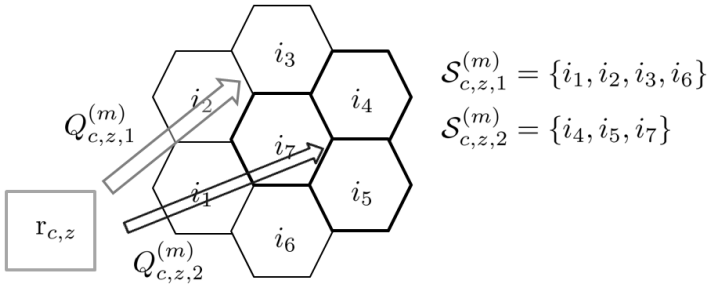

(b) Cell-area group specific configuration.

Figure 7.2. Cell-area specific and cell-area group specific configurations of the handover threshold of area z in cell c with respect to neighboring cells in set $\mathcal{N}_c$.

as shown in Fig. 7.2(a), i.e., index m of (2.32) is equal to 1 and 2 for the serving and target cell handover thresholds, respectively. In contrast, in cell-area group specific configuration a dedicated handover threshold value is configured with respect to each subset of neighboring cells as shown in Fig. 7.2(b). In this example, the set $\mathcal{N}_c$ is

decomposed into two subsets $\mathcal{S}_{c,z,1}^{(m)}$ and $\mathcal{S}_{c,z,2}^{(m)}$. For each handover threshold m, different subsets of neighboring cells can be selected. The handover threshold $Q_{c,z,1}^{(m)}$ and $Q_{c,z,2}^{(m)}$ is configured with respect to subset $\mathcal{S}_{c,z,1}^{(m)}$ and $\mathcal{S}_{c,z,2}^{(m)}$, respectively.

7.3 Formulation of the Optimization Problem

The optimization problem of the handover thresholds is formulated in terms of the KPI values which are collected per area of each cell during T_{CL} time interval. For each mobility failure type defined in Section 3.4, a dedicated KPI exists. Thus, a KPI exists for TLH of type 1, TLH of type 2, TEH, HWC, PP and UH, i.e., six KPIs are defined in total. The index of the KPIs is $a = 1, \ldots, A$ where A is the total number of KPIs. Unlike cell-specific and cell-group specific optimization, the values of the KPIs are differentiated between different areas of each cell. The location of a mobility failure event occurring in cell c with respect to k^{th} neighboring cell i_k is given by the vector $\mathbf{e}_{c,i_k}$. Each mobility failure event occurring in cell c with respect to neighboring cell i_k is assigned to the closest area r_{c,z^*} where

$$z^* = \min_z \|\mathbf{r}_{c,z} - \mathbf{e}_{c,i_k}\|^2. \tag{7.1}$$

The value of KPI a evaluated during a KPI collection period for area $\mathrm{r}_{c,z}$ with respect to neighboring cell i_k is indicated by $f_{c,z,i_k}^{(a)}$. The values of the KPIs evaluated for area $\mathrm{r}_{c,z}$ with respect to each neighbor of cell c are packed in matrix

$$\mathbf{F}_{c,z} = \begin{bmatrix} f_{c,z,i_1}^{(1)} & \cdots & f_{c,z,i_k}^{(1)} & \cdots & f_{c,z,i_K}^{(1)} \\ \vdots & & \ddots & & \vdots \\ f_{c,z,i_1}^{(a)} & \cdots & f_{c,z,i_k}^{(a)} & \cdots & f_{c,z,i_K}^{(a)} \\ \vdots & & \ddots & & \vdots \\ f_{c,z,i_1}^{(A)} & \cdots & f_{c,z,i_k}^{(A)} & \cdots & f_{c,z,i_K}^{(A)} \end{bmatrix} = [\mathbf{f}_{c,z,i_1}, \ldots, \mathbf{f}_{c,z,i_k}, \ldots \mathbf{f}_{c,z,i_K}] \in \mathbb{Z}^{A \times K}. \tag{7.2}$$

The vector $\mathbf{f}_{c,z,i_k}$ is the k^{th} column of matrix $\mathbf{F}_{c,z}$ and comprises the value of each KPI with respect to the neighboring cell i_k. The matrix $\mathbf{F}_c$ and its corresponding element $f_{c,i_k}^{(a)}$ used for cell-specific and cell-group specific optimization approaches can be directly computed by summing up $\mathbf{F}_{c,z}$ and $f_{c,z,i_k}^{(a)}$ of all areas, i.e.,

$$\mathbf{F}_c = \sum_{z=1}^{Z_c} \mathbf{F}_{c,z}, \text{ and} \tag{7.3}$$

$$f_{c,i_k}^{(a)} = \sum_{z=1}^{Z_c} f_{c,z,i_k}^{(a)}. \tag{7.4}$$

The set $\mathcal{N}_c$ of neighboring cells is decomposed into J_m disjoint subsets for each handover threshold m of area $\mathrm{r}_{c,z}$ as follows:

$$\mathcal{S}_{c,z,j}^{(m)} \subseteq \mathcal{N}_c,\ \bigcup_{j=1}^{J_m} \mathcal{S}_{c,z,j}^{(m)} = \mathcal{N}_c, \bigcap_{j=1}^{J_m} \mathcal{S}_{c,z,j}^{(m)} = \emptyset \text{ and } \left|\mathcal{S}_{c,z,j}^{(m)}\right| \geq 1, \tag{7.5}$$

where $j \in \mathcal{J}_m$ is the index for the subsets and $\mathcal{J}_m = \{1, \ldots, J_m\}$. The index for the elements of $\mathcal{S}_{c,z,j}^{(m)}$ is indicated by $v = 1, \ldots, V$ where V is the total number of elements. The v^{th} element of $\mathcal{S}_{c,z,j}^{(m)}$ is denoted by ζ_v, i.e.,

$$\mathcal{S}_{c,z,j}^{(m)} = \{\zeta_1, \ldots, \zeta_v, \ldots, \zeta_V\}. \tag{7.6}$$

In case of cell-area specific handover threshold, $J_m = 1$ and the subset $\mathcal{S}_{c,z,1}^{(m)} = \mathcal{N}_c$. The value of handover threshold m that is configured with respect to the j^{th} subset $\mathcal{S}_{c,z,j}^{(m)}$ of neighboring cells is indicated by $Q_{c,z,j}^{(m)}$.

The optimization of each handover threshold m is based on a fraction or all the columns of $\mathbf{F}_{c,z}$ depending on its configuration. For a cell-area specific handover threshold, the handover threshold $Q_{c,z}^{(m)}$ is optimized with respect to all the columns of $\mathbf{F}_{c,z}$. However, a cell-area group specific handover threshold $Q_{c,z,j}^{(m)}$ is optimized with respect to the columns of $\mathbf{F}_{c,z}$ corresponding to the neighboring cells of $\mathcal{S}_{c,z,j}^{(m)}$. These columns are retrieved from $\mathbf{F}_{c,z}$ using a selection matrix $\mathbf{S}_{c,z,j}^{(m)} \in \mathbb{B}^{K \times V}$ and are packed in matrix $\mathbf{R}_{c,j}^{(m)} \in \mathbb{Z}^{A \times V}$, i.e.,

$$\mathbf{F}_{c,z}\mathbf{S}_{c,z,j}^{(m)} = \mathbf{R}_{c,z,j}^{(m)}. \tag{7.7}$$

For instance, consider the example depicted in Fig. 7.2(b). The two selections matrices $\mathbf{S}_{c,z,1}^{(m)}$ and $\mathbf{S}_{c,z,2}^{(m)}$ are given as

$$\mathbf{S}_{c,z,1}^{(m)} = \begin{bmatrix} 1 & 0 & 0 & 0 \\ 0 & 1 & 0 & 0 \\ 0 & 0 & 1 & 0 \\ 0 & 0 & 0 & 0 \\ 0 & 0 & 0 & 0 \\ 0 & 0 & 0 & 1 \\ 0 & 0 & 0 & 0 \end{bmatrix} \text{ and } \mathbf{S}_{c,z,2}^{(m)} = \begin{bmatrix} 0 & 0 & 0 \\ 0 & 0 & 0 \\ 0 & 0 & 0 \\ 1 & 0 & 0 \\ 0 & 1 & 0 \\ 0 & 0 & 0 \\ 0 & 0 & 1 \end{bmatrix}. \tag{7.8}$$

In case of a cell-area specific handover threshold, $\mathbf{S}_{c,z,1}^{(m)}$ is equal to the identity matrix $\mathbf{I} \in \mathbb{B}^{K \times K}$.

The matrix $\mathbf{R}_{c,z,j}^{(m)}$ is then expressed as

$$\mathbf{R}_{c,z,j}^{(m)} = [\mathbf{f}_{c,z,\zeta_1}, \ldots, \mathbf{f}_{c,z,\zeta_v}, \ldots, \mathbf{f}_{c,z,\zeta_V}] \tag{7.9}$$

where $\mathbf{f}_{c,z,\zeta_v}$ is the column containing the values of the KPIs in area $\mathrm{r}_{c,z}$ with respect to neighboring cell ζ_v. As a single handover threshold is configured with respect to the

neighboring cells in $\mathcal{S}_{c,z,j}^{(m)}$, the values of the KPIs in $\mathbf{R}_{c,z,j}^{(m)}$ are not differentiated between the selected neighboring cells. Thus, the values of the KPIs in $\mathbf{R}_{c,z,j}^{(m)}$ are summed up over the index v resulting in vector $\boldsymbol{\ell}_{c,z,j}^{(m)}$

$$\boldsymbol{\ell}_{c,z,j}^{(m)} = \sum_{v=1}^{V} \mathbf{f}_{c,z,\zeta_v} \in \mathbb{Z}^{A\times 1}. \tag{7.10}$$

Each element of $\boldsymbol{\ell}_{c,z,j}^{(m)}$ is the sum of all the values of a KPI in cell area $\mathrm{r}_{c,z}$ with respect to all neighboring cells in set $\mathcal{S}_{c,z,j}^{(m)}$. Following the same approach of cell-specific and cell-group specific optimizations, the values of the KPIs in $\boldsymbol{\ell}_{c,z,j}^{(m)}$ are grouped into two correction directives: $D_{c,z,j}^{(+),m}$ and $D_{c,z,j}^{(-),m}$ which are the total number of mobility failure events which require an increase and a decrease, respectively, of the value of the threshold $Q_{c,z,j}^{(m)}$. In order to obtain the correction directives, the same matrix $\mathbf{G}_m \in \mathbb{R}^{A\times 2} = [\mathbf{g}_{1,m}, \mathbf{g}_{2,m}]$ which is defined in (5.9) is used to group the values of the KPIs as follows

$$\boldsymbol{\ell}_{c,z,j}^{(m)\,\mathrm{T}} \mathbf{G}_m = \mathbf{d}_{c,z,j}^{(m)}, \tag{7.11}$$

where

$$\mathbf{d}_{c,z,j}^{(m)} = \left[D_{c,z,j}^{(+),m}, D_{c,z,j}^{(-),m} \right]. \tag{7.12}$$

The independent optimization problem which is formulated in (5.6) can be now decomposed into $Z_c \cdot \sum_{m=1}^{M} J_m$ sub-problems as follows:

$$\widehat{Q}_{c,z,j}^{(m)} = \underset{Q_{c,z,j}^{(m)}}{\arg\min} \quad \left(D_{c,z,j}^{(+),m} + D_{c,z,j}^{(-),m} \right) \quad \forall m, z, j \text{ and } c. \tag{7.13}$$

Each handover threshold $Q_{c,z,j}^{(m)}$ is optimized with respect to the sum of its corresponding correction directives. It is shown in Appendix A.3 that

$$\sum_{k=1}^{K} \sum_{a=1}^{A} w_{c,a} f_{c,i_k}^{(a)} = \sum_{m=1}^{M} \sum_{z=1}^{Z_c} \sum_{j=1}^{J_m} \left(D_{c,z,j}^{(+),m} + D_{c,z,j}^{(-),m} \right) \tag{7.14}$$

holds if the constraint of (5.10) is fulfilled, i.e., $\sum_{m=1}^{M} (\mathbf{g}_{1,m} + \mathbf{g}_{2,m}) = \mathbf{w}_c$ where $M = 2$ is the number of handover thresholds and $\mathbf{w}_c$ is the vector containing the weights $w_{c,a}$ of each KPI a.

The value of J_m determines the configuration type of the handover threshold as shown in Table 7.1. The cell-area specific configuration of the handover thresholds is a special case of the cell-area group specific configuration approach. If $J_m = 1$, the set $\mathcal{S}_{c,z,j}^{(m)} = \mathcal{N}_c$ and the handover threshold $Q_{c,z,j}^{(m)}$ is configured with respect to all neighboring cells. On the other hand, if $J_m = |\mathcal{N}_c|$ then each set $\mathcal{S}_{c,z,j}^{(m)}$ consists of a single neighboring cell

Table 7.1. Three different cell-area based handover threshold configurations depending on the value of J_m.

Case	$\mathcal{S}_{c,z,j}^{(m)}$	$Q_{c,z,j}^{(m)}$	Optimization function	Configuration
$J_m = 1$	$\mathcal{N}_c$	$Q_{c,z}^{(m)}$	$\left(D_{c,z}^{(+),m} + D_{c,z}^{(-),m}\right)$	Cell-area specific
$1 < J_m < \lvert\mathcal{N}_c\rvert$	$\mathcal{S}_{c,z,j}^{(m)}$	$Q_{c,z,j}^{(m)}$	$\left(D_{c,z,j}^{(+),m} + D_{c,z,j}^{(-),m}\right)$	Cell-area group specific
$J_m = \lvert\mathcal{N}_c\rvert$	$\left\lvert\mathcal{S}_{c,z,j}^{(m)}\right\rvert = 1$	$Q_{c,z,j}^{(m)}$	$\left(D_{c,z,j}^{(+),m} + D_{c,z,j}^{(-),m}\right)$	Cell-area pair specific

and the handover threshold $Q_{c,z,j}^{(m)}$ is configured with respect to each neighboring cell. In this case, the cell-area group specific configuration approach is denoted by cell-area pair specific. If $1 < J_m < |\mathcal{N}_c|$, then there exists at least one handover threshold $Q_{c,z,j}^{(m)}$ which is not configured with respect to a single neighboring cell. In this case, the configuration of the handover threshold is cell-area group specific.

7.4 Location-Based Application of Handover Thresholds

Each UE is configured by the serving cell with a location-specific configuration map which contains the handover thresholds of all the areas inside the cell. In practice, most of the areas will have default handover threshold values, and in turn only the handover thresholds of few areas need to be specified. A UE approaching an area $\mathrm{r}_{c,z}$ should apply its corresponding handover thresholds ahead of time before it experiences the same mobility failures which had occurred before in $\mathrm{r}_{c,z}$. For instance, a UE approaching an area $\mathrm{r}_{c,z}$ having missed handovers, i.e., TLHs, should apply its corresponding handover threshold early enough so that the entering condition of the measurement event can be fulfilled for TTT time interval before it fails. On the other hand, a UE approaching an area $\mathrm{r}_{c,z}$ having fast handovers, e.g., TEHs, HWC, PP or UH, can apply its corresponding handover thresholds just before it enters the area $\mathrm{r}_{c,z}$ so that the inter-RAT handover is not triggered early. Therefore, a UE applies the handover thresholds if it is inside the area $\mathrm{r}_{c,z}$ or in its proximity. The set of all locations where the UE applies the handover threshold $Q_{c,z,j}^{(m)}$ of area $\mathrm{r}_{c,z}$ is denoted by $\Omega_{c,z,j}^{(m)}$ and is configured by the serving cell.

An example of the definition of $\Omega_{c,z,j}^{(m)}$ is shown in Fig. 7.3. The figure shows a UE moving with a certain estimated velocity $\tilde{v}_{\mathrm{st}}$ on a street passing through area $\mathrm{r}_{c,z}$. The UE starts to apply the handover thresholds when it is $d_{\mathrm{mar}} = \tilde{v}_{\mathrm{st}} \cdot T_{\mathrm{mar}}$ meters away from $\mathrm{r}_{c,z}$, where T_{mar} is the time margin configured by the serving cell. The value of T_{mar}

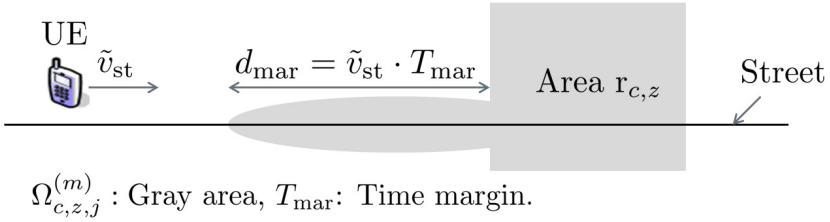

Figure 7.3. The set $\Omega^{(m)}_{c,z,j}$ of all the locations where the UE applies the handover threshold $Q^{(m)}_{c,z,j}$ of area $\text{r}_{c,z}$ is shown in gray.

depends on the number and types of mobility failure events in area $\text{r}_{c,z}$. The mobility failure events of $\text{r}_{c,z}$ are grouped into two correction directives $D^{(+),m}_{c,z,j}$ and $D^{(-),m}_{c,z,j}$ for each handover threshold m. The mobility failure events of $D^{(+),1}_{c,z,j}$, i.e., $m = 1$, and $D^{(-),2}_{c,z,j}$, i.e., $m = 2$, correspond to missed handovers, i.e., TLHs, whereas those of $D^{(-),1}_{c,z,j}$ and $D^{(+),2}_{c,z,j}$ correspond to fast handovers, i.e., TEHs, HWC, PPs and UHs. The value of T_{mar} corresponding to $\Omega^{(1)}_{c,z,j}$, i.e., set of locations where the serving cell threshold $Q^{(1)}_{c,z,j}$ is applied, is set to one of the two values T_{MH} and T_{FH} as follows:

$$T_{\text{mar}} = \begin{cases} T_{\text{MH}}, & \text{if } D^{(+),1}_{c,z,j} > D^{(-),1}_{c,z,j} \\ T_{\text{FH}}, & \text{otherwise.} \end{cases} \tag{7.15}$$

The value T_{MH} is used when the number of missed handovers which are resolved by $Q^{(1)}_{c,z,j}$ is higher than that of fast handovers. Otherwise, T_{mar} is set to T_{FH} which is typically smaller or equal to T_{MH}. Similarly, the value of T_{mar} corresponding to $\Omega^{(2)}_{c,z,j}$, i.e., set of locations where the target cell threshold $Q^{(2)}_{c,z,j}$ is applied, is set as follows:

$$T_{\text{mar}} = \begin{cases} T_{\text{FH}}, & \text{if } D^{(+),2}_{c,z,j} > D^{(-),2}_{c,z,j} \\ T_{\text{MH}}, & \text{otherwise.} \end{cases} \tag{7.16}$$

7.5 Advantages and Limitations of Cell-Area Based Optimization

7.5.1 Advantages over Cell-Based Optimization

The cell-area and cell-area group specific optimization of handover thresholds have a finer granularity than cell-specific and cell-group specific optimization, respectively. The more granular the optimization, the better is the performance of the automatic algorithm. The relationships among all cell-area and cell-based optimization approaches are given in the following.

For all optimization approaches, the handover threshold m is optimized with respect to the sum of its corresponding correction directives. In network-wide optimization, the correction directives are denoted by $D^{(+),m}$ and $D^{(-),m}$ which correspond to the total number of mobility failure events in the whole network requiring an increase and decrease, respectively, in the network-wide handover threshold m. The relationships among the optimization functions of all optimizations approaches of handover thresholds are shown in Fig. 7.4. The optimization approaches are ordered according to their

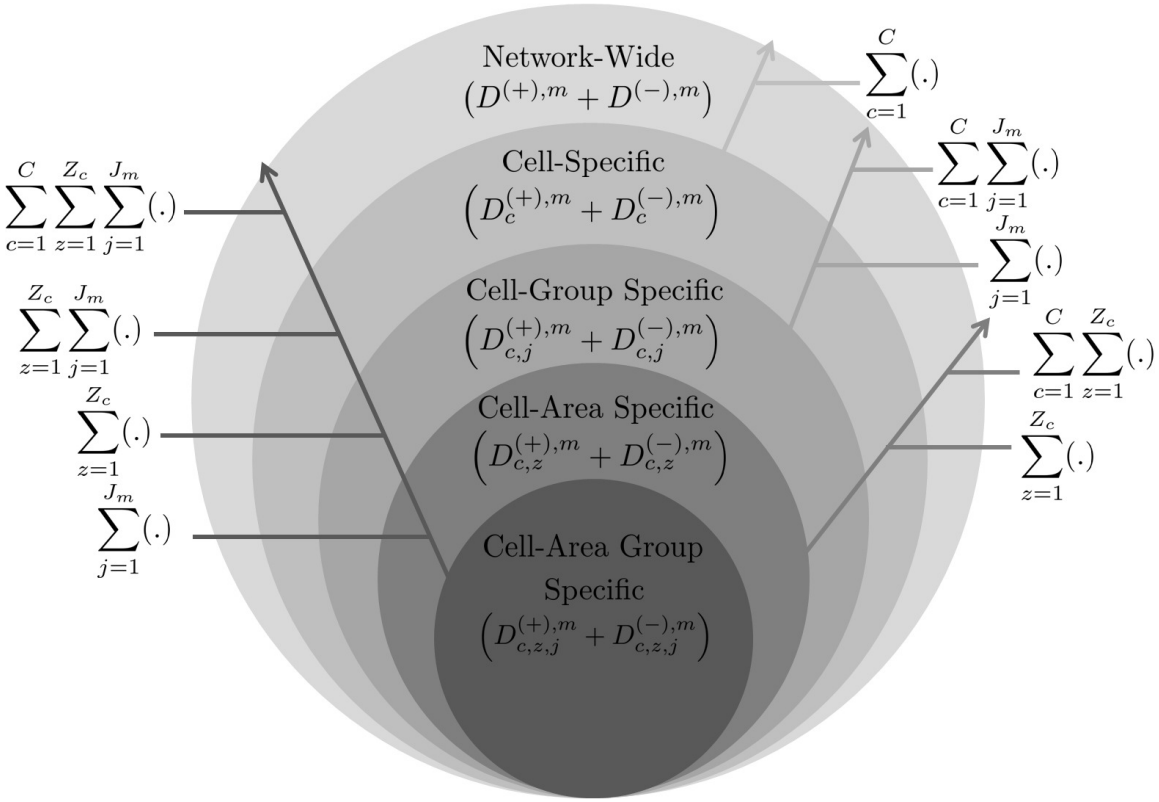

Figure 7.4. Relationships among the optimization functions of all optimizations approaches of handover thresholds.

levels of granularity: The network-wide optimization (largest circle) has the largest granularity whereas the cell-area group specific optimization has the smallest granularity (smallest circle). The optimization function used for each optimization approach is found inside each circle. The relationships among the optimization functions are indicated by arrows. For instance, the optimization function of cell-specific optimization approach can be obtained from that of cell-group specific optimization by summing up the correction directives with respect to all neighboring cells, i.e., sum over index j.

The optimization functions of the cell-specific and network-wide optimization approaches can be obtained from that of the cell-area specific optimization approach.

However, the optimization function of cell-group specific optimization can be obtained only from that of cell-area group specific optimization. This is because in all other optimization approaches, the handover thresholds are not differentiated with respect to neighboring target cells. In addition, the optimization functions of all approaches can be obtained from that of the cell-area group specific optimization approach which has the smallest granularity. Thus, an automatic algorithm optimizing the handover thresholds in cell-area group specific way can be used for all other optimization approaches.

7.5.2 Optimization Limitations

The cell-area specific and cell-area group specific optimization approaches of handover thresholds have two limitations. The first optimization limitation is when the number of mobility failure events requiring an increase and decrease in the same handover threshold $Q^{(m)}_{c,z,j}$ are comparable, i.e.,

$$D^{(+),m}_{c,z,j} \approx D^{(-),m}_{c,z,j}. \tag{7.17}$$

In this case, the automatic algorithm cannot react since none of the two correction directives can be well reduced without a significant increase in the other correction directive. The automatic algorithm can update the handover threshold $Q^{(m)}_{c,z,j}$ only if one of the two correction directives is dominant, i.e., $D^{(+),m}_{c,z,j} >> D^{(-),m}_{c,z,j}$ or $D^{(+),m}_{c,z,j} << D^{(-),m}_{c,z,j}$. However, the optimization limitation of (7.17) is unlikely to happen if the areas are designed small enough to isolate mobility failure events of the same type.

The second optimization limitation occurs when the UE has to select one of several conflicting handover threshold values corresponding to different areas. For clarity, an example is shown in Fig. 7.5. The figure shows a UE moving on a street which passes

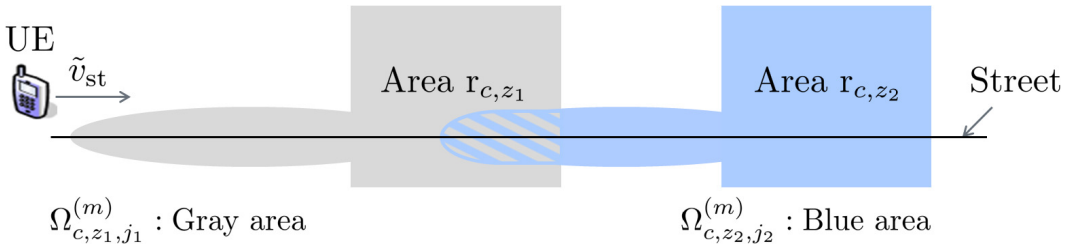

Figure 7.5. Intersection of the two location sets $\Omega^{(m)}_{c,z_1,j_1}$ and $\Omega^{(m)}_{c,z_2,j_2}$ corresponding to two different areas r_{c,z_1} and r_{c,z_2}, respectively.

through two areas: r_{c,z_1} (gray square) and r_{c,z_2} (blue square). The set $\Omega^{(m)}_{c,z_1,j_1}$ of locations

where the UE should apply the handover threshold $Q^{(m)}_{c,z_1,j_1}$ of area r_{c,z_1} is shown in gray. Similarly, the set $\Omega^{(m)}_{c,z_2,j_2}$ of locations where the UE should apply the handover threshold $Q^{(m)}_{c,z_2,j_2}$ of area r_{c,z_2} is shown in blue. The intersection of the two locations sets is shown in gray and blue stripes. Each handover threshold $Q^{(m)}_{c,z_1,j_1}$ and $Q^{(m)}_{c,z_2,j_2}$ is configured with respect to the subset $\mathcal{S}^{(m)}_{c,z_1,j_1}$ and $\mathcal{S}^{(m)}_{c,z_2,j_2}$, respectively. A conflict in selecting the value of handover threshold m occurs when the UE is positioned in the intersection area of the two location sets, and the handover thresholds $Q^{(m)}_{c,z_1,j_1} \neq Q^{(m)}_{c,z_2,j_2}$ are configured with respect to the same subset of neighboring cells, i.e.,

$$\exists\ \mathrm{r}_{c,z_1} \neq \mathrm{r}_{c,z_2} \text{ s.t. } \Omega^{(m)}_{c,z_1,j_1} \bigcap \Omega^{(m)}_{c,z_2,j_2} \neq \emptyset, \mathcal{S}^{(m)}_{c,z_1,j_1} = \mathcal{S}^{(m)}_{c,z_2,j_2} \text{ and } Q^{(m)}_{c,z_1,j_1} \neq Q^{(m)}_{c,z_2,j_2}. \quad (7.18)$$

In this case, the UE can configure only one of the two handover threshold values. For instance, the UE can select the handover threshold of the area having the most mobility problems. This conflict in selecting the value of the handover threshold is not critical if the areas having mobility problems are distant enough from each other.

7.6 Cell Area-Based Optimization Loop of Handover Thresholds

7.6.1 Introduction

The cell-area based optimization loop of the inter-RAT handover thresholds is shown in Fig. 7.6. It is carried out independently per each cell area of LTE and 3G networks.

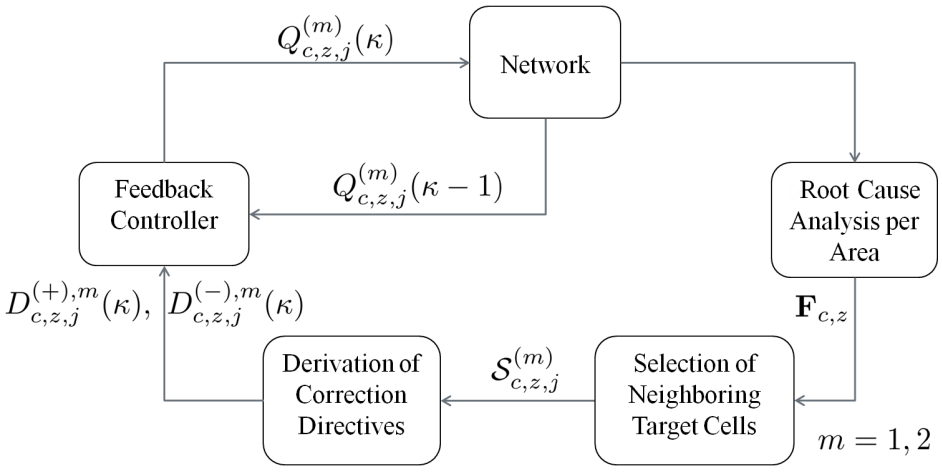

Figure 7.6. The cell-area based optimization loop of the inter-RAT handover thresholds.

A root cause analysis is performed by each cell for the mobility failure events which are collected per area in each KPI period. For each handover threshold m, the subset $\mathcal{S}_{c,z,j}^{(m)}$ of (7.5) are selected. Using these subsets, the two correction directives $D_{c,z,j}^{(+),m}(\kappa)$ and $D_{c,z,j}^{(-),m}(\kappa)$ of (7.11) are calculated for each KPI collection period κ. Finally, the handover threshold $Q_{c,z,j}^{(m)}(\kappa)$ is updated by the feedback controller using the two correction directives and the previous value $Q_{c,z,j}^{(m)}(\kappa-1)$ of the handover threshold. The optimization loop is repeated until the algorithm converges.

7.6.2 Root Cause Analysis per Area

The handover thresholds of each area are updated based on the values of the KPIs which are collected periodically during time interval T_{CL}. A mobility failure event is counted by the responsible cell and is assigned to the area of which the misconfiguration of its handover thresholds is the root cause for that failure. The values of the KPIs collected by area $\mathrm{r}_{c,z}$ with respect to each k^{th} inter-RAT neighboring cell i_k are packed in matrix $\mathbf{F}_{c,z}$ of (7.2). In each KPI collection period κ, a new matrix $\mathbf{F}_{c,z}$ is obtained for each area $\mathrm{r}_{c,z}$.

7.6.3 Selection of Neighboring Target Cells for Handover Thresholds

After the root cause analysis, the subsets $\mathcal{S}_{c,z,j}^{(m)}$ of neighboring cells are selected for each handover threshold m, See Fig. 7.6. The same subsets are used in each KPI collection period for each handover threshold. The investigations in Section 5.5.4.1 have shown that configuring only the target cell threshold in a cell-group specific manner is beneficial. Following the same approach, the serving cell threshold is configured as cell-area specific. In this case, $\mathcal{S}_{c,z,j}^{(1)}$, i.e., $m=1$, is equal to the set of all neighboring cells $\mathcal{N}_c$. As for the target cell threshold, it can be configured either as cell-area or cell-area group specific. In the latter case, the set $\mathcal{N}_c$ is typically decomposed such that each subset $\mathcal{S}_{c,j}^{(m)}$ consists of a single neighboring cell, i.e., $J_m = |\mathcal{N}_c|$.

7.6.4 Derivation of Correction Directives for Handover Thresholds

The two correction directives $D_{c,z,j}^{(+),m}(\kappa)$ and $D_{c,z,j}^{(-),m}(\kappa)$ of KPI collection period κ can now be computed using (7.11). To this end, the matrix $\mathbf{G}_m$ needs to be designed for

each handover threshold m. The matrices $\mathbf{G}_1$ and $\mathbf{G}_2$ corresponding to serving and target cell threshold, respectively, have been already defined for cell-based optimization approaches in (5.46). These two matrices are reused here for the cell-area based optimization approach.

7.6.5 Correction of the Values of Handover Thresholds using Feedback Controller

Each handover threshold m is updated based on the values of its corresponding correction directives provided that at least one of them is higher than $D_{\text{thr}}^{(\text{min})}$. This condition is necessary to avoid reacting on outliers. The handover threshold is increased if $D_{c,z,j}^{(+),m} >> D_{c,z,j}^{(-),m}$, decreased if $D_{c,z,j}^{(+),m} << D_{c,z,j}^{(-),m}$ and not modified if $D_{c,z,j}^{(+),m} \approx D_{c,z,j}^{(-),m}$. The value of increase and decrease is determined for each handover threshold by a feedback controller which is described in Section 5.6.5. The handover thresholds are updated in each KPI collection period until the algorithm converges.

7.7 Performance Evaluation and Analysis

7.7.1 Network Level Performance Evaluation

The network level performance of the cell-area based optimization approach is compared with those of cell-based optimization approaches of handover thresholds and joint cell-based optimization of handover thresholds and TTT. The handover parameter configurations of the investigated optimization approaches are summarized in Table 7.2. The best network-wide setting of handover thresholds (NWS) is found in Section 4.2. For cell-area based optimization approach of handover thresholds, denoted by "C-AS Serv. & C-APS Targ.", the serving and target cell thresholds are configured as cell-area and cell-area pair specific, respectively. A PP is given the same weight as an RLF, i.e., $w_{\text{PP}} = 1$, and the handover thresholds of the cells or cell areas are initialized in the first KPI collection period to the best network-wide setting of handover thresholds (NWS). The inter-RAT TTT $Q_c^{(3)}$ is set to a network-wide value of 100 ms. For joint optimization approaches of handover thresholds and TTT, the value of TTT is changed for each cell during the optimization.

The scenario consists of two fully overlaying co-sited LTE and 3G networks, which is discussed in Section 2.8.3. The simulation parameters which are used for the scenario

Table 7.2. Handover parameter configurations of different optimization approaches.

Optimization approach	Handover parameter	Configuration
Best network-wide setting of handover thresholds		
NWS	Serving cell threshold	Network-wide
	Target cell threshold	Network-wide
	TTT	Network-wide
Cell-based optimization approaches of handover thresholds		
CS Thr.	Serving cell threshold	Cell-specific
	Target cell threshold	Cell-specific
	TTT	Network-wide
CS Serv. & CPS Targ.	Serving cell threshold	Cell-specific
	Target cell threshold	Cell-pair specific
	TTT	Network-wide
Joint cell-based optimization approaches of handover thresholds and TTT		
CS Thr., TTT	Serving cell threshold	Cell-specific
	Target cell threshold	Cell-specific
	TTT	Cell-specific
CS Serv., TTT & CPS Targ.	Serving cell threshold	Cell-specific
	Target cell threshold	Cell-pair specific
	TTT	Cell-specific
Cell-area based optimization approach of handover thresholds		
C-AS Serv. & C-APS Targ.	Serving cell threshold	Cell-area specific
	Target cell threshold	Cell-area pair specific
	TTT	Network-wide

are summarized in Table 3.2 and Table 3.3. The parameters of the cell-area based automatic algorithm are shown in Table 7.3. Each cell is decomposed into small areas of 100 m^2. The two time margins T_{MH}, T_{FH} are set to 3 s and 0.5 s, respectively.

Table 7.3. The parameters that are used by the cell-area based automatic algorithm of the inter-RAT handover thresholds.

Parameter	Value
Minimum threshold $D_{\mathrm{thr}}^{(\mathrm{min})}$	10
Side length d	10 meters
Time margin T_{MH}, T_{FH}	3 s, 0.5 s

The performance comparison is carried out for four different velocities v_{st} of UEs on streets: 30 km/h, 60 km/h, 90 km/h and 120 km/h. The performance of each approach is evaluated using the values of the KPIs which are collected from each LTE and 3G networks during $T_{\mathrm{CL}} = 150$ seconds time interval. The total number of RLFs, PPs and UHs in LTE network is denoted by $N_{\mathrm{LTE}}^{(\mathrm{RLF})}$, $N_{\mathrm{LTE}}^{(\mathrm{PP})}$ and $N_{\mathrm{LTE}}^{(\mathrm{UH})}$, respectively. Similarly,

the total number of RLFs, PPs in 3G network is denoted by $N_{3G}^{(RLF)}$, $N_{3G}^{(PP)}$, respectively.

The performance of all investigated optimization approaches, which are summarized in Table 7.2, is shown in Fig. 7.7 for different velocities v_{st} of UEs on streets. For

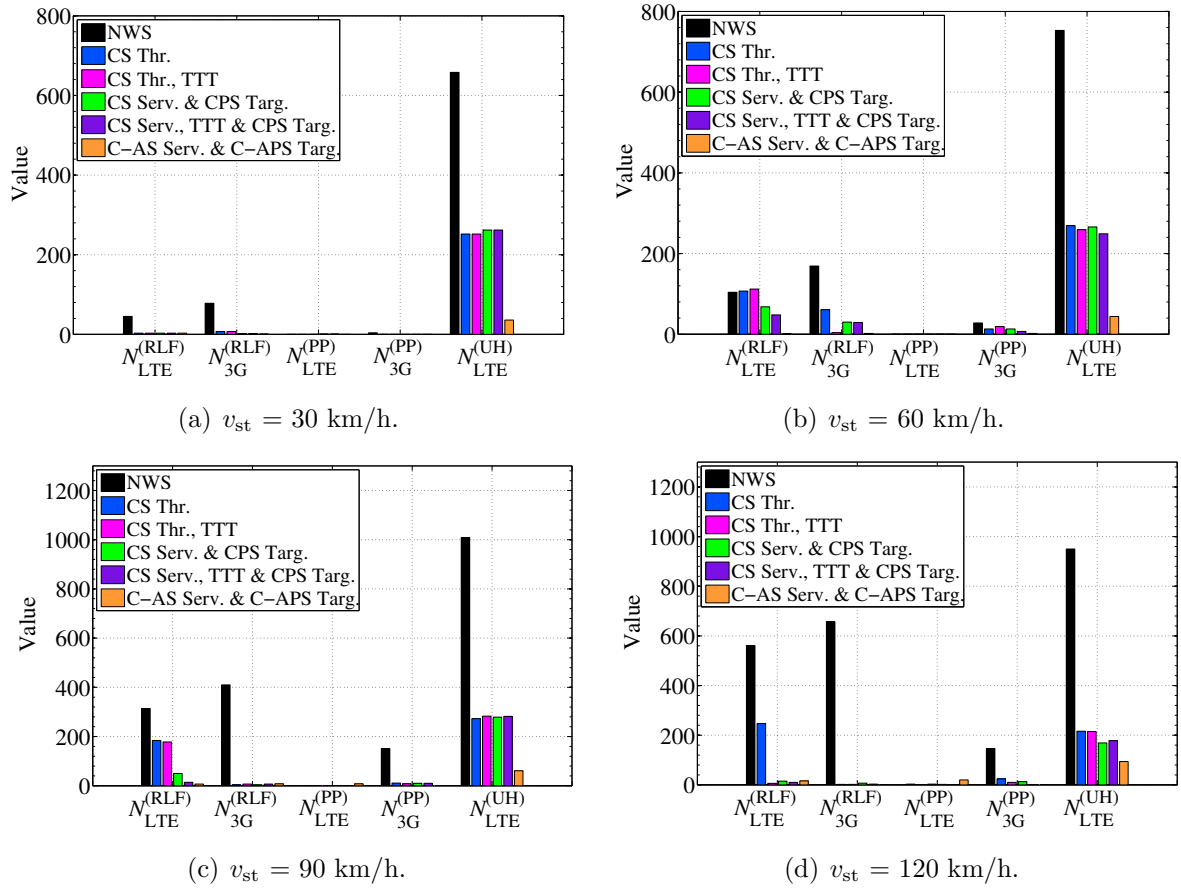

(a) v_{st} = 30 km/h. (b) v_{st} = 60 km/h.

(c) v_{st} = 90 km/h. (d) v_{st} = 120 km/h.

Figure 7.7. Performance comparison of the optimization approaches in Table 7.2 for different velocities v_{st} of UEs on streets.

a speed of 30 km/h, all the optimization approaches achieve the same performance with respect to RLFs and PPs. However, $N_{UH}^{(LTE)}$ of "C-AS Serv. & C-APS Targ." is 85.7% and 86.3% lower than that of "CS Thr." and "CS Serv. & CPS Targ.", respectively. As for the speed of 60 km/h, the cell-area based optimization approach is able to completely resolve the number of RLFs in LTE network in contrast to the other optimization approaches which fail to improve much the performance compared to "NWS". Moreover, $N_{UH}^{(LTE)}$ of "C-AS Serv. & C-APS Targ." is 83.6%, 83.5% lower than that of "CS Thr." and "CS Serv. & CPS Targ.", respectively. A similar performance is also shown in Fig. 7.7(c) where "C-AS Serv. & C-APS Targ." outperforms the other optimization approaches with respect to the number of UHs. For a speed of 120 km/h, all optimization approaches, except "CS Thr.", resolve all RLFs and PPs in LTE and

3G networks. However, $N_{\mathrm{UH}}^{(\mathrm{LTE})}$ of "CS Serv. & CPS Targ." is 56.5% and 44.4% lower than that of "CS Thr." and "CS Serv. & CPS Targ.", respectively. These results show that among the optimization paradigms "C-AS Serv. & C-APS Targ." is the most efficient in tackling all types of mobility problems in LTE and 3G networks.

7.7.2 Cell Level Performance Evaluation

The performance of the cell-area based automatic algorithm is evaluated on a cell level for velocity $v_{\mathrm{st}} = 60$ km/h and inter-RAT TTT $Q_c^{(3)} = 100$ ms. The network level performance of the automatic algorithm has been already shown in Fig. 7.7(b) for these specific values of v_{st} and TTT. The number $N_c^{(\mathrm{RLF})}$ of RLFs, $N_c^{(\mathrm{PP})}$ of PPs and $N_c^{(\mathrm{UH})}$ of UHs is shown in Fig. 7.8 for LTE and 3G cells. According to the figure, it

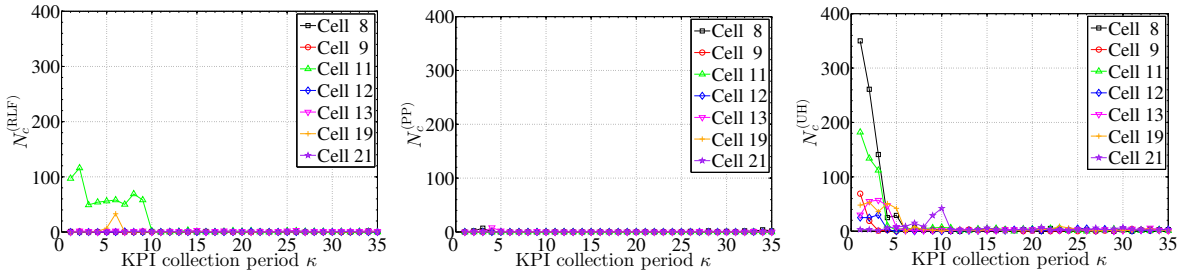

(a) Number $N_c^{(\mathrm{RLF})}$ of RLFs in each LTE cell.

(b) Number $N_c^{(\mathrm{PP})}$ of PPs in each LTE cell.

(c) Number $N_c^{(\mathrm{UH})}$ of UHs in each LTE cell.

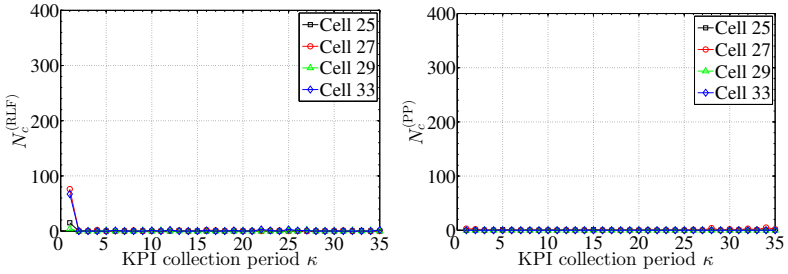

(d) Number $N_c^{(\mathrm{RLF})}$ of RLFs in each 3G cell.

(e) Number $N_c^{(\mathrm{PP})}$ of PPs in each 3G cell.

Figure 7.8. Cell level performance of the cell-area based automatic algorithm of the handover thresholds for velocity $v_{\mathrm{st}} = 60$ km/h and inter-RAT TTT $Q_c^{(3)} = 100$ ms.

is shown that the cell-area based optimization approach can resolve all the mobility problems of all cells. In particular, it can efficiently resolve the numbers of UHs which are the bottleneck for all other optimization approaches.

To highlight the advantage of the cell-area based optimization approach, denoted by "C-AS Serv. & C-APS Targ.", over the cell-pair specific optimization of handover

thresholds, denoted by "CS Serv. & CPS Targ.", the numbers $N_c^{(\mathrm{RLF})}$ and $N_c^{(\mathrm{UH})}$ are shown in Fig. 7.9 for the LTE cells whose mobility problems are not resolved by "CS Serv. & CPS Targ.". It is shown in Fig. 7.9(a) that only cell 11 has initially RLF problems. This is because the initial setting of the handover thresholds has been already optimized by selecting the best network-wide setting. The "CS Serv. & CPS Targ." approach fails to resolve the number of RLFs of cell 11 since its corresponding mobility failure events occurring with respect to the 3G target cell 32 require contradicting actions to be performed on the same cell-pair specific target cell threshold, i.e., $D_{c,j}^{(+),2} \approx D_{c,j}^{(-),2}$. Moreover, it is shown in Fig. 7.9(b) that "CS Serv. & CPS Targ." did not react on UHs of cell 11 since it has already TLHs which have higher priority than UHs. On the other hand, "C-AS Serv. & C-APS Targ." is able to resolve $N_c^{(\mathrm{RLF})}$ and $N_c^{(\mathrm{UH})}$ of cell 11 by exploiting the locations of the mobility failure events and assigning different handover threshold values for each area of the cell.

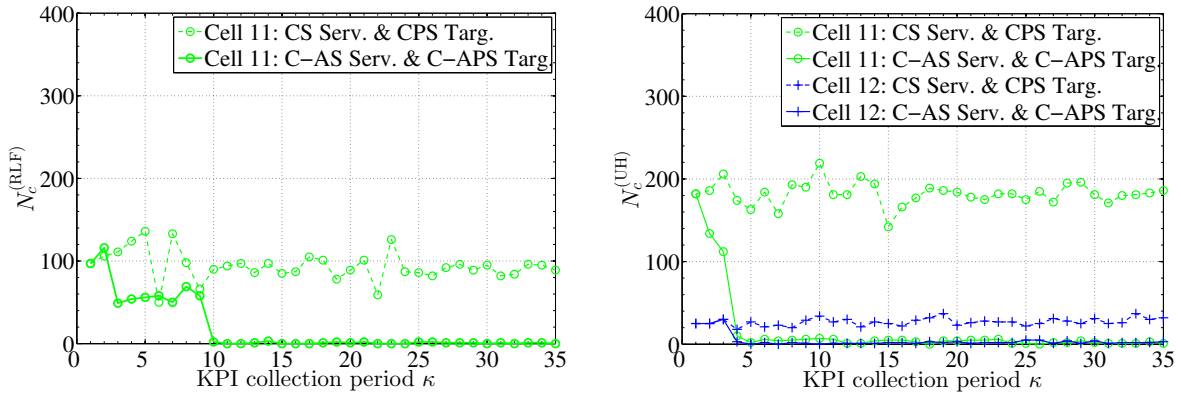

(a) LTE cell having RLF problems.

(b) LTE cells having UH problems.

Figure 7.9. Performance comparison between "C-AS Serv. & C-APS Targ." and "CS Serv. & CPS Targ." with respect to number of RLFs and UHs in LTE cells.

The optimized values of the serving cell threshold $Q_{c,z}^{(1)}$ and target cell threshold $Q_{c,z,j}^{(2)}$ is shown in Fig. 7.10 for each area $\mathrm{r}_{c,z}$ of cell $c = 11$ with respect to the overlaying target cell 32. The white color denotes the initial default configured value of $Q_{c,z}^{(1)} = -121$ dBm and $Q_{c,z,j}^{(2)} = -100$ dBm. According to the figure, most of the areas kept the default setting of handover thresholds. Only few areas, indicated by colored squares, have updated their corresponding handover thresholds. It is shown in Fig. 7.10(a) that areas in region 1 and 2 have $Q_{c,z}^{(1)}$ values which are lower and higher, respectively, than the default one. Thus, "C-AS Serv. & C-APS Targ." has reacted on TLHs and UHs of different areas simultaneously which is not possible for "CS Serv. & CPS Targ." approach. Similarly, Fig. 7.10(b) shows that areas in region 3 and 4 have $Q_{c,z,j}^{(2)}$ values which are higher and lower, respectively, than the default one. This also indicates that

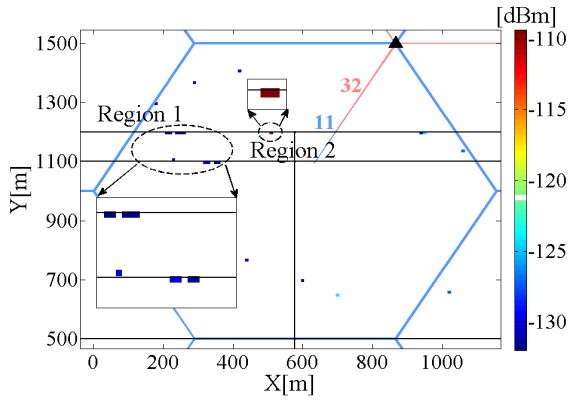

(a) Optimized value of $Q_{c,z}^{(1)}$ in dBm for each area $\mathrm{r}_{c,z}$ of cell $c = 11$.

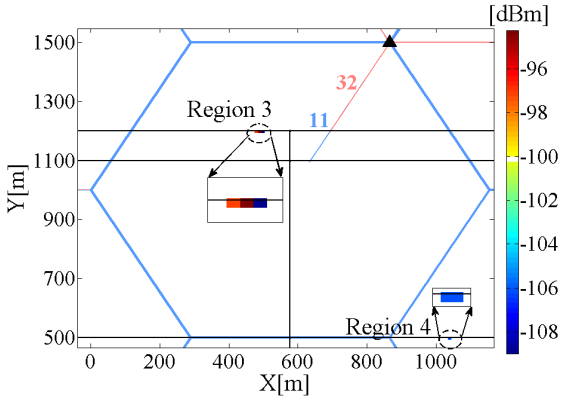

(b) Optimized value of $Q_{c,z,j}^{(2)}$ in dBm for each area $\mathrm{r}_{c,z}$ of cell $c = 11$ with respect to the overlaying target cell 32.

Figure 7.10. The optimized values of $Q_{c,z}^{(1)}$ and $Q_{c,z,j}^{(2)}$ thresholds for each area $\mathrm{r}_{c,z}$ of cell $c = 11$ with respect to the overlaying target cell 32.

the "C-AS Serv. & C-APS Targ." algorithm has reacted on different types of mobility failures in cell 11, i.e., TEH and TLH of type 2, even though they occur with respect to the same target cell 32.

Chapter 8

Summary and Outlook

This thesis has dealt with the automatic optimization of inter-RAT handover parameters in SON. Several optimization approaches to dynamically react on the mobility problems of each cell have been proposed and investigated. The optimization of handover parameters can be performed on either cell or cell-area basis. For both paradigms, the handover thresholds can be optimized cell-specifically with respect to all neighboring target cells, or cell-group specifically with respect to a group of neighboring target cells. The proposed optimization approaches outperform the current network planning optimization methods and reduce CAPEX and OPEX.

Chapter 2 has described the system model used for the evaluation of inter-RAT MRO concepts. The model has allowed the evaluation of several KPI collection periods in order of minutes while keeping the computational complexity low. Moreover, it has considered the impact of L1 filtering of fast fading which operates on much smaller time scale than that used for KPI collection periods. Two deployments scenarios have been proposed for proper investigation of inter-RAT MRO. The first scenario has consisted of two fully overlaying LTE and 3G networks and allowed the study of inter-RAT MRO problem from pure radio driven aspects. The second scenario has considered a partial deployment of an LTE network overlaying with an ubiquitous 3G network. In this scenario, the inter-RAT handovers from LTE to 3G network are radio-driven whereas those from 3G to LTE are triggered by a traffic steering policy.

The inter-RAT handover parameters and mobility failure types have been defined in Chapter 3. An inter-RAT handover is triggered by a dual-threshold measurement event where the first threshold corresponds to the serving cell and the second to the neighboring target cell of another RAT. The most relevant handover parameters are the serving and target cell thresholds of the measurement event, TTT and filter coefficient. In contrast to the intra-RAT case, two types of TLHs exist. The first type refers to TLHs which can be resolved by the serving cell threshold and the second type refers to TLHs which can be resolved by the target cell threshold. This differentiation between the two types of TLHs has been adopted by LTE Rel. 11 standard [3GP12c].

In Chapter 4, the inter-RAT handover thresholds have been optimized using manual optimization methods. Cell-specific configuration of handover thresholds can be obtained either online using drive tests or offline using network planning optimization

methods. The two investigated offline optimization methods are SA and TM. Unlike the SA algorithm that searches locally for new candidates in the neighborhood of the current solution, TM explores a wider search space via the parameter combinations arranged by OA which refer to candidate solutions that are far apart from each other in the search space. TM has been modified by replacing OA with a NOA as it provides more flexibility regarding the number of configuration parameters and experiments, and has statistical properties that are comparable to OA. The simulation results have shown that the newly introduced TM applying NOA has a comparable performance to SA. Moreover, the two methods SA and TM can be used offline in the network planning phase to provide cell-specific configuration of handover thresholds which outperform the best network-wide setting.

The automatic optimization of handover thresholds in SON has been described in Chapter 5. The cell-specific optimization problem has been formulated by the author of this thesis analytically. Moreover, a new cell-group specific optimization approach has been proposed to overcome the limitations of the cell specific optimization approach. For both optimization approaches, the values of the inter-RAT KPIs are collected from each cell in both RATs and are further mapped into correction directives depending on the action required by each mobility problem, i.e., increase or decrease the handover threshold. Modifying the handover thresholds by a fixed and large step size may lead to fluctuations in the values of the KPIs and in turn instability in the network. As a countermeasure, a proportional feedback controller has been used to apply the necessary amount of change to each handover threshold. Moreover, a gain scheduler has been added to adjust the parameters of the controller according to the mobility conditions of each cell. Simulation results have shown that cell-specific handover thresholds are necessary to resolve the mobility failure events of some cells. An additional performance gain has been obtained by optimizing the target cell threshold cell-pair specifically i.e., a dedicated handover threshold is configured with respect to each neighboring cell. Moreover, the performance of the automatic algorithm optimizing only the handover thresholds depends on the initial value of TTT.

In Chapter 6, an automatic algorithm has been proposed to jointly optimize the inter-RAT handover thresholds and TTT. The additional TTT parameter is used to react on mobility failure events which can be resolved by TTT. Simulation results have shown that the performance of the joint optimization approach is to some extent independent of the initial value of TTT as opposed to that of the automatic algorithm optimizing only the handover thresholds. Moreover, an additional performance gain has been shown with respect to RLFs for a cell-specific configuration of handover thresholds. In case of a cell-pair specific target cell threshold, the joint optimization approach could not improve the performance of the automatic algorithm optimizing only the handover

thresholds for small values of TTT. This is because the cell-pair specific optimization approach provides already many degrees of freedom by allowing dedicated handover thresholds to be configured with respect to different neighboring target cells.

An advanced cell-area based optimization approach for the inter-RAT handover thresholds has been presented in Chapter 7. The mobility failure events have been classified per small cell areas and dedicated handover thresholds have been assigned for each area. The handover thresholds of each area can be either configured cell-area specifically with respect to all neighboring target cells, or cell-area group specifically with respect to a group of neighboring target cells. The handover thresholds of the areas having mobility problems have been optimized automatically. Simulation results have shown that the new cell-area based optimization approach can mitigate mobility problems which cell-based optimization approaches fail to resolve.

As a future work, a comprehensive automatic algorithm for the inter-RAT handover thresholds that includes all cell-based and cell-area based optimization approaches can be designed. For each cell, the proper optimization approach can be applied depending on the optimization granularity that the mobility failure events of the cell require. In this way, cell-based optimization approaches are applied in cells having mobility problems which can be easily resolved whereas cell-area based optimization approaches are applied in cells having more difficult mobility problems. Moreover, the optimization of filter coefficients used for filtering fast fading and measurement errors can be as well investigated to check if an additional performance gain can be achieved. The coordination between inter-RAT MRO and other SON use cases such as intra-RAT MRO is also an interesting topic for investigation. Coordinating several SON use cases is a challenging task due to inter-dependencies and interactions among them.

Appendix

A.1 Proof of (5.12)

In this appendix, it is proven that (5.12) of Section 5.4.1:

$$\sum_{k=1}^{K}\sum_{a=1}^{A} w_{c,a} f_{c,i_k}^{(a)} = \sum_{m=1}^{M} \left(D_c^{(+),m} + D_c^{(-),m} \right) \tag{A.1}$$

holds if the design matrix $\mathbf{G}_m \in \mathbb{R}^{A\times 2} = [\mathbf{g}_{1,m}, \mathbf{g}_{2,m}]$ fulfills the following constraint:

$$\sum_{m=1}^{M} (\mathbf{g}_{1,m} + \mathbf{g}_{2,m}) = \mathbf{w}_c. \tag{A.2}$$

As a notation, the $(i,j)^{\text{th}}$ element of a matrix $\mathbf{X}$ is indicated by $[\mathbf{X}]_{i,j}$.

The value of the a^{th} KPI with respect to k^{th} neighboring cell i_k of cell c is expressed by $f_{c,i_k}^{(a)}$ and all values are packed in matrix $\mathbf{F}_c \in \mathbb{Z}^{A\times K}$ as follows:

$$\mathbf{F}_c = \begin{bmatrix} f_{c,i_1}^{(1)} & \cdots & f_{c,i_k}^{(1)} & \cdots & f_{c,i_K}^{(1)} \\ \vdots & & \ddots & & \vdots \\ f_{c,i_1}^{(a)} & \cdots & f_{c,i_k}^{(a)} & \cdots & f_{c,i_K}^{(a)} \\ \vdots & & \ddots & & \vdots \\ f_{c,i_1}^{(A)} & \cdots & f_{c,i_k}^{(A)} & \cdots & f_{c,i_K}^{(A)} \end{bmatrix} = [\mathbf{f}_{c,i_1}, \ldots, \mathbf{f}_{c,i_k}, \ldots \mathbf{f}_{c,i_K}]\,. \tag{A.3}$$

The weights of the KPI values are independent of the neighbor i_k and are given by $\mathbf{w}_c \in \mathbb{R}^{A\times 1}$ as follows:

$$\mathbf{w}_c = \begin{bmatrix} w_{c,1} \\ \vdots \\ w_{c,a} \\ \vdots \\ w_{c,A} \end{bmatrix}. \tag{A.4}$$

The weighted sum of the KPI values of cell c is given by

$$F = \sum_{k=1}^{K}\sum_{a=1}^{A} w_{c,a} f_{c,i_k}^{(a)}. \tag{A.5}$$

Using (A.3) and (A.4), F is rewritten as

$$F = \sum_{k=1}^{K} \left[\mathbf{F}_c^{\mathrm{T}} \mathbf{w}_c \right]_{k,1}. \tag{A.6}$$

Replacing $\mathbf{w}_c$ by the summand in (A.2), F is expressed by

$$F = \sum_{k=1}^{K} \left[\mathbf{F}_c^{\mathrm{T}} \left(\sum_{m=1}^{M} \left(\mathbf{g}_{1,m} + \mathbf{g}_{2,m} \right) \right) \right]_{k,1} . \tag{A.7}$$

Using linear decomposition, F can be written as

$$F = \sum_{k=1}^{K} \left[\mathbf{F}_c^{\mathrm{T}} \sum_{m=1}^{M} \mathbf{g}_{1,m} \right]_{k,1} + \sum_{k=1}^{K} \left[\mathbf{F}_c^{\mathrm{T}} \sum_{m=1}^{M} \mathbf{g}_{2,m} \right]_{k,1} \tag{A.8}$$

$$= \sum_{m=1}^{M} \sum_{k=1}^{K} \left[\mathbf{F}_c^{\mathrm{T}} \mathbf{g}_{1,m} \right]_{k,1} + \sum_{m=1}^{M} \sum_{k=1}^{K} \left[\mathbf{F}_c^{\mathrm{T}} \mathbf{g}_{2,m} \right]_{k,1} . \tag{A.9}$$

Using vector $\boldsymbol{\ell}_c \in \mathbb{Z}^{A \times 1}$ which is defined in (5.7) as

$$\boldsymbol{\ell}_c = \sum_{k=1}^{K} \mathbf{f}_{c,i_k}, \tag{A.10}$$

F can be expressed by

$$F = \sum_{m=1}^{M} \boldsymbol{\ell}_c^{\mathrm{T}} \mathbf{g}_{1,m} + \sum_{m=1}^{M} \boldsymbol{\ell}_c^{\mathrm{T}} \mathbf{g}_{2,m}. \tag{A.11}$$

Moreover, using vector $\mathbf{d}_m \in \mathbb{R}^{1 \times 2}$ which is defined in (5.9) as

$$\mathbf{d}_m = \boldsymbol{\ell}_c^{\mathrm{T}} \mathbf{G}_m = \left[D_c^{(+),m}, D_c^{(-),m} \right], \tag{A.12}$$

F can be written as a function of the correction directives and the proof of (A.1) is completed:

$$F = \sum_{m=1}^{M} \left(D_c^{(+),m} + D_c^{(-),m} \right). \tag{A.13}$$

□

A.2 Proof of (5.26)

In this appendix, it is proven that (5.26) of Section 5.5.3:

$$\sum_{k=1}^{K}\sum_{a=1}^{A} w_{c,a} f_{c,i_k}^{(a)} = \sum_{m=1}^{M}\sum_{j=1}^{J_m}\left(D_{c,j}^{(+),m} + D_{c,j}^{(-),m}\right) \tag{A.14}$$

holds if the design matrix $\mathbf{G}_m \in \mathbb{R}^{A\times 2} = [\mathbf{g}_{1,m}, \mathbf{g}_{2,m}]$ fulfills the following constraint:

$$\sum_{m=1}^{M}(\mathbf{g}_{1,m} + \mathbf{g}_{2,m}) = \mathbf{w}_c. \tag{A.15}$$

As a notation, the $(i,j)^{\text{th}}$ element of a matrix $\mathbf{X}$ is indicated by $[\mathbf{X}]_{i,j}$.

The weighted sum F of the KPI values of matrix $\mathbf{F}_c$, defined in (5.3), is given by (A.9) as follows:

$$F = \sum_{k=1}^{K}\sum_{a=1}^{A} w_{c,a} f_{c,i_k}^{(a)} \tag{A.16}$$

$$= \sum_{m=1}^{M}\sum_{k=1}^{K}\left[\mathbf{F}_c^{\mathrm{T}}\mathbf{g}_{1,m}\right]_{k,1} + \sum_{m=1}^{M}\sum_{k=1}^{K}\left[\mathbf{F}_c^{\mathrm{T}}\mathbf{g}_{2,m}\right]_{k,1}. \tag{A.17}$$

Using matrix $\mathbf{R}_{c,j}^{(m)} \in \mathbb{Z}^{A\times V}$ which is defined in (5.21) as

$$\mathbf{R}_{c,j}^{(m)} = [\mathbf{f}_{c,\zeta_1}, \ldots, \mathbf{f}_{c,\zeta_v}, \ldots, \mathbf{f}_{c,\zeta_V}], \tag{A.18}$$

F can be expressed by

$$F = \sum_{m=1}^{M}\sum_{j=1}^{J_m}\sum_{v=1}^{V}\left[{\mathbf{R}_{c,j}^{(m)}}^{\mathrm{T}}\mathbf{g}_{1,m}\right]_{v,1} + \sum_{m=1}^{M}\sum_{j=1}^{J_m}\sum_{v=1}^{V}\left[{\mathbf{R}_{c,j}^{(m)}}^{\mathrm{T}}\mathbf{g}_{2,m}\right]_{v,1}. \tag{A.19}$$

Moreover, using vector $\boldsymbol{\ell}_{c,j}^{(m)} \in \mathbb{Z}^{A\times 1}$ defined in (5.22) as

$$\boldsymbol{\ell}_{c,j}^{(m)} = \sum_{v=1}^{V}\mathbf{f}_{c,\zeta_v}, \tag{A.20}$$

F can be rewritten as

$$F = \sum_{m=1}^{M}\sum_{j=1}^{J_m}{\boldsymbol{\ell}_{c,j}^{(m)}}^{\mathrm{T}}\mathbf{g}_{1,m} + \sum_{m=1}^{M}\sum_{j=1}^{J_m}{\boldsymbol{\ell}_{c,j}^{(m)}}^{\mathrm{T}}\mathbf{g}_{2,m}. \tag{A.21}$$

Using vector $\mathbf{d}_{c,j}^{(m)} \in \mathbb{R}^{1\times 2}$ which is defined in (5.23) as

$$\mathbf{d}_{c,j}^{(m)} = \boldsymbol{\ell}_{c,j}^{(m)^{\mathrm{T}}} \mathbf{G}_m = \left[D_{c,j}^{(+),m}, D_{c,j}^{(-),m} \right], \tag{A.22}$$

F can be written as a function of the correction directives and the proof of (A.14) is completed:

$$F = \sum_{m=1}^{M} \sum_{j=1}^{J_m} \left(D_{c,j}^{(+),m} + D_{c,j}^{(-),m} \right). \tag{A.23}$$

□

A.3 Proof of (7.14)

In this appendix, it is proven that (7.14) of Section 7.3:

$$\sum_{k=1}^{K}\sum_{a=1}^{A} w_{c,a} f_{c,i_k}^{(a)} = \sum_{m=1}^{M}\sum_{z=1}^{Z_c}\sum_{j=1}^{J_m}\left(D_{c,z,j}^{(+),m} + D_{c,z,j}^{(-),m}\right) \tag{A.24}$$

holds if the design matrix $\mathbf{G}_m \in \mathbb{R}^{A\times 2} = [\mathbf{g}_{1,m}, \mathbf{g}_{2,m}]$ fulfills the following constraint:

$$\sum_{m=1}^{M}(\mathbf{g}_{1,m} + \mathbf{g}_{2,m}) = \mathbf{w}_c. \tag{A.25}$$

As a notation, the $(i,j)^{\text{th}}$ element of a matrix $\mathbf{X}$ is indicated by $[\mathbf{X}]_{i,j}$.

The weighted sum F of KPI values of matrix $\mathbf{F}_c$, defined in (5.3), is given by (A.9) as follows:

$$F = \sum_{k=1}^{K}\sum_{a=1}^{A} w_{c,a} f_{c,i_k}^{(a)} \tag{A.26}$$

$$= \sum_{m=1}^{M}\sum_{k=1}^{K}\left[\mathbf{F}_c^{\mathrm{T}}\mathbf{g}_{1,m}\right]_{k,1} + \sum_{m=1}^{M}\sum_{k=1}^{K}\left[\mathbf{F}_c^{\mathrm{T}}\mathbf{g}_{2,m}\right]_{k,1}. \tag{A.27}$$

The matrix F_c is replaced by the summand of (7.3) which is defined as

$$\mathbf{F}_c = \sum_{z=1}^{Z_c}\mathbf{F}_{c,z}, \tag{A.28}$$

yielding

$$F = \sum_{m=1}^{M}\sum_{z=1}^{Z_c}\sum_{k=1}^{K}\left[\mathbf{F}_{c,z}^{\mathrm{T}}\mathbf{g}_{1,m}\right]_{k,1} + \sum_{m=1}^{M}\sum_{z=1}^{Z_c}\sum_{k=1}^{K}\left[\mathbf{F}_{c,z}^{\mathrm{T}}\mathbf{g}_{2,m}\right]_{k,1}. \tag{A.29}$$

Using matrix $\mathbf{R}_{c,z,j}^{(m)} \in \mathbb{Z}^{A\times V}$ which is defined in (7.9) as

$$\mathbf{R}_{c,z,j}^{(m)} = [\mathbf{f}_{c,z,\zeta_1}, \ldots, \mathbf{f}_{c,z,\zeta_v}, \ldots, \mathbf{f}_{c,z,\zeta_V}], \tag{A.30}$$

F can be expressed by

$$F = \sum_{m=1}^{M}\sum_{z=1}^{Z_c}\sum_{j=1}^{J_m}\sum_{v=1}^{V}\left[\mathbf{R}_{c,z,j}^{(m)\,\mathrm{T}}\mathbf{g}_{1,m}\right]_{v,1} + \sum_{m=1}^{M}\sum_{z=1}^{Z_c}\sum_{j=1}^{J_m}\sum_{v=1}^{V}\left[\mathbf{R}_{c,z,j}^{(m)\,\mathrm{T}}\mathbf{g}_{2,m}\right]_{v,1}. \tag{A.31}$$

Moreover, using vector $\boldsymbol{\ell}_{c,z,j}^{(m)} \in \mathbb{Z}^{A\times 1}$ which is defined in (7.10) as

$$\boldsymbol{\ell}_{c,z,j}^{(m)} = \sum_{v=1}^{V}\mathbf{f}_{c,z,\zeta_v}, \tag{A.32}$$

F can be rewritten as

$$F = \sum_{m=1}^{M} \sum_{z=1}^{Z_c} \sum_{j=1}^{J_m} \boldsymbol{\ell}_{c,z,j}^{(m)\,\mathrm{T}} \mathbf{g}_{1,m} + \sum_{m=1}^{M} \sum_{z=1}^{Z_c} \sum_{j=1}^{J_m} \boldsymbol{\ell}_{c,z,j}^{(m)\,\mathrm{T}} \mathbf{g}_{2,m}. \tag{A.33}$$

Using vector $\mathbf{d}_{c,j}^{(m)} \in \mathbb{R}^{1\times 2}$ which is defined in (7.11) as

$$\mathbf{d}_{c,z,j}^{(m)} = \boldsymbol{\ell}_{c,z,j}^{(m)\,\mathrm{T}} \mathbf{G}_m = \left[D_{c,z,j}^{(+),m}, D_{c,z,j}^{(-),m} \right], \tag{A.34}$$

F can be written as a function of the correction directives and the proof of (A.24) is completed:

$$F = \sum_{m=1}^{M} \sum_{z=1}^{Z_c} \sum_{j=1}^{J_m} \left(D_{c,z,j}^{(+),m} + D_{c,z,j}^{(-),m} \right). \tag{A.35}$$

□

List of Acronyms

2G	2nd Generation
3-D	3-Dimensional
3G	3rd Generation
4G	4th Generation
3GPP	3rd Generation Partnership Project
BS	Base Station
CAPEX	Capital Expenses
CPICH	Common Pilot Channel
GSM	Global System for Mobile Communications
HOF	Handover Failure
HWC	Handover to a Wrong Cell
ISD	Inter-Site Distance
KPI	Key Performance Indicator
L1	Layer 1
L3	Layer 3
LTE	Long Term Evolution
Mb	Megabit
MRO	Mobility Robustness Optimization
NGMN	Next Generation Mobile Networks
NOA	Nearly Orthogonal Array
OA	Orthogonal Array
OAM	Operation and Maintenance
OFDM	Orthogonal Frequency Division Multiplexing
OPEX	Operational Expenses

PCI	Physical Cell ID
pdf	probability distribution function
PP	Ping-Pong
QoS	Quality of Service
RACH	Random Access Channel
RAT	Radio Access Technology
RB	Resource Block
Rel.	Release
RF	Radio Frequency
RLF	Radio Link Failure
RRM	Radio Resource Management
RSCP	Received Signal Code Power
RSRP	Reference Signal Received Power
RSRQ	Reference Symbol Received Quality
RSSI	Received Signal Strength Indicator
RV	Random Variable
SA	Simulated Annealing
SINR	Signal-to-Interference and Noise Ratio
SN	Signal-to-Noise
SNR	Signal-to-Noise Ratio
SON	Self-Organizing Network
TEH	Too Early Handover
TLH	Too Late Handover
TM	Taguchi's Method
TTI	Transmission Time Interval

TTT	Time-to-Trigger
UE	User Equipment
UH	Unnecessary Handover
UMTS	Universal Mobile Telecommunication System
WCDMA	Wideband Code Division Multiple Access
WiMAX	Worldwide Interoperability for Microwave Access

List of Symbols

a	Index for inter-RAT KPIs
a_{gs}	Slope used by the gain scheduler for increasing $\chi_{c,j}^{(m)}$
a_{L3}	Filter factor used for L3 filtering
a'_{L3}	Filter factor used for L3 filtering in case $T_{\mathrm{n}} < 200$ milliseconds
A	Total number of inter-RAT KPIs
$\mathbf{A}$	OA having N_{exp} rows and N_{p} columns
b	Index for BSs
b_{gs}	Constant used by the gain scheduler for increasing $\chi_{c,j}^{(m)}$
B_{a}	Maximum backward attenuation of antenna
B_{h}	Maximum azimuth attenuation of antenna
B_{v}	Maximum elevation attenuation of antenna
$\mathbb{B}$	Set of 0 and 1
c	Index for cells
c_0	Intra-RAT neighbor of cell c
$\mathcal{C}$	Set of LTE and 3G cells
d	Side length of a cell area
d_{corr}	De-correlation distance
$d_{c,u}$	Distance between BS serving cell c and UE u
d_{mar}	Margin distance
$D^{(-),m}$	Total number of mobility failure events in the whole network requiring a decrease in the network-wide handover parameter m
$D^{(+),m}$	Total number of mobility failure events in the whole network requiring an increase in the network-wide handover parameter m
$D_c^{(-),m}$	Number of mobility failure events which require a decrease in $Q_c^{(m)}$
$D_c^{(+),m}$	Number of mobility failure events which require an increase in $Q_c^{(m)}$
$\mathbf{d}_m$	Vector containing $D_c^{(+),m}$ and $D_c^{(-),m}$
$D_{\mathrm{thr}}^{(\mathrm{min})}$	Minimum threshold to react on $D_{c,j}^{(+),m}$ and $D_{c,j}^{(-),m}$
$D_{\mathrm{T}}^{(\mathrm{min})}$	Minimum threshold to react on $D_c^{(+),3}$ and $D_c^{(-),3}$
$D_{c,j}^{(-),m}$	Number of mobility failure events which require a decrease in $Q_{c,j}^{(m)}$
$D_{c,j}^{(+),m}$	Number of mobility failure events which require an increase $Q_{c,j}^{(m)}$
$\mathbf{d}_{c,j}^{(m)}$	Vector containing $D_{c,j}^{(+),m}$ and $D_{c,j}^{(-),m}$
$D_{c,z,j}^{(-),m}$	Number of mobility failure events which require a decrease in $Q_{c,z,j}^{(m)}$
$D_{c,z,j}^{(+),m}$	Number of mobility failure events which require an increase in $Q_{c,z,j}^{(m)}$
$\mathbf{d}_{c,z,j}^{(m)}$	Vector containing $D_{c,z,j}^{(+),m}$ and $D_{c,z,j}^{(-),m}$

e	Index for the number N_{exp} of experiments
$\mathbf{e}_{c,i_k}$	Location of a mobility failure event occurring in cell c with respect to k^{th} neighboring cell i_k
$[Ec/N_0]_{u,c}$	Ec/N_0 of a 3G cell c measured by a UE u in dB
$\mathbf{f}_{c,i_k}$	k^{th} column of matrix $\mathbf{F}_c$
$f_{c,i_k}^{(a)}$	Value of the KPI a in cell c with respect to the neighboring cell i_k
$\mathbf{f}_{c,z,i_k}$	k^{th} column of matrix $\mathbf{F}_{c,z}$
$f_{c,z,i_k}^{(a)}$	Value of KPI a evaluated for area $\mathrm{r}_{c,z}$ with respect to neighboring cell i_k
F	Weighted sum of KPI values in a cell
$\mathbf{F}_c$	Matrix containing the values of the KPIs with respect to each neighbor of cell c
$\mathbf{F}_{c,z}$	Matrix containing the values of the KPIs evaluated for area $\mathrm{r}_{c,z}$ with respect to each neighbor of cell c
$\mathbf{g}_{1,m}$	First column of matrix $\mathbf{G}_m$
$\mathbf{g}_{2,m}$	Second column of matrix $\mathbf{G}_m$
G_{gain}	Antenna gain
$\mathbf{G}_m$	Matrix used to group the values of the KPIs into correction directives
h	Counter of the number of times the temperature T is reduced
h_{bs}	BS height
$H_{c,j}^{(2)}$	Number of missed (TLHs) and successful handovers from cell c with respect to neighboring cells of set $\mathcal{S}_{c,j}^{(2)}$
i_k	k^{th} inter-RAT neighbor of cell c
$\mathbf{I}$	Identity matrix
j	Index for the subsets $\mathcal{S}_{c,j}^{(m)}$ of neighboring cells
J_m	Total number of subsets $\mathcal{S}_{c,j}^{(m)}$
$\mathcal{J}_m$	Set containing the indices j for $\mathcal{S}_{c,j}^{(m)}$
k	Index for inter-RAT neighbors of cell c
k_{L3}	Filter coefficient used for L3 filtering
K	Number of inter-RAT neighbors of cell c
ℓ	Elements of set $\mathcal{L}$
ℓ_c	Index of the network to which cell c belongs to
L_{pn}	Penetration loss
$\boldsymbol{\ell}_c$	Vector containing the values of the KPIs in cell c with respect to all neighboring cells
$\boldsymbol{\ell}_{c,j}^{(m)}$	Vector containing the values of the KPIs in cell c with respect to all neighboring cells in $\mathcal{S}_{c,j}^{(m)}$

$\boldsymbol{\ell}_{c,z,j}^{(m)}$	Vector containing the values of the KPIs in cell area $\mathrm{r}_{c,z}$ with respect to all neighboring cells in $\mathcal{S}_{c,z,j}^{(m)}$
$\mathcal{L}$	Set of levels in an OA
m	Index for the handover parameters
M	Total number of handover thresholds
$M_{c,j}^{(m)}$	Controller metric corresponding to $Q_{c,j}^{(m)}$
$MQ_{u,c}$	L3 filtered measurement of $\widetilde{MQ}_{u,c}$
$\widehat{MQ}_{u,c}$	L1 measured quantity of cell c performed by UE u in dB scale
$\widetilde{MQ}_{u,c}$	$\widehat{MQ}_{u,c}$ impacted by the measurement error
n	Index for simulation time steps
$N^{(\mathrm{PP})}$	Number of PPs occurring per minute and UE
$N^{(\mathrm{RLF})}$	Number of RLFs occurring per minute and UE
$N^{(\mathrm{UH})}$	Number of UHs occurring per minute and UE
N_{bs}	Number of BSs
N_{c}	Number of cells
N_{exp}	Number of experiments in an OA or NOA
N_{FH}	Number of fast handovers which are assigned to handover thresholds
N_{it}	Number of iterations in SA executed at each temperature T
N_{MH}	Number of missed handovers which are assigned to handover thresholds
N_{p}	Total number of configuration parameters in an OA or NOA
N_{samples}	Gain scheduler parameter indicating number of samples for a correction directive
N_{tp}	Number of times the temperature T is reduced
N_{ue}	Number of UEs
N_{v}	Number of levels in an OA or NOA
$N_{\mathrm{3G}}^{(\mathrm{PP})}$	Total number of PPs in 3G network
$N_{\mathrm{3G}}^{(\mathrm{RLF})}$	Total number of RLFs in 3G network
$N_{\mathrm{all}}^{(\mathrm{PP})}$	Total number of PPs in 3G and LTE networks
$N_{\mathrm{all}}^{(\mathrm{RLF})}$	Total number of RLFs in 3G and LTE networks
$N_{\mathrm{all}}^{(\mathrm{UH})}$	Total number of UHs in LTE network
$N_{c}^{(\mathrm{HWC})}$	Number of HWC in cell c
$N_{c}^{(\mathrm{PP})}$	Number of PPs in cell c
$N_{c}^{(\mathrm{RLF})}$	Number of RLFs in cell c
$N_{c}^{(\mathrm{TEH})}$	Number of TEHs in cell c
$N_{c}^{(\mathrm{TLH}-1)}$	Number of TLHs of type 1 in cell c

$N_c^{(\mathrm{TLH-2})}$	Number of TLHs of type 2 in cell c
$N_c^{(\mathrm{UH})}$	Number of UHs in cell c
$N_{\max}^{(\mathrm{osc})}$	Maximum number of oscillations in the value of TTT
$N_{\mathrm{LTE}}^{(\mathrm{PP})}$	Total number of PPs in LTE network
$N_{\mathrm{LTE}}^{(\mathrm{RLF})}$	Total number of RLFs in LTE network
$N_{\mathrm{LTE}}^{(\mathrm{UH})}$	Total number of UHs in LTE network
$\mathrm{N}(\mathbf{x})$	Neighborhood of the current solution $\mathbf{x}$
$\mathcal{N}_c$	Set of inter-RAT neighbors of cell c
o	Index for the elements of set $\mathcal{O}_c^{(2)}$
$\mathcal{O}^{(m)}$	Set of cells which do not require any change in $Q_c^{(m)}$
$\mathcal{O}_c^{(2)}$	Set containing the indices of subsets $\mathcal{S}_{c,j}^{(2)}$ which do not require any change in $Q_{c,j}^{(2)}$
p	Index for the elements in $\mathbf{x}$
$\mathbf{p}_c$	Position vector of BS serving cell c
P_{N}	Total noise power in dBm
$P_{\mathrm{N}}^{(\mathrm{rb})}$	Noise power on a single RB in dBm
$P_c^{(\mathrm{tx})}$	Total transmit power of cell c in dBm
$P_c^{(\mathrm{tx,cpich})}$	Transmit power on CPICH channel in dBm
$P_c^{(\mathrm{tx,rb})}$	Transmit power of cell c on a single RB in dBm
$P_c^{(\mathrm{tx,re})}$	Transmit power of cell c on a single resource element in dBm
$P_{u,c}^{(\mathrm{rx})}$	Total received power of cell c by UE u
$P_{u,c}^{(\mathrm{rx,rb})}$	Received power on a single RB of a cell c measured by a UE u in dBm
q	Repetition counter for SA
$\mathbf{q}_c$	Vector containing the cell-specific handover thresholds of cell c
$\widehat{\mathbf{q}}_c$	Optimized vector of $\mathbf{q}_c$
$Q_c^{(1)}$	Cell-specific serving threshold of cell c
$Q_c^{(2)}$	Cell-specific target threshold of cell c
$Q_c^{(3)}$	Cell-specific TTT of cell c
$\widetilde{Q_c^{(3)}}$	Value of TTT which is required to resolve a missed or fast handover
$Q_c^{(m)}$	Cell-specific value of inter-RAT handover parameter m
$\widehat{Q}_c^{(m)}$	Optimized value of $Q_c^{(m)}$
$Q_{c,j}^{(m)}$	Value of the handover parameter m configured with respect to all neighbors of set $\mathcal{S}_{c,j}^{(m)}$
$\widehat{Q}_{c,j}^{(m)}$	Optimized value of $Q_{c,j}^{(m)}$
$Q_{c,z}^{(m)}$	Value of the handover parameter m configured by cell c for area z with respect to all neighboring cells $\mathcal{N}_c$

$Q_{c,z,j}^{(m)}$	Value of the handover parameter m configured by cell c for area z with respect to all neighbors of set $\mathcal{S}_{c,z,j}^{(m)}$
$\widehat{Q}_{c,z,j}^{(m)}$	Optimized value for $Q_{c,z,j}^{(m)}$
Q_{HC}	Threshold for detecting a failure in the handover command transmission
Q_{RACH}	Threshold for detecting a RACH failure
Q_{RLF}	Threshold for detecting an RLF
Q_{RSRQ}	Threshold for the RSRQ level of the previously serving LTE cell
Q_{ts}	Threshold for measurement event 3C used for traffic steering from 3G to LTE
r	Iteration index for TM
$\mathrm{r}_{c,z}$	z^{th} area of cell c
$\mathbf{r}_{c,z}$	Position vector of the center of area $\mathrm{r}_{c,z}$
$RSCP_{u,c}$	RSCP of a 3G cell c measured by a UE u in dBm
$\widehat{RSCP}_{u,c}$	L1 filtered measurement of $RSCP_{u,c}$
$RSRP_{u,c}$	RSRP of an LTE cell c measured by a UE u in dBm
$\widehat{RSRP}_{u,c}$	L1 filtered measurement of $RSRP_{u,c}$
$RSRQ_{u,c}$	RSRQ of an LTE cell c measured by a UE u in dB
$RSSI_u$	RSSI measured by UE u in dBm
$R_{c,j}^{(-),2}$	Difference between $H_{c,j}^{(2)}$ and $D_{c,j}^{(+),2}$
$\mathbf{R}_{c,j}^{(m)}$	Matrix containing the columns of $\mathbf{F}_c$ corresponding to neighboring cells of $\mathcal{S}_{c,j}^{(m)}$
$\mathbf{R}_{c,z,j}^{(m)}$	Matrix containing the columns of $\mathbf{F}_{c,z}$ corresponding to neighboring cells of $\mathcal{S}_{c,z,j}^{(m)}$
$\mathbb{R}$	Set of real numbers
S	Strength parameter of an OA
SN_e	SN ratio evaluated in e^{th} experiment
$\mathbf{S}_{c,j}^{(m)}$	Selection matrix used to retrieve the columns in $\mathbf{F}_c$ corresponding to the neighboring cells in $\mathcal{S}_{c,j}^{(m)}$
$\mathcal{S}_{c,j}^{(m)}$	j^{th} subset of neighbors of cell c for handover parameter m
$\mathbf{S}_{c,z,j}^{(m)}$	Selection matrix used to retrieve the columns in $\mathbf{F}_{c,z}$ corresponding to the neighboring cells in $\mathcal{S}_{c,z,j}^{(m)}$
$\mathcal{S}_{c,z,j}^{(m)}$	j^{th} subset of neighbors of cell c corresponding to area $\mathrm{r}_{c,z}$ and handover parameter m
t_0	Time step when the entering condition of the measurement event has been fulfilled for TTT time interval

t_1	Time step when the entering condition of the measurement event is fulfilled for the first time prior to RLF
t_2	Time step when the entering condition of the measurement event is not fulfilled for the first time after the inter-RAT handover is executed
t_n	n^{th} simulation time step
t_{HO}	Time step of handover execution
t_{RLF}	Time step of RLF
T	Temperature parameter for SA
$\mathcal{T}$	Set of TTT values
T_0	Initial value of temperature T
T_{cst}	Time constant corresponding to a filter coefficient
T_{n}	Time elapsed between any two simulation time steps
$T_{\text{hp}}^{(\text{inter})}$	Handover preparation time in milliseconds for inter-RAT handover
$T_{\text{hp}}^{(\text{intra})}$	Handover preparation time in milliseconds for intra-RAT handover
T_{CL}	Time interval during which the number of mobility failure events are collected from the network
T_{FH}	A value of T_{mar}
T_{mar}	Time margin
T_{MH}	A value of T_{mar}
T_{PP}	Time interval for detecting a PP
T_{RLF}	Time interval for detecting an RLF
T_{RSRQ}	Time interval for detecting an UH
$T_{\text{T}}^{(\text{intra})}$	TTT used for intra-RAT handover
$T_{\text{T}}^{(\text{ts})}$	Time interval for measurement event 3C used for traffic steering from 3G to LTE
T_{TE}	Time interval for detecting TEH and HWC
u	Index for UEs
$\mathcal{U}^{(m)}$	Set of the cells which require an increase in $Q_c^{(m)}$
$\mathcal{U}_c^{(2)}$	Set containing the indices j of the subsets $\mathcal{S}_{c,j}^{(2)}$ requiring an increase in $Q_{c,j}^{(2)}$
v	Index for the elements of a subset of neighboring cells
v_{mr}	Velocity of UEs moving randomly in the network
v_{st}	Velocity of UEs moving on streets
$\tilde{v}_{\text{st}}$	Estimated velocity of UEs moving on streets
$\mathbf{v}_u$	Position of UE u
V	Total number of elements in a subset of neighboring cells

$\mathcal{V}^{(m)}$	Set of the cells which require a decrease in $Q_c^{(m)}$
$\mathcal{V}_c^{(2)}$	Set containing the indices of the subsets $\mathcal{S}_{c,j}^{(2)}$ requiring a decrease in $Q_{c,j}^{(2)}$
$V_p^{(\max)}$	Maximum value of parameter x_p
$V_p^{(\min)}$	Minimum value of parameter x_p
$V_p^{(r)}$	A testing value of parameter x_p in iteration r
$V_p^{(\text{best},r)}$	Best testing value of parameter x_p in iteration r
w	Index for LTE and 3G networks
$\mathbf{w}_c$	Vector containing the weights of KPI values of cell c
$w_{c,a}$	Weight for the value of KPI a of cell c
w_{PP}	Weight for the value of PP KPI
w_{UH}	Weight for the value of UH KPI
W	System bandwidth
$\mathbf{x}$	Vector containing the handover thresholds of all cells in 3G and LTE networks
$\mathbf{x}'$	New candidate solution vector obtained from $\mathbf{x}$
$\mathbf{x_0}$	Initial candidate solution
x_p	p^{th} element in $\mathbf{x}$
$x_{p'}$	Element in $\mathbf{x}$ which is different than x_p
y	Optimization function for SA and TM
y_e	Value of the optimization function y evaluated in e^{th} experiment
z	Index for the areas of a cell
Z_c	Total number of areas in cell c
$\mathbb{Z}$	Set of integers
α_{p}	Propagation constant
$\alpha_{u,c}$	Power envelope of the multipath fading channel on the link between cell c and UE u
$\widehat{\alpha}_{u,c}$	L1 filtered value of $\alpha_{u,c}$
$\bar{\alpha}_{u,c}$	Average of the first five consecutive samples of $\alpha_{u,c}$ of each 50 milliseconds block
$\alpha_{u,c}^{(\text{me})}$	Measurement error pertaining to $\widehat{MQ}_{u,c}$
β_{p}	Path loss exponent
$\beta_p^{(r)}$	Step size corresponding to parameter x_p in iteration r
$\gamma_{u,c}$	SINR in dB of a UE u served by cell c
δ	Value of increase in optimization function y
$\delta_{\max}$	Maximum increase in optimization function y

Δ_1	Difference between the value of serving cell threshold and its corresponding measured quantity
Δ_2	Difference between the value of target cell threshold and its corresponding measured quantity
Δ_θ	Elevation beam width
Δ_ϕ	Azimuth beam width
$\Delta_{c,j}^{(-),2}$	Factor corresponding to $D_{c,j}^{(-),2}$
$\Delta_{c,j}^{(+),2}$	Factor corresponding to $D_{c,j}^{(+),2}$
ϵ	Termination threshold for TM
$\varepsilon^{(\max)}$	Maximum error value
$\varepsilon_{c,j}^{(m)}$	Error value corresponding to $Q_{c,j}^{(m)}$
ζ_{bs}	Shadowing correlation coefficient between two BSs of same network
ζ_{nw}	Shadowing correlation coefficient between two BSs of different networks
ζ_v	v^{th} element of a subset of neighboring cells
θ	Angle pertaining to vertical beam pattern
ϑ	Random number which is uniformly distributed between 0 and 1
Θ_c	Tilt of antenna serving cell c
κ	Index for KPI collection periods
λ	Index parameter of an OA
$\lambda_{c,j}^{(2)}$	Factor corresponding to the sum of $D_{c,j}^{(+),2}$ and $D_{c,j}^{(-),2}$
$\lambda_{c,j}^{(+),2}$	Factor corresponding to $D_{c,j}^{(+),2}$
$\lambda_{c,j}^{(-),2}$	Factor corresponding to $D_{c,j}^{(-),2}$
Λ_{dB}	Quantization step size for $\widetilde{\mu_{c,j}^{(m)}}$
μ	Index for the elements of set $\mathcal{U}_c^{(2)}$
$\mu^{(\max)}$	Maximum change in $Q_{c,j}^{(m)}$
$\mu_{c,j}^{(m)}$	Absolute change in the value of $Q_{c,j}^{(m)}$
$\widetilde{\mu_{c,j}^{(m)}}$	Change in the value of $Q_{c,j}^{(m)}$
$\widehat{\mu_{c,j}^{(m)}}$	Quantized value of $\widetilde{\mu_{c,j}^{(m)}}$
μ_{pb}	Initial acceptance probability value for SA
ν	Index for the elements of set $\mathcal{V}_c^{(2)}$
ν_{T}	Temperature reduction ratio for SA
ξ	Reduction ratio of the optimization range in TM
ϖ	Reduction ratio for $\chi_{c,j}^{(m)}$
ρ_c	Load of cell c
$\varrho^{(+)}$	Change in the value of $D_{c,j}^{(+),m}$

$\varrho^{(\max)}$	Threshold for the maximum change in a correction directive
$\varrho^{(\min)}$	Threshold for the minimum change in a correction directive
σ_{me}	Standard deviation of the measurement error
σ_{sf}	Standard deviation of shadow fading
υ	Random displacement value
$\upsilon_{\max}$	Maximum displacement value
ϕ	Angle pertaining to horizontal beam pattern
φ	Intra-RAT handover offset
Φ_c	Azimuth orientation of the antenna serving cell c
$\chi_{c,j}^{(m)}$	Controller gain corresponding to $\mu_{c,j}^{(m)}$
Ψ_c	Sum of the correction directives corresponding to $Q_c^{(2)}$
Ω	Solution space of $\mathbf{x}$
$\Omega_{c,z,j}^{(m)}$	Set of all the locations where the UE applies the handover threshold $Q_{c,z,j}^{(m)}$ of area $\mathrm{r}_{c,z}$

Bibliography

[3GP06] 3GPP, "TR 25.814: Technical specification group radio access network; physical layer aspects for evolved Universal Terrestrial Radio Access (UTRA) (Release 7)," 3GPP, Tech. Rep., 2006.

[3GP07] ——, "TR 32.816: Telecommunication management; study on management of Evolved Universal Terrestrial Radio Access Network (E-UTRAN) and Evolved Packet Core (EPC) (Release 8)," 3GPP, Tech. Rep., 2007.

[3GP10] ——, "TR 36.814: Technical specification group radio access network; Evolved Universal Terrestrial Radio Access (E-UTRA), further advancements for E-UTRA physical layer aspects (Release 9)," 3GPP, Tech. Rep., 2010.

[3GP11] ——, "TR 36.902: Technical specification group radio access network; Evolved Universal Terrestrial Radio Access Network (E-UTRAN); self-configuring and Self-Optimizing Network (SON) use cases and solutions (Release 9)," 3GPP, Tech. Rep., 2011.

[3GP12a] ——, "TS 25.133: Technical specification group radio access network; requirements for support of radio resource management (FDD) (Release 11)," 3GPP, Tech. Rep., 2012.

[3GP12b] ——, "TS 25.331: Technical specification group radio access network; radio resource control; protocol specification (Release 10)," 3GPP, Tech. Rep., 2012.

[3GP12c] ——, "TS 32.425: Technical specification group services and system aspects; telecommunication management; Performance Management (PM); performance measurements Evolved Universal Terrestrial Radio Access Network (E-TRAN) (Release 11)," 3GPP, Tech. Rep., 2012.

[3GP12d] ——, "TS 36.133: Technical specification group radio access network; Evolved Universal Terrestrial Radio Access (E-UTRA); requirements for support of radio resource management (Release 11)," 3GPP, Tech. Rep., 2012.

[3GP12e] ——, "TS 36.214: Technical specification group radio access network; Evolved Universal Terrestrial Radio Access (E-UTRA); physical layer; measurements (Release 11)," 3GPP, Tech. Rep., 2012.

[3GP12f] ——, "TS 36.300: Technical specification group radio access network; Evolved Universal Terrestrial Radio Access (E-UTRA) and Evolved Universal Terrestrial Radio Access Network (E-UTRAN); overall description; stage 2 (Release 11)," 3GPP, Tech. Rep., 2012.

[3GP12g] ——, "TS 36.331: Technical specification group radio access network; Evolved Universal Terrestrial Radio Access (E-UTRA); Radio Resource Control (RRC); protocol specification (Release 11)," 3GPP, Tech. Rep., 2012.

[ABH+04] S. Allen, B. Belloul, S. Hurley, S. Saunders, and R. Whitaker, "Smart cell planning and optimisation for UMTS," in *Proc. IEEE International Conference on 3G Mobile Communication Technologies*, 2004, pp. 34–38.

[ACMS02] E. Almadi, A. Capone, F. Malucelli, and F. Signori, "UMTS radio planning: optimizing base station configuration," in *Proc. IEEE Vehicular Technology Conference (VTC)*, vol. 2, December 2002, pp. 768–772.

[ADCO+07] M. Anas, F. D. Calabrese, P.-E. Östling, K. I. Pederson, and P. E. Mogensen, "Performance analysis of handover measurements and layer 3 filtering for UTRAN LTE," in *Proc. IEEE Symposium on Personal, Indoor and Mobile Radio Communications (PIMRC)*, September 2007, pp. 1–5.

[AEaG13] S. Abd El-atty and Z. Gharsseldien, "On performance of HetNet with coexisting small cell technology," in *Wireless and Mobile Networking Conference (WMNC)*, 2013, pp. 1–8.

[ALS+08] M. Amirijoo, R. Litjens, K. Spaey, M. Döttling, T. Jansen, and N. Scully, "Use cases, requirements and assessment criteria for future self-organizing radio access networks," in *International Workshop on Self-Organizing Systems (IWSOS)*, 2008, pp. 275–280.

[Ame11] G. Americas. (2011) Self-optimizing networks-The benefits of SON in LTE. [Online]. Available: http://www.4gamericas.org/

[AWR+11] A. Awada, B. Wegmann, D. Rose, I. Viering, and A. Klein, "Towards self-organizing mobility robustness optimization in inter-RAT scenario," in *Proc. IEEE Vehicular Technology Conference (VTC)*, May 2011, pp. 1–5.

[AWV+11] A. Awada, B. Wegmann, I. Viering, , and A. Klein, "A mathemetical model for user traffic in coverage and capacity optimization of a cellular network," in *Proc. IEEE Vehicular Technology Conference (VTC)*, May 2011, pp. 1–5.

[AWVK10a] A. Awada, B. Wegmann, I. Viering, and A. Klein, "Application of game theory for load balancing in long term evolution networks," *in Frequenz Journal of RF-Engineering and Telecommunications*, vol. 64, no. 9, pp. 180–184, 2010.

[AWVK10b] ——, "A game-theoretic approach to load balancing in cellular radio networks," in *Proc. IEEE International Symposium on Personal Indoor and Mobile Radio Communications (PIMRC)*, September 2010, pp. 1184–1189.

[AWVK11a] ——, "Optimizing the radio network parameters of the long term evolution system using Taguchi's method," *IEEE Transactions on Vehicular Technology (TVT)*, vol. 60, no. 8, pp. 3825–3839, October 2011.

[AWVK11b] ——, "Self-optimization algorithm for inter-RAT configuration parameters," in *Proc. IEEE International Symposium on Wireless Communication Systems (ISWCS)*, August 2011, pp. 311–316.

[AWVK11c] ——, "A joint optimization of antenna parameters in a cellular network using Taguchi's method," in *Proc. IEEE Vehicular Technology Conference (VTC)*, May 2011, pp. 1–5.

[AWVK12a] ——, "Cell-pair specific optimization of the inter-RAT handover parameters in SON," in *Proc. IEEE International Symposium on Personal, Indoor and Mobile Radio Communications (PIMRC)*, September 2012, pp. 1168–1173.

[AWVK12b] ——, "Performance comparison of signal strength and signal quality based inter-RAT MRO," in *Proc. IEEE International Symposium on Wireless Communication Systems (ISWCS)*, August 2012, pp. 11–15.

[AWVK13a] ——, "A location-based self-optimizing algorithm for the inter-RAT handover parameters," in *Proc. IEEE International Conference on Communications (ICC)*, June 2013, pp. 6168–6173.

[AWVK13b] ——, "A SON-based algorithm for the optimization of inter-RAT handover parameters," *IEEE Transactions on Vehicular Technology (TVT), Special issue on SON*, vol. 62, no. 5, pp. 1906–1923, June 2013.

[BABS+11] O. Bulakci, A. Awada, A. Bou Saleh, S. Redana, J. Hamalainen, B. Wegmann, B. Raaf, and I. Viering, "Joint optimization of uplink power control parameters in LTE-advanced relay networks," in *Proc. IEEE International Wireless Communications and Mobile Computing Conference (IWCMC)*, July 2011, pp. 2064–2069.

[BABS+13] O. Bulakci, A. Awada, A. Bou Saleh, S. Redana, and J. Hamalainen, "Automated uplink power control optimization in LTE-advanced relay networks," *in EURASIP Journal on Wireless Communications and Networking*, vol. 2013, no. 8, January 2013.

[BAE+09] J. Belschner, P. Arnold, H. Eckhardt, E. Kuhn, E. Patouni, A. Kousaridas, N. Alonistioti, A. Saatsakis, K. Tsagkaris, and P. Demestichas, "Optimisation of radio access network operation introducing self-x functions: Use cases, algorithms, expected efficiency gains," in *Proc. IEEE Vehicular Technology Conference (VTC)*, April 2009, pp. 1–5.

[BB08] U. Bakshi and M. V. Bakshi, *Modern Control Theory*. Technical Publications Pune, 2008.

[BGM+06] C. Brunner, A. Garavaglia, M. Mittal, M. Narang, and J. Bautista, "Inter-system handover parameter optimization," in *Proc. IEEE Vehicular Technology Conference (VTC)*, 2006, pp. 1–6.

[BJAPO05] S. Ben Jamaa, Z. Altman, J.-M. Picard, and A. Ortega, "Steered optimization strategy for automatic cell planning of UMTS networks," in *Proc. IEEE on Vehicular Technology Conference (VTC)*, vol. 1, 2005, pp. 359–362.

[BJS+11] I. Balan, T. Jansen, B. Sas, I. Moerman, and T. Kürner, "Enhanced weighted performance based handover optimization in LTE," in *Future Network Mobile Summit 2011*, June 2011, pp. 1–8.

[Cel08] J. Celentano, "Carrier capital expenditures," *IEEE Communications Magazine*, vol. 46, no. 7, pp. 82–88, 2008.

[CL05] Y. Cai and D. Liu, "Multiuser detection using the Taguchi method for DS-CDMA systems," *IEEE Transactions on Wireless Communications*, vol. 4, no. 4, pp. 1594–1607, July 2005.

[ERX+13] A. Engels, M. Reyer, X. Xu, R. Mathar, J. Zhang, and H. Zhuang, "Autonomous self-optimization of coverage and capacity in LTE cellular networks," *IEEE Transactions on Vehicular Technology (TVT)*, vol. 2013, no. 5, pp. 1989–2004, 2013.

[FS08] S. Feng and E. Seidel, "Self-organizing networks (SON) in 3GPP Long Term Evolution," Nomor Research GmbH, Munich, Germany, May 2008.

[FSL+07] I. Forkel, M. Schmocker, L. Lazin, M. Becker, F. Debus, and F. Winnewisser, "Cell-specific optimized parameterization of compressed mode operation and inter-system handovers in UMTS/GSM overlay networks," in *European Wireless (EW)*, Paris, France, April 2007.

[Gol05] A. Goldsmith, *Wireless Communications*. Cambridge University Press, 2005.

[Has12] P. P. Hasselbach, "Capacity optimization for self-organizing networks: Analysis and algorithms," Ph.D. dissertation, Technical University of Darmstadt, 2012. [Online]. Available: http://tuprints.ulb.tu-darmstadt.de/id/eprint/3047

[HHL+05] G. Y. Hwang, S. M. Hwang, H. J. Lee, J. H. Kim, K. S. Hong, and W. Y. Lee, "Application of Taguchi method to robust design of acoustic performance in IMT-2000 mobile phones," *IEEE Transactions on Magnetics*, vol. 41, no. 5, pp. 1900–1903, May 2005.

[HJJ03] D. Henderson, S. H. Jacobson, and A. Johnson, *The Theory and Practice of Simulated Annealing*, F. Glover and G. A. Kochenberger, Eds. Kluwer Academic Publishers, 2003.

[HL12] G. Hui and P. Legg, "Soft metric assisted mobility robustness optimization in LTE networks," in *Proc. IEEE International Symposium on Wireless Communication Systems (ISWCS)*, 2012, pp. 1–5.

[Hop03] R. Hoppe, "Comparison and evaluation of algorithms for the interpolation of 3D antenna patterns based on 2D horizontal and 2D vertical patterns," Study AWE Communications GmbH, Tech. Rep., 2003.

[HSS99] A. S. Hedayat, N. Sloane, and J. Stufken, *Orthogonal Arrays: Theory and Applications*. New York: Springer-Verlag, 1999.

[HSS12] S. Hämäläinen, H. Saneck, and C. Sartori, *LTE Self-Organizing Network (SON): Network Management Automation for Operational Efficiency*. John Wiley & Sons, 2012.

[HT04a] K. Höglund and B. Ternby, "Co-siting solutions," Ericsson, Tech. Rep., 2004.

[HT04b] H. Holma and A. Toskala, *WCDMA for UMTS*, 3rd ed. John Wiley & Sons, 2004.

[HT07] ——, *HSDPA/HSUPA for UMTS: High Speed Radio Access for Mobile Communications*. John Wiley & Sons, 2007.

[HT09] ——, *LTE for UMTS: OFDMA and SC-FDMA Based Radio Access*. John Wiley & Sons Ltd., 2009.

[Hur02] S. Hurley, "Planning effective cellular mobile radio networks," *IEEE Transactions on Vehicular Technology (TVT)*, vol. 51, no. 2, pp. 243–253, March 2002.

[IHTT06] H. Ikeda, T. Hanamoto, T. Tsuji, and M. Tomizuka, "Design of vibration suppression controller for 3-inertia systems using Taguchi method," in *International Symposium on Power Electronics, Electrical Drives, Automation and Motion*, 2006, pp. 1045–1050.

[Jak74] W. C. Jakes, *Microwave Mobile Communications*. Wiley, 1974.

[JBS+11] T. Jansen, I. Balan, S. Stefanski, I. Moerman, and T. Kürner, "Weighted performance based handover parameter optimization in LTE," in *Proc. IEEE Vehicular Technology Conference (VTC)*, May 2011, pp. 1–5.

[JBT+10] T. Jansen, I. Balan, J. Turk, I. Moerman, and T. Kürner, "Handover parameter optimization in LTE self-organizing networks," in *Proc. IEEE Vehicular Technology Conference (VTC)*, September 2010, pp. 1–5.

[KGV83] S. Kirkpatrick, C. D. Gelatt, and M. P. Vecchi, "Optimization by simulated annealing," *Science*, vol. 220, no. 4598, pp. 671–680, May 1983.

[KH08] J. Kurjenniemi and T. Henttonen, "Effect of measurement bandwidth to the accuracy of inter-frequency RSRP measurements in LTE," in *Proc. IEEE Symposium on Personal, Indoor and Mobile Radio Communications (PIMRC)*, September 2008, pp. 1–5.

[KKYK11] K. Kitagawa, T. Komine, T. Yamamoto, and S. Konishi, "A handover optimization algorithm with mobility robustness for LTE systems," in *Proc. IEEE International Symposium on Personal Indoor and Mobile Radio Communications (PIMRC)*, 2011, pp. 1647–1651.

[KRR08] S. R. Karnik, A. B. Raju, and M. S. Raviprakasha, "Genetic algorithm based robust power system stabilizer design using Taguchi principle," in *First International Conference on Emerging Trends in Engineering and Technology*, July 2008, pp. 887–892.

[LF06] P. Loannou and B. Fidan, *Adaptive Control Tutorial*. Society for Industrial and Applied Mathematics, 2006.

[LH11] J. Lim and D. Hong, "Management of neighbor cell lists and physical cell identifiers in self-organizing heterogeneous networks," *Journal of Communications and Networks*, vol. 13, no. 4, pp. 367–376, 2011.

[LSJB10] A. Lobinger, S. Stefanski, T. Jansen, and I. Balan, "Load balancing in downlink LTE self-optimizing networks," in *Proc. IEEE Vehicular Technology Conference (VTC)*, 2010, pp. 1–5.

[MN00] R. Mathar and T. Niessen, "Optimum positioning of base stations for cellular radio networks," *Wireless Networks*, vol. 6, no. 6, pp. 421–428, December 2000.

[Mol03] A. F. Molisch, *Wireless Communications*. Wiley & Sons, November 2003.

[MPJC10] N. Marchetti, N. Prasad, J. Johansson, and T. Cai, "Self-organizing networks: State-of-the-art, challenges and perspectives," in *International Conference on Communications (COMM)*, 2010, pp. 503–508.

[MTR00] H. Meunier, E.-G. Talbi, and P. Reininger, "A multiobjective genetic algorithm for radio network optimization," in *Proceedings of the 2000 Congress on Evolutionary Computation*, vol. 1, July 2000, pp. 317–324.

[MYYZ12] C. Ma, R. Yin, G. Yu, and J. Zhang, "Reference signal power control for load balancing in downlink LTE-A self-organizing networks," in *Proc. IEEE International Symposium on Personal Indoor and Mobile Radio Communications (PIMRC)*, 2012, pp. 460–464.

[MZMT12] S. Mwanje, N. Zia, and A. Mitschele-Thiel, "Self-organized handover parameter configuration for LTE," in *Proc. IEEE International Symposium on Wireless Communication Systems (ISWCS)*, 2012, pp. 26–30.

[NDA06] M. J. Nawrocki, M. Dohler, and A. H. Aghvami, *Understanding UMTS radio network modelling, planning and automated optimisation.* John Wiley & Sons, 2006.

[NGM06] NGMN. (2006) Next generation mobile networks beyond HSPA & EVDO. [Online]. Available: www.ngmn.org

[NGM07] ——. (2007, May) NGMN use cases related to self organizing network, overall description. [Online]. Available: www.ngmn.org

[NGM08] ——. (2008, December) Next generation mobile networks recommendation on SON and O&M requirements. [Online]. Available: www.ngmn.org

[NN12] NSN and Nokia, "Cell-pair specific inter-RAT measurement configuration," Nokia Siemens Networks and Nokia Corporation, Tech. Rep. R2-122292, May 2012. [Online]. Available: http://www.3gpp.org/ftp/tsg_ran/WG2_RL2/TSGR2_78/Docs/R2-122292

[NPS11] M. D. Nisar, V. Pauli, and E. Seidel, "Multi-RAT traffic steering - why, when, and how could it be benefecial?" Nomor Research, Tech. Rep., 2011.

[NSN12] NSN, "Deployment strategies for heterogeneous networks," Nokia Siemens Networks, Tech. Rep., 2012.

[NuIAJHMT10] M. Naseer ul Islam, R. Abou-Jaoude, C. Hartmann, and A. Mitschele-Thiel, "Self-optimization of antenna tilt and pilot power for dedicated channels," in *International Symposium on Modeling and Optimization in Mobile, Ad Hoc and Wireless Networks (WiOpt)*, 2010, pp. 196–203.

[NuIMT12a] M. Naseer ul Islam and A. Mitschele-Thiel, "Cooperative Fuzzy Q-learning for self-organized coverage and capacity optimization," in *Proc. IEEE International Symposium on Personal Indoor and Mobile Radio Communications (PIMRC)*, 2012, pp. 1406–1411.

[NuIMT12b] ——, "Reinforcement learning strategies for self-organized coverage and capacity optimization," in *Proc. IEEE Wireless Communications and Networking Conference (WCNC)*, 2012, pp. 2818–2823.

[ONY+11] K. Okino, T. Nakayama, C. Yamazaki, H. Sato, and Y. Kusano, "Pico cell range expansion with interference mitigation toward LTE-advanced heterogeneous networks," in *Proc. IEEE International Conference on Communications Workshops (ICC)*, 2011, pp. 1–5.

[PDH97] R. Palm, D. Driankov, and H. Hellendoorn, *Model Based Fuzzy Control.* Springer-Verlag Berlin New York Heidelberg, 1997.

[PYS08] N. Pang, Y. You, and Y. Shi, "Application research on the simulated annealing in balance optimization of multi-resource network planning," in *Second International Symposium on Intelligent Information Technology Application*, vol. 2, December 2008, pp. 113–117.

[PZW11] K. Pentikousis, D. Zhu, and H. Wang, "Network infrastructure at the crossroads the emergence of smart cities," in *International Conference on Intelligence in Next Generation Networks (ICIN)*, 2011, pp. 109–114.

[Rao47] C. R. Rao, "Factorial experiments derivable from combinatorial arrangements of arrays," *Journal of the Royal Statistical Society*, vol. 9, no. 1, pp. 128–139, 1947.

[Rap02] T. S. Rappaport, *Wireless Communications: Principles and Practice*, 2nd ed. Prentice Hall PTR, 2002.

[Roy90] R. Roy, *A Primer on the Taguchi Method*. Society of Manufacturing Engineers, 1990.

[Roy01] ——, *Design of Experiments Using the Taguchi Approach: 16 Steps to Product and Process Improvement*. Wiley, 2001.

[Sau10] M. Sauter, *From GSM to LTE: An Introduction to Mobile Networks and Mobilie Broadband*. John Wiley & Sons, 2010.

[Sha11] P. M. Shankar, *Fading and Shadowing in Wireless Systems*. Springer, December 2011.

[She05] S. Shen, "How to cut mobile network costs to serve emerging markets," Gartner Inc., November 2005.

[Sin10] T. L. Singal, *Wireless Communications*. Tata McGraw Hill, 2010.

[Slo] N. J. A. Sloane, "A library of orthogonal arrays." [Online]. Available: http://www2.research.att.com/∼njas/oadir

[SOC08a] SOCRATES. (2008, May) Requirements for self-organizing networks. [Online]. Available: http://www.fp7-socrates.eu

[SOC08b] ——. (2008) Self-optimization and self-configuration in wireless networks, european research project. [Online]. Available: http://www.fp7-socrates.eu

[SOZ11] A. Sibille, C. Oestges, and A. Zanella, *MIMO from Theory to Implementation*. Academic Press, 2011.

[SPRSG+11] O. Sallent, J. Pérez-Romero, J. Sánchez-González, R. Agusti, M. Díazguerra, D. Henche, and D. Paul, "A roadmap from UMTS optimization to LTE self-optimization," *IEEE Communications Magazine*, vol. 49, no. 6, pp. 172–182, 2011.

[SS10] L. Song and J. Shen, *Evolved Cellular Network Planning and Optimization for UMTS and LTE*. CRC Press, 2010.

[SSJC05] N. Saravanan, N. Sreenivasulu, D. Jayaram, and A. Chockalingam, "Design and performance evaluation of an inter-system handover algorithm in UMTS/GSM networks," in *Proc. IEEE TENCON*, 2005, pp. 1–6.

[SVY06] I. Siomina, P. Varbrand, and D. Yuan, "Automated optimization of service coverage and base station antenna configuration in UMTS networks," *IEEE Wireless Communications*, vol. 13, no. 6, pp. 16–25, 2006.

[SY08] I. Siomina and D. Yuan, "Enhancing HSDPA performance via automated and large-scale optimization of radio base station antenna configuration," in *Proc. IEEE Vehicular Technology Conference (VTC)*, May 2008, pp. 2061–2065.

[Tag01] G. Taguchi, "Taguchi methods in LSI fabrication process," in *Proc. IEEE International Workshop on Statistical Methodology*, June 2001.

[TK05] U. Turke and M. Koonert, "Advanced site configuration techniques for automatic UMTS radio network design," in *Proc. IEEE Vehicular Technology Conference (VTC)*, vol. 3, May 2005, pp. 1960–1964.

[Tol11] M. Tolstrup, *Indoor Radio Planning: A Practical Guide for GSM, DCS, UMTS, HSPA and LTE*. John Wiley & Sons, 2011.

[vdBLE+08] J. L. van den Berg, R. Litjens, A. Eisenblätter, M. Amirijoo, O. Linnell, C. Blondia, T. Kürner, N. Scully, J. Oszmianski, and L. C. Schmelz, "Self-organisation in future mobile communications networks," in *ICT-Mobile Summit 2008*, June 2008.

[VDL09] I. Viering, M. Döttling, and A. Lobinger, "A mathematical perspective of self-optimizing wireless networks," in *Proc. IEEE International Conference on Communications (ICC)*, June 2009, pp. 1–6.

[VE93] K. L. Virga and R. J. Engelhardt, Jr, "Efficient statistical analysis of microwave circuit performance using design of experiments," in *Proc. IEEE MTT-S International Microwave Symposium Digest*, vol. 1, June 1993, pp. 123–126.

[VVGZ94] A. Viterbi, A. Viterbi, K. Gilhousen, and E. Zehavi, "Soft handoff extends CDMA cell coverage and increases reverse link capacity," *IEEE Journal on Selected Areas in Communications*, vol. 12, no. 8, pp. 1281–1288, Oct 1994.

[VWL+11] I. Viering, B. Wegmann, A. Lobinger, A. Awada, and H. Martikainen, "Mobility robustness optimization beyond doppler effect and WSS assumption." in *Proc. IEEE International Symposium on Wireless Communication Systems (ISWCS)*, August 2011, pp. 186–191, Invited paper.

[WAKV13] B. Wegmann, A. Awada, K. Kordybach, and I. Viering, "Inter-RAT MRO in 3GPP Rel.11: What works, and what does not," in *Proc. IEEE Vehicular Technology Conference (VTC)*, June 2013.

[Wei10] Z. Wei, "Mobility robustness optimization based on UE mobility for LTE system," in *Proc. IEEE International Conference on Wireless Communications and Signal Processing (WCSP)*, October 2010, pp. 1–5.

[WYE07] W.-C. Weng, F. Yang, and A. Elsherbeni, "Linear antenna array synthesis using Taguchi's method: A novel optimization technique in electromagnetics," *IEEE Transactions on Antennas and Propagation*, vol. 55, no. 3, pp. 723–730, March 2007.

[Xu02] H. Xu, "An algorithm for constructing orthogonal and nearly-orthogonal arrays with mixed levels and small runs," *American Statistical Association and the American Society for Quality*, vol. 44, no. 4, pp. 356–368, Technometrics, November 2002.

[ZYAW06] J. Zhang, J. Yang, M. Aydin, and J. Wu, "Mathematical modeling and comparisons of four heuristic optimization algorithms for WCDMA radio network planning," in *Proc. IEEE International Conference on Transparent Optical Networks*, vol. 3, 2006, pp. 253–257.

Lebenslauf

Name:	Ahmad Awada
Geburtsdatum:	30.04.1985
Geburtsort:	Beirut, Libanon

Schulausbildung

1988-1996	Lycée Verdun, Beirut, Libanon
1996-2003	Lycée Abdel Kader, Beirut, Libanon

Studium

2003-2007	Bachelor of Engineering in Computer and Communications an der American University of Beirut
2007-2009	Master of Science in Communications Engineering an der Technischen Universität München

Berufstätigkeit

2009-2013	Wissenschaftliche Tätigkeit in der Radio Systems Forschungsabteilung von Nokia Siemens Networks in München

Erklärung laut §9 der Promotionsordnung

Ich versichere hiermit, dass ich die vorliegende Dissertation allein und nur unter Verwendung der angegebenen Literatur verfasst habe. Die Arbeit hat bisher noch nicht zu Prüfungszwecken gedient.

Darmstadt, 31. August 2013